

# Symmetries & Tensor Networks in Two-Dimensional Quantum Physics

Henrik Dreyer

Ludwig-Maximilian Universität



and Max-Planck-Institute of Quantum Optics



Supervised by  
Prof. Norbert Schuch  
and  
Prof. Ignacio Cirac



# Symmetries & Tensor Networks in Two-Dimensional Quantum Physics

Dissertation an der  
Ludwig-Maximilian Universität  
München

vorgelegt von  
Henrik Dreyer  
aus Wesel, Deutschland

München, den 13.08.2020

Tag der mündlichen Prüfung: 28.09.2020

Erstgutachter: Prof. Jan von Delft

Zweitgutachter: Prof. Norbert Schuch

Vorsitzender der Kommission: Prof. Roland Kersting

Protokollantin: Prof. Barbara Ercolano

Stellvertretung: Prof. Emiliano Cortez

# Zusammenfassung

Die allgemeinste Beschreibung eines Quanten-Vielteilchensystems ergibt sich aus einer Wellenfunktion, die in einem Hilbert-Raum lebt, dessen Dimension exponentiell in der Anzahl der Teilchen ist. Dies macht es äußerst schwierig, stark korrelierte Phänomene wie den fraktionalen Quanten-Hall-Effekt und die Hochtemperatursupraleitung zu untersuchen. Wenn die Wechselwirkungen ausreichend lokal sind und die Temperatur niedrig ist, steht dem System nicht der gesamte Hilbert-Raum zur Verfügung. Sein Grundzustand befindet sich in der kleinen “Ecke” des Hilbert-Raums, die durch das *area law* beschrieben wird. Mit wenig Verschränkung können die Zustände dann als Tensornetzwerke ausgedrückt werden, eine Familie von Wellenfunktionen mit einer polynomiellen Anzahl von Parametern.

Einerseits können Tensornetzwerke als variationelle Ansätze bei numerischen Berechnungen verwendet werden. Auf der anderen Seite ermöglichen sie das Erstellen von Modellwellenfunktionen. Diese Modelle ermöglichen nicht nur eine analytische Behandlung, sondern gewähren auch Zugang zu den physikalischen und den Verschränkungsfreiheitsgraden.

Dies ist besonders nützlich bei der Klassifizierung von Phasen der Materie. Eine große Anzahl von Phasen kann mit Landaus Theorie der Symmetriebrechung erklärt werden. Diese Beschreibung ist jedoch nicht vollständig, was durch die Existenz von Phasen mit intrinsischer topologischer Ordnung in zwei Dimensionen veranschaulicht wird. Es war ein großer konzeptioneller Fortschritt, als Tensornetzwerke (nicht-chirale) topologische Phasen als solche identifizieren konnten, bei denen die Symmetrie in den Verschränkungsfreiheitsgraden liegt.

Die diesen topologischen Phasen entsprechenden Symmetrien wirken als diskrete, endliche Gruppen auf den virtuellen Freiheitsgraden. Der Zweck dieser Arbeit ist es, dieses Programm auf andere Symmetrien zu verallgemeinern. Wir untersuchen eine Klasse von Tensornetzwerken mit kontinuierlichen Symmetrien und stellen fest, dass sie keine mit eindeutigen Grundzustand unter einer Energielücke beschreiben können. Der abelsche Fall beschreibt einen nicht-Lorentz-invarianten Phasenübergangspunkt in eine topologisch geordnete Phase. Die Physik des nicht-abelschen Falls ist die eines Plaquette-Zustands, der spontan die Translationssymmetrie des Gitters bricht. Der nicht-abelsche PEPS entsteht als Grundzustand eines lokalen *parent*-Hamiltonians, dessen Grundzustandsunterraum vollständig durch das Tensornetzwerk beschrieben wird. In beiden Fällen finden wir zwei Arten von Korrekturen an der Verschränkungsentropie: Erstens gibt es eine Korrektur, die in der Größe der Grenze logarithmisch und unabhängig von der Form ist. Eine weitere Korrektur hängt nur von der Form des Schnitts ab, wodurch ausreichend dünne Bereiche weiter eingeschränkt werden.

Schließlich untersuchen wir Symmetrien, die virtuelle und physikalische Freiheitsgraden mischen und darüber hinaus anisotrop sind. Ihre Physik wird durch topologische Ordnung beschrieben, die stabil ist solange bestimmte Subsystem-

---

Symmetrien nicht gebrochen werden. Insbesondere konzentrieren wir uns auf die Verschränkungsentropie in der Clusterphase und zeigen, dass die Entropie in der gesamten Phase universell eine konstante Korrektur erhält. Dies ist wichtig im Programm zur Etablierung der Verschränkungsentropie als Detektionsmechanismus für topologisch geordnete Phasen. Wir schlagen einen numerischen Algorithmus vor, um die Korrektur zu berechnen und entdecken eine neue Phase der Materie, in die die Clusterphase eingebettet ist.

# Abstract

The most general description of a quantum many-body system is given by a wavefunction that lives in a Hilbert space with dimension exponential in the number of particles. This makes it extremely hard to study strongly correlated phenomena like the fractional quantum Hall effect and high-temperature superconductivity. Whenever interactions are sufficiently local and temperature is low, the system does not explore the full Hilbert space, but its ground state resides in the small corner of Hilbert space described by the area law. Containing little entanglement, the states can then be expressed as tensor networks, a family of wavefunctions with a polynomial number of parameters.

On the one hand, tensor networks can be used as a variational manifold in numerical computations. On the other hand, they allow building model wavefunctions much like locality allows writing down physically realistic Hamiltonians. Besides allowing for an analytical treatment, these models grant access both to the physical and the entanglement degrees of freedom.

This is particularly useful in classifying phases of matter. A large number of phases can be explained in terms of Landau's symmetry-breaking paradigm. This framework, however, is not complete, as exemplified by the existence of phases with intrinsic topological order in two dimensions. It was a major conceptual advance when tensor networks could explain (non-chiral) topological phases as those where the symmetry resides in the entanglement degrees of freedom.

The symmetries corresponding to those topological phases act as discrete, finite groups on the virtual degrees of freedom. The purpose of this Thesis is to generalize this program to include other symmetries. We investigate a class of tensor networks with continuous symmetries and find that they cannot describe gapped physics with a unique ground state. The abelian case is found to describe a non-Lorentz invariant phase transition point into a topologically ordered phase. The physics of the non-abelian case is that of a plaquette state that spontaneously breaks the translation symmetry of the lattice. The non-abelian PEPS arises as the ground state of a local parent Hamiltonian whose ground state manifold is completely characterized by the tensor network. In both cases, we find two types of corrections to the entanglement entropy: first there is a correction that is logarithmic in the size of the boundary and independent of the shape. A further correction depends only on the shape of the partition, imposing further restrictions on regions that are sufficiently thin.

Finally, we investigate symmetries that mix the virtual with the physical degrees of freedom and are furthermore anisotropic. Their physics is described by subsystem symmetry protected topological order. In particular, we focus on the entanglement entropy in the cluster phase and show that there is a universal constant correction to the entropy throughout the phase. This is important in the program of establishing the entanglement entropy as a detection mechanism for topologically ordered phases. We put forward a numerical algorithm to compute the correction and use it to

---

discover a novel phase of matter in which the cluster phase is embedded.



*Dedicated to Ruben, from whom I learned so much*

# Publications

This Thesis contains material from the following publications:

- Projected Entangled Pair States with Continuous Virtual Symmetries, Henrik Dreyer, Ignacio Cirac, Norbert Schuch, Physical Review B **98**, 115120 (2018)
- Detecting Subsystem Symmetry Protected Topological Order via Entanglement Entropy, David T. Stephen, Henrik Dreyer, Mohsin Iqbal, Norbert Schuch, Physical Review B **100**, 115112 (2019)
- Robustness of critical U(1) spin liquids and emergent symmetries in tensor networks, Henrik Dreyer, Laurens Vanderstraeten, Ji-Yao Chen, Ruben Verresen, Norbert Schuch, arXiv:2008.04833 (2020)

Chapter 4 contains passages that are reprinted verbatim with permission from the American Physical Society ©2018. Chapter 5 contains figures that are reprinted with permission from the American Physical Society ©2019.

# Contents

<b>1</b>	<b>Introduction</b>	<b>12</b>
1.1	Notation & Tensor Network Basics . . . . .	18
1.1.1	Matrix Product States . . . . .	18
1.1.2	Projected Entangled Pair States . . . . .	21
1.2	Example of a model MPS: The AKLT model . . . . .	23
1.2.1	Wave function and Symmetry . . . . .	24
1.2.2	Correlations . . . . .	25
1.2.3	Entanglement and the Bulk-Boundary Correspondence . . . . .	25
1.2.4	Symmetry-Protected Topological Order . . . . .	28
<b>2</b>	<b><math>U(1)</math>-symmetry</b>	<b>30</b>
2.1	Ground State Properties . . . . .	30
2.1.1	The Entanglement-Restricted Subspace . . . . .	32
2.1.2	Entanglement Entropy . . . . .	33
2.1.3	Symmetries of the Transfer Matrix . . . . .	36
2.2	Example: The Six-Vertex PEPS . . . . .	37
2.3	Low-Lying Excitations . . . . .	42
2.3.1	A Virtual Lieb-Schultz-Mattis Theorem . . . . .	43
2.3.2	Virtual Photons . . . . .	48
2.4	Conclusion . . . . .	51
<b>3</b>	<b>Dimer &amp; Resonating Valence Bond models</b>	<b>53</b>
3.1	The Resonating Valence PEPS . . . . .	55
3.2	Field Theory of the RVB state . . . . .	56
3.2.1	Interlude: The Classical Dimer Model . . . . .	57
3.2.2	From Orthogonal Dimers to Resonating Valence Bonds . . . . .	60
3.3	The Transfer Matrix . . . . .	61
3.4	Perturbing the Transfer Matrix . . . . .	63
3.5	Gap Scaling . . . . .	66
3.6	Floating $K$ and the Sine-Gordon Model . . . . .	68
3.7	Conclusion . . . . .	72
<b>4</b>	<b><math>SU(2)</math>-symmetry</b>	<b>75</b>
4.1	The wave function . . . . .	75
4.1.1	The Loop Picture . . . . .	77
4.1.2	Combinatorics of Loop Configurations . . . . .	79
4.1.3	Entanglement Entropy . . . . .	92
4.1.4	Physical Interpretation of the State . . . . .	94
4.2	Parent Hamiltonians . . . . .	98

4.2.1	Construction of the Hamiltonian and intersection property . . .	99
4.2.2	Open boundary conditions and unique ground state . . . . .	101
4.2.3	Periodic Boundary Conditions . . . . .	105
4.3	Conclusion . . . . .	112
<b>5</b>	<b>Subsystem Symmetry Protected Topological Order</b>	<b>114</b>
5.1	The Cluster State . . . . .	115
5.1.1	Symmetries . . . . .	115
5.1.2	Parent Hamiltonian . . . . .	117
5.1.3	Entropy . . . . .	117
5.2	The Cluster Phase . . . . .	118
5.2.1	An Exactly Solvable Perturbation . . . . .	118
5.2.2	Generic Ground States . . . . .	120
5.2.3	Generic Perturbations - Numerics . . . . .	124
5.3	Conclusion . . . . .	132
<b>6</b>	<b>Conclusion and Outlook</b>	<b>133</b>
	<b>Bibliography</b>	<b>137</b>

# Chapter 1

## Introduction

It is only slightly overstating the case to say that physics is the study of symmetry.

---

Philip W. Anderson, [1]

When Schrodinger wrote down his famous equation 1925, the fundamental laws of physics could have been considered complete. His equation equips us with a way to compute the behaviour of the system if we know the underlying interactions, taking into account the best theory we have for our universe, quantum mechanics. As such, the equation gave birth to two diverging paths of scientific inquiry. On the one hand, one may ask what *are* the fundamental interactions of our universe. This *reductionist* viewpoint leads one down into the microcosmos of particle physics, where few-body phenomena are understood up to high energies. On the other hand, one may ask if one can reconstruct the world starting from a complete understanding of the fundamental laws.

This *completionist* approach fails spectacularly across many scales even in the classical world: No single water molecule is wet, no single bird flocks and no single neuron can feel pride and joy.

The first layer at which collective behavior occurs is *quantum many-body physics*. Classic examples in this field are antiferromagnetism, liquid crystals, superfluidity and superconductivity. Clearly, even at this fundamental level, the study of emergent phenomena is both *rich* and technologically *useful*. It is also *hard*: It took 30 years to understand the mechanism of superconductivity even though the fundamental laws were known all the while. It is hard because of *complexity* and *scale*: A typical sample comprises  $10^{23}$  particles, a number so large that it is often easier to work in the *thermodynamic limit* of infinite particle number. To make matters worse, interactions are often sufficiently complex such that any attempt at divide-and-conquer strategies is futile. Finally, a complete *quantum mechanical* description requires a vector in

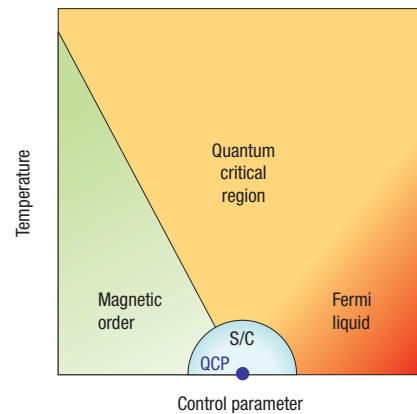


Figure 1.1: Phase diagram of a strongly correlated material showing a variety of phases. Reprinted with permission from Springer Nature Customer Service Centre GmbH: Nature Physics “What lies beneath the dome?”, D. M. Broun, ©2008 [2]

a Hilbert space of a corresponding dimension e.g.,  $2^{10^{23}}$ . To put this number into perspective: the largest computer-simulated Hilbert space to date is of dimension  $\sim 2^{45}$  [3].

Keeping track of every degree of freedom is thus a hopeless task. Fortunately, achieving this task would also be useless: The goal must be a humanly intelligible prediction for a macroscopic observable like whether the system has a magnetic moment or how well it conducts electricity. Reducing a complex system into a small number of macroscopic properties is the essence of the concept of *phases*. A trained scientist can infer all relevant information by a single glance at a phase diagram (Fig. 1.1), in which parameter regions are labeled by the kind of *order* that is present. It is the basic goal of condensed matter physics to understand and classify all possible types of orders and transitions between them.

It was realized by Landau in 1936 that order is intricately linked with *symmetry* [4]. More concretely, the microscopic laws exhibit a number of symmetries that may or may not be reflected by the macroscopic behavior of the system. This concept of *spontaneous symmetry breaking* has firmly established symmetry as the main protagonists across multiple branches of physics for many years to come.

There are two types of symmetries: *Discrete* and *Continuous*. They play rather distinct roles in the classification of phases: Due to a theorem by Hohenberg, Mermin and Wagner, continuous symmetries cannot spontaneously be broken at any finite temperature [5, 6]. In Landau's symmetry-breaking classification, therefore, there can only be a single phase associated to such continuous symmetries. This is why it was quite surprising, when Berezinskii, Kosterlitz and Thouless discovered a phase transition in the two-dimensional classical XY-model [7, 8]. The symmetry of the model is  $U(1)$ , the simplest example of a continuous group. Nevertheless, the model exhibits two distinct phases, separated by a transition at finite temperature.

If BKT's discovery cast a shadow of doubt on the completeness of the symmetry-breaking paradigm, then the lethal strike was delivered by von Klitzing's experimental discovery of the Quantum Hall effect [9]. He observed signatures of sharp phase transitions while varying the strength of a transverse magnetic field applied to an electron gas confined to two dimensions at low temperature. Crucially, the transitions could not be attributed to any spontaneously broken symmetry. What's more, the transitions occur without any change in temperature, indicating a *quantum phase transition*. Unlike thermal order-disorder transitions, in which entropy and energy compete, a quantum phase transition embodies the competition between different types of quantum order. These transitions happen at zero temperature, but their presence can be felt in large regions of the finite temperature phase diagram. The central object in the study of quantum phases is the *ground state*. If there is a finite energy gap above the ground state, it completely dominates the physics at sufficiently small temperatures. Furthermore, slight perturbations of the system induce only small changes in the ground state as long as the gap does not close.

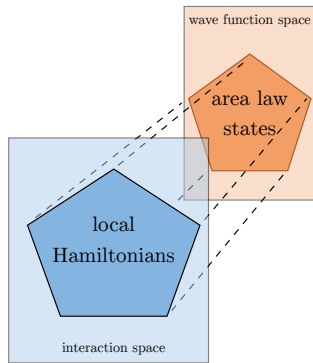
The key to understanding the new Quantum Hall phases is *topology*. It's role is most easily understood in the *Fractional* Quantum Hall effect: The ground state manifold is degenerate and the number of ground states depends on the topology of the surface on which the system lives. On the one hand, these topological systems exhibit exotic emergent properties like fractionalized excitations that are neither bosons nor fermions. These *anyons* could be used as the building blocks of a topological quantum computer. On the other hand, such interacting topologically

ordered systems are hard to control both from a theoretical as well as experimental perspective: While many symmetry breaking phases can be described perturbatively starting from a classical product state, no such luck is to be had in the presence of strong interactions. The phase is disconnected from any product state and can in principle explore the whole exponentially large Hilbert space.

But can it *really*? Consider for a moment describing the quantum system by its interactions rather than its state. In principle the two must contain precisely the same information. Realistic interactions, however, satisfy a severe constraint: *locality*. For example, the dimension of the space of nearest-neighbour Hamiltonians on a chain of  $d$ -level systems is  $d^4 N$ , while arbitrary interactions span a space of dimension  $d^{2N}$ . Ground states of such local Hamiltonians therefore only contain a polynomial amount of information. How can we characterize those states?

The answer was provided by a separate scientific field. *Quantum Information Theory* is the study of *entanglement*. In particular, it seeks to quantify the information stored in a quantum mechanical state in terms of the *entanglement entropy*. This quantity is defined in terms of a partition of the system into two subsystems and quantifies the amount of information that can not be inferred from measuring the subsystems alone. Ground states of local Hamiltonians turn out to be those that have relatively little entanglement. More precisely, while random states possess entanglement extensive in the size of the smaller subsystem, entanglement in ground states only grows with the boundary of the partition. This atypical behavior, the *area law*, has been rigorously proven in spatial dimension one and is widely believed to hold in higher dimensions as well [10]. Strictly speaking, all of these results hold away from phase transition points at which slight violations of the area law occur.

The novel, entanglement-based perspective led to the development of *Tensor Network States (TNS)*. They are constructed by introducing *virtual* degrees of freedom in which the entanglement is explicit.



The role of tensor networks in Hilbert space is roughly the same as that of local Hamiltonians in interaction space: they occupy the (tiny) corner of physically realistic systems. This realization has been exploited in two ways: First, the exponential reduction in complexity led to the development of efficient *numerical algorithms*. In fact, the success of the Density Matrix Renormalization Group (DMRG) [11] relies on the fact that only a tiny corner of Hilbert space has to be explored variationally. On the other hand, tensor networks allow for unprecedented *analytical* control on the level of the wave function. One particularly radical approach is the *model*

*wave function*. In this “wave function-first” approach, rather than variationally minimizing the energy with respect to some model Hamiltonian, a ground state candidate is simply written down in terms of a tensor network. This has four major advantages: First, unlike the “Hamiltonian-first” approach, one has direct access to the entanglement degrees of freedom. What’s more, symmetries can be directly encoded. In some sense, this is the reason that the “Hamiltonian-first” approach has been so powerful: as long as the correct symmetries are incorporated, it does not matter so much if one gets the microscopic details wrong. The difference is that, in a tensor network, not only the presence of a symmetry but also the way the entan-

glement and physical degrees of freedom transform is important in the classification of phases. We will have a lot more to say on that later. Third, observables in a tensor network model can be extracted using efficient numerical methods. Last, if it possesses a reasonable analytical structure, one can gain a deep understanding from the wave function. This has been carried out with great success for the Laughlin wave function of odd-filling fractional quantum Hall states [12] (although this is an example of the wave function approach independent of tensor networks), and the *Affleck-Kennedy-Lieb-Tasaki (AKLT)* model [13].

The AKLT state is a *Matrix Product State (MPS)*, i.e., a one-dimensional tensor network that occupies a sweet spot in the world of model wave functions. Typically, model wave functions are not *exact* ground states of simple Hamiltonians and there is a tradeoff in the complexity of the state and the interactions. This is not the case for the AKLT model. It is one of the rare non-integrable models where the ground state physics of a realistic system can be understood perfectly. The AKLT model is only slightly more complicated than (and adiabatically connected to) the spin-1 Heisenberg antiferromagnet. Prior to AKLT's work, Haldane had made the surprising conjecture that integer spin antiferromagnets are gapped [14, 15] (it had been known since Bethe's work [16] that the spin-1/2 antiferromagnet is gapless). The AKLT model did not only corroborate the conjecture, but it also clarified *why* such a distinction exists: Unlike spin-1/2, spin-1 systems allow for non-trivial gapped topological order, even in one dimension. A whole new class of phases was discovered as a consequence: those with *Symmetry Protected Topological (SPT) order*. This new type of order is manifestly characterized by entanglement: As long as the protecting symmetry is not explicitly broken, no ground state in the phase can be disentangled without crossing a phase transition. Furthermore, MPS enabled to prove that the classification of phases in one dimension is now actually *complete*: gapped phases either have symmetry-breaking, SPT or trivial order and that is all there is [17, 18].

Much effort has been made to carry over the success of tensor networks to dimension greater than one. Higher-dimensional tensor networks are usually called Projected Entangled Pair States (PEPS). Two-dimensional systems are particularly interesting: quantum fluctuations (which are favored by low spatial dimension) are still strong enough, while at the same time there is “enough space” for more interesting topological phenomena to occur. It is therefore not surprising that prominent open problems in the field, like high-temperature superconductivity and the fractional quantum Hall effect are effectively two-dimensional. A milestone in the classification of topological order was the complete characterization of the *Quantum Double Models* and, more generally, string-net models [19] in terms of PEPS [20–22]. The programme has been extended to include several examples of chiral topological order [23–25].

The key ingredient in all of these constructions lies in the symmetry of the entanglement degrees of freedom. These symmetries, as well as symmetry twists, are locally undetectable yet show up in the global topological properties of the systems. For discrete groups, they allow to parametrize the ground space manifold, to study anyonic excitations and their statistics, and to determine the entanglement properties of the system. Topological order can be understood in terms of the symmetry breaking pattern in the virtual degrees of freedom [26].

With this, we have come full circle: Landau told us that order means breaking a



symmetry. Topological order shows the shortcomings of Landau’s theory and pushes symmetry to the sideline. Finally, the tensor network formalism reconciles the two by reinterpreting topological order in terms of symmetry in the entanglement degrees of freedom, putting symmetry back front and centre.

While there are decades of research concerning the breaking of various physical symmetries, the study of symmetries in the entanglement is still in its infancy. For example, there is no framework for the context of continuous symmetries. This topic is particularly timely due to recent developments in Lattice Gauge Theory that are now studied with PEPS [27–32]. Furthermore, one can investigate non-trivial mixtures of physical and entanglement symmetries and even the effect of anisotropic symmetries. The central question of this Thesis is therefore:

Which are the phases that correspond to symmetric PEPS?

We will restrict the discussion to tensor networks describing neither fermionic nor bosonic, but spin degrees of freedom. On the one hand this description is sufficient to describe the relevant low-temperature physics in various models, like the Mott insulator phase of the Hubbard model which we discuss more concretely in chapter 3. On the other hand, simple spin systems without any immediate relevance to realistic systems can still show the same types of phases and phase transitions that are realized in actual materials.

The outline of this Thesis is as follows: we introduce tensor networks more rigorously in section 1.1 and establish some useful diagrammatic notation. In section 1.2 we showcase how symmetries are encoded in a model tensor network using the example of the AKLT chain. The original contributions of this Thesis are chapters 2 through 5. Apart from using the notation introduced in this chapter as well as a few cross-references, the following chapters are self-contained. In chapter 2, we study the simplest *continuous* symmetry,  $U(1)$ . Beyond its simplicity, the study is also motivated by the fact that any other compact Lie group has a subgroup isomorphic to  $U(1)$  which means that the results from this section hold more generally.  $U(1)$  is the relevant symmetry in Berezinskii-Kosterlitz-Thouless’ discovery of phases beyond the symmetry-breaking paradigm and we will find the physics of  $U(1)$ -PEPS to be closely related. Indeed, we will show that such PEPS generically cannot be the unique ground states of gapped local Hamiltonians, indicating criticality, symmetry-breaking or topologically ordered scenarios. The critical points can describe transitions into topologically ordered phases with a characteristic dynamical critical exponent  $z = 2$ . We investigate the entanglement entropy and find two separate mechanisms that lead to corrections to the area law. First, there is a *logarithmic* correction corresponding to the dimension of the singlet space under the  $U(1)$ -symmetry. Furthermore, there is a *geometric* correction arising from the finite entanglement mediated through thin channels. We establish a connection with vertex models of classical statistical mechanics.

In chapter 3, we study the *Resonating Valence Bond (RVB)* state. Relevant in the theory of high-temperature superconductivity and quantum spin liquids, this model wave function is also one of the simplest  $U(1)$ -PEPS. Physically, the state corresponds to covering the square lattice with spin-1/2 nearest-neighbour singlet pairs. A more realistic scenario is one in which pairings exist between more distant spins. In terms of PEPS, long-range singlets correspond to an explicit breaking of the  $U(1)$ -symmetry. Previous studies have observed critical behavior of the PEPS

even when the symmetry is broken. In light of our findings in chapter 2, this comes as a surprise: Is the presence of  $U(1)$ -symmetry not essential, after all, for the existence of low-lying excitations? We reconcile these findings by showing that breaking  $U(1)$  *does* induce a finite gap, albeit one which is so small that it can only be detected on lattices with thousands of spins in each direction. The required system sizes are way beyond reach of the best currently existing numerical algorithms. To nevertheless show the existence of a gap, we combine PEPS techniques with *Conformal Field Theory* (CFT). Tailored to gapless critical points, CFT provides a useful complementary approach to tensor network methods. After translating key objects from the PEPS into the CFT and vice-versa, we use this correspondence to establish a scaling hypothesis for the gap which is then numerically corroborated. Furthermore, we identify the perturbed PEPS with a symmetry broken phase of a Sine-Gordon field theory, before proposing a PEPS with an *emergent*  $U(1)$ -symmetry.

In chapter 4, we shift our attention from  $U(1)$  to  $SU(2)$ , as a first example of a non-abelian continuous group. We have found the  $U(1)$ -PEPS to lie at the boundary of a topological phase, on which one of the abelian anyons has condensed into the ground state. In the context of topological quantum computation, non-abelian anyons are much more attractive, since they enable universal quantum computation. We find, however, that an elementary class of  $SU(2)$ -PEPS does not describe a topological phase transition, but instead has translation symmetry-breaking plaquette order. As opposed to the abelian case, we show that the classical model corresponding to the non-abelian symmetry is a *non-local loop model*, due to the fact that singlets of the non-abelian symmetry are necessarily entangled. The PEPS is an exact ground state of a “loop surgery” Hamiltonian. The ground state manifold consists of two types of states: the Hamiltonian decomposes into a polynomial number of blocks which can be accessed by inserting topologically non-trivial string-operators. On the other hand, there is an exponential number of “frozen” product ground states. We investigate the entanglement entropy and find stricter logarithmic and geometric restrictions than in the  $U(1)$  case.

In chapter 5, we take a step back from continuous symmetries. The anisotropic symmetry we study gives rise to physical *subsystem symmetries*. These rigid lower-dimensional symmetries are sufficient to protect a topological phase, the so-called *Cluster Phase*. The presence of such subsystem symmetries induces a constant correction to the area law. Such corrections are important in the study of systems with intrinsic topological order, where they are referred to as the *topological entanglement entropy*  $\gamma$  [33, 34]. The value of  $\gamma$  derived from these subsystem-symmetries can be precisely identical to that of systems with intrinsic topological order. This is a problem when using the entanglement entropy in order to distinguish different phases. There has been a recent debate about whether such coincidence is generic or fine-tuned. We settle this argument by showing that the Cluster phase has a uniform correction to the entanglement entropy, the *Symmetry-Protected Entanglement Entropy* (SPEE). While doing so, we develop a novel numerical tool and discover a new, larger subsystem-symmetry protected topological phase in which the Cluster phase is embedded.

We conclude in Chapter 6 and present an outlook for further research directions.

## 1.1 Notation & Tensor Network Basics

The purpose of this section is to introduce basic notation, theorems and methods that will be used throughout this Thesis.

### 1.1.1 Matrix Product States

Matrix Product States are defined by a collection  $n = 1, 2, \dots, L$  of three-legged tensors  $A[n]_{lr}^i$ , depicted graphically by

$$\begin{array}{c} i \\ | \\ \boxed{A[n]} \\ | \\ l \quad r \end{array} \quad (1.1)$$

where  $i = 1, 2, \dots, d$  and  $l, r = 1, 2, \dots, \chi$ . Here,  $L$  is the number of sites,  $d$  is the *physical dimension* and  $\chi$  is the *bond dimension*. Identifying these labels with bases  $\{|i\rangle\}, \{|l\rangle\}, \{|r\rangle\}$  of the *physical (Hilbert) space* and the *virtual space*, respectively, these tensors can be *contracted*:

$$\begin{aligned} |\psi(\{A[n]\}_n)\rangle &:= \sum_{i_1, i_2, \dots, i_L} \text{Tr} \left[ A[1]^{i_1} A[2]^{i_2} \dots A[L]^{i_L} \right] |i_1, i_2, \dots, i_L\rangle \\ &= \begin{array}{c} i_1 \quad i_2 \quad i_L \\ | \quad | \quad | \\ \boxed{A[1]} \quad \boxed{A[2]} \quad \dots \quad \boxed{A[L]} \\ | \quad | \quad | \end{array} \end{aligned} \quad (1.2)$$

The number of parameters in (1.2) is  $\chi^2 d L$ ; exponentially less than the  $2^L$  coefficients naively used to describe the wave function.

In all parts of this Thesis, we will deal with states that are *translation invariant*, i.e. they do not change under  $i_1 \rightarrow i_2 \rightarrow i_3 \rightarrow \dots i_L \rightarrow i_1$ . In this case, we may restrict (1.2) to a single tensor that is repeated along the chain,  $A[n] \equiv A$ . This *elementary tensor* defines both a tripartite *fiducial state*

$$|A\rangle := \sum_{ilr} A_{lr}^i |i\rangle |l\rangle |r\rangle \quad (1.3)$$

as well as a *fiducial map*

$$M_A := \sum_{ilr} A_{lr}^i |i\rangle \langle l| \langle r| \quad (1.4)$$

that maps the virtual into the physical subspace. An MPS is called *invertible* if there exists a left inverse  $M_A^{-1}$ , such that  $M_A^{-1} M_A = \mathbb{1}_{\text{virtual}}$ . This is only possible if

$\chi^2 < d$ . However, MPS tensors can be *blocked*

$$\begin{array}{c} | \\ \hline \boxed{B} \\ \hline \end{array} = \begin{array}{c} | \\ \hline \boxed{A} \\ \hline \end{array} \begin{array}{c} | \\ \hline \boxed{A} \\ \hline \end{array} \quad (1.5)$$

to yield tensors with the same bond dimension, but larger physical dimension  $d'_B = d_A^2$ . An MPS is *normal*, if it is injective after blocking a finite number of times.

The map  $M_A$  can be used to construct Hamiltonians that have the MPS as a ground state. To this end, define the image of  $M_A$  after blocking e.g., 2 tensors by

$$\mathcal{S}_2 = \text{span} \left\{ \begin{array}{c} \begin{array}{c} | \\ \hline \boxed{A} \end{array} \begin{array}{c} | \\ \hline \boxed{A} \end{array} \\ \hline \bigcirc X \end{array} \left| X \right. \right\}. \quad (1.6)$$

The *parent Hamiltonian* is then defined by local projectors onto the orthogonal complement

$$h := \mathbb{1} - \Pi_{\mathcal{S}_2}. \quad (1.7)$$

Clearly, such Hamiltonians are hermitian, semi-positive and annihilate the MPS. Of course, writing down such a Hamiltonian is easy; simply taking  $h = 0$  would do the trick. If the MPS is injective, however, the parent Hamiltonian has a *unique* ground state which is given by the MPS. Furthermore, on open boundaries, the ground space of the Hamiltonian is given precisely by the states that are generated from the MPS with different boundary conditions.

A central element in the study of Matrix Product States is the *transfer matrix*

$$T_A = \sum_i A^i \otimes \overline{A^i} \quad (1.8)$$

$$= \begin{array}{c} \begin{array}{c} | \\ \hline \boxed{\overline{A}} \\ \hline \end{array} \\ | \\ \begin{array}{c} \boxed{A} \\ \hline \end{array} \end{array} \quad (1.9)$$

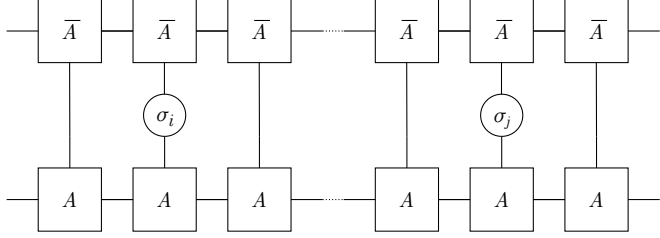
For notational clarity, we will suppress the dependence of the transfer matrix on the underlying tensor throughout this Thesis. The norm of the quantum state can be expressed in terms of the transfer matrix

$$\langle \psi(A) | \psi(A) \rangle = \text{Tr}(T^L). \quad (1.10)$$

As we will discover later, the norm of a tensor network can sometimes be interpreted as a partition function. On the other hand, we typically want to deal with normalized quantum states. Therefore, unless otherwise stated, we will normalize our tensor

networks in such a way that the magnitude of the largest eigenvalue of the transfer matrix is 1.

The transfer matrix also carries all information about correlation functions. Indeed, consider the connected two-point functions of a local operator  $\sigma$

$$\langle \psi(A) | \sigma_i \sigma_j | \psi(A) \rangle =$$

(1.11)

$$=: \text{Tr} (T(\sigma) T^{|i-j|-1} T(\sigma) T^{L-|i-j|-1}) \quad (1.12)$$

In the thermodynamic limit  $L \rightarrow \infty$ , we can replace  $T^{L-|i-j|-1}$  by the projector onto its leading left and right eigenvectors  $\langle \sigma_L |$  and  $|\sigma_R \rangle$ . Assume for now that  $T$  has a unique largest eigenvalue  $\lambda_1 = 1$ . Denoting eigenvectors corresponding to smaller eigenvalues by  $\langle L_i |$  and  $|R_i \rangle$  (for  $i = 2, \dots, \chi^2$ ) and the distance by  $x := |i - j| - 1$ , we have

$$\begin{aligned} \dots &= \langle \sigma_L | T(\sigma) T^{|i-j|-1} T(\sigma) | \sigma_R \rangle \\ &= | \langle \sigma_L | T(\sigma) | \sigma_R \rangle |^2 + \sum_{i=2}^{\chi^2} \lambda_i^x \langle \sigma_L | T(\sigma) | R_i \rangle \langle L_i | T(\sigma) | \sigma_R \rangle \end{aligned} \quad (1.13)$$

Identifying  $| \langle \sigma_L | T(\sigma) | \sigma_R \rangle |^2 = \langle \psi(A) | \sigma_i | \psi(A) \rangle \langle \psi(A) | \sigma_j | \psi(A) \rangle$ , we can bound the connected part


$$| \langle \psi(A) | \sigma_i \sigma_j | \psi(A) \rangle - \langle \psi(A) | \sigma_i | \psi(A) \rangle \langle \psi(A) | \sigma_j | \psi(A) \rangle | = \mathcal{O}(e^{-x/\xi}) \quad (1.14)$$

where we have defined  $\xi = -1/\log(|\lambda_2|)$ , or, more generally,

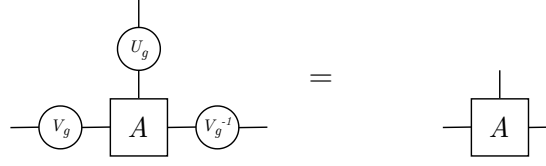
$$\xi = -\frac{1}{\log(|\lambda_2/\lambda_1|)}. \quad (1.15)$$

Under general circumstances, we can therefore identify the maximum correlation length of an MPS with the gap of its transfer matrix, where special care has to be taken in the case of exact degeneracies.

In this Thesis, we are particularly interested in tensor networks with symmetries. *On-site symmetries* are unitary representations  $U_g$  of a group  $G$  that act on an MPS as


(1.16)

A great virtue of tensor networks comes from the fact that such symmetries can be encoded *locally*. Indeed, a tensor that fulfills

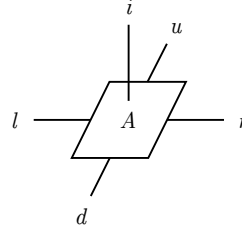


$$(1.17)$$

also satisfies (1.16). On the other hand, the *fundamental theorem* of MPS states that, as long as the MPS is normal, the reverse is also the case: Eq. (1.16) implies the existence of  $V_g$  for which (1.17) holds [35, 36] and for which  $V_g^{-1} = V_g^\dagger$  for unitary representations [37].

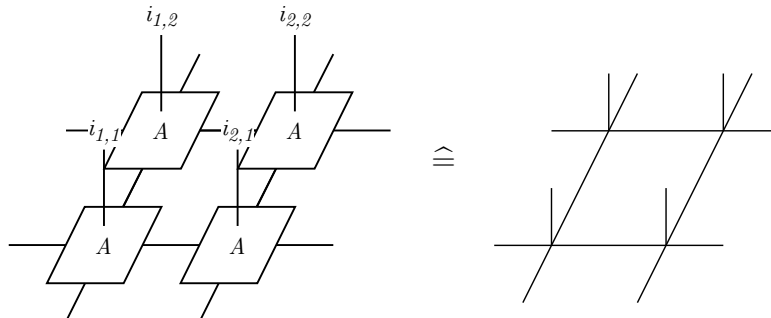
### 1.1.2 Projected Entangled Pair States

Higher-dimensional generalization of Matrix Product States are generally called Projected Entangled Pair States (PEPS) and, owing to the richer geometry of lattices in higher dimension, this name can refer to a multitude of constructions. In this Thesis, we will work exclusively on the square lattice in two dimensions. While being mainly a conceptual tool, the square lattice is actually an accurate effective description of physical systems of interests like the cuprates. For our purposes, we define a PEPS from an elementary five-legged tensor  $A_{uldr}^i$



$$(1.18)$$

Translational invariant states are obtained by distributing such an elementary tensor across the lattice (cf. 1.2)



$$(1.19)$$

where we have introduced more economical notation. In terms of this notation, the transfer matrix now reads

$$T = \begin{array}{c} \diagup \\ \text{---} \\ \diagdown \\ \text{---} \\ \diagup \\ \text{---} \\ \diagdown \\ \text{---} \\ \diagup \\ \text{---} \\ \diagdown \\ \text{---} \\ \diagup \end{array} \quad (1.20)$$

An elementary building block of the transfer matrix is the *double tensor*

$$\begin{array}{c} \diagup \\ \text{---} \\ \diagdown \\ \text{---} \\ \diagup \\ \text{---} \\ \diagdown \\ \text{---} \\ \diagup \end{array} = \begin{array}{c} \text{---} \\ \boxed{\mathbb{E}} \\ \text{---} \end{array} \quad (1.21)$$

The eigenvectors of the transfer matrix are themselves one-dimensional objects. In many occasions throughout this Thesis, we will attempt to describe them in terms of Matrix Product States. For example, if the transfer matrix runs from bottom to top, the MPS representing the top fixed point is simply denoted

$$\begin{array}{|c|c|c|c|c|} \hline & & & & \\ \hline & & & & \\ \hline \end{array} = \begin{array}{|c|c|c|c|c|} \hline & & & & \\ \hline \end{array} \quad (1.22)$$

At several occasions, we will find such MPS fixed points numerically, using the *Corner Transfer Matrix method* [38–41].

Sometimes, the interesting physics will take place exclusively on the virtual level of the PEPS. In this case, we adopt a top view in which we suppress the physical legs of the tensor

$$\begin{array}{c} \text{---} \\ \boxed{A} \\ \text{---} \end{array} \quad (1.23)$$

Like Matrix Product States, Projected Entangled Pair States enjoy the property of having a non-trivial local Hamiltonian that is guaranteed to have the PEPS in its ground space. Such *parent* Hamiltonians are defined by blocking a number of tensors

until the corresponding map  $M$  from the virtual to physical degrees of freedom fails to be surjective. Denote the image of  $M$  by

$$\mathcal{S} = \text{span} \left\{ \left( \begin{array}{c} \boxed{\begin{array}{cc} A & A \\ A & A \end{array}} \quad X \quad \bigg| \quad X \right) \right\}. \quad (1.24)$$

and define the projector onto the orthogonal complement of  $\mathcal{S}$

$$h = \mathbb{1} - \Pi_{\mathcal{S}} \quad (1.25)$$

Setting  $H = \sum_p h_p$  yields a local, hermitian and semipositive Hamiltonian that annihilates the PEPS. The notion of injectivity carries over from matrix product states and parent Hamiltonians of injective PEPS fulfil the intersection property, i.e., their ground is completely characterized by the PEPS. The concept of injectivity can be weakened such that the map  $M$  is only injective on the symmetric subspace of a finite group. In one dimension, such MPS correspond to cat states describing one of the ground states in symmetry-breaking phases. In two dimensions, *G-injective* PEPS have intrinsic topological order: their parent Hamiltonians do not have unique ground states, but a finite topological ground states degeneracy. In spatial dimension larger than one, more exotic behaviour than injectivity or G-injectivity is possible. In chapters 2-5, we study some of those possibilities. Before doing so, we need to introduce some final concepts. We will illustrate these using the ancestor of all tensor network models.

## 1.2 Example of a model MPS: The AKLT model

There is a number of concepts that are relevant for the main discussion of this Thesis. Rather than dealing with them abstractly, we review the paradigmatic AKLT model, where these ideas are exemplified.

Consider the *bilinear-biquadratic* spin chain with local spin-1 degrees of freedom,  $L$  sites and periodic boundary conditions described by the Hamiltonian

$$H = \sum_{i=1}^L \vec{S}_i \cdot \vec{S}_{i+1} + \beta (\vec{S}_i \cdot \vec{S}_{i+1})^2 \quad (1.26)$$

For  $\beta = 0$ , the model becomes the spin-1 Heisenberg Antiferromagnet (AFM). Bethe solved the spin-1/2 antiferromagnet using his celebrated Bethe ansatz [16]. It is gapless and can be seen as a transition of Kosterless-Thouless type from the disordered, critical phase of the XXZ chain into an antiferromagnetic ordered phase. The nature of the spin-1 AFM remained unclear for a long time, until Haldane predicted the existence of a unique ground state and a finite excitation gap implying exponential decay of local correlation functions [14, 15]. We will prove this statement using the modern approach and start with a model MPS wave function.



### 1.2.1 Wave function and Symmetry

Since (1.26) is manifestly  $SU(2)$  and translational invariant, let us write down the simplest MPS wave function respecting those symmetries. Define the MPS tensor  $A$ , with bond dimension  $\chi = 2$  and physical dimension  $d = 3$  (spin-1) by

$$A^+ = \sqrt{\frac{2}{3}} \begin{pmatrix} 0 & 0 \\ 1 & 0 \end{pmatrix} \quad (1.27a)$$

$$A^0 = -\sqrt{\frac{1}{3}} \begin{pmatrix} 1 & 0 \\ 0 & -1 \end{pmatrix} \quad (1.27b)$$

$$A^- = -\sqrt{\frac{2}{3}} \begin{pmatrix} 0 & 1 \\ 0 & 0 \end{pmatrix} \quad (1.27c)$$

The continuous  $SU(2)$ -symmetry is encoded in the local tensor in terms of the generators:

$$\begin{array}{c} \text{---} \square \text{---} \\ | \\ \bigcirc \text{---} \\ | \\ \text{---} \end{array} \quad \begin{array}{c} \text{---} \square \text{---} \\ | \\ \bigcirc \text{---} \\ | \\ \text{---} \end{array} = \begin{array}{c} \text{---} \bigcirc \text{---} \\ | \\ \text{---} \end{array} \begin{array}{c} \text{---} \square \text{---} \\ | \\ \text{---} \end{array} - \begin{array}{c} \text{---} \square \text{---} \\ | \\ \text{---} \end{array} \begin{array}{c} \text{---} \bigcirc \text{---} \\ | \\ \text{---} \end{array} \quad (1.28)$$

where  $Z$  is the spin- $S$  representation of the generator of rotations around the z-axis corresponding to the dimension of the link that it is acting on, i.e., the usual Pauli- $Z$  matrix in the virtual space and  $\text{diag}(1, 0, -1)$  in the physical space. For the global wave function this implies that

$$\begin{aligned} S^z |\psi\rangle &= \sum_i \cdots \begin{array}{c} \text{---} \square \text{---} \\ | \\ \text{---} \end{array} \begin{array}{c} \text{---} \square \text{---} \\ | \\ \bigcirc \text{---} \\ | \\ \text{---} \end{array} \begin{array}{c} \text{---} \square \text{---} \\ | \\ \text{---} \end{array} \cdots \\ &= \cdots \begin{array}{c} \text{---} \square \text{---} \\ | \\ \text{---} \end{array} \begin{array}{c} \text{---} \bigcirc \text{---} \\ | \\ \text{---} \end{array} \begin{array}{c} \text{---} \square \text{---} \\ | \\ \text{---} \end{array} \begin{array}{c} \text{---} \square \text{---} \\ | \\ \text{---} \end{array} \cdots - \cdots \begin{array}{c} \text{---} \square \text{---} \\ | \\ \text{---} \end{array} \begin{array}{c} \text{---} \square \text{---} \\ | \\ \text{---} \end{array} \begin{array}{c} \text{---} \bigcirc \text{---} \\ | \\ \text{---} \end{array} \begin{array}{c} \text{---} \square \text{---} \\ | \\ \text{---} \end{array} \cdots \\ &+ \cdots \begin{array}{c} \text{---} \square \text{---} \\ | \\ \text{---} \end{array} \begin{array}{c} \text{---} \square \text{---} \\ | \\ \text{---} \end{array} \begin{array}{c} \text{---} \bigcirc \text{---} \\ | \\ \text{---} \end{array} \begin{array}{c} \text{---} \square \text{---} \\ | \\ \text{---} \end{array} \cdots + \dots \\ &= 0 \end{aligned} \quad (1.29)$$

and similarly for  $S^x$  and  $S^y$ . Since each of the generators of  $SU(2)$  annihilates  $|\psi\rangle$ , we have shown that (1.28) implies

$$\begin{aligned} U^{\otimes L} |\psi\rangle &= e^{i\vec{\theta}\vec{S}} |\psi\rangle \\ &= |\psi\rangle \end{aligned} \quad (1.30)$$

for all  $U \in SU(2)$ . Let us compute the parent Hamiltonian of the MPS. The AKLT tensor is normal but it is only injective after blocking at least two sites. According

to the last section, one would expect that we need to take more than two sites to set up an appropriate parent Hamiltonian. As it turns out, the model is exceptional in the sense that two sites already suffice. Let us calculate the span of the map from the virtual to the physical degrees of freedom given by two single-site tensors:

$$M = \begin{array}{c} \uparrow \quad \uparrow \\ \boxed{A} \text{---} \boxed{A} \\ \leftarrow \quad \rightarrow \end{array} \quad (1.31)$$

Both the input and output spaces can be labelled by  $SU(2)$  quantum numbers. The virtual space decomposes as  $1/2 \otimes 1/2 = 0 \oplus 1$ , while the physical space can be written as  $1 \otimes 1 = 0 \oplus 1 \oplus 2$ . The map (1.31) preserves spin quantum numbers by virtue of equation (1.28). The subspace of the physical space spanned by  $M_2$  is therefore given by the orthogonal complement of the spin-2 space:

$$\mathcal{S}_2 = \{|S, z\rangle\}_{\substack{S=0,1 \\ z=-S,\dots,S}} \quad (1.32)$$

The corresponding parent Hamiltonian is the projector onto the spin-2 space

$$h_{i,i+1} = \mathbb{1} - \Pi_{\mathcal{S}_2} \quad (1.33)$$

$$= \frac{1}{3}\mathbb{1} + \frac{1}{2}\vec{S}_i\vec{S}_{i+1} + \frac{1}{6}(\vec{S}_i\vec{S}_{i+1})^2 \quad (1.34)$$

where we have rewritten the projector onto the spin-2 space in terms of  $\vec{S}_i\vec{S}_{i+1}$  operators. The final Hamiltonian is simply the bilinear-biquadratic chain (1.26) at  $\beta = 1/3$ .

### 1.2.2 Correlations

Using the explicit representation (1.27) of the AKLT tensors, we find that

$$T = \frac{1}{3} \begin{pmatrix} 1 & & & 2 \\ & -1 & & \\ & & -1 & \\ 2 & & & 1 \end{pmatrix} \quad (1.35)$$

$$= \begin{array}{c} \text{---} \text{---} \\ \bigcirc \text{---} \bigcirc \\ \text{---} \text{---} \end{array} \quad - \frac{1}{3} \sum_{\alpha \in \{x,y,z\}} \begin{array}{c} \text{---} \text{---} \\ \bigcirc^\alpha \text{---} \bigcirc^\alpha \\ \text{---} \text{---} \end{array}, \quad (1.36)$$

in which form

$$\xi_{\text{AKLT}} = \frac{1}{\ln 3} \quad (1.37)$$

is obvious due to (1.15).

### 1.2.3 Entanglement and the Bulk-Boundary Correspondence

Let us now focus on the entanglement properties of the AKLT state. Given a state  $|\psi\rangle$  and a bipartition into regions  $A$  and  $B$ , the  $\alpha$ -**Renyi entanglement entropy**

is given by

$$S_\alpha(A) = \frac{1}{1-\alpha} \log \text{Tr}(\rho_A^\alpha), \quad (1.38)$$

where  $\rho_A = \text{Tr}_B(|\psi\rangle\langle\psi|)$  is the reduced density matrix of region  $A$  after tracing out the complement. Three particular values are of special interest for the remainder of this Thesis:

$$\alpha = 0 : \quad S_0 = \log \text{rank}(\rho_A) \quad (\text{max-entropy}) \quad (1.39)$$

$$\alpha = 1: \quad S_1 = -\text{Tr}(\rho_A \log \rho_A) \quad (\text{von Neumann entropy}) \quad (1.40)$$

$$\alpha = 2: \quad S_2 = -\text{Tr}(\rho_A^2) \quad (\text{2-entropy}) \quad (1.41)$$

The entanglement entropy assigns a single number to a bipartition of a many-body quantum state that contains surprisingly accurate information about the nature of the underlying system. As we will see in later chapters, a single number extracted from the entanglement entropy can be used to detect and characterize whole quantum phases. Nevertheless, there is also a more fine-grained characterization of entanglement given by the spectrum of the reduced density matrix  $\rho_A$ , also called the **entanglement spectrum**. The entanglement spectrum is equal to the spectrum of (squared) Schmidt coefficients.

The entanglement spectrum of the AKLT-chain is computed as follows. We consider an open chain with  $L$  sites and a bipartition into regions  $A$  and  $B$  which contain the left and right half-chain with  $L/2$  spins, respectively. We choose to terminate the open virtual legs of the MPS on the left and right with  $|0\rangle$ . The following result is independent of the boundary conditions, so long as we take  $L \rightarrow \infty$  at some point. Making this particular choice of boundary conditions simply streamlines the discussion. The reduced density matrix is now schematically given by

$$\rho_A = \begin{array}{c} \text{Diagram (1.42): A quantum circuit with two horizontal rows of qubits. The top row starts with a qubit in state $|0\rangle$, followed by three blue boxes labeled $\bar{A}$, then three red boxes labeled $\bar{A}$, and ends with a qubit in state $|0\rangle$. The bottom row starts with a qubit in state $|0\rangle$, followed by three blue boxes labeled $A$, then three red boxes labeled $A$, and ends with a qubit in state $|0\rangle$. Vertical lines connect the corresponding boxes in the top and bottom rows. The blue region is labeled $A$ and the red region is labeled $B$. \end{array} \quad (1.42)$$

First consider the  $A$ -subregion. We can block all of the  $L/2$  tensors to form one large matrix

$$\begin{array}{c} \boxed{A_{L/2}} \\ \vdots \\ \vdots \\ \vdots \end{array} \text{---} := \langle 0| \text{---} \boxed{A} \text{---} \cdots \text{---} \boxed{A} \text{---} \boxed{A} \text{---} \quad (1.43)$$

acting from  $\mathbb{C}^x \rightarrow (\mathbb{C}^d)^{L/2}$ . We will now use the *polar decomposition* on  $A_{L/2}$ . This factorization is a direct consequence of the singular value decomposition. We may write

$$A_{L/2} = W \Sigma V^\dagger \quad (1.44)$$

$$= \underbrace{(W\Sigma W^\dagger)}_{=:P>0} \underbrace{(WV^\dagger)}_{=:U} \quad (1.45)$$

since  $\Sigma \geq 0$  and  $U$  is an isometry  $U^\dagger U = \mathbb{1}_{\chi \times \chi}$ , since  $W^\dagger W = \mathbb{1}_{\chi \times \chi} = V^\dagger V$ . Furthermore,  $P$  is the unique square root of  $A_{L/2}^\dagger A_{L/2}$ , which is given by

$$(1.46)$$

Here, and in the following, we use  $|\sigma_L\rangle$  when we mean the left fixed point *vector* of the transfer matrix and  $\sigma_L$  when referring to the operator that is the left fixed point of the transfer matrix seen as a superoperator. Since such operators are positive [42], they possess a unique square root that we denote by  $\sqrt{\sigma_L}$ .

In the  $B$ -subregion we recognize the object  $T^{L/2} \rightarrow |\sigma_R\rangle \langle \sigma_L|$ . Taking everything together, we have

$$\rho_A = U \sqrt{\sigma_L} \sigma_R \sqrt{\sigma_L^T} U^\dagger \quad (1.47)$$

This result is the so-called bulk-boundary correspondence [43]. It tells us that the spectrum of the physical reduced density matrix is equal to that of the virtual object  $\sigma := \sqrt{\sigma_L} \sigma_R \sqrt{\sigma_L^T}$ , padded with zeros. While  $\rho_A$  grows with system size, the latter object is a  $\chi \times \chi$ -matrix, regardless of system size. This has one important immediate implication on the entanglement entropy of any Matrix Product State. The entropy is maximal if the spectrum of  $\sigma$  is flat in which case all Renyi entropies are given by  $S = \log \chi$ , which is therefore an upper bound on the entanglement entropy with respect to any bipartition. The saturation of the entanglement entropy to a constant value is remarkable: the entropy of random quantum state on  $L$  sites is typically on the order of  $L$  [44], which is what we refer to as a *volume law*. In contrast, we have just shown that MPS satisfy an *area law* of entanglement.

For the AKLT MPS considered before, we have that  $\sigma_L = \sigma_R = \mathbb{1}$  and the only two eigenvalues contributing to the entanglement spectrum are degenerate. One could argue that this is a fine-tuned property of the AKLT point, but we are now going to show that this degeneracy is indeed a hallmark of a much deeper phenomenon.

### 1.2.4 Symmetry-Protected Topological Order

The state (1.27) is invariant under global spin rotations (1.29) and therefore also under  $180^\circ$  rotations about the  $x$ - and  $z$ -axes

$$\begin{aligned} R_x &= e^{\frac{\pi i}{\sqrt{2}}} \begin{pmatrix} 0 & 1 & 0 \\ 1 & 0 & 1 \\ 0 & 1 & 0 \end{pmatrix} \\ &= \begin{pmatrix} 0 & 0 & -1 \\ 0 & -1 & 0 \\ -1 & 0 & 0 \end{pmatrix} \end{aligned} \quad (1.48a)$$

$$\begin{aligned} R_z &= e^{\pi i} \begin{pmatrix} 1 & & \\ & 0 & \\ & & -1 \end{pmatrix} \\ &= \begin{pmatrix} -1 & & \\ & 1 & \\ & & -1 \end{pmatrix}. \end{aligned} \quad (1.48b)$$

Since  $R_x^2 = R_z^2 = \mathbb{1}$  and  $R_x R_z = R_z R_x$ , the four elements  $\{\mathbb{1}, R_x, R_z, R_x R_z\}$  form a unitary representation  $\{U_g\}$  of the group  $\mathbb{Z}_2 \times \mathbb{Z}_2$ . Using (1.17), we have that the symmetry pushes through *locally*

$$\begin{array}{c} | \\ \textcircled{U_g} \\ | \\ \boxed{A} \\ | \end{array} = \begin{array}{c} | \\ \textcircled{V_g} \\ | \end{array} \begin{array}{c} | \\ \boxed{A} \\ | \end{array} \begin{array}{c} \textcircled{V_g^{-1}} \\ | \end{array} \quad (1.49)$$

Where the  $V_g$  also form a unitary representation of the same group. By direct inspection, we find that  $\{V_g\} = \{\mathbb{1}, X, Z, XZ\}$ . Being a representation implies that

$$V_g V_h = e^{i\phi(g,h)} V_{gh} \quad (1.50)$$

The phases  $\phi(g, h)$  are called the *factor system* of the representation. The trivial factor system  $\phi \equiv 1$  corresponds to a *linear* representation. This is the case for the physical spin-1 representation (1.48). On the other hand,

$$\phi(Z, X) = \pi. \quad (1.51)$$

Of course, (1.49) holds even if we redefine  $V_g \rightarrow e^{i\alpha_g} V_g$ , since  $V_g$  and  $V_g^\dagger$  always appear together. Can we use this freedom to make the factor system trivial? To rectify (1.51), we might be tempted to set  $Z \rightarrow -Z$ . But doing so sacrifices  $\phi(X, Z)$ . Clearly, it is not possible to have both  $\phi(Z, X)$  and  $\phi(X, Z)$  be trivial. We say that  $\{V_g\}$  forms a *non-trivial projective representation*.

The type of virtual representation has far-reaching physical consequences. Note that a nontrivial factor system cannot be continuously deformed into a trivial one. Indeed for the present case of  $\mathbb{Z}_2 \times \mathbb{Z}_2$  there are only two discrete inequivalent classes of projective representations, the trivial (i.e., linear) representation and the so-called maximally non-commutative case. On the other hand, Matrix Product States correspond precisely to the ground states of gapped local Hamiltonians. Therefore, as

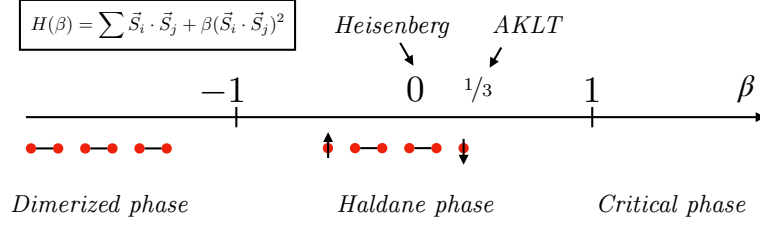


Figure 1.2: Phase Diagram of the bilinear-biquadratic chain (1.26). Having an exact MPS representation at one point allows us to understand the entire adiabatically connected *Haldane* phase.

long as the  $\mathbb{Z}_2 \times \mathbb{Z}_2$ -symmetry is preserved, the type of projective virtual representation cannot be changed without crossing a phase transition [17, 18]. We say that the symmetry *protects* a topologically ordered phase.

Physically, the nontrivial projective representation implies the existence of both *edge modes* as well as a degenerate entanglement spectrum. In a gapped phase, the fixed point of the transfer matrix is unique and therefore inherits the commutation properties of the transfer matrix, i.e.,  $[\sigma_R, V_g \otimes V_g^\dagger] = 0$ . Assume that  $v$  is a non-degenerate eigenvector of  $\sigma_R$ . Then,  $v$  must be invariant under  $V_{R_x}$  and  $V_{R_z}$ . But then, as long as  $V_{R_x}$  and  $V_{R_z}$  anti-commute

$$v = V_{R_z} V_{R_x} v = -V_{R_x} V_{R_z} v = -v = 0. \quad (1.52)$$

Therefore, as long as no phase transition is crossed and the nontrivial projective symmetry prevails, the entire entanglement spectrum must necessarily be degenerate. A similar argument can be repeated for the Hamiltonian, leading to a robust nontrivial ground space in which one can move around by applying operators that are exponentially localized at the edge.

# Chapter 2

## $U(1)$ -symmetry

This chapter is devoted to the study of PEPS with the arguably simplest continuous group,  $U(1)$ . The motivation to investigate this setup is two-fold: The first is *practical*, since a number of physically interesting PEPS naturally exhibit a  $U(1)$ -symmetry, among them Resonating Valence Bond States [45, 46], Chiral Topological States [47–49] and Lattice Gauge Theories [50]. The second motivation is *fundamental*: In spatial dimension one, studying the symmetries of Matrix Product States has led to a complete classification of gapped phases of matter [17, 18]. Naturally, phases in higher dimensions can be a lot richer and many open questions remain, especially for  $D \geq 3$ . Nonetheless, the success of the symmetry-based perspective was carried over to two dimensions, where a wide class of topological phases, the so-called Quantum Double Models, have been completely characterized in the PEPS framework [51]. The key observation in this formalism is that the virtual legs of the fundamental PEPS tensor are symmetric under the action of a *finite* group. We seek to continue this program by initiating the study of *continuous* groups. The circle group  $U(1)$  is a natural first candidate owing to its simplicity. At the same time, the results derived here should apply to any compact Lie group (of non-zero dimension), since every such group has a subgroup isomorphic to  $U(1)$ .

The outline of this chapter is as follows: In section 2.1, we will establish the general setup as well as some useful notation, before moving on to studying the general ground state properties of a system defined by the PEPS. In order to gain first insights into the physics of such systems, in section 2.2, we turn to the study of the Six-Vortex PEPS. We will find that a key role is played by the existence of *low-lying* excitations whose energy gap to the PEPS ground state (with respect to a reasonable Hamiltonian) is vanishing in the thermodynamic limit. Turning again to a more general perspective, we explain the origin of those states and give general conditions for their existence in section 2.3.

### 2.1 Ground State Properties

Throughout the chapter, we consider a PEPS-tensors  $A$  with virtual symmetry

$$\begin{array}{c} | \\ \hline -Z \boxed{A} \\ \hline | \end{array} + \begin{array}{c} | \\ \hline \boxed{A} \\ \hline Z \\ | \end{array} - \begin{array}{c} | \\ \hline \boxed{A} \\ \hline | \end{array} Z - \begin{array}{c} | \\ \hline \boxed{A} \\ \hline | \end{array} \overset{Z}{\uparrow} = 0, \quad (2.1)$$

where  $Z$  is a Hermitian operator with an integer gap between each pair of eigenvalues such that  $U_\phi = \exp(i\phi Z)$  forms a unitary representation of  $U(1)$ . In the following, we will use primed sums

$$\sum' Z |A\rangle = 0 \quad (2.2)$$

to mean  $+Z$  for bonds pointing up or left and  $-Z$  for bonds pointing down or right. Without loss of generality, we can assume the eigenvalues of  $Z$  to be in  $\mathbb{Z}_{\geq 0}$  since (2.2) is invariant under  $Z \rightarrow \alpha Z + \beta \mathbf{1}$ . Note that (2.1) is the infinitesimal version of and equivalent to

$$-U_\phi \begin{array}{c} \uparrow \\ \boxed{A} \\ \downarrow \\ U_\phi^\dagger \end{array} = \begin{array}{c} \boxed{A} \\ \downarrow \end{array} \quad (2.3)$$

and we will use the two interchangeably. We can split the tensor into a projector that enforces the virtual symmetry and the usual mapping from the virtual to the physical degrees of freedom:

$$\begin{array}{c} \diagup \boxed{A} \diagdown \end{array} = \frac{1}{2\pi} \int_0^{2\pi} d\phi \begin{array}{c} \uparrow \\ \textcircled{\Gamma} U_\phi' \\ \downarrow \\ U_\phi^\dagger \end{array} \begin{array}{c} \boxed{A} \\ \downarrow \end{array} \quad (2.4)$$

A further simplification arises if we choose  $\Gamma$  diagonal in the same basis as the symmetry generator  $Z$ . Then, for the double tensor we have a single-leg  $U(1)$ -symmetry

$$\begin{array}{c} \boxed{E} \\ \downarrow \end{array} U_\phi^{\text{bra}} \otimes U_\phi^{\text{ket}} = \begin{array}{c} \boxed{E} \\ \downarrow \end{array} \quad (2.5)$$

that allows us to compress each leg individually

$$\begin{array}{c} \boxed{E} \\ \downarrow \end{array} \rightarrow \begin{array}{c} \triangleup \\ \triangleleft \boxed{E} \triangleright \\ \triangleleft \end{array} . \quad (2.6)$$

If additionally,  $\Gamma > 0$ , the resulting state becomes a *Rokhsar-Kivelson* state

$$|\psi\rangle = \sum_{\{\sigma\}} e^{-\frac{H(\{\sigma\})}{2}} |\sigma\rangle, \quad (2.7)$$

where the eigenstates of  $Z$  have been elevated to classical configurations on the links of the lattice and  $H(\{\sigma\})$  is a classical (potentially non-local) Hamiltonian.



### 2.1.1 The Entanglement-Restricted Subspace

Equation (2.3) is useful because the invariance property of the local tensor *concatenates* and has implications on the global state:

$$\begin{aligned}
 \begin{array}{c} | \\ \hline \boxed{A} \\ \hline | \end{array} & \begin{array}{c} | \\ \hline \boxed{A} \\ \hline | \end{array} = \begin{array}{c} | \\ \hline U_\phi \boxed{A} U_\phi^\dagger \\ \hline U_\phi^\dagger \end{array} \begin{array}{c} | \\ \hline U_\phi \boxed{A} U_\phi^\dagger \\ \hline U_\phi^\dagger \end{array} \\
 & = \begin{array}{c} | \\ \hline U_\phi \boxed{A} U_\phi^\dagger \\ \hline U_\phi^\dagger \end{array} \begin{array}{c} | \\ \hline U_\phi \boxed{A} U_\phi^\dagger \\ \hline U_\phi^\dagger \end{array} \quad (2.8)
 \end{aligned}$$

This property restricts the boundary of the PEPS to the symmetric subspace. A natural question is then whether the PEPS can explore the whole virtual space at its boundary. This is equivalent to the existence of an inverse that, when applied to the physical legs of the tensors yields a projector onto the full symmetric subspace at the boundary. In the case of injective PEPS, or  $G$ -injective PEPS of finite groups, it can be shown that, similar to the invariance property (2.8), the existence of a *local* inverse implies the existence of a global one [51]; the concatenation of local inverses simply yields the global one. We will show now that this is *not* the case in the presence of a  $U(1)$ -virtual symmetry. The boundary of the PEPS is not allowed to explore the full charge-neutral space at the boundary, but only an *entanglement-restricted subspace*. Intuitively, large charges on the boundary must be neutralised along every cut in the bulk. For sufficiently “non-square” cuts, there are not enough Schmidt vectors available for this information to propagate through. This is formalised in the following

**Claim 2.1.** Consider a PEPS-tensor and a symmetry generator  $Z$  fulfilling (2.3) and a bipartition of a patch of such tensors  $S = A \cup B$  that cuts  $L$  bonds pointing left or up and  $R$  bonds pointing right or down with respect to  $A$ . Let  $M_S$  be the corresponding matrix that maps virtual  $\rightarrow$  physical. Denote by  $\partial A$  the virtual bonds only contained in the  $A$  subsystem and let  $\sum' Z |v\rangle_{\partial A} = Q |v\rangle_{\partial A}$  be a state with fixed  $U(1)$  charge  $Q < \lambda_{\min}(Z)L - \lambda_{\max}(Z)R$  or  $Q > \lambda_{\max}(Z)L - \lambda_{\min}(Z)R$ . Then  $M |v\rangle_{\partial A} |w\rangle_{\partial B} = 0$  for any  $|w\rangle_{\partial B}$ .

*Proof.* For any state  $|j\rangle$  along the cut with fixed charge  $q$ , we have  $q \in [\lambda_{\min}(Z)L - \lambda_{\max}(Z)R, \lambda_{\max}(Z)L - \lambda_{\min}(Z)R]$ . By assumption, for each such  $q$ , there exists a  $\phi$ ,

such that  $\phi(Q - q) \notin 2\pi\mathbb{Z}$ . Thus we have

$$\begin{array}{c} \text{Diagram 1: A box labeled } A \text{ with two vertical lines entering from the top, labeled } |v\rangle_{\partial A} \text{ and } \dots. \text{ A horizontal line exits from the right, labeled } |j\rangle. \\ \text{Diagram 2: A box labeled } A \text{ with two vertical lines entering from the top, labeled } |v\rangle_{\partial A} \text{ and } \dots. \text{ A horizontal line exits from the right, labeled } |j\rangle. \text{ Above the box is a box labeled } e^{i\phi \sum' Z}. \end{array} = \quad (2.9)$$

$$\begin{array}{c} \text{Diagram 3: A box labeled } A \text{ with two vertical lines entering from the top, labeled } |v\rangle_{\partial A} \text{ and } \dots. \text{ A horizontal line exits from the right, labeled } |j\rangle. \end{array} = e^{i\phi(Q+q)} \quad (2.10)$$

$$= 0. \quad (2.11)$$

Inserting an orthogonal eigenbasis of the Hermitian operator  $\sum' Z$  on the cut yields the result

$$M |v\rangle_{\partial A} |w\rangle_{\partial B} = \sum_j \begin{array}{c} \text{Diagram 4: Two boxes labeled } A \text{ and } B. \text{ Box } A \text{ has two vertical lines entering from the top, labeled } |v\rangle_{\partial A} \text{ and } \dots. \text{ Box } B \text{ has two vertical lines entering from the top, labeled } |w\rangle_{\partial B} \text{ and } \dots. \text{ A horizontal line connects the right side of } A \text{ to the left side of } B, \text{ labeled } |j\rangle \text{ and } \langle j|. \end{array} \quad (2.12)$$

$$= 0. \quad (2.13)$$

□

A priori, the properties of the virtual space of a PEPS may not directly translate to the properties of the state after contraction. This begs the following question: Does the emergence of an entanglement-restricted subspace have any *physical* ramifications? We will answer this question in the affirmative in the next section.

### 2.1.2 Entanglement Entropy

In this subsection, we study the effect of the symmetry (2.3) on the entanglement of the physical state that is left after contraction. We will see that there are two independent mechanisms at play: First, the restriction to the symmetric virtual subspace induces a logarithmic correction to the area law. Second, the restriction to the entanglement-restricted subspace yields further corrections that depend on the geometry of the partition rather than the size of the cut.

Using the symmetry property (2.3), one can derive a bound on the Rényi zero-entropy of a  $U(1)$ -symmetric PEPS (the zero-entropy is the maximal attainable entropy that bounds from above all other Rényi entropies including the von-Neumann entanglement entropy).


**Claim 2.2.** Let  $|\psi\rangle_S$  be a state constructed from PEPS-tensors and a symmetry generator  $Z$  with spectrum  $\Omega$  in  $\mathbb{Z}_{\geq 0}$  fulfilling (2.3). Consider a bipartition  $S = A \cup B$

and let  $\rho_A$  be the reduced density matrix on  $A$ . Then

$$S_0(\rho_A) \leq \log \sum_{Q=|\partial A|\lambda_{\min}(Z)/2}^{|\partial A|\lambda_{\max}(Z)/2} p_Q^2, \quad (2.14)$$

where  $|\partial A|$  is the size of the boundary of  $A$  and  $p_Q$  is the number of partitions of  $Q$  into  $|\partial A|/2$  integers drawn from  $\Omega$ .

*Proof.* The rank of

$$\rho_A = \text{Tr}_B |\psi\rangle \langle \psi|$$


is bounded by the rank of  $A$ . Since the symmetry concatenates (2.8),  $A$  has to be charge neutral. By assumption, the spectrum of  $Z$  is positive, so a given positive charge  $+Q$  on the up- and left-pointing legs has to be exactly compensated by the  $-Q$  on the down- and right-pointing legs. Since we can pick the positive and negative configurations individually, for each  $Q$ , there are  $p_Q^2$  options to do this and the maximal charge is  $|\partial A|\lambda_{\max}(Z)/2$ , due to the fact that there are as many up-/left-legs as down-/right-legs.  $\square$

Claim 2.2 is not very illuminating with respect to the asymptotic behaviour of the entropy for large cuts. Let us look at the simple case of spin-1/2 virtual particles,  $\Omega = \{0, 1\}$ . In this case

$$\begin{aligned} S_0(\rho_A) &= \log \sum_{j=0}^{|\partial A|/2} \binom{|\partial A|/2}{j}^2 \\ &= \log \binom{|\partial A|}{|\partial A|/2} \\ &\sim \log \frac{2^{|\partial A|}}{\sqrt{\pi|\partial A|/2}} \\ &= |\partial A| \log 2 - \frac{1}{2} \log |\partial A| - \log \sqrt{\frac{2}{\pi}} \end{aligned} \quad (2.16)$$

The first part corresponds to the area law of the bond dimension  $D = 2$  PEPS. Second, we observe a negative logarithmic correction to the area law and finally a constant independent of the size of the boundary. While we have used a particular representation of  $U(1)$ , arguments from analytic combinatorics indicate that both the existence of the logarithmic correction as well as its prefactor  $1/2$  is universal for so-called “bridge” problems, which are loosely defined by counting the number of charge neutral configurations [52, p. 539]. Logarithmic corrections to the entanglement entropy have first appeared in the study of *Quantum Conformal Critical*

*Points (CQCP)* [53]. As we will see in section 2.2, the above counting corresponds to an exact lattice regularization of such a field theory. For these models, a negative logarithmic correction was observed for non-smooth bipartitions: each corner contributes a universal term to the von-Neumann entropy from which the central charge of the underlying 2+0-dimensional CFT can be extracted [54]. For example, the prefactor of the logarithmic correction to the von-Neumann entropy in the Quantum Dimer Model [55] is consistent with a description of a  $c = 1$  CFT [56]. For smooth boundaries, the logarithmic contribution in the field theory vanishes. In this scenario, it is likely that there is some mechanism by which the logarithmic contribution in (2.16) vanishes when shifting focus from the zero Renyi- to the von Neumann-entropy. Finally, *positive* logarithmic corrections to the area law have been observed in two-dimensional critical systems [57], in the presence of broken continuous symmetry, where the prefactor is believed to be  $1/2$  times the number of Goldstone Bosons, i.e., the number of generators of the symmetry that are broken.

Potentially more interesting regarding the discussion on universality is the effect of the entanglement-restricted subspace introduced in the previous section. To study its effect, we consider an  $L_x \times L_y$  torus that is divided into a cylinder  $A$  of length  $l$  and its complement  $B$  (Fig. 2.1a). Varying  $l$  keeps the size of the boundary  $|\partial A|$  in (2.14) constant. Nonetheless, we will now show that for thin enough cylinders, the bound (2.14) can be tightened. We take again the simplest possible case of spin-1/2 particles on the boundary of the PEPS,  $\Omega = \{0, 1\}$ . Then, one may derive the dimension of the entanglement-restricted subspace (which bounds  $S_0(\rho_A)$ ) as follows. First consider  $l = 1$ . The set of charge neutral configurations decomposes into *allowed* and *forbidden* configurations. Fig. 2.1c shows such a forbidden configuration: Each vertex along the cylinder is either a *source* ( $\oplus \oplus \ominus$ ), a *sink* ( $\ominus \oplus \oplus$ ) or neutral ( $\oplus \oplus \oplus$  or  $\ominus \oplus \ominus$ ). Crucially, a configuration with two adjacent sources or sinks (neglecting potentially intermediate neutral vertices) contracts to zero. Applying this rule for consecutive columns, we see that the presence of  $l + 1$  successive sinks or sources result in the configuration being forbidden. Scanning the strip from top to bottom, one can map each configuration to a bridge diagram, where each step takes values in  $\{+1, 0_{\text{blue}}, 0_{\text{red}}, -1\}$  (as there are two species of neutral configurations). The entanglement restriction is tantamount to requiring the resulting bridge to have no consecutive  $l + 1$  up- or down-steps (ignoring intermediate flat steps). Counting the number of such paths for a given  $l < L_x$  and  $L_y$  is a linear problem: Given  $l$ , one may set up a *counting vector*  $v$  of size  $(2l + 1)^2$  and a matrix  $M$  such that  $(M^n v)_{(h,c)}$  contains the number of allowed bridges of length  $n$ . Then,  $\sum_c (M^{L_y} v)_{(0,c)}$  is the dimension of the entanglement-restricted subspace. The result for  $L_x = L_y = 60$  is shown in Fig. 2.1b. In [58], different Rényi  $n$ -entropies for the Quantum Dimer models have been obtained on the same geometry. We conjecture that the curve we have obtained by our counting argument is the limiting case for  $n \rightarrow 0$  (inset of 2.1b). As it turns out (cf. chapter 3), the Dimer model has an exact  $U(1)$ -symmetric PEPS representation, so the agreement should may not be too surprising. It is interesting to note however, that the behaviour we have discovered persists when looking at other Rényi entropies and the von Neumann entropy. Furthermore, the thin-cylinder limit is expected to contain features of universality. More explicitly, for the geometry considered, the Rényi  $n$ -entropy should generically

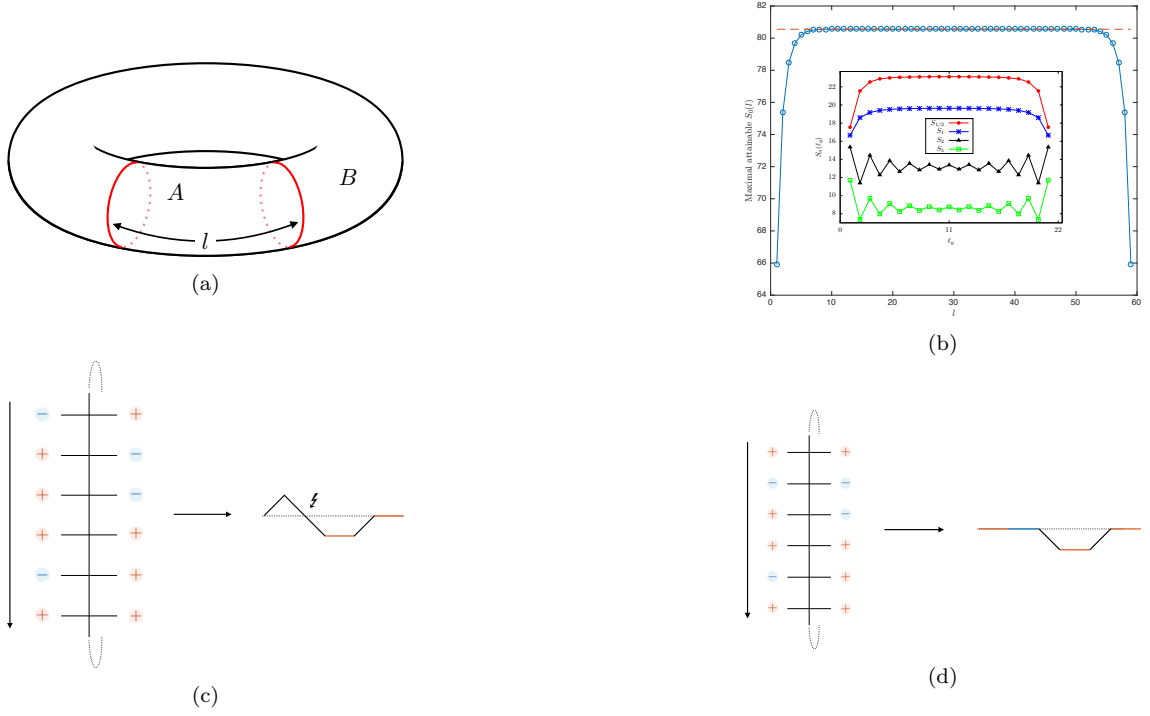


Figure 2.1: Setup considered in section 2.1.2. (a) Bipartition of a torus into two cylinders. (b) Maximal attainable Rényi zero-entropy for a torus of size  $L_x = L_y = 60$  as a function of the width  $l$  of the  $A$  subsystem. Inset: Different Rényi entropies in the Quantum Dimer model with respect to the same geometry, except  $L_x = L_y = 22$ . Figure courtesy of J.M. Stéphan [58] and reprinted with permission from the New Journal of Physics). (c) A forbidden configuration of the  $l = 1$  setup. In the corresponding height diagram  $l + 1$  down-steps occur without an intermediate up-step. (d) An allowed configuration. For  $l = 1$ , for a given total of  $k$  up- and down-steps, these paths can be mapped  $2^{N-k}$ -to-1 to partitions of  $L_y$ .

follow

$$S_n = a_n L_y - \kappa_n \left( \frac{L_x}{l} \right) + \dots, \quad (2.17)$$

with some universal constant  $\kappa_n$  that depends on the Rényi index [59, 60] (the dots represent further subleading terms). The dimension of the complement of the entanglement-restricted subspace in the whole symmetric subspace may therefore yield information about  $\kappa_0$ .

### 2.1.3 Symmetries of the Transfer Matrix

In this section we will show that the local symmetry of the PEPS induces a symmetry on the transfer matrix of the PEPS. Again, there are two aspects that need to be taken into account. First, the local symmetry of the tensor enforces a block structure on the transfer matrix, corresponding to different charge sectors of *two* independent  $U(1)$ -symmetries. Second, because the geometry of the transfer matrix is essentially a long thin strip (cf. Fig 2.1a), the geometric restriction is especially severe. We will see that this restriction enforces a sort of weak *locality* on the transfer matrix: the  $U(1)$ -charge is not just conserved globally, but also approximately locally.

Consider an elementary PEPS tensor fulfilling (2.3). Then, the double tensor

inherits two copies of the same symmetry, for the bra- and ket-layer individually.

$$\begin{array}{c}
 U_\phi^{\text{bra}} \\
 | \\
 - U_\phi^{\text{bra}} \boxed{E} U_\phi^{\dagger \text{bra}} - \\
 | \\
 U_\phi^{\dagger \text{bra}} \\
 |
 \end{array}
 =
 \begin{array}{c}
 U_\phi^{\text{ket}} \\
 | \\
 - U_\phi^{\text{ket}} \boxed{E} U_\phi^{\dagger \text{ket}} - \\
 | \\
 U_\phi^{\dagger \text{ket}} \\
 |
 \end{array}
 =
 \begin{array}{c}
 \boxed{E} \\
 |
 \end{array}
 \quad (2.18)$$

Putting the double-tensor on a cylinder, we may use (2.18) repeatedly to obtain

$$\begin{array}{c}
 \circlearrowleft U_\phi \\
 | \\
 \boxed{E} \\
 | \\
 \circlearrowright U_\phi^\dagger
 \end{array}
 \begin{array}{c}
 \circlearrowleft U_\phi \\
 | \\
 \boxed{E} \\
 | \\
 \circlearrowright U_\phi^\dagger
 \end{array}
 \begin{array}{c}
 \circlearrowleft U_\phi \\
 | \\
 \boxed{E} \\
 | \\
 \circlearrowright U_\phi^\dagger
 \end{array}
 \cdots
 \begin{array}{c}
 \circlearrowleft U_\phi \\
 | \\
 \boxed{E} \\
 | \\
 \circlearrowright U_\phi^\dagger
 \end{array}
 \circlearrowright
 =
 \begin{array}{c}
 \boxed{E} \\
 |
 \end{array}
 \begin{array}{c}
 \boxed{E} \\
 |
 \end{array}
 \begin{array}{c}
 \boxed{E} \\
 |
 \end{array}
 \cdots
 \begin{array}{c}
 \boxed{E} \\
 |
 \end{array}
 \circlearrowright
 \quad (2.19)$$

for either bra- or ket-layer, resulting in a  $U(1) \times U(1)$ -symmetry of the transfer matrix

$$[T, (U_\phi^{\text{ket}})^{\otimes L}] = [T, (U_\phi^{\text{bra}})^{\otimes L}] = 0 \quad \forall \phi \in U(1). \quad (2.20)$$

In order to observe the implications of the entanglement-restricted subspace, consider two states with fixed local charges on, say, the ket-level  $\sum_{j=j_0}^{j_0+l} Z_j^{\text{ket}} |v^{\text{in}}\rangle = Q^{\text{in}} |v^{\text{in}}\rangle$ ,  $\sum_{j=j_0}^{j_0+l} Z_j^{\text{ket}} |v^{\text{out}}\rangle = Q^{\text{out}} |v^{\text{out}}\rangle$ . Assume further that  $|Q^{\text{in}} - Q^{\text{out}}| > \lambda_{\max}(Z) - \lambda_{\min}(Z)$ . Then

$$\langle v^{\text{out}} | T | v^{\text{in}} \rangle = 0 \quad (2.21)$$

is an immediate consequence of claim 2.1. For a region of  $l$  consecutive spins, the transfer matrix therefore only changes the charge density by  $\mathcal{O}(1/l)$ . In the simplest case  $Z = \text{diag}(1/2, -1/2)$  it is also implied that, when expanding the transfer matrix in terms of local operators, terms like

$$\begin{array}{c}
 | \\
 \circ \sigma^+ \\
 |
 \end{array}
 \begin{array}{c}
 | \\
 | \\
 |
 \end{array}
 \begin{array}{c}
 | \\
 \circ \sigma^+ \\
 |
 \end{array}
 \begin{array}{c}
 | \\
 \circ \sigma^- \\
 |
 \end{array}
 \begin{array}{c}
 | \\
 | \\
 |
 \end{array}
 \begin{array}{c}
 | \\
 \circ \sigma^- \\
 |
 \end{array}
 \quad (2.22)$$

on either layer are forbidden despite respecting the  $U(1)$ -symmetry ( $\sigma^+$  and  $\sigma^-$  correspond precisely to up- and down-steps in the path-mapping in Fig. 2.1c).

## 2.2 Example: The Six-Vortex PEPS

We now turn to the study of the simplest non-trivial  $U(1)$ -invariant PEPS. The goal of this section is to gain some insight into the physics that these states generically

represent. For the parameters we consider, we will first show that there exists a family of commuting transfer matrices that can be continuously connected to the lattice shift operator. This is the basic prerequisite for *integrability*: An extensive number of locally conserved charges exists and the phase diagram of the model can be obtained by Bethe ansatz techniques. While useful in deriving these results, we stress that  $U(1)$ -symmetry is *not* sufficient for integrability. By virtue of being integrable, we can then access the physics of this PEPS in a wide parameter regime and observe a phase diagram with both critical and symmetry-breaking phases. The interpretation of the phase diagram will naturally guide us to the subsequent section, where we both show how to understand such “anomalous” behaviour and tackle the issue of its genericity.

The simplest non-trivial model fulfilling (2.3) is given by  $Z = \text{diag}(1/2, -1/2)$ . Let us introduce graphical notation for the computational basis of the  $D = 2$ -dimensional Hilbert space on the links

$$\begin{aligned}
 Z \left| \begin{array}{c} \rightarrow \\ \rightarrow \end{array} \right\rangle &= +1/2 \left| \begin{array}{c} \rightarrow \\ \rightarrow \end{array} \right\rangle \\
 Z \left| \begin{array}{c} \leftarrow \\ \leftarrow \end{array} \right\rangle &= -1/2 \left| \begin{array}{c} \leftarrow \\ \leftarrow \end{array} \right\rangle \\
 Z \left| \begin{array}{c} \downarrow \\ \downarrow \end{array} \right\rangle &= +1/2 \left| \begin{array}{c} \downarrow \\ \downarrow \end{array} \right\rangle \\
 Z \left| \begin{array}{c} \uparrow \\ \uparrow \end{array} \right\rangle &= -1/2 \left| \begin{array}{c} \uparrow \\ \uparrow \end{array} \right\rangle
 \end{aligned} \tag{2.23}$$

For simplicity let us pick  $\Gamma$  diagonal with matrix elements given by

$$\begin{array}{cccccc}
 \begin{array}{c} \uparrow \\ \rightarrow \circ \rightarrow \\ \downarrow \end{array} & \begin{array}{c} \downarrow \\ \leftarrow \circ \leftarrow \\ \uparrow \end{array} & \begin{array}{c} \uparrow \\ \leftarrow \circ \leftarrow \\ \downarrow \end{array} & \begin{array}{c} \downarrow \\ \rightarrow \circ \rightarrow \\ \uparrow \end{array} & \begin{array}{c} \downarrow \\ \leftarrow \circ \leftarrow \\ \uparrow \end{array} & \begin{array}{c} \uparrow \\ \rightarrow \circ \rightarrow \\ \downarrow \end{array} \\
 \sqrt{a} & \sqrt{a} & \sqrt{b} & \sqrt{b} & \sqrt{c} & \sqrt{c}
 \end{array} \tag{2.24}$$

and all other configurations are trivially zero due to the  $U(1)$ -projector in (2.4)<sup>1</sup>. Fortunately, assessing the physics of this PEPS is simple, since the spectrum of its transfer matrix is - as we will now show - exactly solvable. To this end, we first compress the double tensor via (2.6) and study for which triples  $E = E(a, b, c); E' =$

---

<sup>1</sup>Note that this PEPS breaks the  $C4v$ -symmetry of the square lattice. In fact it can be checked that the only bond dimension  $D = 2$ -PEPS with virtual  $U(1)$ -symmetry and complete lattice symmetry is given by  $a = b = c$ , also called *square ice*.

$E(a', b', c'); E'' = E(a'', b'', c'')$  the *Yang-Baxter equation*

$$(2.25)$$

is fulfilled. Here

$$(2.26)$$

This is a system of  $D^6$  equations that generically needs a fair amount of fine tuning to be satisfied. The concatenated  $U(1)$ -symmetry combined with the arrow-reversal symmetry of (2.24) implies that there are only three independent equations (instead of the naive 64), corresponding to the boundary conditions

$$(2.27)$$

which yield

$$ac'a'' = bc'b'' + ca'c'' \quad (2.28a)$$

$$ab'c'' = ba'c'' + cc'b'' \quad (2.28b)$$

$$cb'a'' = ca'b'' + bc'c'' \quad (2.28c)$$

respectively. The solution to (2.28) is written more succinctly if we reparametrise

$$a = \rho \sin(\lambda - u) \quad (2.29a)$$

$$b = \rho \sin(u) \quad (2.29b)$$

$$c = \rho \sin(\lambda). \quad (2.29c)$$

Such a reparametrisation is possible if  $|a^2 + b^2 - c^2/2ab| < 1|$ , otherwise one has to modify the parametrisation to include hyperbolic instead of trigonometric functions. For what follows, either parametrisation will yield the final result, so we will assume (2.29). Furthermore, without loss of generality, we drop any dependence of  $a, b, c$  on  $\rho$  from here on out. In these variables, (2.25) is true if and only if

$$\lambda = \lambda' = \lambda'' \quad (2.30a)$$

$$u'' = u - u' \quad (2.30b)$$





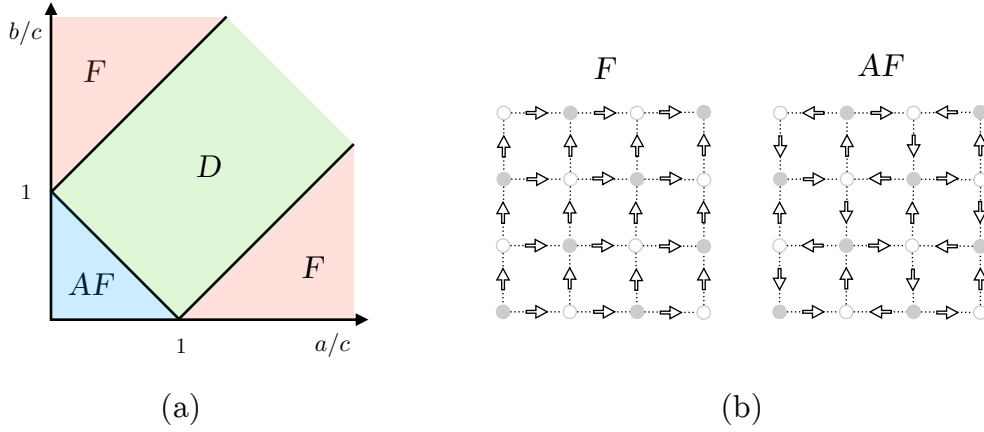


Figure 2.2: Phase Diagram of the Six-Vertex PEPS. (a) Ferromagnetic phases are labeled  $F$ ,  $AF$  is an anti-ferromagnetic phase and  $D$  is a disordered phase with algebraically decaying correlations. Deep in the ordered phases, the PEPS becomes an equal superposition cat state over the states shown in (b) and their counterparts with all arrows reversed. The ferromagnet ( $F$ ) refers to the lower right triangle (the corresponding state in the other ferromagnetic phase has all horizontal arrows reversed).

More conserved quantities can be constructed from considering higher order derivatives in (2.34). The local operator appearing at first order is simply given by the sum of

$$2 \left[ \frac{\partial E}{\partial u} \Big|_{u=0} \right] = XX + YY + \Delta(ZZ + \mathbb{1}), \quad (2.36)$$

where we have introduced

$$\begin{aligned} \Delta &= -\cos(\lambda) \\ &= \frac{a^2 + b^2 - c^2}{2ab}. \end{aligned} \quad (2.37)$$

We conclude that the PEPS' transfer matrix shares a set of eigenstates with the well-known XXZ chain<sup>2</sup>. At this point it is not clear whether there is any relationship between the *eigenvalues* of  $H_{\text{XXZ}}$  and  $T$ . It has been the remarkable achievement of [61–63] (for special cases) and [64] (for the general case) to show that the fixed point of the transfer matrix is indeed equal to the ground state of  $H_{\text{XXZ}}$ , whose phase diagram is well-known. The phase diagram of the Six-Vertex PEPS follows (Fig. 2.2). We note the existence of three qualitatively different phases: A ferromagnetic  $U(1)$ -breaking phase, an antiferromagnetic phase that breaks translation symmetry and a disordered, critical phase. At no point in the phase diagram do we find a state that would be consistent with being the unique ground state of a local, gapped Hamiltonian. Indeed, one may try to construct a parent Hamiltonian for the PEPS defined by (2.24) using the construction of (1.24) and (1.25). For the PEPS considered in

<sup>2</sup>Bearing in mind that we compressed the transfer matrix via (2.6), the eigenstates of  $T$  are actually eigenstates of two *coupled* XXZ chains  $H = H_{\text{XXZ}}^{\text{ket}} + H_{\text{XXZ}}^{\text{bra}} + H_{\text{coupling}}$ , where  $H_{\text{coupling}}$  gives an infinite energy penalty for states with different  $U(1)$ -charges in bra- and ket-layer on any site.

this example, a  $2 \times 2$  plaquette is sufficient to set up a non-trivial Hamiltonian and for  $a = b = c = 1$  in (2.24), the Hamiltonian becomes the Rokhsar-Kivelson point of the Quantum Six-Vortex model that has been studied in [65–67]

$$H = \sum_{\text{plaquettes}} \left( \left| \begin{array}{c} \circ \rightarrow \bullet \\ \bullet \rightarrow \circ \\ \bullet \rightarrow \bullet \\ \bullet \rightarrow \circ \end{array} \right\rangle - \left| \begin{array}{c} \bullet \rightarrow \bullet \\ \bullet \rightarrow \bullet \\ \bullet \rightarrow \bullet \\ \bullet \rightarrow \bullet \end{array} \right\rangle \right) \left( \left\langle \begin{array}{c} \bullet \rightarrow \bullet \\ \bullet \rightarrow \bullet \\ \bullet \rightarrow \bullet \\ \bullet \rightarrow \bullet \end{array} \right| - \left\langle \begin{array}{c} \circ \rightarrow \bullet \\ \bullet \rightarrow \circ \\ \bullet \rightarrow \bullet \\ \bullet \rightarrow \circ \end{array} \right| \right). \quad (2.38)$$

We now close the discussion of the Six-Vortex as an example of a  $U(1)$ -invariant PEPS. The most striking feature is exposed in Fig. 2.2(a): The absence of regions in the phase diagram with unique gapped ground states. Is this a fundamental property of  $U(1)$ -symmetric PEPS? Or is this merely an artefact of the fine-tuned integrability that we have used to study the example? After all, while the  $U(1)$ -constraint severely reduced the number of Yang-Baxter equations, it is by no means a sufficient criterion<sup>3</sup>. In the next section, we will answer this question in favor of the former.

## 2.3 Low-Lying Excitations

In the previous section, we have studied an example of a  $U(1)$ -invariant PEPS that described symmetry-breaking or critical phases in a wide parameter regime of its phase diagram. The purpose of this section is to find conditions under which this behaviour is generic. Both symmetry-breaking and critical phases feature low-lying excitations above the ground state. Of course, in order to make a statement about the energy of a state one has to specify the Hamiltonian of the system. Throughout this section, we will use the natural parent Hamiltonian of the PEPS (1.24) and (1.25). To streamline the graphical notation, we will assume the parent Hamiltonian to act on  $2 \times 2$ -plaquettes but we stress that this is not necessary for the discussion. We mention again that such a  $2 \times 2$  parent Hamiltonian captures relevant models, such as the Quantum Six Vertex (cf. (2.38)) and the Quantum Dimer Models [55].

First, we will derive a criterion for the system to be *either* symmetry-breaking, critical or topologically ordered, by constructing *one* low-lying state. Second, we will give requirements to *distinguish* symmetry-breaking scenarios from criticality. While in the former case there typically is an exact finite degeneracy (up to exponential splitting) and a finite gap to the excitations, critical systems have a full band of excitations that touch the ground state as  $\mathcal{O}(1/N)$ . Under these requirements, we will derive an explicit expression for these excitations.

Throughout this section, our goal is to set up criteria that are feasible to check in practice. In particular, we wish to avoid any reference to a proper two-dimensional contraction of the PEPS, especially when working with finite systems. The trial states we construct will therefore be localized on the virtual space in one direction of the torus. Note that this may not translate into localization on the physical level of the PEPS. One might argue that these requirements are too stringent: In a critical system, localizing a state close to the gapless point typically comes with an energy cost proportional to the linear length  $L$  of the system. If the theory is Lorentz invariant, we expect a dispersion  $E \sim k$ , i.e., the lowest-lying state has

---

<sup>3</sup>Instead, there is a stricter *quantum* group symmetry underlying the solution to the Yang-Baxter equation which does not generally follow from  $U(1)$ -invariance.

energy  $\sim 1/L$ . The localized wavepacket will therefore acquire a finite gap above the ground state. The key observation is that all known examples of critical PEPS at finite bond dimension are *not* Lorentz invariant [68, 69] and, in the particular case of a virtual  $U(1)$ -symmetry, possess a dynamical critical exponent  $z = 2$  [70]. The low-energy dispersion is  $E \sim k^2$  and we can afford to localize the excitations and still get a gapless band. Our construction both illuminates why the exponent  $z = 2$  is typical at  $U(1)$ -invariant points and establishes this behavior for a wide range of systems.

### 2.3.1 A Virtual Lieb-Schultz-Mattis Theorem

We will use an argument first made by Lieb, Schultz and Mattis in the context of the one-dimensional Heisenberg antiferromagnet [71]. The key ingredient is the fact that continuous on-site symmetries allow for infinitesimally small twists of the symmetry to be well-defined. While these states locally look like the ground state, certain topological properties of the system nevertheless enforce the resulting global state to be orthogonal. The advantage of using such an approach is that the Lieb-Schultz-Mattis argument has since been shown to be remarkably stable: While initially formulated for spin-1/2-particles and  $SU(2)$ -symmetry, the behaviour persists when introducing an anisotropy that explicitly breaks  $SU(2)$  to  $U(1)$  [72, 73]. This result might seem questionable at first, since it is clear that for very strong anisotropy a trivial paramagnet must arise as the unique, gapped ground state of the system. However, it was shown that criticality generically persists for an extended region in the phase diagram, as long as the ground state magnetisation per spin is non-integer [74]. An alternative route was taken in [75], where the  $U(1)$ -symmetry is dropped altogether and replaced by a  $\mathbb{Z}_2 \times \mathbb{Z}_2$  symmetry. The modern version of this statement is sometimes informally referred to as the “projective-is-gapless-theorem”: As an example, the one-dimensional XXZ chain is symmetric under both  $\pi$ -rotations around the  $Z$ - and the  $X$ -axis, generated by the Pauli matrices. Crucially,  $Z$  and  $X$  anticommute, meaning the onsite symmetry is a *projective* representation of  $\mathbb{Z}_2 \times \mathbb{Z}_2$ . Assume that the ground state is a gapped, injective MPS. By the fundamental theorem of Matrix Product States [36, 76], this symmetry must be represented on the virtual level by  $V_g \otimes V_g^\dagger$ . The representation on the virtual level, however, is clearly always linear, leading to a contradiction. Carrying over the arguments of Lieb, Schultz, Mattis, Oshikawa and co-workers to higher dimensions is of great interest, since there is certainly a richer variety of possible phases on the one hand, while general theorems are almost non-existent. One seminal contribution is the generalisation of the spin-1/2  $SU(2)$ -case to two dimensions [77]. The approach we will take is inspired by the above results, it is, however, orthogonal in the sense that no *physical* symmetry is required at all.

Our strategy is to carry over the original argument of Lieb-Schultz-Mattis to the PEPS setting, with one modification: In the original setting, the symmetry twist acts unitarily on the ground state such that the excitation is automatically normalized. Special care has to be taken when inserting symmetry-strings on the virtual level since those need not correspond to unitary actions on the physical state. Indeed consider the Six-Vertex PEPS with  $\Gamma_{ij} = 1 \forall i, j$  in (2.4). The fixed point of the transfer matrix is then given by  $|F\rangle = |\text{XXZ}\rangle \otimes |\text{XXZ}\rangle$ , where  $|\text{XXZ}\rangle$  is the ground state of the XXZ chain at  $\Delta = 1/2$ . Thus the norm of the trial state (to be defined shortly (2.39))



45

symmetry strings can be deformed arbitrarily without changing the state (2.8).

$$\begin{aligned}
 \langle \phi_L | H | \phi_L \rangle &= \sum_{x=1}^L \left\langle \begin{array}{c} \vdots \\ \text{---} A \text{---} A \text{---} \\ \vdots \\ \text{---} U_{x\phi} \text{---} U_{x\phi+\phi} \text{---} \\ \vdots \\ \text{---} A \text{---} A \text{---} \\ \vdots \end{array} \middle| h \middle| \begin{array}{c} \vdots \\ \text{---} A \text{---} A \text{---} \\ \vdots \\ \text{---} U_{x\phi} \text{---} U_{x\phi+\phi} \text{---} \\ \vdots \\ \text{---} A \text{---} A \text{---} \\ \vdots \end{array} \right\rangle \\
 &= \sum_{x=1}^L \left\langle \begin{array}{c} U_{x\phi} \quad \vdots \quad U_{x\phi} \\ \text{---} A \text{---} A \text{---} \\ \vdots \\ \text{---} \mathbb{1} \text{---} U_\phi \text{---} \\ \vdots \\ \text{---} A \text{---} A \text{---} \\ \vdots \end{array} \middle| h \middle| \begin{array}{c} U_{x\phi} \quad \vdots \quad U_{x\phi} \\ \text{---} A \text{---} A \text{---} \\ \vdots \\ \text{---} \mathbb{1} \text{---} U_\phi \text{---} \\ \vdots \\ \text{---} A \text{---} A \text{---} \\ \vdots \end{array} \right\rangle \\
 &= \sum_{x=1}^L \phi^2 \left\langle \begin{array}{c} U_{x\phi} \quad \vdots \quad U_{x\phi} \\ \text{---} A \text{---} A \text{---} \\ \vdots \\ \text{---} \mathbb{1} \text{---} Z \text{---} \\ \vdots \\ \text{---} A \text{---} A \text{---} \\ \vdots \end{array} \middle| h \middle| \begin{array}{c} U_{x\phi} \quad \vdots \quad U_{x\phi} \\ \text{---} A \text{---} A \text{---} \\ \vdots \\ \text{---} \mathbb{1} \text{---} Z \text{---} \\ \vdots \\ \text{---} A \text{---} A \text{---} \\ \vdots \end{array} \right\rangle + \mathcal{O}(\phi^3) \\
 &\leq L\phi^2 \|h\|_2 \text{Tr} \left[ \begin{array}{c} \text{---} \text{---} \\ \text{---} Z^{\text{bra}} \otimes Z^{\text{ket}} \text{---} \\ \text{---} \text{---} \end{array} \left( V_\phi \begin{array}{c} \text{---} \text{---} \\ \text{---} \text{---} \end{array} \right)^{L-1} \right] + L\mathcal{O}(\phi^3) \quad (2.44)
 \end{aligned}$$

Setting  $\phi = 2\pi/L$  gives the result

$$\frac{\langle \frac{2\pi}{L} | H | \frac{2\pi}{L} \rangle}{\langle \frac{2\pi}{L} | \frac{2\pi}{L} \rangle} = \mathcal{O}\left(\frac{1}{L}\right). \quad (2.45)$$

Finally, we need to show that  $|\phi_L\rangle$  is orthogonal to the ground state. Since  $Z$  has





than sufficient coupling is

$$\text{Tr} \left[ V_\phi \begin{array}{c} \text{---} \\ | \\ \text{---} \end{array} \right]^L = \Omega(1). \quad (2.47)$$

Practically, one may gather evidence for the sufficient coupling criterion from e.g., CTM calculations, using the boundary bond dimension as a refinement parameter. Special care has to be taken to impose  $U(1)$ -symmetry by hand which would otherwise be broken in this situation. Let us also mention that a generalization similar to [75] can be made: The half-integer spin assumption may be weakened in favor of *non-integer filling*. As long as the magnetization per site is non-integer,  $|\phi_L\rangle$  remains orthogonal to the ground state.

### 2.3.2 Virtual Photons

A large portion of the phase diagram Fig. 2.2(a) is characterized by algebraically decaying ground state correlations. We therefore expect that there exists a whole band of excitations  $|k\rangle$  in momentum space such that  $E(k) \rightarrow 0$  at some gapless point  $k_0$ . The purpose of this subsection is to show that - under certain conditions - such a band can be constructed explicitly. Similarly to the preceding discussing, we will insert small symmetry twists on the virtual level, this time taking care that the resulting states are momentum eigenstates.

A model whose ground state is also represented by a  $U(1)$ -invariant PEPS is the *Quantum Dimer Model* [55]: The configurations of the classical Dimer model on the square lattice are lifted to orthogonal quantum states and a Hamiltonian is defined whose ground state is the equal superposition of all dimer coverings of the lattice<sup>4</sup>. It was noted early on that the model possesses gapless excitations owing to the algebraic correlations of the classical Dimer model. Rokhsar and Kivelson used the *Single-Mode Approximation* (SMA) [78] to construct the gapless band explicitly. The Dimer occupation of a given link is Fourier transformed, yielding a momentum eigenstate whose energy is given by the so-called oscillator strength

$$f(\vec{k}) \propto (\vec{k} \times \tau)^2, \quad (2.48)$$

which vanishes at the gapless point due to the local conservation of Dimers (on any bipartite patch, the number of Dimers sticking out of the A-sublattice is equal to the number of Dimers originating from the B-sublattice). Here, the *polarization*  $\tau = (1, 0)^T$  for horizontal Dimers and  $\tau = (0, 1)^T$  for vertical Dimers. The norm of the excitation is given by the structure factor of the (classical) Dimer-Dimer correlator, which is a transverse projector, i.e., for two horizontal Dimers

$$S(\vec{k}) = \frac{k_y^2}{k_x^2 + k_y^2}, \quad (2.49)$$

yielding

$$E(\vec{k}) = \frac{f(\vec{k})}{S(\vec{k})} \propto \vec{k}^2. \quad (2.50)$$

---

<sup>4</sup>Technically, this state is just *one* of the extensively many ground states of the model, as there exists one ground state for each of the non-maximal *winding sectors* and an exponential number of ground states in the maximal winding sector (cf. chapter 3 for the Classical and Quantum Dimer models and chapter 4 for a model with winding-induced ground state degeneracy).

These modes were named *resonons* by Rokhsar-Kivelson, since they introduce dephasing of the constituents of the ground state that lie in different topological sectors. Later on, considering the  $U(1)$ -symmetry of the model as well as the transverse nature of the excitations, the term *photon* gained popularity [79, 80].

A few observations are worth noting: We immediately note the soft dispersion  $E \sim k^2$ , meaning that we can hope to identify fingerprints of such excitations in the PEPS even after a localizing the photon along one direction of the lattice. By virtue of dimensionality reduction, we may then reduce the existence of a gapless band to the properties of the entanglement spectrum of the one-dimensional fixed point of the transfer matrix. Second, we may focus our attention on particles of a fixed polarization and create arbitrary polarizations by taking linear superpositions later on. Throughout this subsection, we will focus on vertically polarized excitations.

**Proposition 2.2.** Let  $A$  be a tensor giving rise to a normalized square-lattice PEPS  $|\psi_L\rangle$  on an infinite cylinder of circumference  $L$  fulfilling (2.3) for some  $Z$ . Let  $H$  be the parent Hamiltonian as defined in (1.24) and (1.25). Denote

$$|x, y\rangle = \begin{array}{c} \vdots \\ \begin{array}{|c|c|c|c|} \hline & & & \\ \hline & & & \\ \hline & & & \\ \hline & & & \\ \hline \end{array} \\ \vdots \end{array} \quad (2.51)$$

and define a vertically polarized photon localized at an arbitrary  $y_0$

$$|k\rangle = \frac{1}{\sqrt{kL}} \sum_{x=1}^L e^{ikx} |x, y_0\rangle, \quad (2.52)$$

If the fixed point of the transfer matrix is unique, we may define the channels

$$\mathcal{E} := \begin{array}{|c|} \hline \text{---} \\ | \\ \text{---} \\ \hline \end{array} \quad E^{\text{bra}} := \begin{array}{|c|} \hline \text{---} \\ | \\ Z^{\text{bra}} \\ | \\ \text{---} \\ \hline \end{array} \quad E^{\text{ket}} := \begin{array}{|c|} \hline \text{---} \\ | \\ Z^{\text{ket}} \\ | \\ \text{---} \\ \hline \end{array} \quad E^{\text{mix}} := \begin{array}{|c|} \hline \text{---} \\ | \\ Z^{\text{bra}} \otimes Z^{\text{ket}} \\ | \\ \text{---} \\ \hline \end{array} \quad (2.53)$$

and the structure factor

$$S_L(k) := \frac{1}{k} \left( \text{Tr} [E^{\text{mix}} \mathcal{E}^{L-1}] + 2\text{Re} \sum_{x=1}^L e^{ikx} \text{Tr} [E^{\text{bra}} \mathcal{E}^{x-1} E^{\text{ket}} \mathcal{E}^{L-x-1}] \right). \quad (2.54)$$

If, for sufficiently large  $L$ , the structure factor is uniformly bounded from zero on an interval  $(0, k_0]$ , i.e.,  $\exists c_0, k_0 > 0$ , s.t.  $\exists L_0 > 0$ , s.t.  $S_L(k) \geq c_0 \forall L > L_0, k \in (0, k_0]$ , then the Hamiltonian (1.25) has a band of excitations that are well-defined  $\langle k|k\rangle > c_0$  for some  $c_0 > 0$  and have low energy

$$\frac{\langle k|H|k\rangle}{\langle k|k\rangle} \leq 2\langle h\rangle \frac{1 - \cos(k)}{k} \quad (2.55)$$

for some constant  $\langle h\rangle$  independent of  $L$  and  $k$ .

*Proof.* Working with a unique fixed point on an infinite cylinder, we simply have

$$\langle k|k\rangle = S_L(k) > c_0, \quad (2.56)$$

for some  $c_0$  that exists by assumption. We compute the energy of this state with respect to (1.25):

$$\begin{aligned} \langle k|H|k\rangle &= \frac{1}{kL} \sum_{x_1, x_2, p} e^{ik(x_1-x_2)} \langle x_1, y_0 | h_p | x_2, y_0 \rangle \\ &= \frac{1}{k} \left[ \underbrace{\left\langle \begin{array}{|c|c|} \hline \vdots & \vdots \\ \hline \vdots & \vdots \\ \hline \end{array} \right| h \left| \begin{array}{|c|c|} \hline \vdots & \vdots \\ \hline \vdots & \vdots \\ \hline \end{array} \right\rangle}_{=:\langle h \rangle} + \left\langle \begin{array}{|c|c|} \hline \vdots & \vdots \\ \hline \vdots & \vdots \\ \hline \end{array} \right| h \left| \begin{array}{|c|c|} \hline \vdots & \vdots \\ \hline \vdots & \vdots \\ \hline \end{array} \right\rangle \right. \\ &\quad \left. + \left( e^{ik} \left\langle \begin{array}{|c|c|} \hline \vdots & \vdots \\ \hline \vdots & \vdots \\ \hline \end{array} \right| h \left| \begin{array}{|c|c|} \hline \vdots & \vdots \\ \hline \vdots & \vdots \\ \hline \end{array} \right\rangle + h.c. \right) \right] \end{aligned} \quad (2.57)$$

Now we combine use symmetry (2.3) to move the generators underneath the Hamiltonian

$$h \left| \begin{array}{|c|c|} \hline \vdots & \vdots \\ \hline \vdots & \vdots \\ \hline \end{array} \right\rangle = -h \left| \begin{array}{|c|c|} \hline \vdots & \vdots \\ \hline \vdots & \vdots \\ \hline \end{array} \right\rangle \quad (2.58)$$

and arrive at

$$\langle k|H|k\rangle = 2 \langle h \rangle \frac{1 - \cos k}{k} \quad (2.59)$$

□

We briefly discuss the assumptions and an extension of this proposition. First, while it is easy to write down models that satisfy the prerequisites of Proposition 2.1 (e.g., all models with half-integer spin and  $\Gamma$  diagonal in the basis of the  $U(1)$ -generators), the present theorem offers no such “free lunch”. This represents the fact that rigorously distinguishing symmetry-breaking scenarios from criticality is typically only feasible in the presence of exact (e.g., Bethe ansatz) solutions.

It is straightforward to further reduce the energy of the photon from  $E \sim k$  to  $E \sim k^2$  by defining

$$|k\rangle = \frac{1}{\sqrt{L_h L_v}} \sum_{x,y} e^{i(k_x x + k_y y)} |x, y\rangle. \quad (2.60)$$

It is trivial to show that  $\langle k|H|k\rangle \propto (1 - \cos k)$  remains true. Denoting  $|k^{\text{top}}\rangle = \sum_x e^{ik_x x} Z_x^{\text{ket}} |\text{top fixed point}\rangle$  and  $|k^{\text{bottom}}\rangle = \sum_x e^{ik_x x} Z_x^{\text{ket}} |\text{bottom fixed point}\rangle$ , the norm of this state becomes

$$\frac{1}{L_v} \left\langle k^{\text{top}} \left| \frac{1 - T^2}{1 - 2 \cos k_y T + T^2} \right| k^{\text{bottom}} \right\rangle, \quad (2.61)$$

which contains information beyond just the fixed point of the transfer matrix. In practice, one may compute the low-lying states of the transfer matrix using an excitation ansatz [81, 82], since only eigenstates of the transfer matrix with  $\lambda = 1 - \mathcal{O}(1/L)$  contribute to (2.61).

## 2.4 Conclusion

In this chapter, we have introduced  $U(1)$ -symmetric PEPS and studied both their ground state properties and natural candidates for their low-lying excitations. Strikingly, as opposed to injective or G-injective PEPS, their ground state entanglement entropy generally possesses both a logarithmic correction to the area law *and* a geometric contribution due to the existence of the entanglement-restricted subspace. A natural follow-up question is to investigate whether the geometric contribution persists to other Rényi- and the von Neumann-entropy. For example,  $S_2$  could be evaluated numerically in an efficient way using PEPS techniques (cf. chapter 5). In the exactly solvable Quantum Dimer and Six-Vertex Models, such computations may even be accessible analytically, highlighting the value of connecting these PEPS to integrable models. If answered affirmatively, this question can be useful as a stepping stone towards formulating measures of universality in the entanglement entropy of two-dimensional quantum systems [60].

Connecting to ideas from integrability, we mapped out the phase diagram of a family of  $U(1)$ -invariant PEPS and concluded that the corresponding family of parent Hamiltonians must describe symmetry-breaking phases or critical behaviour. We then put forward two propositions, a virtual Lieb-Schultz-Mattis theorem, that we argue to be satisfied generically, and a more refined virtual photon theorem, that provides an explicit representation of the excitations in critical systems.

A key assumption in the former is the fact that the fixed point of the transfer matrix inherits its  $U(1) \times U(1)$ -symmetry. While this is clear for any finite system, it is interesting to study whether  $U(1)$ -symmetry breaking can occur in the thermodynamic limit. On the one hand, the spectrum of transfer matrices is typically closely related to the spectrum of some local Hamiltonian (cf. (2.34) for example). The Hohenberg-Mermin-Wagner theorem [6, 83] precludes any continuous symmetry to be spontaneously broken at any non-zero temperature for classical two-dimensional models. The quantum-classical correspondence maps two-dimensional models at *finite* temperature to one-dimensional quantum models at a temperature proportional to the inverse width of the system, i.e.,  $T = 0$  in the genuine 2D limit. It is therefore unlikely that transfer matrices corresponding to such Hamiltonians can have  $U(1)$ -breaking fixed points. On the other hand, the Hohenberg-Mermin-Wagner theorem requires interactions to be local and indeed,  $U(1)$ -breaking phases have been observed for sufficiently long-range interactions [84]. It is likely that such long-range interactions are incompatible with transfer matrices of constant bond dimension. However, to date no rigorous proof has been made.

The criteria we derived in the virtual photon theorem only detect gapless excitations if they disperse (at least) quadratically. To date, no PEPS with  $U(1)$ -symmetry is known with dynamical critical exponent  $z \neq 2$ . This is because those wave functions are generally described by the *Quantum Lifshitz Model* [85]

$$H = \int d^2x \left[ \frac{\Pi^2}{2} + \frac{\kappa^2}{2} (\nabla^2 \phi)^2 \right]. \quad (2.62)$$

which manifestly has a dynamical critical exponent  $z = 2$ . The Quantum Lifshitz Model has two remarkable features: It has been shown in [53] that ground state expectation values of the two-dimensional quantum theory (2.62) are given by the

two-dimensional Euclidean free boson

$$\langle \text{gs} | \sigma | \text{gs} \rangle = \int [\mathcal{D}\phi] \sigma e^{-\kappa \int d^2x (\nabla\phi)^2} \quad (2.63)$$

On the other hand, from the field theoretic perspective, the mechanism forbidding a term like  $(\nabla\phi)^2$  in the action is that, in the ground state of a Quantum Conformal Critical Point, the resistance to shear stress must vanish. While we have used the equivalence of the ground state correlators to map out the phase diagram Fig. 2.2(a), it would be very interesting to define and measure the effect of such a shearing operator in the PEPS framework. This would lead to a deeper understanding of the universality classes that critical PEPS can represent. The latter is particularly relevant when using such PEPS as a variational ansatz.

Finally, as noted in [86], the quadratic dispersion characterises a point that is on the boundary of a phase with linearly dispersing gapless modes. This suggests that such Lorentz-invariant phases might more generally be found in the vicinity of critical PEPS with constant bond dimension.

# Chapter 3

## Dimer & Resonating Valence Bond models

In the last chapter, we studied general features of Projected Entangled Pair States with  $U(1)$  virtual symmetry. It is the purpose of this chapter to investigate a physically relevant  $U(1)$ -PEPS: The square lattice *Resonating Valence-Bond (RVB)* model. The RVB state was first proposed by Anderson as a candidate for a *Quantum Spin Liquid (QSL)* state [87]. At the time, it was believed that all spin models order magnetically at zero temperature. The RVB was invented to be an exception. It is defined in terms of spin-1/2 degrees of freedom living on the vertices of some lattice. The state is defined as an equal superposition of nearest neighbour singlet pairings.

As such, it has neither magnetic order (being a superposition of  $SU(2)$ -invariant singlets), nor crystalline order (as translation invariance gets restored by taking the superposition). At the time, the state was constructed as a candidate for the ground state of the spin-1/2 square lattice Heisenberg antiferromagnet. Today, we know that its ground state has a non-vanishing magnetization, since it spontaneously breaks the  $SU(2)$  symmetry. After enjoying a brief moment in the sun, it was forgotten for about a decade until the discovery of high-temperature superconductors. It was again Anderson who proposed the ground state of the cuprates to be a Mott insulator, in which the charge degrees of freedom are frozen and the remaining spin degrees of freedom of the copper ions sit on the vertices of an effectively

two-dimensional square lattice. These would then interact antiferromagnetically to form a translation- and  $SU(2)$ -invariant superposition of singlet coverings of the lattice [88]. The key observation in the context of superconductivity was the fact that the RVB state hosts spinon excitations, which carry the spin but not the charge of the original electrons. Upon doping, these spinons could form bosonic bound states with unpaired holes and condense [89]. The RVB state did not explain the rich phase diagram of the cuprates (the understanding of which remains an important problem to this day), but it has enjoyed considerable interest ever since.

Already in his initial paper, Anderson remarked that the expressive power of

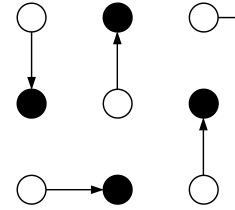


Figure 3.1: Schematic drawing of an RVB configuration. The connecting lines are spin-1/2-singlets  $|\psi^-\rangle = |\uparrow\downarrow\rangle - |\downarrow\uparrow\rangle$ . The pairing breaks the lattice symmetry, a so-called *Valence Bond Solid (VBS)*. To remedy this, one can take an equal superposition  $|\text{nnRVB}\rangle = \sum_{\text{nearest neighbour pairings } P} |P\rangle$ .

the *nearest-neighbour* RVB wave function (nnRVB) is severely restricted: While the dimension of the total spin-0 subspace of  $2N$  spin-1/2-particles grows as  $\sim 4^N / \sqrt{N^3}$ , there are only  $\sim 1.791^N$  nearest-neighbour pairing configurations [90]. A more realistic scenario includes pairings that connect more distant spins on the lattice. Such a variational ansatz has been shown to deliver good ground state energies for the frustrated  $J_1 - J_2$  Heisenberg model [91, 92]. There are of course many ways in which long-range pairing can be introduced. While the nnRVB state has long been shown to be gapless [93, 94], the nature of some of these long-range RVB states is unclear. Two long-range RVB (lrRVB) ansatzes have been proposed that can be written directly in the language of PEPS [92, 95]. It has been argued that these long-range RVB states are surrounded by a critical phase. According to this hypothesis, a  $\mathbb{Z}_2$  Quantum Spin Liquid phase is entered only when the amplitude of long-range bonds is on the order of the nearest-neighbour coupling. The extent of such a gapped spin liquid phase, as well as the size of the associated gap is important in the context of anyonic excitations. Such excitations are the theoretical building blocks of topological quantum computers, in which they are moved in such a way to apply non-trivial unitary gates [96, 97]. In order for the computation to be robust, there must be an energy gap, such that braiding can be carried out adiabatically. The magnitude of the gap sets the time scale on which such a computation may take place.

In light of the previous chapter, an extended critical phase beyond the  $U(1)$ -symmetric nnRVB point comes as a surprise since we have identified the  $U(1)$  virtual symmetry to be the key ingredient for the construction of gapless excitations. One possible explanation is that the  $U(1)$ -symmetry *reemerges* in the low-energy sector of the theory. In this chapter, we show that this is *not* the case, but the lrRVB state is actually *gapped*. However, the methods we develop allow us to understand why the gap has not been observed in previous studies: It is extremely small, even for large densities of long-range valence bonds. Using arguments from Conformal Field Theory (CFT), we place an estimate on the numerical value of the gap and show that, for length scales of thousands of lattice sites, the description as a gapless Spin Liquid is actually correct. We also elucidate the physical mechanism which causes huge correlation lengths.

The outline of the chapter is as follows: We define both the nearest-neighbour as well as long-range RVB in terms of a tensor network construction in section 3.1. We then move on to describe the nnRVB state both in terms of its field theoretic content (section 3.2) and on the lattice via its transfer matrix (section 3.3). This correspondence allows us to extract the field operator associated with the perturbation from a perturbed transfer matrix in section 3.4. The operator is *relevant* and a gap must open for any finite density of long-range singlets. We use dimensional analysis in section 3.5 to put forward a hypothesis for the scaling of the gap. This hypothesis is subsequently shown to be correct for a family of models connecting the lrRVB to a Dimer-Solidomer model. Close to the RVB point, however, substantial corrections to our scaling hypothesis arise. In section 3.6, we explain these corrections by mapping the long-range RVB state to a Sine-Gordon model. Finally, in section 3.7, we propose PEPS with an actual emergent  $U(1)$ -symmetry and conclude.



### 3.1 The Resonating Valence PEPS

The nearest-neighbour RVB state shown in Fig. 3.1 has a simple representation in terms of a PEPS. The wave function is built from a single tensor  $A_1$  that is repeated in a translationally invariant fashion across the lattice. Its virtual degrees of freedom carry a  $\text{spin-}1/2 \oplus 0$  degree of freedom, where we will refer to the 0-subspace as an “empty” virtual site. An elementary configuration has one of the virtual spin-1/2s maximally entangled with the local physical spin into a triplet state, while the other three directions are empty (Fig. 3.2(a)). The tensor  $A_1$  is obtained by summing over all such configuration in such a way that the complete  $C_{4v}$  symmetry of the square lattice is recovered. Technically this will give rise to an equal superposition of *triplet* coverings. Due to the bipartiteness of the square lattice, however, the triplet and singlet nnRVB states are equivalent up to a local Pauli- $Y$  rotation of one the sublattices.

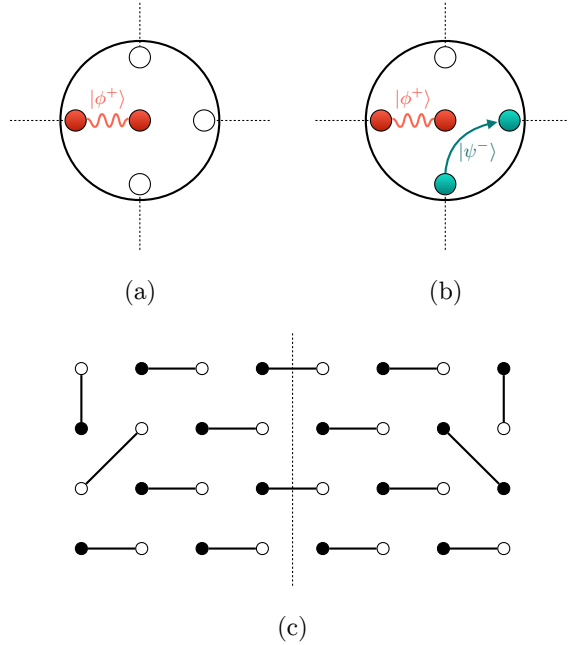


Figure 3.2: (a,b) Diagrammatic representation of one of the terms in the definition of the tensors. The peripheral dots are the virtual degrees of freedom (which are later projected out) and the physical degree of freedom sits in the middle of the tensor. Colorless dots depict empty spin 0 sites. Red wavy lines refer to triplets  $|\phi^+\rangle = |00\rangle + |11\rangle$  while the oriented teal-colored bonds denote singlets  $|\psi^-\rangle = |01\rangle - |10\rangle$ . The tensor  $A_1$  ( $A_2$ ) is obtained by summing over all  $90^\circ$  rotations and reflections about the axes of the square lattice of diagram a (b), respectively. (c) A typical configuration when inserting two test AA/BB-dimers into the classical Dimer model. The intermediate region has maximal winding number in the  $y$ -direction.


To allow for longer-range singlets, we define a *teleportation tensor*  $A_2$ , which differs from  $A_1$  by an additional singlet pairing between neighbouring virtual spin-1/2 degrees of freedom (Fig. 3.2(b)). Regarding the long-range bonds as a perturbation to the nnRVB state, we define

$$A(\lambda) := A_1 + \lambda A_2. \quad (3.1)$$

and denote by  $|\psi(\lambda)\rangle$  the state that results from contracting a translational invariant network of  $A(\lambda)$ . This family of states has been studied in [95] after a slight variation



thereof has been introduced in [92]. A couple of comments are in order. We can expand the wave function in orders of  $\lambda$ ,  $|\psi(\lambda)\rangle = |\text{nnRVB}\rangle + \lambda |\delta\psi\rangle + \lambda^2 |\delta^2\psi\rangle + \dots$ . Assuming an even number of sites in both directions, one may convince oneself that all odd orders vanish, e.g.,  $|\delta\psi\rangle = 0$ . One can further make the observation that certain next-nearest neighbour singlets (“AA singlets”) cancel locally:



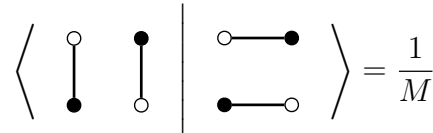
$$= 0. \quad (3.2)$$

Flipping one of the triplets in eq. (3.2), however, changes the nature of the interference from destructive to constructive. Note that the relative signs are uniquely fixed by demanding both  $A_1$  and  $A_2$  to exhibit  $C_{4v}$  symmetry. The case is slightly different in the PEPS studied in [92], where the  $A_2$  tensor is antisymmetric under reflections (which still leads to a fully symmetric wave function due to the cancellation of odd powers mentioned before). There, indeed all next-nearest neighbour singlets cancel. Going beyond next-nearest neighbours, AA singlets will exist in either case, since the destructive-interference argument hinges on the fact that one finds two teleportation paths *while keeping the physical pairing pattern fixed*. For the family of states considered here, this has been confirmed through Marshall sign computations [95]. Let us quickly address the current understanding of the physics of the this one-parameter family of PEPS. The nnRVB state ( $\lambda = 0$ ) is critical with two types of operators: Singlet-singlet correlations decay algebraically with an exponent  $\alpha_{\text{DD}} \approx 1.2$ , while Spin-Spin correlators exhibit exponential clustering [93, 94, 98]. A previous study has found singlet-singlet correlations to remain critical until  $\lambda_c^{(1)} \approx 0.85$  upon which a  $\mathbb{Z}_2$  Spin Liquid phase is entered. The gap closes again around  $\lambda_c^{(2)} \approx 3.85$  and remains zero for all  $\lambda > \lambda_c^{(2)}$  [95].

On the contrary, we claim that the gapped  $\mathbb{Z}_2$  is entered *immediately* upon introducing an infinitesimal amount of long-range singlets, but that the induced correlation lengths are indeed on the order of thousands of sites or more for extended regions in parameter space. Clearly, to make such a claim, numerical evidence alone cannot suffice. In the absence of exact solutions, we instead turn to the continuum.

## 3.2 Field Theory of the RVB state

The study of RVB physics is complicated by the fact that the basis states of the intuitive valence bond basis are not orthogonal. To understand the impact of this feature, one may regard the nnRVB as a member of a more general family of  $SU(M)$  nnRVB states, defined by



$$= \frac{1}{M}. \quad (3.3)$$

In the limit  $M \rightarrow \infty$ , one recovers the Quantum Dimer Model (QDM) [55].

$$|\text{QDM}\rangle = \sum_{\{\sigma\}} e^{-\frac{\beta}{2} H_{\text{Classical Dimer}}(\{\sigma\})}. \quad (3.4)$$

The correlators in this Rokhsar-Kivelson wave function are clearly identical to thermal correlators of the classical Dimer model.

### 3.2.1 Interlude: The Classical Dimer Model

The classical Dimer model facilitates our goal of a continuum description. The degrees of freedom are two-level systems living on the links of the square lattice. There is a hard constraint, namely that around each vertex only one of the links can be occupied by a dimer (see Fig. 3.3 for a typical configuration). Physically this can arise from a quasi-infinite energy scale in the Hamiltonian. The partition function of the model is equal to the number of allowed dimer configurations. This problem has been solved exactly in [90, 99]. The correlation functions, i.e., the probability of finding dimers on links separated by a distance  $\vec{d}$  has also been obtained [100]. They decay as

$$C_{\text{Dimer-Dimer}}(\vec{d}) \sim \frac{1}{|\vec{d}|^2}, \quad (3.5a)$$

i.e., the system possesses critical power-law correlations. An interesting generalization of the Dimer model consists in introducing other objects like monomer defects, longer dimers, or even groupings of more than two sites (Figs. 3.2(c) and 3.9). These models are generally not exactly solvable anymore. However, correlations of test monomers in an otherwise dimerized background, for example, are known to decay as

$$C_{\text{Monomer-Monomer}}(\vec{d}) = \frac{1}{\sqrt{|\vec{d}|}} \quad (3.5b)$$

Introducing objects other than nearest-neighbour dimers makes the model non-integrable, but the physics can still be understood by going to the *continuum*.

Since the dimer problem is purely entropic, we look for a free energy that essentially counts the number of microconfigurations corresponding to a coarse-grained variable.

To find this variable, we map the model onto a *height model*<sup>1</sup>. We follow [103–105]. To each configuration, we can assign a landscape of heights according to the following rule: we pick an arbitrary plaquette (the choice is arbitrary, but we have to pick the same for each configuration) and assign it a height  $\phi = 0$ . For the adjacent heights, we add  $+1/4$  when we go around the A-sublattice and do not encounter a dimer and  $-3/4$  if we cross a dimer and vice versa for the B-sublattice. For a given region, we define a coarse-grained height as the average of the heights of all the plaquettes contained within the region.

There are three desiderata: First, by locality, the entropy of a given region should not depend on changes far away from the region. However, as we see in Fig. 3.3, shifting dimers in a closed loop surrounding the region will transform  $\phi \rightarrow \phi + 1$ . Therefore, the free energy should not depend on  $\phi$  itself, but only on derivatives or periodic functions thereof. Second, the free energy should reflect the rotation symmetry of the lattice. Indeed, as shown in Fig. 3.3, rotating a region by  $90^\circ$  maps the local height  $\phi \rightarrow -\phi$ . For this reason, we can exclude odd powers as well as odd periodic functions (e.g.,  $\sin(\phi)$ ). Finally, we impose translation symmetry. As

<sup>1</sup>While this mapping has been proven rigorously [101, 102], we describe the mapping on an intuitive level.

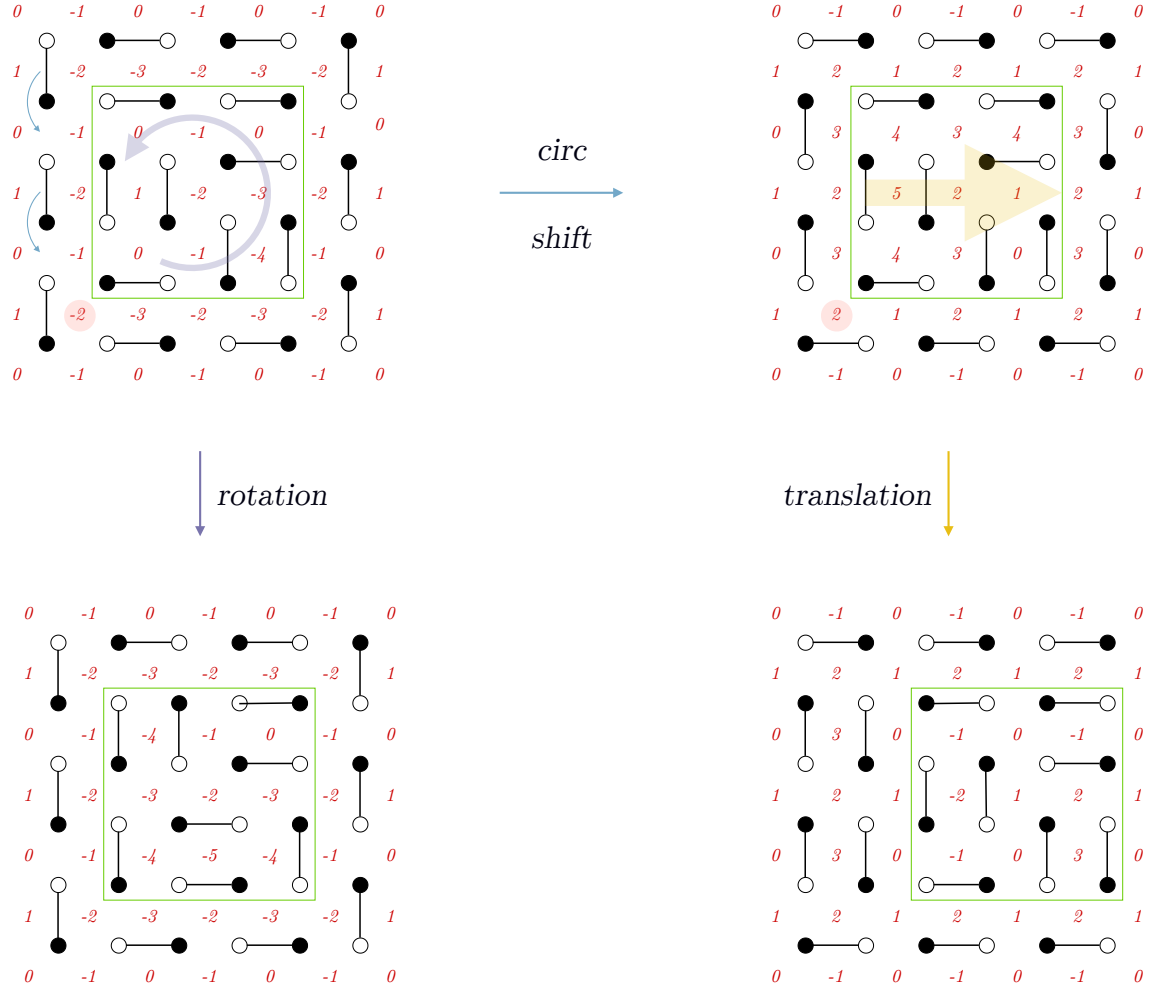


Figure 3.3: Typical configurations of the classical Dimer model. Red numbers indicate local heights on the plaquettes (for better readability, they have been multiplied by a factor 4). *Circular shift*: Shifting a ring of dimers outside the region of interest shifts the heights by  $+4/4$ . *Rotation*: Rotating a patch of dimers by  $90^\circ$  maps the heights inside from  $z_0 + d(r) \rightarrow z_0 - d(\mathcal{R}(r))$ . The reference plaquette with height  $z_0$  is marked in red. *Translation*: Shifting a patch of dimers by  $90^\circ$  maps the heights from  $z_0 + d(r) \rightarrow z_0 - 1/4 - d(r - 1)$ . The reference plaquette with height  $z_0$  is again marked in red.

shown in Fig. 3.3, moving the region by one lattice spacing, maps the heights to  $\phi \rightarrow -\phi - 1/4$ . Combining all these requirements, the simplest action compatible with the symmetries is:

$$S = \int d^2x \frac{\pi}{2K} |\nabla \phi(x)|^2 + \sum_{p=4,8,12,\dots} V_p \cos(2\pi p \phi(x)) \quad (3.6)$$

where  $K$  is a constant and  $\phi$  takes values in  $[0, 1]$  (it is *compactified*). In the following, we will find it more convenient to work with fields that are  $2\pi$ -periodic. We therefore take  $\phi \rightarrow 2\pi\phi$ .

For  $V_p = 0$ , (3.6) is a *Conformal Field Theory (CFT)*. We will not attempt any detailed review over this field, but merely mention some facts that are relevant to the present discussion [106]. Furthermore, we restrict ourselves to two dimensions (due to Lorentz invariance it does not matter whether these are space or space-time dimensions). A CFT is characterized by a set of operators called primary fields  $\phi_1, \phi_2, \dots$  and their scaling dimensions  $\Delta_1, \Delta_2, \dots$ . The correlation function of two such operators is given by:

$$\langle \phi_i(x_1) \phi_j(x_2) \rangle = \frac{\delta_{ij}}{|x_1 - x_2|^{2\Delta_i}} \quad (3.7)$$

In particular, correlation functions generally decay as polynomials in the distance, indicating critical behavior. The CFT also makes a prediction for when it is perturbed by one of its primary operators. We can group primary fields into *irrelevant* ( $\Delta > 2$ ), *marginal* ( $\Delta = 2$ ) and *relevant* ( $\Delta < 2$ ) perturbations. Irrelevant and marginal perturbations drive the system into either the same or a different critical state, while relevant perturbations produce a gap and hence exponential decay of correlations. Equation (3.6) permits two interpretations: In two-dimensional Euclidean space, the model is typically referred to as the *Coulomb Gas*. Alternatively, one can map one of the spatial dimensions into a time dimension by a Wick rotation  $x \rightarrow i\tau$ . It is then called the *Compactified Boson* or *Luttinger Liquid*, which is why we will refer to the parameter  $K$  as the *Luttinger parameter*. The operator content of the CFT is as follows: There are three types of primary operators. First, there is the derivative of the height field with scaling dimension  $[\nabla\phi] = 1$  (the field  $\phi$  has correlations that diverge with distance and is not a local operator). The operator  $|\nabla\phi|^2$  therefore has scaling dimension 2 and is marginal. Second, the height field has *vertex operators*  $[\cos(n\phi)] = Kn^2$ . Their relevance depends on the value of the constant  $K$  in the action. In particular,  $\cos(4\phi)$  is relevant if

$$K < 1/8 \quad (3.8)$$

and all higher order terms are less relevant. Finally, there are vertex operators corresponding to the *dual* field  $[\cos(m\theta)] = m^2/4K$ . Generally, when acting with two or more operators on points that are close in space-time, some nontrivial fusion can occur. Our case, however, is simple and the scaling dimension of an arbitrary vertex operator is given by

$$[\cos(n\phi) \cos(m\theta)] = Kn^2 + \frac{m^2}{4K}. \quad (3.9)$$

In some instances, the operators of a CFT have a direct correspondence with lattice operators, in the sense that their long-distance correlation functions decay with the same exponent. For example, measuring the presence of a dimer on a given link in the lattice has been shown to correspond to [107–109]

$$\text{Dimer} \sim \nabla\phi + \cos(\phi). \quad (3.10)$$

A monomer, on the other hand, creates vortices in the height field and corresponds to

$$\text{Monomer} \sim \cos(\theta) \quad (3.11)$$

Comparing (3.9) to (3.5) fixes the value of the constant

$$K = 1 \quad (3.12)$$

in (3.6). The point  $K = 1$  is also called the *free fermion* point of the Luttinger Liquid. Since the condition for relevance of the height-locking potential (3.8) is not met, the action (3.6) will flow towards

$$S_0 = \int d^2x \frac{1}{8\pi K} |\nabla\phi(x)|^2 \quad (3.13)$$

under renormalization.

### 3.2.2 From Orthogonal Dimers to Resonating Valence Bonds

We are now ready to roll back the limit  $M \rightarrow \infty$  in (3.3). The exact Rokhsar-Kivelson-correspondence (3.4) ceases to exist for finite  $M$ , but the norm of the quantum states remains equal to the partition function of a classical model [110]. The key insight is that the norm is a sum over transition graphs, in which  $SU(M)$  dimer patterns on the ket- and bra-layers form closed loops (Fig. 3.5). While the classical Dimer model strictly precludes any finite amount of non-trivial loops, larger loops become more and more likely for  $M \rightarrow 2$ . These loops effectively introduce an aligning interaction on the level of the classical Hamiltonian<sup>2</sup>. The interacting model in turn has been found to be in the same critical phase as the pure Dimer model [103]. This phase is characterized by a Coulomb Gas description (3.13) where the parameter  $K$  decreases smoothly from the free fermionic Dimer point ( $K = 1$ ) to the  $SU(2)$ -RVB state ( $K \approx 0.6$ ). Note that the renormalization of  $K$  due to long loops makes the RVB state more stable against monomer perturbations than the Quantum Dimer model (cf. (3.9)). An intuitive picture of this mechanism can be gained as follows: On periodic boundaries, the height field  $\phi(x)$  is allowed to differ by integer multiples when going around the torus, defining a winding number  $(W_x, W_y)$ . The total amplitude of a given winding sector is given by  $\exp(-S(W_x, W_y))$ . Separating the tilt from smaller fluctuations, one can derive that  $P(W_x, W_y) = P(0, 0) \exp(-8\pi(W_x^2 + W_y^2)/K)$  [94], i.e., higher winding sectors are more and more suppressed with decreasing  $K$ . In the pure Dimer model, correlation functions of the operator  $\cos(2\theta)$  are computed by inserting two test

<sup>2</sup>Technically long loops induce an extra *non-local* potential that can be truncated to the leading aligning term with small error.

AA/BB-dimers and summing over the compatible configurations (Fig. 3.2(c)). The resulting imbalance of available A vs. B sites entails that the region between the test dimers must exhibit a large local winding number. Consequently, smaller values of  $K$  leads to more rapidly decaying correlations. The RVB point in particular is already relatively close to  $K = 1/2$ , at which this operator becomes marginal.

### 3.3 The Transfer Matrix

We would now like to recover the CFT operators discussed in the previous section in our lattice model. The right place to look for them is the PEPS transfer matrix, as it contains all information about the long-distance behaviour. To get a one-dimensional object in the CFT, we employ the *quantum-classical correspondence* [111]. This mapping simply amounts to performing a Wick rotation  $dy \rightarrow id\tau$  followed by a Legendre transform from which a quantum Hamiltonian is obtained.

On the other hand, in cases where exact solutions are at hand, a one-dimensional lattice Hamiltonian can be found which is the logarithmic derivative of the transfer matrix (cf. (2.34)). This suggests the definition

$$H = -\log(T). \quad (3.14)$$

Let us check the validity of this hypothesis in an exactly solvable example. For the pure Dimer model (classical or quantum), we can expand  $-\log(T)$  numerically on a finite cylinder<sup>3</sup> and obtain the quasi-local free fermion Hamiltonian

$$H_{\text{Dimer}} = \sum_{i=1}^N \sum_{d=0}^{N-1} e^{-d/\xi} \left( a_i^\dagger a_{i+d} + \text{h.c.} \right) \quad (3.15)$$

after a Jordan-Wigner transformation. The model (3.15) realizes the free fermion point of a Luttinger Liquid<sup>4</sup>.

For the nnRVB state, we consider the natural transfer matrix of the PEPS (3.1). In this case, the expansion in terms of local operators is numerically unfeasible due to the larger on-site Hilbert space and the double-layer nature of the state. We conjecture that nevertheless an appropriate Hamiltonian  $H_{\text{RVB}}$  exists where the degrees of freedom are two chains of spinful fermions with exponentially decaying hopping amplitudes, no double occupancy and an infinitely strong antiferromagnetic Heisenberg coupling between the chains, leading to gapless charge and gapped spin degrees of freedom.

Despite not being able to find the exact form of  $H_{\text{RVB}}$ , we can still provide evidence for eq. (3.14) by extracting CFT data from the finite size spectrum of  $-\log(T)$ . This is because the energy eigenvalues of  $H$  coincide with the eigenvalues of the dilation operator in two-dimensional space-time [114]. If the hypothesis (3.14) is correct, the finite-size spectrum of  $T$  should be given by

$$E_n(N) = E_0(N) + a \frac{\Delta_n}{N}, \quad (3.16)$$

<sup>3</sup>Here and in the remainder of the chapter we regard  $T$  as the *double* row transfer matrix to ensure positivity, as is customary in the study of Dimer models.

<sup>4</sup>There is a second, strictly local Hamiltonian which also commutes with  $T$  and has the same ground state [112]. This latter model falls into the  $f(z)$ -classification in which its central charge and  $U(1)$  symmetry can be read off directly [113].

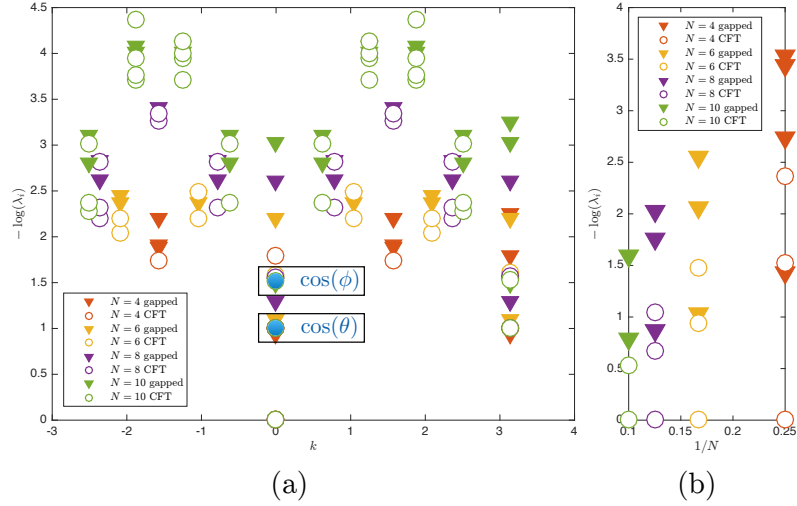


Figure 3.4: Finite-size spectrum of the nnRVB-PEPS transfer matrix on a cylinder of circumference  $N = 4, 6, 8, 10$ . (a) Dispersion relation. Empty dots stand for eigenvectors with  $\Delta q = 0$  and have been labeled ‘CFT’. Among the diagonally neutral states, the first state with off-diagonal charge  $|q_{\text{ket}}| = |q_{\text{bra}}| = 1(0)$  has been labeled  $\cos(\theta)$  ( $\cos(\phi)$ ) in accordance with the CFT prediction. (b) Lowest lying states at momentum  $k = 0$  for different cylinder sizes. The lowest lying  $\Delta q = 0$  states go to zero as  $1/N$ , while the lowest gapped states cross over and saturate at a finite value.

where  $E_n = -\log(\lambda_n)$  are the eigenenergies of  $T$ ,  $a$  is a non-universal constant and  $\Delta_n$  are the scaling dimensions of the primary and descendant operators of the CFT. Normalizing the PEPS amounts to shifting the ground state energy  $E_0 = 0$ . In the present regime  $K \in [0.5, 1]$ , according to (3.9), the operator with the smallest scaling dimension is  $[\cos(\theta)] = 1/4K$ , followed by  $[\cos(\phi)] = K$ . By taking the ratio of the eigenvalues corresponding to those states one can get rid of the non-universal constant and read off the Luttinger parameter

$$\frac{E[\cos(\phi)]}{E[\cos(\theta)]} = 4K^2. \quad (3.17)$$

An analysis of the finite-size spectrum of the RVB transfer matrix is presented in Fig. 3.4. We draw the following conclusions: First, due to the double-layer structure of the transfer matrix possesses an enlarged  $U(1) \times U(1)$  symmetry. The diagonal charge  $\Delta q := q_{\text{ket}} - q_{\text{bra}}$  splits the Hilbert space into two sectors. The charge neutral sector becomes gapless as  $1/N \rightarrow 0$  and is thus identified with the CFT degrees of freedom. Within this sector, the single-layer charge specifies the  $U(1)$  quantum number of the corresponding operator in the Luttinger Liquid, e.g., the lowest state which we identify with  $\cos(\theta)$  has charge  $|q_{\text{ket}}| = |q_{\text{bra}}| = 1$ . The diagonally charged sector is gapped and accounts for the exponentially decaying spinon-spinon correlators. Seeing the Dimer and RVB states as extremes of a more general  $SU(M)$ -RVB family, it seems plausible that the spinon gap is monotonically diverging with vanishing local overlap  $M \rightarrow \infty$ . In summary,

$$-\log(T) = \underbrace{H_{\text{CFT}}}_{\Delta q=0} \oplus H_{\text{gapped}}. \quad (3.18)$$

As a side remark, let us mention that the CFT sector contains only a small fraction  $(1/3)^N \sum_{n=0}^{N/2} \binom{N}{n} \binom{N-n}{n} (4/9)^n$  of the overall  $6^N$ -dimensional Hilbert space, which could potentially be used to target the gapless degrees of freedom numerically much



more efficiently. Furthermore, the ratio of the first and second eigenvalues in the CFT sector predicts  $K = 0.6170$ , which is in good agreement with the known value  $K \approx 0.6$  [93, 94, 110].

### 3.4 Perturbing the Transfer Matrix

Now that we have given some evidence regarding the validity of our assumption for the nnRVB state, we will broaden the discussion to include long-range singlets

$$T(\lambda) \sim e^{-H+\lambda V}. \quad (3.19)$$

Since the transfer matrix mediates correlations in the PEPS,  $|\psi(\lambda)\rangle$  can only be critical if  $-H + \lambda V$  is. Now that we have shown that  $H$  is a Luttinger Liquid, we will investigate whether  $V$  forms a relevant, irrelevant or marginal perturbation. To this end, we assume that the potential is local  $V = \sum v_i$ . The relevance of  $V$  can then be determined by computing the ground state correlator  $\langle v_i v_j \rangle - \langle v_i \rangle \langle v_j \rangle \sim |i-j|^{-\alpha}$ . If  $\alpha \geq 4$ , the perturbation is irrelevant/marginal and the state remains critical. On the other hand, a gap will necessarily open if  $\alpha < 4$ . Remarkably, it is possible to compute such a correlator in general, despite not having access to  $V$  directly. The key is to introduce inhomogenous fields for each individual tensor:

$$e^{-H+\sum \lambda_i v_i} = \cdots \begin{array}{c} \text{---} \square_{\mathbb{E}(\lambda_{i-1})} \text{---} \square_{\mathbb{E}(\lambda_i)} \text{---} \square_{\mathbb{E}(\lambda_{i+1})} \text{---} \cdots \\ \text{---} \quad \quad \quad \text{---} \quad \quad \quad \text{---} \end{array} \quad (3.20)$$

To obtain (connected) correlation functions, we take derivatives at zero with respect to the local fields and compute the expectation value of the operator thus obtained with respect to the fixed point  $|F\rangle$  of the unperturbed transfer matrix. A complication arises because  $[H, \sum \lambda_i v_i] \neq 0$ , so we have to use the Lie-Trotter formula to arrive at

$$\begin{aligned} C(|i-j|) &= \frac{\partial^2 T}{\partial \lambda_i \partial \lambda_j} \\ &= \langle F | v_i \left( \int_0^1 \tau e^{-\tau H} d\tau \right) v_j | F \rangle + (i \leftrightarrow j) \\ &= l \begin{array}{c} \text{---} \square_{\frac{\partial \mathbb{E}}{\partial \lambda_i}} \text{---} \square_{\mathbb{E}} \text{---} \cdots \text{---} \square_{\mathbb{E}} \text{---} \square_{\frac{\partial \mathbb{E}}{\partial \lambda_j}} \text{---} r \\ \text{---} \quad \quad \quad \text{---} \quad \quad \quad \text{---} \end{array} . \end{aligned} \quad (3.21)$$

$\longleftarrow \quad \quad \quad |i-j| \quad \quad \quad \longrightarrow$

For the sake of readability, we have suppressed the evaluation of the derivative at zero. In the last diagram, intersections of lines denote a translational invariant MPS tensor that describes the fixed point of the transfer matrix. Boxes labeled  $\mathbb{E}$  refer to the unperturbed double tensor and  $l$  and  $r$  are the left and right fixed points of the resulting zero-dimensional channel operator.

Eq. (3.21) differs from the pure correlation function by an intermediate relaxation that suppresses highly excited states by a factor  $1/E^2$ . More importantly,



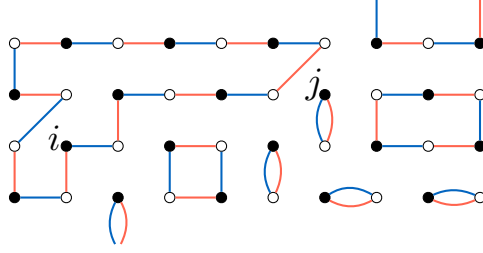


Figure 3.5: Part of the transition graph corresponding to the overlap of the red Dimer pattern in the bra with the blue Dimer pattern in the ket. The presence of an  $A_2$  tensor at sites  $i$  and  $j$  necessitates the existence of at least one long loop in the graph. The number associated to this transition graph is  $2^8$  times the weight corresponding to the loops outside of this section. The other  $A_2$  tensors are located far away.

the imaginary time evolution term possesses the  $U(1)$ -symmetry of the unperturbed Hamiltonian. Therefore, if  $V$  has no overlap with a given  $\cos(m\theta)$  operator (which has charge  $\pm m$  under that symmetry), the time-evolved operator will also not contain that operator. Any long-distance behaviour of (3.21) corresponding to a given charged operator must therefore also be present in the pure correlator  $\langle F|v_i v_j|F \rangle$ .

Before moving on to the result, we should make a comment concerning the double-layer structure of the PEPS. The double tensor has both a linear and quadratic perturbation term  $\mathbb{E}(\lambda) = \mathbb{E} + \lambda\delta\mathbb{E} + \lambda^2\delta^2\mathbb{E}$ , corresponding to two independent potentials, i.e.,  $T(\lambda) \sim \exp(-H + \lambda V^{(1)} + \lambda^2 V^{(2)})$ . In principle, we need to assess the relevance of each perturbation individually. However, we will now adapt a topological argument from [115] to show that  $V^{(1)}$  only affects the gapped degrees of freedom, exhibits exponential decay of correlations and is therefore irrelevant. According to (3.21), we have to evaluate the overlap  $\langle \psi_i | \psi_j \rangle$ , where  $|\psi_j\rangle$  has a single  $A_2$  tensor at site  $j$  and  $A_1$ -tensors everywhere else (technically there must be a second  $A_2$  tensor in each layer to avoid the PEPS to contract to zero. For the following argument we can assume those to be very far from both  $i$  and  $j$ ). This overlap can be expanded in terms of transition graphs, where each term in the sum must be compatible with an AA-singlet around site  $i$  and a BB-singlet around site  $j$  (Fig. 3.5). The contribution to the overlap of a given transition graph is simply  $2^{n_L}$ , where  $n_L$  is the number of loops in the graph. Crucially, it is impossible to locally close the loop opened up by e.g., the AA-singlet which must necessarily lie on the same loop as the BB-singlet. Therefore, each term in the sum must have at least one loop of size  $2|i - j|$ . We can therefore bound the correlator by

$$\langle \psi_i | \psi_j \rangle \leq e^{-|i-j|\ln 2} \sum_{\text{compatible transition graphs } T} Z(T), \quad (3.22)$$

where  $Z(T)$  is the partition function after removal of the long loop. Since the unperturbed partition function is dominated by configurations with short loops and we have normalized the overall norm of the unperturbed PEPS, the sum should evaluate to  $\mathcal{O}(1)$ . The crude estimate for the correlation length thus obtained  $\xi = 1/\ln 2 \approx 1.4$  is not far from the spin-spin correlation length  $\xi_{\text{Spin-Spin}} \approx 1.3$  [116, 117]. We remark that this argument would indicate a correlation length that vanishes as  $\xi(M) \sim 1/\ln M$  for  $SU(M)$  Dimer models on the square lattice and mention in passing that this is similar to the asymptotic behaviour the correlation length in

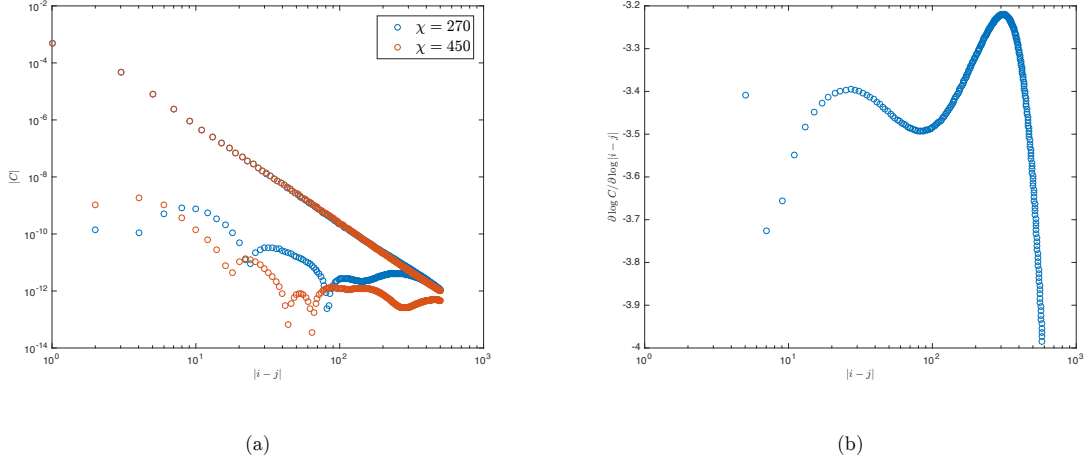


Figure 3.6: (a) The correlator (3.21) evaluated for the second order potential  $\partial^2 \mathbb{E} / \partial \lambda_i^2 = \delta^2 \mathbb{E}$  at the RVB point  $\lambda = 0$ . To extract the exponent  $\alpha$ , the odd-distance data was used. (b) The local slope in the loglog-plot (a) obtained from numerical differentiation at  $\lambda = 0, \chi = 306$ . There is a pronounced dip at small distances.

$Q$ -state Potts models at their first order transition  $\sim 1/\log \sqrt{Q}$ . As we will discuss in detail in chapter 4, such models can be seen as  $SU(\sqrt{Q})$  loop models.

An alternative argument for the exponential decay of the  $V^{(1)}$  potential is given by the observation that, in the finite size spectrum, all low-lying states belonging to the CFT sector are only affected at second order in perturbation theory when turning on  $\lambda$  (which was confirmed numerically).

The second-order potential  $V^{(2)}$ , on the other hand, shows clear algebraic decay over  $\sim 500$  sites (Fig. 3.6(a)). For the employed boundary bond dimensions, the exponent of the decay has saturated to the value

$$\alpha = 3.2 \quad (3.23)$$

This is in good agreement with the operator  $\cos(2\theta)$  that is predicted to decay with exponent  $2/K \approx 3.33$ .

There is a second way in which one can probe the field operator corresponding to the perturbation. Applying  $\cos(2\theta)$  to the vacuum of the field theory breaks the  $U(1)$ -symmetry generated by  $\theta \rightarrow \theta + \alpha$  to its  $\mathbb{Z}_2$  subgroup. Since we have direct access to the generator of the lattice  $U(1)$ -symmetry, we can extract the symmetry properties of the fixed point by computing the *Rayleigh quotient*. The latter is defined by inserting a candidate symmetry representation  $U$  between two fixed point tensors and measuring the largest eigenvalue of the corresponding transfer matrix. This eigenvalue corresponds to the norm  $\langle F | U^{\otimes L} | F \rangle = \lambda_{\max}^L$  and should be 1 if and only if the fixed point is symmetric (the Rayleigh quotient typically does not saturate to 1 exactly, since it is advantageous for the algorithm to break the  $U(1)$ -symmetry). In principle, we can probe either of the  $U(1)$ -symmetries of the transfer matrix. In the previous section, we have identified the counter-rotating  $Z^{\text{ket}} - Z^{\text{bra}}$ -symmetry to be the relevant one for the low-energy subspace. The values of the corresponding Rayleigh quotient are shown in Fig. 3.7. Even for small values of  $\lambda$ , it is maximal and very close to 1 only for  $\phi = 0, \pi$ . Hence, the lattice fixed point breaks  $U(1) \rightarrow \mathbb{Z}_2$ , providing further evidence for a relevant perturbing  $\cos(2\theta)$ -operator.

Equipped with this knowledge, we expect  $|\psi(\lambda)\rangle$  to be gapped for any  $\lambda > 0$ . On the other hand, we can now use our theory to make quantitative predictions.

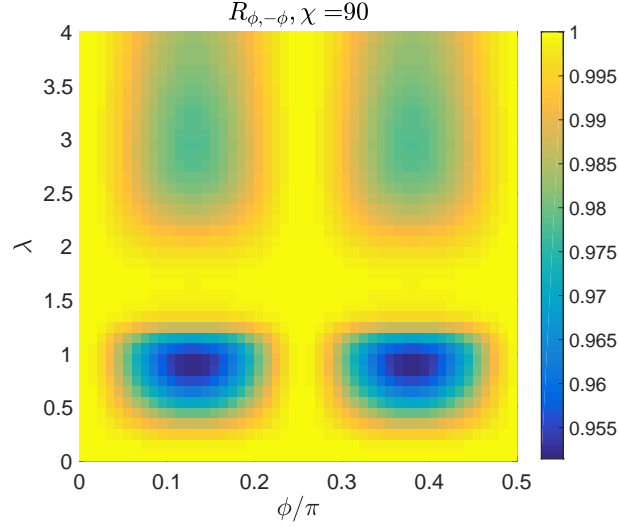


Figure 3.7: The Reyleigh quotient per site  $R(\lambda, \phi) := \langle F(\lambda) | U(\phi, -\phi) | F(\lambda) \rangle^{1/L}$  measures how well the initial diagonal  $U(1)$ -symmetry is preserved. For small perturbations, the symmetry is clearly broken to  $\mathbb{Z}_2$ , indicating a perturbing operator  $\cos(2\theta)$ . Figure courtesy of J.-Y. Chen.

### 3.5 Gap Scaling

For the present family of states, previous studies observed critical behaviour in a regime of finite  $\lambda$ . We will now argue that a gap is present but indeed too small for even high-precision numerics to detect. The key is that, at the nnRVB point, the operator  $\cos(2\theta)$  is rendered *almost irrelevant* by the interplay of two mechanisms: i) stabilization of the nnRVB state with respect to Classical Dimers due to the long-loop renormalization of the Luttinger parameter and ii) the double-layer nature of the state. A simple calculation will yield some quantitative understanding: We have argued that the action is

$$S(\lambda) = S_0 + \lambda^2 \int d^2x \cos(2\theta(x)) \quad (3.24)$$

Since the above expression has to be dimensionless, the dimension of  $\lambda$  has to be  $[\lambda] = 1 - 1/2K$ . On the other hand, if a gap opens as  $\Delta \sim \lambda^u$ , in order for  $\Delta$  to have dimensions of energy, we need

$$u = \frac{1}{1 - \frac{1}{2K}}. \quad (3.25)$$

In particular, at the Dimer point  $K = 1$ , the gap opens as  $\lambda^2$ , while the RVB point  $K \approx 0.6$  has  $\Delta \approx \lambda^6$ . For the optimal parameter with respect to the Heisenberg  $J1 - J2$  model,  $\lambda = 0.26$ , eq. (3.25) entails a correlation length of  $\sim 3200$  sites, which is hardly distinguishable from true criticality<sup>5</sup>.

The validity of this argument can be tested by considering a hole-doped RVB state [118]. Doping completely breaks the  $U(1)$  symmetry of the PEPS tensor, which is compatible with the  $\cos(\theta)$  operator. The above argument would predict the

<sup>5</sup>The cited value differs from the one found in [92] due to a different normalization of the tensors.

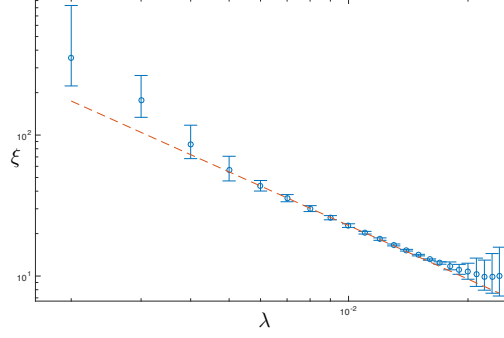


Figure 3.8: Correlation Length versus hole density in the hole-doped RVB state. Error bars represent the quality of a linear  $\delta$ - $\varepsilon$  fit [119]. The orange dotted line is the scaling prediction  $\xi \sim \lambda^{-1.26}$ .

correlation length to diverge as  $\xi \approx \lambda^{-1.26}$ , which we can indeed confirm numerically (Fig. 3.8).

To further strengthen the above argument in the present case, we will now introduce a Dimer-Solidomer model and show that it is in the same gapped  $\mathbb{Z}_2$  topological phase as the long-range RVB state. This model is a relaxation of the Classical Dimer Model, where solidomer vertices are allowed but obtain a penalizing energy  $-\log(\lambda)$  (Fig. 3.9). The quantum wave function is simply the Rokhsar-Kivelson state of the form (3.4). For any finite  $\lambda$ , the model is equivalent to a Toric Code (or an eight-vertex model from the classical perspective) with a uniform background charge of one unit per site. The model is dual under transforming  $\lambda \leftrightarrow 1/\lambda$  plus conjugation of each spin by Pauli- $X$ . The RG fixed point  $\lambda = 1$  is self-dual and the Hamiltonian is simply  $H = \sum_i X_i X_{i+1}$ .

To connect this model to the RVB state, we interpolate in two steps. First, we equip each occupied edge with an additional maximally entangled state, i.e., each dimer/solidomer has both a spin and compass degree of freedom, the latter of which keeps different configurations orthogonal. At the same time, we transform the virtual solidomers into singlet bonds. At this point, the family of states still realizes a  $K = 1$  Luttinger Liquid with a relevant  $\cos(2\theta)$  perturbation which drives the system into a gapped topological phase for any  $\lambda > 0$ . In a second step, we slowly forget the compass degrees of freedom, introducing a parameter

$$g = \left\langle \begin{array}{c} \circ \\ \circ \text{---} \bullet \text{---} \circ \\ \circ \end{array} \middle| \begin{array}{c} \circ \text{---} \circ \\ \circ \text{---} \bullet \text{---} \circ \\ \circ \end{array} \right\rangle \quad (3.26)$$

and interpolating from  $g = 0$  (Dimer) to  $g = 1$  (RVB). At various intermediate values of  $g$ , we compute the Luttinger parameter  $K(g)$  in three ways: First, we measure the finite-size spectrum as described in section 3.3. Second, we fit the algebraic decay of both the Dimer-Dimer and the  $\cos(2\theta)$  correlations to field theoretic predictions (for  $K \leq 1$  the dominant operator in the Dimer correlators is  $\cos(\phi)$  which is expected to decay with exponent  $2K$ ). These measurements are strictly confined to the critical line  $\lambda = 0$ . Crucially, if our prediction (3.25) is correct, we should be able to extract  $K$  from the critical exponent corresponding to the divergence of the correlation length. To assess the exponent, we need to pick a window of parameters at which  $\lambda$  is large enough to obtain converged values for the correlation length. On the other

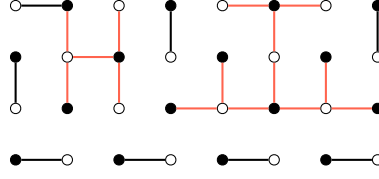


Figure 3.9: A configuration of the Dimer-Solidomer model. Solidomer vertices have three edges. The Boltzmann weight of the above configuration is  $\lambda^6$ .

hand, we may not choose  $\lambda$  too large for two reasons: First, universality is lost as we move deeper into the gapped phase (Fig. 3.10(b-d)). Second, we employ a  $\delta - \varepsilon$ -extrapolation to accurately measure the correlation length [119]. This procedure relies on the fact that correlation functions typically follow an Ornstein-Zernike form  $\langle v_i v_j \rangle \sim c + |i - j|^{-\alpha} \exp(-|i - j|/\xi)$  with both an algebraic and an exponential part. We have noticed that this extrapolation performs significantly worse both at Dimer and the RVB points when we bring  $\lambda$  close to 1 (inset of Fig. 3.10(c)). In the Dimer-Solidomer model, this is of course not surprising: Since the self-dual fixed point is a symmetry-breaking product state, the subleading algebraic part is non-existent. We therefore conjecture that an exact MPS solution, or at least a solution with pure exponential decay, might also exist along the long-range RVB line.

The numerical results are shown in Fig. 3.10. We observe that the stiffness parameter changes smoothly from  $K = 1$  to  $K \approx 0.6$  as expected, indicating that our model realizes a line of Luttinger Liquid fixed points. Turning on the teleportation perturbation is compatible with opening a gap of size given by (3.25) up to  $g \sim 0.75$ . Closer to the RVB point, we can neither confirm nor refute our scaling hypothesis:  $\xi$  vs.  $\lambda$  is not a straight line (in the loglog-plot), indicating that there is no single exponent that captures the opening of the gap. Can we still argue that there is a non-vanishing gap at the RVB point? What is the nature of the floating exponent in Fig. 3.10? We set out to answer these questions in the next section.

### 3.6 Floating $K$ and the Sine-Gordon Model

For a large fraction of models connecting the Quantum Dimer Model to the Resonating Valence Bond state, we have gathered evidence that the teleportation perturbation opens up a finite gap. Close to the RVB point, our simple scaling argument is not sufficient: we need to assist it with more a detailed analysis. This section will provide the two missing pieces. First, by identifying subleading operators in the expansion of the teleportation tensor, we identify a marginal perturbation, which accounts for the varying slope in Fig. 3.10. We postulate an action for the effective field theory. In a second step, we map this field theory to the *Sine-Gordon Model*. By virtue of being integrable, the model offers exact numerical values for the hypothetical gaps which can be compared to numerical PEPS simulations. We find that, in a regime where converged numerical data is available, the data confirms our hypothesis.

In the analysis surrounding (3.23), we have used both symmetry analysis as well as correlator scaling to infer that the leading field theory operator contained in  $\delta^2 E$  is  $\cos(2\theta)$ . The key to understanding our numerical data is to look at the effect of subleading operators. In particular, consider the operator  $(\nabla\phi)^2$ . Being a marginal

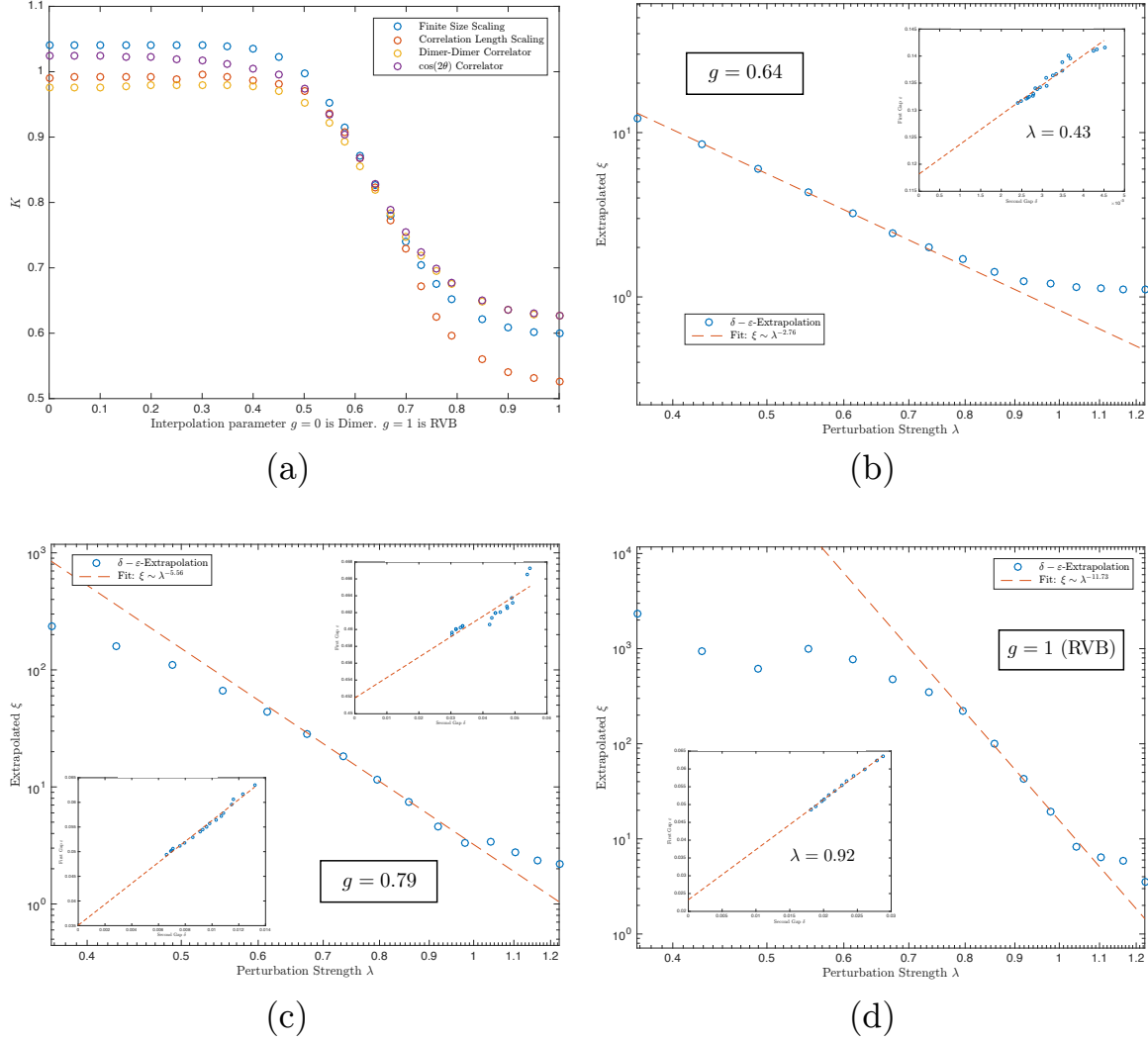


Figure 3.10: (a) Extracted values for the Luttinger parameter. Finite-Size Scaling is done for  $N = 6, 8, 10$  and using  $1/N$  extrapolation. The correlator exponents were fitted to the algebraic decay over distances up to 100 sites. For the correlation length scaling we used a window of  $\lambda$  that shifts up with increasing  $g$ . (b-d) Loglog plot of the extrapolated correlation length at a few points along the interpolation. At the RVB point, there is no regime in which a linear fit is accurate and the best guess deviates from the scaling prediction  $\xi \sim \lambda^{-6}$ . Inset:  $\delta - \varepsilon$ -extrapolation at a few values of  $\lambda$ .

operator, its correlators decay as

$$\langle (\nabla\phi(x))^2 (\nabla\phi(y))^2 \rangle \sim \frac{1}{|x-y|^4} \quad (3.27)$$

and are therefore invisible to our numerical approach (cf. Fig. 3.6(a)). Furthermore a linear combination

$$\delta^2\mathbb{E} \sim (\nabla\phi)^2 + \cos(2\theta) \quad (3.28)$$

transforms correctly under the  $U(1)$ -symmetry. Crucially, (3.28) implies that the perturbed action (3.24) has to be modified

$$S(\lambda) = \int \frac{1}{8\pi K(\lambda)} (\nabla\phi(x))^2 + \lambda^2 \cos(2\theta(x)) d^2x. \quad (3.29)$$

This action is compatible with the data in Fig. 3.10 since the local slope  $\xi \sim \lambda^u(K)$  depends on  $K$  which is allowed to float. Furthermore, it is expected that this effect is much stronger close to the RVB point, because the dependence of  $u$  on  $K$  blows up for  $K \rightarrow 1/2$ . Equation (3.29) is therefore our refined hypothesis. The remainder of this section is concerned with accumulating appropriate evidence.

A first confirmation of (3.29) is found by investigating the  $\delta^2\mathbb{E}$ - $\delta^2\mathbb{E}$  correlation function in more detail. If the component of  $(\nabla\phi)^2$  is sufficiently large, there can exist a regime in which correlators will seem to decay with a larger exponent  $|x-y|^{-4}$  before this contribution vanishes in the long-range asymptotics. Indeed we observe two distinct regions in Fig. 3.6(b), corresponding to fast decay at short distances and slower decay over intermediate length scales, which is compatible with our hypothesis.

The second piece of evidence is that (3.29) delivers the correct quantitative prediction for the correlation length of the PEPS. It is a useful duality of the Coulomb Gas (also known as *T-Duality*) that perturbing the theory (3.6) at Luttinger parameter  $K$  with an operator  $\cos(n\theta)$  is equivalent to perturbing with  $\cos(n\phi)$  at a value of  $K' = 1/4K$ . The correlation length of our model is therefore equal to the one corresponding to

$$S'(\lambda) = \int \frac{K(\lambda)}{2\pi} (\nabla\phi(x))^2 + \lambda^2 \cos(2\phi(x)) d^2x, \quad (3.30)$$

The action (3.30) is known as the *Sine-Gordon Model*. Let us quickly state some known facts about the model that will turn out to be useful for the discussion [120]. The Sine-Gordon model is integrable. The lightest particle in the theory is a *Soliton*, a topological excitation that is created by acting with the non-local operator  $\cos(\phi/2)$  on the vacuum. Its mass is given by

$$M = \frac{2\Gamma(\Xi/2)}{\sqrt{\pi}\Gamma(1/2 + \Xi/2)} \left( \frac{\Gamma(1 - \beta^2)\pi\mu}{\Gamma(\beta^2)} \right)^{\frac{1}{2-2\beta^2}}, \quad (3.31)$$

where  $\beta^2 = 1/2K$ ,  $\Xi = \beta^2/(1 - \beta^2)$ ,  $\mu = \lambda^2/2$  and  $\Gamma$  is the Gamma function. The maximum correlation length in the Sine-Gordon model

$$\xi = \frac{1}{M}, \quad (3.32)$$



is a quantity that can be directly compared to numerical simulations of the PEPS. Crucially, the correlation length (3.31) only depends on  $\lambda$  and  $K(\lambda)$  which can be accessed through measurements of correlation functions.

Before we launch into the comparison of (3.31) with our PEPS data, it is important to fix the correct quantity to compare with. In fact, there is a multitude of length scales that can be associated with the PEPS (corresponding to gaps in the entanglement spectra); the correct one should reproduce the mass of the Soliton operator  $\cos(\phi/2)$ . Technically,  $\cos(\phi/2)$  is not well-defined but is instead shorthand for

$$\cos(\phi/2) = e^{i\pi \int_{-\infty}^x \nabla \phi(x') dx'} + \text{h.c.} \quad (3.33)$$

The operator  $\nabla \phi$ , is simply the generator of the  $U(1)$ -symmetry and can be identified with the lattice operator  $Z = \text{diag}(3/4, 3/4, -1/4)$ . The above equation can therefore be interpreted as a string of  $\pi$ -rotations  $\prod_j e^{i\pi Z_j}$ , i.e., a domain-wall excitation of the transfer matrix. We therefore identify

$$\langle \cos(\phi(x)/2) \cos(\phi(y)/2) \rangle \sim \begin{array}{c} \cdots \quad \begin{array}{|c|c|c|c|c|c|} \hline & & & & & \\ \hline & Z_x & Z & \cdots & Z_y & \\ \hline & & & & & \\ \hline \end{array} \quad \cdots \end{array} . \quad (3.34)$$

Note that this is compatible with

$$\lim_{y \rightarrow x} \cos(\phi(x/2)) \cos(\phi(y/2)) \sim \cos(\phi(x)) \sim Z \quad (3.35)$$

which is indeed the dominant contribution to the dimer operator. The correlation length of the domain wall excitation (3.34) is given by the gap of the dressed channel operator

$$\begin{array}{c} \text{---} \\ | \\ Z \\ | \\ \text{---} \end{array} \quad (3.36)$$

In Fig. 3.11(a), we show the correlation length for both the trivial and the domain wall excitation. In anticipation of classifying the finite- $\lambda$  phase as a  $\mathbb{Z}_2$  Spin Liquid, we dub these particles *Visons*. As it turns out, this Vison correlation length is indeed the largest length scale in the system.

Furthermore, the Vison-Vison correlator unlocks a new way of computing the Luttinger parameter  $K$ : According to (3.9), the scaling dimension of  $\cos(\phi/2)$  is

$$[\cos(\phi/2)] = K/4. \quad (3.37)$$

Thus, a correlator like (3.34) decays as  $|x-y|^{-K/2}$ . Extracting  $K$  from this correlator agrees with the previously discussed means of obtaining  $K$ , but is more reliable since the window of algebraic decay is largest for the vison.

We are now ready to compare the values on the correlation length in the PEPS with the prediction from the Sign-Gordon model. To obtain correlation lengths in the Sine-Gordon model, the value of  $K(\lambda)$  from the Vison correlator (Fig. 3.11(a))



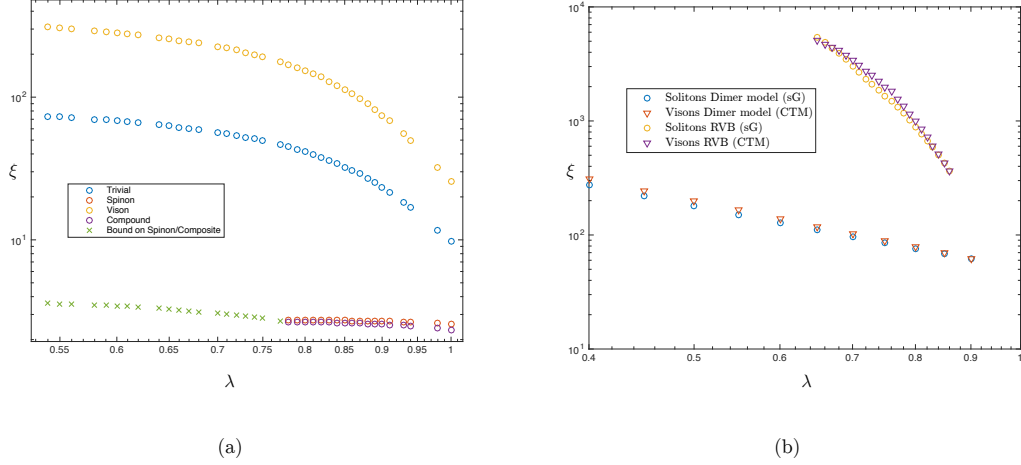


Figure 3.11: (a) Correlation Lengths at of trivial and Vison excitations  $\chi = 270$  for various perturbation strengths away from the RVB point. The dual *Spinon* excitations are seen to saturate at a finite value, in accordance with the transition graph argument in section 3.4. For  $\lambda \leq 0.77$ , all the computed eigenvalues live in the trivial or vison on sector, which is why only an upper bound is given. (b) Extrapolated Vison correlation length for the Dimer-Solidomer (red triangles) and long-range RVB models (purple triangles), together with the corresponding prediction from Sine-Gordon model (blue and yellow circles, respectively). Lengths in the field theory have been “right-normalized” such that the data agrees on the largest available perturbation.

is used. The result is shown in Fig. 3.11(b). Values are displayed in log log-scale for both for the RVB as well as the Dimer-Solidomer model, wherever data is available that is either converged or extrapolated with high confidence. We point out that we have “right-normalized” our data, i.e., we multiply the prediction from the Sine-Gordon by a constant independent of  $\lambda$ . We do this because the numerical overlap of a lattice operator with a field includes UV-contributions that we do not access: We are less interested in predicting the absolute numerical value of  $\xi$ , but more in retracing the non-trivial slope that deviates from a simple scaling analysis with constant  $K$ .

The Dimer length follows a straight line that is compatible with a simple scaling analysis cf. (3.25). There are no signs of an effective floating  $K$  corresponding to a marginal operator. The RVB data on the other hand is clearly curved downwards, in agreement with our hypothesis of floating  $K$ , indicating a significant contribution of  $|\nabla\phi|^2$  to the perturbation. Since the Sine-Gordon hypothesis is able to explain the non-trivial curvature of  $\xi$  vs.  $\lambda$ , it is likely that this gapped theory is the correct description for all  $\lambda > 0$ .

### 3.7 Conclusion

We have shown that the RVB state on the square lattice is a gapped  $\mathbb{Z}_2$  Spin Liquid for any finite density of long-range singlets. Furthermore, we explain the previous difficulties to detect the gap by giving a field theoretic argument for its extremely small magnitude. We stress that the argument does not depend on the microscopic details of the RVB state. Instead, whenever we can understand a  $\mathbb{Z}_2$  Spin Liquid to live in the vicinity of a  $U(1)$ -invariant point, it seems likely that a universal argument like (3.25) will hold. The only free parameter in this discussion is the Luttinger parameter  $K$ , which is fixed by the additional  $SU(2)$ -symmetry. We can therefore

generically expect competing phases, e.g., Valence-Bond Solids, Topological Phases and non-Fermi Liquids to live in close vicinity of one another in the phase diagrams of such models. This may also explain why naturally occurring candidates for Quantum Spin Liquids in which antiferromagnetic Heisenberg physics is relevant, tend to have very small or vanishing excitation gaps [121]. This also points towards a potential avenue for finding topological phases that are more stable than the long-range RVB state. Since the gap depends sensitively on the Luttinger parameter, which is in turn given by the local overlap of Dimer configurations, our findings suggest that antiferromagnetic  $SU(M)$  models may be more stable than their  $SU(2)$  counterparts. Recently, these models have been subject to both theoretical and experimental interest [122–124]. Our results also reopen the issue whether there can be a critical RVB-state without bipartiteness.

The major part of this chapter has been devoted to refuting the hypothesis of an emergent  $U(1)$ -symmetry in the long-range RVB state. One might ask if such a thing is possible in principle. We now put forward a candidate PEPS with an emergent virtual  $U(1)$ -symmetry. To this end, we revisit a system we studied in depth in section 2.2: The Six-Vertex Model. Like the RVB and Dimer states, the model is described by a Coulomb Gas CFT. The difference is that the  $K$ -parameter is very well under control: It is related via

$$K = \frac{\pi}{2(\pi - \arccos(\Delta))} \quad (3.38)$$

to the anisotropy parameter, which can in turn be tuned by the vertex weights, cf. (2.37). We have two choices for perturbing the Six-Vertex Model with an irrelevant, symmetry-breaking operator: One may choose a simple  $\cos(\theta)$  or  $\cos(2\theta)$  as in the RVB case. This has the advantage that it is easily implemented on the level of the local PEPS-tensor. On the other hand, for these operators to be irrelevant we would need  $K < 1/2$ , which is manifestly impossible in (3.38). Alternatively, one could circumvent this problem by choosing a less relevant primary like  $\cos(3\theta)$ . This perturbation, however, consists of large clusters of same-sublattice defects, which increase the size of the unit cell and make our numerical algorithms unfeasible. The trick is to introduce an external field, which allows to break the  $K = 1/2$ -barrier.

Perturbing the system at  $K < 1/2$  with an “all-in”- or “all-out”-vertex (rather than “2-in-2-out”) results in an explicit breaking of the  $U(1)$ -symmetry, that should reemerge in the long-distance limit. More explicitly, we set up a tensor  $A(\lambda, h) = A_{\text{Six-Vertex}}(h) + \lambda A_{\text{all-in/all-out}}$ , where  $A_{\text{Six-Vertex}}(h)$  is the Six-Vertex tensor from chapter 2 at  $a = b = 1$ ,  $c = 3$  and each up-pointing (down-pointing) arrow receives an additional multiplicative weight  $e^{-h}$  ( $e^h$ ).  $A_{\text{all-in/all-out}}$  is the  $U(1) \rightarrow \mathbb{Z}_2$ -breaking tensor that is the equal superposition of all arrows pointing in and all arrows pointing out and the transfer matrix acts from bottom to top.

Probing an emergent symmetry on the lattice is subtle: the ground state will generally not be symmetric under the unperturbed  $U(1)$ -symmetry. Instead, emergent symmetries in field theories are typically identified by correlation functions. A correlator that transforms non-trivially under the symmetry is given by

$$\langle F | X_i^{\text{ket}} X_i^{\text{bra}} X_j^{\text{ket}} X_j^{\text{bra}} | F \rangle. \quad (3.39a)$$

Out of the two  $U(1)$ -symmetries, the double-layer symmetry is trivially present in the classical model. Under a  $\pi/2$ -rotation of the single-layer symmetry, the above

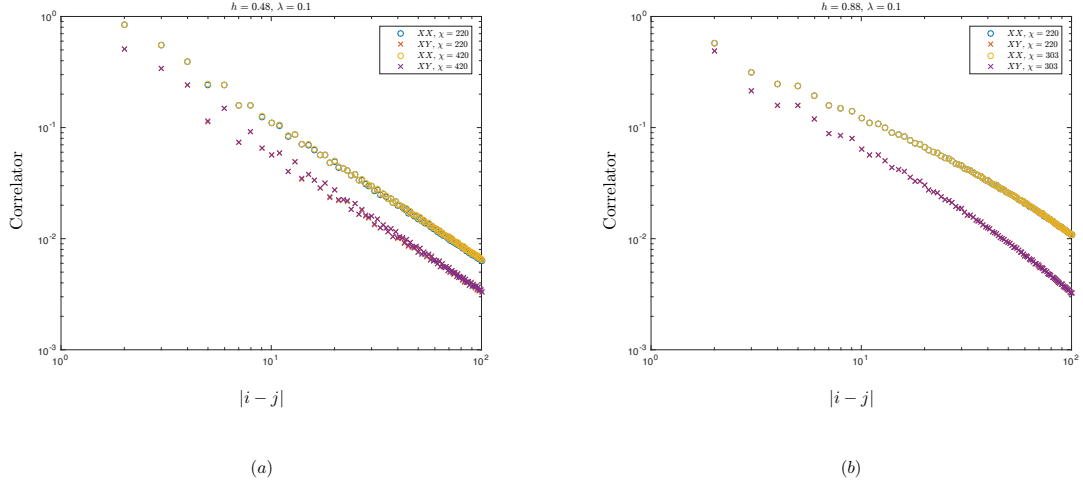


Figure 3.12: Correlation function of the operators  $X^{\text{ket}}X^{\text{bra}} \sim \cos(\theta)$  and  $X^{\text{ket}}Y^{\text{bra}} \sim \sin(\theta)$  for an equal perturbation at two different points of the non-zero field Six-Vortex PEPS. Convergence has been reached for the available bond dimension. The external field strengths (a)  $h = 0.48$  and (b)  $h = 0.88$  correspond to  $K = 0.435$  and  $K = 0.593$ , respectively, as computed from the  $\mathbb{E}_{\text{all-in/all-out}}$ -correlators at  $\lambda = 0$ .

correlator transforms into

$$\langle F | X_i^{\text{ket}} Y_i^{\text{bra}} X_j^{\text{ket}} Y_j^{\text{bra}} | F \rangle. \quad (3.39b)$$

Physically, (3.39) corresponds to inserting test defect “3-in-1-out”-vertices into the partition function.

In cases where the perturbation is relevant, we expect the correlators to decay independently of each other. On the other hand, in the presence of an emergent  $U(1)$ -symmetry, the correlators should decay with the same slope (even though their overlap with the field operators  $\cos(\theta)$  and  $\sin(\theta)$  does not necessarily need to be of the same magnitude). These correlators are shown in Fig. 3.12. The data at  $K < 1/2$  ( $h = 0.48$ ) is indeed compatible with an emergent  $U(1)$ -symmetry, unlike the  $K > 1/2$ -data where we know that the  $U(1)$ -symmetry is irreversibly lost.

# Chapter 4

## $SU(2)$ -symmetry

In the previous chapters, we have focused on  $U(1)$ -symmetric PEPS and found that these corresponds to critical systems in a number of examples. This chapter is devoted to the symmetry group  $SU(2)$ . On the one hand, we expect to find critical or symmetry-breaking behaviour, since  $U(1)$  is a subgroup of  $SU(2)$  and proposition 2.1 should hold. On the other hand, due to its non-abelian nature,  $SU(2)$  may also exhibit distinctive features.

In section 4.1, we set up the most general PEPS with virtual  $SU(2)$ -symmetry for the fundamental representation. Singlets of the non-abelian group are necessarily maximally entangled which leads to a natural description of the wave function in terms of a loop picture. The combinatorics of these loop patterns places stricter bounds on the entanglement entropy and the size of the entanglement-restricted subspace than in the  $U(1)$ -case: the counting problem now belongs to the universality class of mountain diagrams. Physically, we show that the PEPS spontaneously breaks the lattice symmetry and orders in a plaquette phase. To arrive at this result, we map the norm of the PEPS to a classical Delta Potts model with  $Q = 16$  states.

In section 4.2 we turn our attention to the natural parent Hamiltonian of the PEPS. This *loop surgery Hamiltonian* acts on a  $2 \times 2$  patch, and the PEPS exactly parametrizes its ground space manifold on any region with open boundary conditions (the intersection property). Subsequently, we show that by a suitable choice of boundary terms, the parent Hamiltonian can be modified such as to exhibit a unique ground state in any finite volume. While this behavior is closely resemblant to that of PEPS with finite virtual symmetry group, we find that with periodic boundaries, the ground states cannot be parametrized purely in terms of symmetry twists, and the system keeps a ground space degeneracy which is *exponential* in the size of the boundary. A closer analysis reveals that there are at least two types of ground states: Those which can be parameterized through symmetry twists and which span a space of linear dimension in the system size, and a distinct class of ground states which correspond to extremal “frozen” spin configurations which are not coupled to other configurations by the Hamiltonian, and which contribute an exponential number of states. Closing remarks are given in section 4.3.

### 4.1 The wave function

In this section, we define the PEPS, introduce the formalism used for its analysis, and analyse the entanglement properties. We will focus on the case where the bond dimension  $D = 2$ , and  $U_g \equiv g$  is the fundamental representation of  $g \in$

$SU(2)$ . A basis for the two-dimensional subspace of  $(\mathbb{C}^2)^{\otimes 4}$  that is invariant under  $U_g \otimes U_g \otimes \overline{U_g} \otimes \overline{U_g}$  is given by  $\{|\psi^-\rangle_{ul}|\psi^-\rangle_{dr}, |\phi^+\rangle_{ur}|\phi^+\rangle_{dl}\}$ , where  $|\psi^-\rangle = |01\rangle - |10\rangle$ . Therefore, up to a constant factor the most general fiducial state  $\tilde{A}$  is of the form

$$\text{---} \boxed{\tilde{A}} \text{---} = \lambda |0\rangle_p |\psi^-\rangle_{ul} |\psi^-\rangle_{dr} + |1\rangle_p |\phi^+\rangle_{ur} |\phi^+\rangle_{dl} \quad (4.1)$$

where  $\lambda \in \mathbb{C}$ , and  $|0\rangle$  and  $|1\rangle$  are normalized and linearly independent, but not necessarily orthogonal. Throughout this chapter, we will denote fiducial states by  $|\psi_{N_h \times N_v}(A)\rangle$ , e.g.,

$$\begin{aligned} |\psi_{2 \times 1}(A)\rangle &= \text{---} \boxed{A} \text{---} \boxed{A} \text{---} \\ &= \langle \phi^+ |_{r_1, l_2} |\psi_{1 \times 1}(A)\rangle \otimes |\psi_{1 \times 1}(A)\rangle \end{aligned} \quad (4.2)$$

where  $|\phi^+\rangle = \sum_{i=1}^D |ii\rangle$ . Physical states obtained by imposing boundary conditions  $|X\rangle \in (\mathbb{C}^D)^{\otimes (2N_h + 2N_v)}$  are denoted

$$\begin{aligned} |\psi_{2 \times 1}(A, X)\rangle &= \boxed{\begin{array}{c} \partial u_1 \quad \partial u_2 \\ \begin{array}{|c|c|} \hline u_1 \quad u_2 \\ \hline \end{array} \\ \partial l_1 \quad \partial l_2 \\ \begin{array}{|c|c|} \hline d_1 \quad d_2 \\ \hline \end{array} \\ \partial d_1 \quad \partial d_2 \end{array}} X \\ &= \langle \phi^+ |_{\partial u_1, u_1} \langle \phi^+ |_{\partial u_2, u_2} \dots |\psi_{2 \times 1}(A)\rangle |X\rangle, \end{aligned} \quad (4.3)$$

where  $\partial u_1, \partial u_2, \dots$  are the indices of  $|X\rangle$ ,  $u_1, u_2, \dots$  are the indices of  $|\psi_{2 \times 1}(A)\rangle$  and the  $\langle \phi^+ |$  contract them. For the particular choice of periodic boundary conditions we write

$$|X = \text{PBC}\rangle = |\phi^+\rangle_{\partial u_1, \partial d_1} |\phi^+\rangle_{\partial u_2, \partial d_2} \dots \quad (4.4)$$

A complication of the tensor  $\tilde{A}$  is that it involves different entangled states and is not rotationally invariant. We will now introduce another tensor  $A$  which only requires one kind of entangled state, is rotationally invariant for  $\lambda = 1$ , yet generates the same family of states. Specifically, we will show that for any region, there exists an invertible operator  $B$  acting on the virtual indices at the boundary such that

$$|\psi_{N_h \times N_v}(A, X)\rangle = |\psi_{N_h \times N_v}(\tilde{A}, BX)\rangle. \quad (4.5)$$

In the special case of even  $N_h$  and  $N_v$  and periodic boundary conditions (PBC),  $B|X = \text{PBC}\rangle = |X = \text{PBC}\rangle$ . The price we pay is that  $A$  will no longer be explicitly  $SU(2)$ -invariant. Yet, we will see that using  $A$  instead of  $\tilde{A}$  simplifies the majority of the derivations in this paper. Specifically, define

$$\text{---} \boxed{A} \text{---} = \lambda |0\rangle_p |\phi^+\rangle_{ul} |\phi^+\rangle_{dr} + |1\rangle_p |\phi^+\rangle_{ur} |\phi^+\rangle_{dl} \quad (4.6)$$

The tensor  $A$  is clearly rotationally invariant for  $\lambda = 1$ .

To show Eq. (4.5), note that

$$\text{---} \boxed{A} \text{---} = \text{---} \boxed{\tilde{A}} \text{---} \begin{array}{c} \circlearrowleft Y \\ \circlearrowright Y^T \end{array} = \begin{array}{c} \circlearrowleft Y \\ \circlearrowright Y^T \end{array} \text{---} \boxed{\tilde{A}} \text{---} \quad (4.7)$$

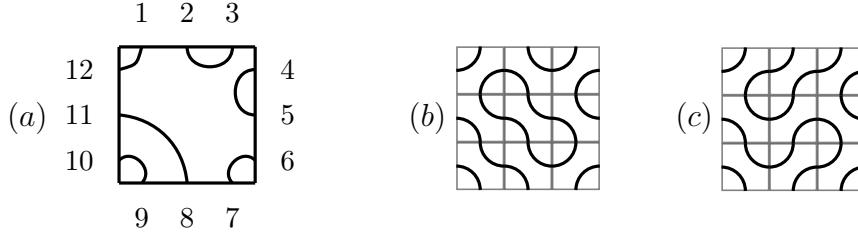


Figure 4.1: Connectivity patterns and classes. (a) shows a connectivity pattern, here  $\{(1, 12), (2, 3), (4, 5), (6, 7), (8, 11), (9, 10)\}$ . (b) and (c) show two loop patterns which are compatible with the connectivity pattern in (a). All compatible patterns form the *connectivity class* corresponding to (a). For the loop pattern shown in (b),  $n_L = 1$  and  $b_L = 3$ .

where  $Y = \begin{pmatrix} 0 & 1 \\ -1 & 0 \end{pmatrix}$  and all matrices act from left to right and from top to bottom. Inserting now the middle form of (4.7) into the even and the right-hand side into the odd sublattice of the square lattice, we obtain

$$\begin{aligned}
 & \begin{array}{c} \text{---} \square A \text{---} \square A \text{---} \\ | \quad | \\ \text{---} \square A \text{---} \square A \text{---} \\ | \quad | \end{array} = \begin{array}{c} \begin{array}{c} \text{---} \square \tilde{A} \text{---} \text{---} \square \tilde{A} \text{---} \\ | \quad | \\ \text{---} \square \tilde{A} \text{---} \text{---} \square \tilde{A} \text{---} \\ | \quad | \end{array} \\ \begin{array}{c} \text{---} \square \tilde{A} \text{---} \text{---} \square \tilde{A} \text{---} \\ | \quad | \\ \text{---} \square \tilde{A} \text{---} \text{---} \square \tilde{A} \text{---} \\ | \quad | \end{array} \end{array} \\
 & \qquad \qquad \qquad = \begin{array}{c} \begin{array}{c} \text{---} \square \tilde{A} \text{---} \text{---} \square \tilde{A} \text{---} \\ | \quad | \\ \text{---} \square \tilde{A} \text{---} \text{---} \square \tilde{A} \text{---} \\ | \quad | \end{array} \\ \begin{array}{c} \text{---} \square \tilde{A} \text{---} \text{---} \square \tilde{A} \text{---} \\ | \quad | \\ \text{---} \square \tilde{A} \text{---} \text{---} \square \tilde{A} \text{---} \\ | \quad | \end{array} \end{array}
 \end{aligned} \tag{4.8}$$

which proves (4.5) with

$$B = Y \otimes \mathbb{1} \otimes Y \otimes \mathbb{1} \cdots \otimes Y^T \otimes \mathbb{1} \otimes \cdots \tag{4.9}$$

The states generated by  $A$  are therefore equivalent to those generated by the  $SU(2)$ -invariant tensor  $\tilde{A}$  up to invertible boundary terms which can be absorbed into the boundary conditions  $X$ . In the following, we will therefore work with the tensor  $A$ , and thus restrict to  $N_h, N_v$  even on PBC.

### 4.1.1 The Loop Picture

We will now introduce graphical notation that will provide a convenient way of expressing configurations of the PEPS through loop patterns. To this end we introduce the rule

$$\begin{aligned}
 |0\rangle & \rightarrow |\boxplus\rangle \\
 |1\rangle & \rightarrow |\boxminus\rangle
 \end{aligned} \tag{4.10}$$

This prescription leads to e.g.,

$$\left| \begin{array}{cccc} 1 & 0 & 1 & 0 \\ 0 & 1 & 1 & 1 \\ 1 & 0 & 0 & 0 \\ 1 & 1 & 0 & 1 \end{array} \right\rangle \rightarrow \begin{array}{|c|c|c|c|} \hline \text{---} & \text{---} & \text{---} & \text{---} \\ \hline \text{---} & \text{---} & \text{---} & \text{---} \\ \hline \text{---} & \text{---} & \text{---} & \text{---} \\ \hline \text{---} & \text{---} & \text{---} & \text{---} \\ \hline \end{array} \quad (4.11)$$

To each such physical configuration corresponds a configuration of virtual states, obtained by contracting the tensors with the corresponding physical states on that patch with open boundaries (note that for  $\langle 0|1 \rangle \neq 0$ , this requires projecting the physical state onto the *dual* basis vector). Since the virtual  $|\phi^+\rangle$  form the same pattern as the  $\boxplus$  and  $\boxminus$ , and are connected by projecting onto  $\langle \phi^+|$ , which yet again yields  $|\phi^+\rangle$ , each open loop corresponds to a virtual state  $|\phi^+\rangle$  at the corresponding virtual indices at the boundary, while each closed loop contributes a factor of 2 (due to our choice of normalization).

Let us now rigorously establish such a framework. In the following, we always consider an  $N_h \times N_v$  patch. The degrees of freedom at the boundary are numbered from  $1, \dots, 2N$ ,  $N = N_h + N_v$ , as shown in Fig. 4.1(a).

A *connectivity pattern*  $p$  on the boundary of the patch is a pairing of the numbers  $1, \dots, 2N$ ,  $N = N_h + N_v$ , into non-crossing tuples  $\{(a_1, b_1), \dots, (a_N, b_N)\}$ , see Fig. 4.1(a).

A *loop pattern*  $L$  is a tiling of the patch with tiles  $\boxplus$  and  $\boxminus$ , such as in Fig. 4.1(b,c). To each loop pattern  $L$ , there is a corresponding *loop state*  $|L\rangle$  of the physical system, namely the product state that is obtained by replacing  $\boxplus$  with  $|0\rangle$  and  $\boxminus$  with  $|1\rangle$ . For a loop pattern  $L$ , we denote by  $n_L$  the number of closed loops in  $L$  and  $b_L$  is the number of  $\boxplus$ -tiles in  $L$ . Each loop pattern  $L$  is *compatible* with a single connectivity pattern,  $p(L)$ , namely the one which is obtained by reading off the boundary pairs which are connected by  $L$ . A *connectivity class*  $C_p$  for a given connectivity pattern is the set of all loop patterns which are compatible with  $p$ . We will denote the vector space spanned by all loop states  $|L\rangle$  in the connectivity class  $C_p$  by  $V(C_p)$ .

A *boundary matching* is a state on the virtual degrees of freedom at the boundary corresponding to a connectivity pattern  $p = \{(a_1, b_1), \dots, (a_N, b_N)\}$ , this is,

$$|m(p)\rangle = |\phi^+\rangle_{a_1, b_1} \otimes \dots \otimes |\phi^+\rangle_{a_N, b_N} . \quad (4.12)$$

This terminology permits us to write down the wave function of our PEPS in a concise way:

$$|\psi_{N_h \times N_v}(A)\rangle = \sum_{\substack{\text{connectivity} \\ \text{patterns} \\ p}} |m(p)\rangle \otimes \sum_{L \in C_p} |L\rangle 2^{n_L} \lambda^{b_L} \quad (4.13)$$

The proof is immediate from the definition of the tensors, and the fact that each closed loop contributes a factor of 2, as discussed above.

The set of all boundary matchings  $|m(p)\rangle$  is linearly independent and forms a basis of the space of all staggered spin-0 states (i.e., spin-0 up to an action of  $Y$  on every second site). This can be seen as follows: Different  $|m(p)\rangle$  correspond to different non-crossing partitions of the boundary points into pairs which form maximally entangled states. Application of  $Y$  on every other boundary site turns such a matching of  $|\phi^+\rangle$  into a matching of singlets, i.e.

$$\begin{aligned} Y \otimes \mathbb{1} \otimes \dots \otimes Y \otimes \mathbb{1} |\phi^+\rangle_{a_1, b_1} \otimes \dots \otimes |\phi^+\rangle_{a_N, b_N} \\ = |\psi^-\rangle_{a_1, b_1} \otimes \dots \otimes |\psi^-\rangle_{a_N, b_N} \end{aligned} \quad (4.14)$$

The set of non-crossing singlet matchings is a minimal basis for the spin-0 space, in particular, the matchings are mutually linearly independent as shown in [125–127]. There this is proven as follows: First, all singlet matchings, non-crossing or otherwise, form an overcomplete basis of the spin-0 space. However, each crossing matching can be ‘uncrossed’ using the relation

$$\begin{array}{c} \bullet \quad \bullet \\ \diagdown \quad \diagup \\ \bullet \quad \bullet \end{array} = \frac{1}{2} \begin{array}{c} \bullet \quad \bullet \\ \text{---} \quad \text{---} \\ \bullet \quad \bullet \end{array} + \frac{1}{2} \begin{array}{c} \bullet \quad \bullet \\ \text{---} \quad \text{---} \\ \bullet \quad \bullet \end{array} \quad (4.15)$$

where the points are spin-1/2 particles and the lines indicate singlet pairings with a suitably chosen orientation. Using this relation iteratively, one can express every spin-0 state as a superposition of crossing-free singlet pairings. Since there are  $\frac{1}{N+1} \binom{2N}{N}$  non-crossing matchings which coincides with the dimension of the spin-0 subspace of  $2N$  qubits, these form a minimal basis. Since  $Y \otimes \mathbb{1} \otimes \cdots \otimes Y \otimes \mathbb{1}$  is an invertible operator, the  $|m(p)\rangle$  form a minimal basis of the staggered spin-0 space.

This implies two things: First, we can restrict any boundary condition  $X$  to the staggered spin 0 space. Second, there exists a dual basis  $\{\langle m^*(p)|\}_p$  of that space such that  $\langle m^*(p)|m(q)\rangle = \delta_{pq}$ .

Using the dual basis, we can construct states which are superpositions of all loop patterns in the same connectivity class,

$$|\psi_{N_h \times N_v}(A, X = |m^*(p)\rangle)\rangle = \sum_{L \in C_p} |L\rangle 2^{n_L} \lambda^{b_L} \quad (4.16)$$

For instance, for  $p = \begin{array}{|c|} \hline \square \\ \hline \end{array}$  and  $\lambda = 1$ ,

$$|\psi_{3 \times 3}(A, X = |m^*(p)\rangle)\rangle = 2 \begin{array}{|c|c|c|} \hline \text{---} & \text{---} & \text{---} \\ \hline \end{array} + \begin{array}{|c|c|c|} \hline \text{---} & \text{---} & \text{---} \\ \hline \end{array} + \dots \quad (4.17)$$

Moreover, since  $\{|m^*(p)\rangle_p\}$  forms a basis of the space of staggered singlets (and thus of all relevant boundary conditions), we can express the PEPS obtained from any boundary condition  $X$  as

$$\begin{aligned} |\psi_{N_h \times N_v}(A, X)\rangle &= \sum_p \langle X|m(p)\rangle \sum_{L \in C_p} |L\rangle 2^{n_L} \lambda^{b_L} \\ &= \sum_p \langle X|m(p)\rangle |\psi_{N_h \times N_v}(A, |m^*(p)\rangle)\rangle \quad (4.18) \end{aligned}$$

### 4.1.2 Combinatorics of Loop Configurations

In the following, we will determine the dimension of the space

$$\mathcal{S}_{N_h \times N_v} := \text{span}\{|\psi_{N_h \times N_v}(A, X)\rangle | X \in \mathbb{C}^{2N_h + 2N_v}\} \quad (4.19)$$

of all physical configurations accessible with our tensor network. This will on the one hand be relevant when computing the entanglement entropy in Sec. 4.1.3, and on the other hand when determining the ground space degeneracy with open boundaries in Sec. 4.2. As we have just seen in Eq. (4.18),  $\mathcal{S}_{N_h \times N_v}$  is spanned exactly by the states given in (4.16).



These states are linearly independent – unless they are zero – due to the linear independence of different  $|L\rangle$  which follows from the linear independence of  $|0\rangle$  and  $|1\rangle$ . In order for Eq. (4.16) to be non-zero for a given connectivity pattern  $p$ , it must hold that  $C_p$  is non-empty. We will call connectivity patterns  $p$  for which  $C_p$  is empty *forbidden*, otherwise we call  $p$  *allowed*.

An example of a forbidden connectivity pattern on a  $2 \times 2$  patch is


(4.20)

The intuitive reason for this connectivity class to be empty is the fact that it requests too large amounts of entanglement between the upper and lower boundary of the system, more than can be mediated by the bulk: The connectivity pattern requires four maximally entangled states between top and bottom half, while the PEPS only has two bonds along that cut. If we tried to find a loop pattern that matches the connectivity pattern, we would see that the first two north-south connections fill up all available space:


(4.21)

In particular, notice that this entanglement restriction is more severe than for  $U(1)$ , cf. section 2.1.1.

In order to compute the dimension of  $\mathcal{S}_{N_h \times N_v}$ , we therefore need to determine the number of allowed connectivity patterns for that given system size, which we denote by  $\mathcal{N}(N_h, N_v)$ . It is the purpose of the remainder of this section to compute this number rigorously. Before diving into the computation, we first give the end result for its asymptotic behaviour: If we take  $N_h$  and  $N_v$  to the thermodynamic limit in a fixed aspect ratio  $N_v/N_h =: \alpha - 1$ , then the asymptotic behaviour is essentially that of the Catalan numbers<sup>1</sup>. Specifically, denoting the size of the boundary by  $N = N_h + N_v$ , we find that  $\mathcal{N}$  scales asymptotically as

$$\mathcal{N}(\alpha, N) = \frac{4^N}{N^{3/2}} \left[ k(\alpha) + \mathcal{O}\left(\frac{1}{N}\right) \right] \quad (4.22)$$

with  $k(\alpha)$  a function of the aspect ratio that is independent of  $N$ .

### Allowed Connectivity Patterns and the Canonical Loop Pattern

In this section, we give a more formal definition of what we have previously called *allowed* and *forbidden* connectivity patterns. This will set us up to rigorously count their number in the next section. The central object is the *flow* of entanglement through subsystems. We start by introducing some definitions:

#### Definition 4.1. (Lattice & Boundary)

Define

$$\mathcal{X} := \left\{ \frac{1}{2}, \frac{3}{2}, \dots, \frac{2N_h - 1}{2} \right\} \times \{0, 1, \dots, N_v\} \quad (4.23)$$

$$\mathcal{Y} := \{0, 1, \dots, N_h\} \times \left\{ \frac{1}{2}, \frac{3}{2}, \dots, \frac{2N_v - 1}{2} \right\} \quad (4.24)$$

---

<sup>1</sup>This remains true as long as one of the dimensions does not grow faster than the other dimension squared, i.e., if the patch is “square enough”.

The  $(N_h, N_v)$ -Lattice is defined as

$$\mathcal{L}_{N_h, N_v} = \mathcal{X} \cup \mathcal{Y} \quad (4.25)$$

The boundary  $\mathcal{B}_{N_h, N_v} \subset \mathcal{L}_{N_h, N_v}$  is

$$\mathcal{B}_{N_h, N_v} = \left\{ (x, y) \in \mathcal{L}_{N_h, N_v} \mid x \in \{0, N_h\} \text{ or } y \in \{0, N_v\} \right\} \quad (4.26)$$

**Definition 4.2. (Tuple Distance)**

Let  $a, b \in \mathcal{L}_{N_h, N_v}$ ,  $a \neq b$  and writing  $a = (a_x, a_y)$ ,  $b = (b_x, b_y)$ , the  $x$ -distance ( $y$ -distance) of the tuple  $(a, b)$  is

$$\begin{aligned} \Delta x(a, b) &= b_x - a_x \\ \Delta y(a, b) &= b_y - a_y \end{aligned} \quad (4.27)$$

A tuple  $(a, b)$  is

$$\begin{aligned} &\text{horizontal, if } |\Delta x(a, b)| > |\Delta y(a, b)|, \\ &\text{vertical, if } |\Delta x(a, b)| < |\Delta y(a, b)| \text{ and} \\ &\text{diagonal, if } |\Delta x(a, b)| = |\Delta y(a, b)|. \end{aligned} \quad (4.28)$$

A horizontal tuple  $(a, b)$  is *upper* if  $a_y + b_y \leq N_v$ , otherwise it is *lower*. A vertical tuple  $(a, b)$  is *left* if  $a_x + b_x \leq N_h$ , otherwise it is *right*.

We previously defined allowed and forbidden matchings by the existence of at least one compatible loop pattern. We will now give a more useful definition in terms of *Flow* and then show that the definitions are equivalent, i.e. show that for each allowed connectivity pattern as defined here there exists at least one loop pattern: the canonical loop pattern. The fact that there cannot exist a loop pattern for forbidden matchings will be easy to see with this new definition.

**Definition 4.3. (Flow)**

For  $i \in \{1, N_h - 1\}$  ( $i \in \{1, N_v - 1\}$ ) and  $a, b \in \mathcal{L}_{N_h, N_v}$ , the tuple  $(a, b)$  goes through vertical (horizontal) cut  $i$  if  $(a, b)$  is horizontal (vertical) and

$$\begin{aligned} &a_x < i \quad \text{and} \quad b_x > i \\ &(a_y < i \quad \text{and} \quad b_y > i) \end{aligned} \quad (4.29)$$

For  $p$  a connectivity pattern, the flow through vertical (horizontal) cut  $i$ , denoted by  $\text{Flow}(p, i, \text{vert})$  ( $\text{Flow}(p, i, \text{hor})$ ) is the number of bonds  $t \in p$  that go through vertical (horizontal) cut  $i$ .

**Definition 4.4. (Forbidden Matchings)**

We call a connectivity pattern  $p$  *vertically forbidden* if there exists  $i \in \{1, 2, \dots, N_h - 1\}$  such that

$$\text{Flow}(p, i, \text{vert}) \geq N_v + 1 \quad (4.30)$$

or *horizontally forbidden* if there exists  $i \in \{1, 2, \dots, N_v - 1\}$  such that

$$\text{Flow}(p, i, \text{hor}) \geq N_h + 1 \quad (4.31)$$

A connectivity pattern which is not forbidden, is *allowed*.

**Definition 4.5. (The Canonical Loop Pattern)**

Given an allowed connectivity pattern  $p = \{(a_1, b_1), \dots, (a_N, b_N)\}$ , we construct the loop pattern explicitly:

1. We start with the empty loop pattern  $L = \{\}$ .
2. (*Initial and final pieces*) For each  $t_i = (a_i, b_i)$ , determine whether it is horizontal, diagonal or vertical. If  $t_i$  is horizontal or diagonal and  $a_i(b_i) \in \mathcal{X}$  then define  $\bar{a}_i = a_i + (1/2, \pm 1/2)$  and  $\bar{b}_i = b_i + (-1/2, \pm 1/2)$ , depending on whether  $a_i(b_i)$  are located on the top or bottom boundary. Similarly, if  $t_i$  is vertical and  $a_i(b_i) \in \mathcal{Y}$ , define  $\bar{a}_i = a_i + (\pm 1/2, 1/2)$  and  $\bar{b}_i = b_i + (\pm 1/2, -1/2)$ . Else, just set  $\bar{a}_i = a_i$  and  $\bar{b}_i = b_i$ . This causes all horizontal and diagonal bonds effectively go from  $\mathcal{Y}$  to  $\mathcal{Y}$  and all vertical bonds to go from  $\mathcal{X}$  to  $\mathcal{X}$ .
3. (*Choosing a bond*) Pick a bond  $t = (a, b) \in p$ , such that all bonds inside  $t$  have been picked already. Since two path cannot be mutually inside each other, there always exists such a path, except if all bonds have been chosen. In that case, continue with step 8. Define a new partial path  $m = \{(a), \bar{a}\}$  (the brackets indicate to only add  $a$  if  $a \neq \bar{a}$ ).
4. Set  $j = 1$  and  $v_1 = \bar{a}$ .
5. If  $v_j = \bar{b}$ , add the completed path  $m = \{(a), \bar{a}, v_2, \dots, \bar{b}, (b)\}$  to  $L$  and go back to step 3. Otherwise continue with the step 6.
6. (*Diagonal partial paths*) If the pair  $(v_j, \bar{b})$  is diagonal, consider without loss of generality the case where  $x(\bar{b}) > x(v_j)$  and  $y(\bar{b}) > y(v_j)$ . Then, set  $v_{j+1} = v_j + (1/2, 1/2)$ . In the other cases, extend the path towards  $\bar{b}$  analogously. In principle,  $v_{j+1}$  could already be occupied by a path  $q$ . However, as will become clear in the next step, all paths are constructed *monotonously*, i.e. horizontal paths advance towards the right in each step and vertical paths advance towards the bottom. Therefore one can draw a horizontal (vertical) cone if  $q$  is horizontal (vertical) and the endpoints, lets call them  $a_q$  and  $b_q$  must lie inside the cone as well, one to the right (top) of  $v_{j+1}$  and one to the left (bottom). It is easy to see that the bonds  $(a_q, b_q)$  and  $(a, b)$  are crossing, violating the assumption that  $m$  is a valid matching. Add  $v_{j+1}$  to  $p$ , set  $j \leftarrow j + 1$  and go back to step 5.
7. (*All other types of partial paths*) If  $(v_j, \bar{b})$  is not diagonal, consider without loss of generality  $(a, b)$  to be a lower horizontal bond (all other cases follow analogously). By construction (see below), at any point  $(v_j, \bar{b})$  remains horizontal. Define

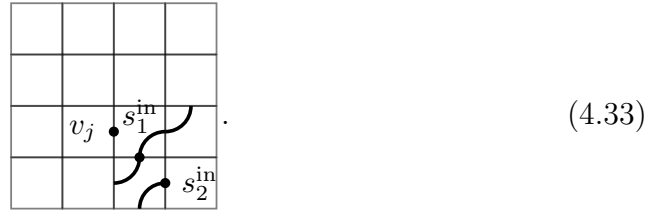
$$\begin{aligned}
 s_1^{in} &= v_j + (1/2, 1/2) \\
 s_1^{out} &= v_j + (1/2, -1/2) \\
 s_2^{in} &= s_1^{in} + (1/2, 1/2) \\
 s_2^{out} &= s_1^{out} + (1/2, -1/2)
 \end{aligned} \tag{4.32}$$

If neither of  $s_1^{in}$  and  $s_2^{in}$  is occupied or in the boundary, set  $v_{j+1} = s_1^{in}$  and  $v_{j+2} = s_2^{in}$ . Otherwise, set  $v_{j+1} = s_1^{out}$  and  $v_{j+2} = s_2^{out}$ . Add  $v_{j+1}$  and  $v_{j+2}$  to  $p$ , set  $j \leftarrow j + 1$  and go back to step 5.

Again, in principle one of  $s_1^{in}$  and  $s_2^{in}$  and one of  $s_1^{out}$  and  $s_2^{out}$  could be occupied

or in the boundary. We are now going to show that in this case  $p$  is forbidden, i.e. there is too much flow going through a horizontal/vertical line.

First, let us assume that  $s_2^{in}$  is occupied. Denote by  $q$  the path that contains  $s_2^{in}$  and call its endpoints  $(a_q, b_q)$ . Then  $q$  must be horizontal, which can be verified using the fact that  $(v_j, b)$  is horizontal. As such,  $v_j + (1/2, 3/2) \in q$ , since  $v_j$  is still free. Now we have two horizontal paths,  $p$  and  $q$ , both go through  $x(v_j)$  and their vertical distance at that point is 2. By construction, the vertical distance must remain even all the way through to the initial and final points of paths  $q$  and  $m$ , which implies that there is an odd number of boundary points between  $a_m$  and  $a_q$  and between  $b_m$  and  $b_q$ . Hence, there is one horizontal bond  $(a_r, b_r)$  that goes through  $x(s_2^{in})$  and  $(a_q, b_q)$  lies inside it. Consider now  $s_1^{in'} = s_1^{in} + (0, 1)$  and  $s_2^{in'} = s_2^{in} + (0, 1)$ . If either of them are in the boundary, the situation is depicted as



Otherwise, consider the progression from  $v_j + (1/2, 3/2)$  to  $s_2^{in}$ : It is an up-move and it is occurring in a lower horizontal path. Hence, either of  $s_1^{in'}$  or  $s_2^{in'}$  must be occupied. If  $s_2^{in'}$  is occupied, the above argument can be repeated until one reaches the boundary to find  $N_v - y(v_j) + 1/2$  horizontal bonds that go through  $x(s_2^{in})$ . If  $s_1^{in'}$  is occupied, its path must be horizontal and running parallel to  $q$ , in particular making an up-step around  $s_1^{in'}$ . Again, we can continue the argument until we arrive at the boundary. The same argument can be used if initially  $s_1^{in}$  is occupied instead of  $s_2^{in}$ . In either case, we find  $N_v - y(v_j) + 1/2$  horizontal bonds that go through  $x(s_2^{in})$ .

Now, by assumption, also either  $s_1^{out}$  or  $s_2^{out}$  is occupied. We can reverse top and bottom in the argument above to find another  $y(v_j) + 1/2$  horizontal bonds which go through  $x(s_2^{in})$ . Note, that the path that contains  $s_2^{out}$  is necessarily upper, since otherwise,  $m$  would be inside it and it could not exist yet by construction.

We have hence found  $N_v + 1$  bonds in  $p$  that go through a single vertical cut, contradicting the assumption that  $p$  is allowed.

8. (*Adding bubbles*) Now for each bond, we have created a connecting path. It is possible, however, that not all points in  $\mathcal{L}_{N_h, N_v}$  are occupied. In this case we add small bubbles to the pattern.

It remains to show that the loop pattern thus created is compatible with  $p$ , i.e. that the boundary points of all paths correspond to tuples in the connectivity pattern, or - differently phrased - for a tuple  $(a, b) \in p$ , whether the corresponding path in  $L$  starting with  $a$  can end at a point  $b' \neq b$ . By construction, once  $(v_j, b)$  becomes diagonal, it will surely have the correct ending point. Again, let us consider without loss of generality a horizontal path. Then, after  $\Delta x$  steps, the horizontal distance to the target is zero. Hence, either we have arrived at the correct ending point, or the partial path has become vertical during the construction. To become

vertical, however, the path must have gone through a point where its remainder was diagonal, hence ensuring that the correct ending point was reached. The resulting loop pattern is the *canonical loop pattern* of  $p$ .

### The number $\mathcal{N}(N_h, N_v)$

Now that we have seen that there is at least one loop pattern for each allowed connectivity pattern, we can count the forbidden connectivity patterns. We will proceed in three steps: first, we show that the problem of counting a forbidden connectivity patterns can be broken down into individually counting horizontally and vertically forbidden ones. Each of those is subsequently mapped to a *height-restricted Dyck path*. Finally, we find expressions for these combinatorial objects.

**Claim 4.1.** A connectivity pattern cannot be both horizontally and vertically forbidden.

*Proof.* Let  $p$  be a connectivity pattern and assume it is both horizontally and vertically forbidden. Then denote the vertical lines at which there is an oversaturated cut by  $x$  and  $y$ , respectively. These lines cut the patch into four areas,  $A, B, C$  and  $D$ :

$$\begin{array}{c}
 x \\
 \begin{array}{|c|c|}
 \hline
 A & B \\
 \hline
 C & D \\
 \hline
 \end{array} \\
 y
 \end{array} \tag{4.34}$$

Now if each of the bonds cuts only either the horizontal *or* vertical line, then there would need to be at least  $N_h + N_v + 2$  bonds in total, hence at least two bonds cut both lines, without loss of generality going from boundary  $A$  to boundary  $D$  in the figure. There could be more than two bonds crossing from  $A$  to  $D$  - let us denote the total number by  $\kappa$ , the lowest one by  $a$  and the highest one by  $b$ . These bonds partition the areas  $A$  and  $D$  into  $A_L, A_R$  and  $D_L, D_R$ , respectively. For their size, clearly

$$\begin{aligned}
 |A_L| + |A_R| + \kappa &\leq |A| \\
 |D_L| + |D_R| + \kappa &\leq |D|
 \end{aligned} \tag{4.35}$$

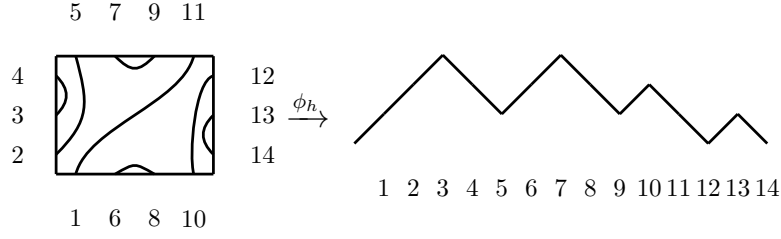
holds. There remain  $N_h - \kappa + 1$  bonds to be found for the horizontal violation and all of these must have boundary points in  $A_R$  and  $D_R$ . Similarly, there remain  $N_v - \kappa + 1$  bonds to be found for the vertical violation and all of these must have boundary points in  $A_L$  and  $D_L$ . Hence we have the inequalities

$$\begin{aligned}
 |A_L| + |D_L| &\geq N_v - \kappa + 1 \\
 |A_R| + |D_R| &\geq N_h - \kappa + 1.
 \end{aligned} \tag{4.36}$$

Adding the two inequalities and inserting inequalities (4.35), we obtain

$$|A| + |D| \geq N_v + N_h + 2 \tag{4.37}$$

and since  $|A| + |D| = N_v + N_h$ , we arrive at a contradiction.  $\square$

Figure 4.2: The mapping  $\phi_h$  for an allowed connectivity pattern

**Definition 4.6. (Dyck paths)**

A *Dyck path* or *mountain diagram* of size  $n$  is a lattice path in  $\mathbb{Z}^2$  from  $(0,0)$  to  $(2n,0)$  consisting of  $n$  up steps of the form  $(1,1)$  and  $n$  down steps of the form  $(1,-1)$  which never goes below the x-axis  $y = 0$ . The *maximal height* of a Dyck path is the maximum  $y$ -coordinate of the path. Denote all Dyck paths of size  $n$  by  $\mathcal{D}_n$ .

**Definition 4.7. (Bijection between connectivity patterns and Dyck paths)**

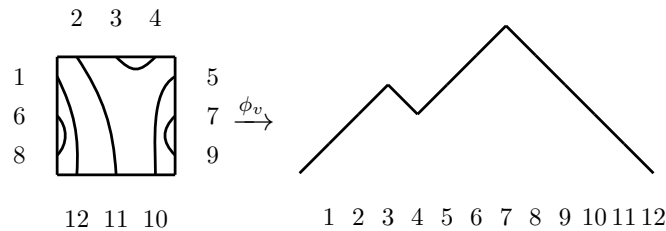
We define two maps

$$\begin{aligned}\phi_h &: (N_h, N_v)\text{-connectivity patterns} \mapsto \mathcal{D}_{N_h+N_v} \\ \phi_v &: (N_h, N_v)\text{-connectivity patterns} \mapsto \mathcal{D}_{N_h+N_v}\end{aligned}$$

The image of a given connectivity patterns  $p$  under the map  $\phi_h$  is given as follows. We start with the empty Dyck path and sequentially look at the boundary points in the order given in figure 4.2. Then, we add an up-step to the Dyck path if the partner of the boundary point we are currently reading has not been read yet. Otherwise we add a down-step. For  $\phi_v$ , we follow the same procedure with the labelling given by figure 4.3 instead.

A couple of remarks are in order:

- The resulting path is a Dyck path: For it to pierce through the x-axis, one would need to read more second halves than first halves up to a given point which is clearly impossible. Also, there is an equal number of second halves and first halves in total, so the final step ends up on the x-axis again.
- The maps  $\phi_h$  and  $\phi_v$  are bijective. The map  $\phi_h^{-1}$  reads the Dyck path sequentially from start to end, while scanning through the boundary points in the order given in figure 4.2. Whenever a down-step is encountered, a bond is added to the connectivity pattern by matching the currently active boundary point with the last open one. Again,  $\phi_v^{-1}$  works analogously with the labelling given in figure 4.3.


 Figure 4.3: The mapping  $\phi_v$  for a forbidden connectivity pattern

- For  $i \in \{1, 2, \dots, N_h - 1\}$ ,  $Flow(p, i, vert)$  is given by the height of  $\phi_h(p)$  after  $N_v + 2i$  steps. Similarly, for  $j \in \{1, 2, \dots, N_v - 1\}$ ,  $Flow(p, j, hor)$  is given by the height of  $\phi_v(p)$  after  $N_h + 2j$  steps. In particular,  $p$  is horizontally (vertically) forbidden if the maximal height of  $\phi_h(p)$  ( $\phi_v(p)$ ) is greater than  $N_h$  ( $N_v$ ).

We are now ready to give three expressions for the number of allowed matchings.

**Claim 4.2. (Number of allowed matchings)** Let  $C_n = \frac{1}{n+1} \binom{2n}{n}$  be the regular Catalan number. For a given  $N_h, N_v \in \mathbb{N}$ , the number of horizontally (vertically) forbidden connectivity pattern is given by  $C_{N_h+N_v} - f(N_h, N_v)$  ( $C_{N_h+N_v} - f(N_v, N_h)$ ), where we can give three expressions for the numbers  $f(N_h, N_v)$ :

$$\begin{aligned}
 f(N_h, N_v) &= \frac{4^N}{1 + \frac{N_h}{2}} \sum_{j=1}^{N_h+2} \sin\left(\frac{\pi j}{N_h+2}\right) \left(\cos\left(\frac{\pi j}{N_h+2}\right)\right)^{2N} \\
 &= \sum_{k \geq 1} \binom{2N}{N - k(N_h+2) - 1} - 2 \binom{2N}{N - k(N_h+2)} + \binom{2N}{N - k(N_h+2) + 1} \\
 &= \left(\frac{d}{dz}\right)^{2N} \bigg|_{z=0} \frac{1}{1 - \frac{z^2}{\ddots - \frac{1}{z^2}}}
 \end{aligned} \tag{4.38}$$

where the continued fraction has  $N_h$  instances of  $z^2$  and  $N = N_h + N_v$ . As a direct corollary, since forbidden matchings are either horizontally or vertically forbidden and the number of all matchings is  $C_{N_h+N_v}$ , we obtain the total number of allowed matchings:

$$\mathcal{N}(N_h, N_v) = f(N_h, N_v) + f(N_v, N_h) - C_{N_h+N_v}. \tag{4.39}$$

For later convenience, we will introduce  $f(N_h, \alpha)$ , with the aspect ratio  $\alpha N_v = N = N_h + N_v$ . Since the number of vertically forbidden matchings is equal to the number of horizontally forbidden matchings on a  $90^\circ$  rotated patch and a  $90^\circ$  rotation corresponds to  $\alpha \rightarrow \frac{\alpha}{\alpha-1}$ , we can rewrite equation (4.39) as

$$\mathcal{N}(N_h, \alpha) = f(N_h, \alpha) + f\left(N_h, \frac{\alpha}{\alpha-1}\right) - C_{\alpha N_h}. \tag{4.40}$$

*Proof.* Let  $N_h, N_v \in \mathbb{N}$ . We are going to count the horizontally allowed connectivity pattern and show that they are equal to  $C_{N_h+N_v} - f(N_h, N_v)$ . From the definition of Dyck paths, we need to count all mountain diagrams of half-length  $N_h + N_v$  whose maximum height exceeds  $N_h$ . To this end, we set up a sequence of counting vectors  $v_i \in \mathbb{N}^{N_h+1}$ . After  $n$  steps, we would like the number of paths with height  $h$  that never exceed  $N_h$  in height to be given by  $(v_n)_h$ . Hence, set  $v_0 = (1, 0, \dots, 0)$ , indicating a single path with height 0, the empty path. Now we are going to sequentially apply linear operations

$$v_{i+1} = M v_i, \tag{4.41}$$

for  $i \in \{1, \dots, 2N\}$ , where  $M$  is an  $N_{h+1} \times N_{h+1}$ -matrix, defined as

$$M = \begin{bmatrix} 0 & 1 & & \\ 1 & \ddots & \ddots & \\ & \ddots & \ddots & 1 \\ & & 1 & 0 \end{bmatrix} \tag{4.42}$$

For each existing path of length  $n$  and height  $h$ , the matrix  $M$  has the effect of creating two new paths of height  $h + 1$  and  $h - 1$ , while automatically cutting off paths with height greater than  $N_h$  and smaller than 0.

Finally, the vector  $v_{2N_h+2N_v}$  contains the number of paths of all heights after  $2N_h + 2N_v$  steps, out of which we are only interested in proper Dyck paths, the number of which is stored in  $(v_{2N})_1 = (M^{2N}v_0)_1$ . The matrix  $M$  is a tridiagonal Toeplitz matrix with eigenvalues  $D_j = 2 \cos \left( \frac{\pi j}{N_h+2} \right)$  and eigenvectors  $S_{ij} = \frac{1}{\sqrt{1+\frac{N_h}{2}}} \sin \left( \frac{\pi i j}{N_h+2} \right)$ . Since  $S$  is orthogonal,

$$\begin{aligned} (M^{2N}v_0)_1 &= \sum_{j=1}^{N_h+2} S_{1j} D_j^{2N} (S^{-1})_{j1} \\ &= \sum_{j=1}^{N_h+2} (S_{1j})^2 D_j^{2N} \\ &= f(N_h, N_v) \end{aligned} \quad (4.43)$$

The second form is an application of the combinatorics of *watermelons* [128]. For the last expression, we allude to a tool from analytical combinatorics, the *symbolic method* [52]. Assume that we want to calculate the number  $b_n$  of binary words of length  $n$ . Then we can write down a combinatorial equation

$$B = \underbrace{\epsilon}_{\text{empty word}} \cup \underbrace{B \times 0}_{\text{append a zero}} \cup \underbrace{B \times 1}_{\text{append a one}} \quad (4.44)$$

meaning “A binary word is either the empty word or a binary word ending on zero or a binary word ending on one”. The machinery of the symbolic method teaches us to translate this equation into a generating function

$$\begin{aligned} B(z) &= 1 + zB(z) + zB(z) \Rightarrow \\ B(z) &= \frac{1}{1-2z} \\ &= \sum_{n \geq 0} 2^n z^n \end{aligned} \quad (4.45)$$

such that we can extract the numbers  $b_n = (d/dz)^{2N} B(z)|_{z=0}$  from the coefficients of the Taylor series. To calculate the number  $D_{2n}$  of Dyck paths of length  $2n$ , we use *the first passage decomposition*:

$$D = \underbrace{\epsilon}_{\text{empty path}} \cup \underbrace{\uparrow \times D \times \downarrow D}_{\substack{\text{an up-step followed by a Dyck path,} \\ \text{a down-step and another Dyck path}}} \quad (4.46)$$

meaning “A Dyck path is either empty or an up-step followed by a Dyck path, a down-step and another (possibly empty) Dyck path”. Similarly, this translates to

$$\begin{aligned} D(z) &= 1 + zD(z)zD(z) \Rightarrow \\ D(z) &= \frac{1 - \sqrt{1-4z}}{2z} \\ &= \sum_{n \geq 0} C_n z^{2n} \end{aligned} \quad (4.47)$$



where  $C_n$  is the  $n$ -th Catalan number. Finally, to obtain a generating function  $D_h(z)$  for the number of Dyck paths with maximal height  $h$ , we start with  $D_0(z) = 1$ , since there is exactly one path with length zero: the empty path. Again, we decompose the path to the left and right of its first passage of zero:

$$\begin{aligned} D_h(z) &= 1 + zD_{h-1}(z)zD_h(z) \quad \Rightarrow \\ D_h(z) &= \frac{1}{1 - \frac{z^2}{1 - \frac{z^2}{\ddots - \frac{1}{z^2}}}} \\ &= \sum_{N_v \geq 0} f(h, N_v) z^{2(h+N_v)} \end{aligned} \tag{4.48}$$

□

Finally, we determine the asymptotic number of allowed matchings, if the system grows to the thermodynamic limit in a fixed aspect ratio. Namely, we want to show that

$$\mathcal{N}(N, \alpha) = \frac{4^N}{N^{3/2}} \left[ k(\alpha) + \mathcal{O}\left(\frac{1}{N}\right) \right] \tag{4.49}$$

cf. equation (4.40) with the function  $k(\alpha)$  given by

$$k(\alpha) = \frac{\sqrt{\pi}}{2} + \frac{\sqrt{\pi}}{2}(\alpha - 1)^{3/2} - \pi^{-1/2} \tag{4.50}$$

In order to calculate  $\mathcal{N}(N_h, \alpha)$ , it is sufficient to compute the asymptotic behaviour of  $f(N, \alpha)$  since the vertically forbidden loop patterns can be transformed into horizontally forbidden ones under the  $90^\circ$  rotation  $\alpha \rightarrow \frac{\alpha}{\alpha-1}$ . The asymptotic behaviour of the Catalan numbers is known to be  $4^N/N^{3/2}\sqrt{\pi}$ . It remains to calculate the expression

$$g(N_h, \alpha) := \sqrt{N_h} \sum_{j=1}^{N_h+2} \sin\left(\frac{\pi j}{N_h+2}\right) \cos\left(\frac{\pi j}{N_h+2}\right)^{2N} \tag{4.51}$$

First observe that the summand is symmetric around  $j = \frac{N_h+2}{2}$  (if  $N_h$  is odd, we can omit the  $(\lceil \frac{N_h+2}{2} \rceil)$ th term from the sum as this term is exponentially small in  $N_h$ ). Therefore

$$g(N_h, \alpha) := 2\sqrt{N_h} \sum_{j=1}^{N_h+2/2} \sin\left(\frac{\pi j}{N_h+2}\right) \cos\left(\frac{\pi j}{N_h+2}\right)^{2\alpha N_h} \tag{4.52}$$

We will proceed with the computation of the sum in four steps. First, we will truncate the sum, using the exponential suppression of terms with  $j$  on the order of  $N_h$ . Second, we will replace the cosine by a Gaussian. Third, we Taylor expand the sine and finally, we replace the sum by an integral that we can compute analytically. All of these approximations induce an error  $\mathcal{O}(1/N)$ .

Let us now establish the relevant claims:

**Claim 4.3. (Truncation of the sum)**

$$\sqrt{N} \sum_{j=\lfloor N/\pi \rfloor}^{N/2} \sin^2 \left( \frac{\pi j}{N} \right) \cos^{2\alpha N} \left( \frac{\pi j}{N} \right) = \mathcal{O} \left( N^{3/2} 2^{-\alpha N} \right) \quad (4.53)$$

*Proof.* For  $j$  in the interval  $[\lfloor N/\pi \rfloor, N/2]$ , for  $N$  large enough we have that  $j\pi/N \geq \pi/4$  and therefore

$$\begin{aligned} \sqrt{N} \sum_{j=\lfloor N/\pi \rfloor}^{N/2} \sin^2 \left( \frac{\pi j}{N} \right) \cos^{2\alpha N} \left( \frac{\pi j}{N} \right) &\leq \sqrt{N} \sum_{j=\lfloor N/\pi \rfloor}^{N/2} \sin^2 \left( \frac{\pi j}{N} \right) \cos^{2\alpha N} (\pi/4) \\ &= \sqrt{N} \sum_{j=\lfloor N/\pi \rfloor}^{N/2} \sin^2 \left( \frac{\pi j}{N} \right) 2^{-\alpha N} \\ &\leq N^{3/2} 2^{-\alpha N} \end{aligned} \quad (4.54)$$

□

To clean up notation in preparation for the next step, we define

$$e_2(N) := \sqrt{N} \sum_{j=1}^{\lfloor N/\pi \rfloor} \sin^2 \left( \frac{\pi j}{N} \right) \left[ e^{-\alpha N \left( \frac{\pi j}{N} \right)^2} - \cos^{2\alpha N} \left( \frac{\pi j}{N} \right) \right] \quad (4.55)$$

**Claim 4.4. (A cosine raised to a high power becomes a Gaussian)**

$$e_2(N) = \mathcal{O} \left( \frac{1}{N} \right) \quad (4.56)$$

*Proof.* For simplicity, define  $x_j = \frac{\pi j}{N}$  and  $M = 2\alpha N$ . Using  $\cos(x) \geq 1 - \frac{1}{2}x^2 > 0$  in the interval  $x \in [0, 1]$  and the fact that each term in the sum is positive, we have:

$$\begin{aligned} e_2(N) &\leq \sqrt{N} \sum_{j=1}^{\lfloor N/\pi \rfloor} \sin^2(x_j) \left[ e^{-\frac{x_j^2}{2}M} - \left( 1 - \frac{1}{2}x_j^2 \right)^M \right] \\ &= \sqrt{N} \sum_{j=1}^{\lfloor N/\pi \rfloor} \sin^2(x_j) \left[ e^{-\frac{x_j^2}{2}M} - \left( 1 - \frac{\frac{1}{2}x_j^2 M}{M} \right)^M \right] \end{aligned} \quad (4.57)$$

Since  $\frac{1}{2}x_j^2 < 1$ , we can use the inequality  $\left( 1 - \frac{\frac{1}{2}x_j^2 M}{M} \right)^M \geq e^{-\frac{x_j^2}{2}M \left( \frac{1 - \frac{1}{2}x_j^2}{1 - \frac{x_j^2}{2}} \right)}$ , combined

with  $0 < \sin(x_j) < x_j$  and  $e^{-y} \geq 1 - y$  to arrive at

$$\begin{aligned}
 e_2(N) &\leq \sqrt{N} \sum_{j=1}^{\lfloor N/\pi \rfloor} x_j^2 \left[ e^{-\frac{x_j^2 M}{2}} - e^{-\frac{x_j^2}{2} M \frac{1}{1 - \frac{x_j^2}{2}}} \right] \\
 &= \sqrt{N} \sum_{j=1}^{\lfloor N/\pi \rfloor} x_j^2 e^{-\frac{x_j^2 M}{2}} \left[ 1 - e^{\frac{x_j^2}{2} M \left( 1 - \frac{1}{1 - \frac{x_j^2}{2}} \right)} \right] \\
 &\leq \sqrt{N} \sum_{j=1}^{\lfloor N/\pi \rfloor} x_j^2 e^{-\frac{x_j^2 M}{2}} \left( -\frac{x_j^2}{2} M \left( 1 - \frac{1}{1 - \frac{x_j^2}{2}} \right) \right) \\
 &\leq \frac{\sqrt{N} M}{2} \sum_{j=1}^{\lfloor N/\pi \rfloor} x_j^6 e^{-\frac{x_j^2 M}{2}} \underbrace{\frac{1}{1 - \frac{x_j^2}{2}}}_{\leq 2} \\
 &\leq N^{5/2} \frac{2\alpha}{\pi} \frac{1}{\lfloor N/\pi \rfloor} \sum_{j=1}^{\lfloor N/\pi \rfloor} x_j^6 e^{-\frac{x_j^2 M}{2}}
 \end{aligned} \tag{4.58}$$

The sum is the right Riemann sum of the function  $f(x) = \pi^2 x^6 e^{-x^2 \alpha N \pi^2}$ , with an error given by

$$\left| \frac{1}{\lfloor N/\pi \rfloor} \sum_{j=1}^{\lfloor N/\pi \rfloor} x_j^6 e^{-\frac{x_j^2 M}{2}} - \int_0^1 \pi^2 x^6 e^{-x^2 \alpha N \pi^2} dx \right| \leq \frac{d_{\max}}{2\lfloor N/\pi \rfloor}, \tag{4.59}$$

where  $d_{\max}$  is the maximum of the derivative  $f'(x)$  in the interval  $[0, 1]$ . A direct calculation reveals that

$$d_{\max} = c(N\alpha)^{-5/2} \tag{4.60}$$

for some constant  $c$ . Plugging (4.60) and (4.59) into (4.58) yields

$$\begin{aligned}
 e_2(N) &= N^{5/2} 2\alpha\pi \int_0^1 x^6 e^{-x^2 \alpha N} dx + \mathcal{O}\left(\frac{1}{N}\right) \\
 &\leq N^{5/2} 2\alpha\pi \int_0^\infty x^6 e^{-x^2 \alpha N} dx + \mathcal{O}\left(\frac{1}{N}\right) \\
 &= N^{5/2} 2\alpha\pi \frac{15\sqrt{\pi}}{16} (N\alpha\pi^2)^{-7/2} + \mathcal{O}\left(\frac{1}{N}\right) \\
 &= \mathcal{O}\left(\frac{1}{N}\right)
 \end{aligned} \tag{4.61}$$

□

**Claim 4.5. (Replacing the sine)**

$$\sqrt{N} \sum_{j=1}^{\lfloor N/\pi \rfloor} e^{-\alpha N \left(\frac{\pi j}{N}\right)^2} \left[ \sin^2\left(\frac{\pi j}{N}\right) - \left(\frac{\pi j}{N}\right)^2 \right] = \mathcal{O}\left(\frac{1}{N}\right) \tag{4.62}$$

*Proof.* Taylor expanding the sine yields

$$\sin^2(x) = x^2 - \frac{1}{3} \cos(2\xi)x^4 \quad (4.63)$$

for some  $\xi \in [0, x]$ . Plugging (4.63) into (4.62) and using a Riemann sum bound akin to (4.59) leads to

$$\begin{aligned} \sqrt{N} \sum_{j=1}^{\lfloor N/\pi \rfloor} e^{-\alpha N \left(\frac{\pi j}{N}\right)^2} \left[ \sin^2\left(\frac{\pi j}{N}\right) - \left(\frac{\pi j}{N}\right)^2 \right] &\leq \sqrt{N} \sum_{j=1}^{\lfloor N/\pi \rfloor} e^{-\alpha N \left(\frac{\pi j}{N}\right)^2} \left(\frac{\pi j}{N}\right)^4 \\ &\leq N^{3/2} \pi^2 \int_0^1 x^4 e^{-\alpha N x^2 \pi^2} dx \\ &\leq N^{3/2} \pi^2 \int_0^\infty x^4 e^{-\alpha N x^2 \pi^2} dx \\ &\leq N^{3/2} \pi^2 \frac{3}{8} \sqrt{\pi} (\alpha \pi^2 N)^{-5/2} \\ &= \mathcal{O}\left(\frac{1}{N}\right) \end{aligned} \quad (4.64)$$

□

**Claim 4.6. (Computation of the integral)**

$$\sqrt{N} \sum_{j=1}^{\lfloor N/\pi \rfloor} x_j^2 e^{-\alpha N x_j^2} := \frac{\sqrt{\pi}}{4\alpha^{3/2}} + \mathcal{O}\left(\frac{1}{N}\right) \quad (4.65)$$

*Proof.* The usual bound for the Riemann sum (4.59) implies

$$\begin{aligned} \sqrt{N} \sum_{j=1}^{\lfloor N/\pi \rfloor} x_j^2 e^{-\alpha N x_j^2} &= \sqrt{N} \lfloor N/\pi \rfloor \frac{1}{\lfloor N/\pi \rfloor} \sum_{j=1}^{\lfloor N/\pi \rfloor} x_j^2 e^{-\alpha N x_j^2} \\ &= \sqrt{N} \lfloor N/\pi \rfloor \pi^2 \int_0^1 x^2 e^{-\alpha N x^2 \pi^2} dx + \mathcal{O}\left(\frac{1}{N}\right) \end{aligned} \quad (4.66)$$

We can extend the integral to infinity by noting that  $x^2 \leq x e^{x^2}$ :

$$\begin{aligned} \int_1^\infty x^2 e^{-\alpha N x^2} dx &\leq \int_1^\infty x e^{1-\alpha N x^2} dx \\ &= \frac{e^{-\alpha N + 1}}{2(\alpha N - 1)} \\ &= \mathcal{O}(e^{-N}), \end{aligned} \quad (4.67)$$

implying that

$$\begin{aligned} \sqrt{N} \sum_{j=1}^{\lfloor N/\pi \rfloor} x_j^2 e^{-\alpha N x_j^2} &= \sqrt{N} \lfloor N/\pi \rfloor \pi^2 \int_0^\infty x^2 e^{-\alpha N x^2 \pi^2} dx + \mathcal{O}\left(\frac{1}{N}\right) \\ &= \sqrt{N} \lfloor N/\pi \rfloor \pi^2 \frac{\sqrt{\pi}}{4(\alpha N \pi^2)^{3/2}} + \mathcal{O}\left(\frac{1}{N}\right) \\ &= \frac{\sqrt{\pi}}{4\alpha^{3/2}} + \mathcal{O}\left(\frac{1}{N}\right) \end{aligned} \quad (4.68)$$

□

**Corollary 4.1.**

$$g(N_h, \alpha) = \frac{\sqrt{\pi}}{2\alpha^{3/2}} + \mathcal{O}\left(\frac{1}{N_h}\right) \quad (4.69)$$

*Proof.* This follows directly from the four previous claims.  $\square$

**Corollary 4.2.**

$$\mathcal{N}(\alpha, N) = \frac{4^N}{N^{3/2}} \left[ k(\alpha) + \mathcal{O}\left(\frac{1}{N}\right) \right] \quad (4.70)$$

*Proof.* For large  $N$ , we have

$$\begin{aligned} \mathcal{N}(\alpha, N) &= 4^N \left[ N_h^{-3/2} g(N_h, \alpha) + N_h^{-3/2} g\left(N_h, \frac{\alpha}{\alpha-1}\right) - N^{-3/2} \pi^{-1/2} \right] \\ &= 4^N \left[ N_h^{-3/2} \frac{\sqrt{\pi}}{2\alpha^{3/2}} + N_h^{-3/2} \frac{\sqrt{\pi}}{2\frac{\alpha}{\alpha-1}^{3/2}} - N^{-3/2} \pi^{-1/2} \right] \\ &= \frac{4^N}{N^{3/2}} \left[ \frac{\sqrt{\pi}}{2} + \frac{\sqrt{\pi}}{2} (\alpha-1)^{3/2} - \pi^{-1/2} + \mathcal{O}\left(\frac{1}{N}\right) \right] \end{aligned}$$

$\square$

### 4.1.3 Entanglement Entropy

We are now ready to determine the scaling behavior of the entanglement in our model. To this end, consider a partition of the  $N_h \times N_v$ -torus into a (small) rectangle  $Q$  of size  $L_h \times L_v$ , and the (large) rest  $R$ . Our goal is to determine the zero Renyi entropy  $S_0(\rho_Q)$  of the reduced state on  $Q$ , this is, the logarithm of the Schmidt rank of  $|\psi_{N_h \times N_v}(A, \text{PBC})\rangle$  in said partition. To this end, note that by construction

$$|\psi_{N_h \times N_v}(A, \text{PBC})\rangle = (\Psi_Q \otimes \Psi_R) |\phi^+\rangle^{|\partial Q|}, \quad (4.71)$$

where  $\Psi_Q$  is the linear map  $|\psi_{L_h \times L_v}(A, \bullet)\rangle$  from the boundary to the bulk in  $Q$  and correspondingly for  $\Psi_R$ , and the  $|\phi^+\rangle^{|\partial Q|}$  are placed along the boundary between  $Q$  and  $R$  which has length  $|\partial Q| = 2L_h + 2L_v =: L$ .

As we have seen in the section 4.1.1, the map  $\Psi_Q$  provides a bijection between the space  $\mathcal{V}_{\text{allowed}}$  spanned by all  $|m^*(p)\rangle$  with  $p$  an allowed matching, and its image  $\mathcal{S}_{L_h \times L_v}$ . If  $\Psi_R$  is also bijective between the full staggered spin-0 space  $\mathcal{V}_0$  and its image in  $R$ , then  $|\psi_{N_h \times N_v}(A, \text{PBC})\rangle$  equals  $(\Pi_{\mathcal{V}_{\text{allowed}}} \otimes \Pi_{\mathcal{V}_0}) |\phi^+\rangle^{|\partial Q|}$ , which has Schmidt rank equal to  $\dim \mathcal{V}_{\text{allowed}} = \mathcal{N}(L_h, L_v)$ . Using (4.22), we obtain that for a fixed aspect ratio of  $Q$ ,  $S_0(\rho_Q)$  scales as

$$S_0(\rho_Q) = L \log 2 - \frac{3}{2} \log(L/2) + \log k + \mathcal{O}\left(\frac{1}{L}\right) \quad (4.72)$$

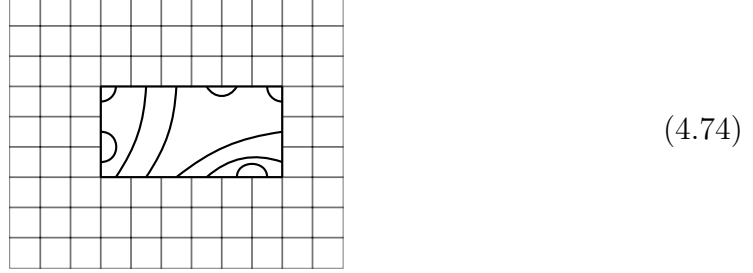
with a non-universal constant  $\log k$  that depends on the aspect ratio of  $Q$ .

It remains to show that the matrix  $\Psi_R : V_{\text{matchings}} \mapsto V_{\text{loops}}^B$  is indeed bijective. We will now demonstrate this assuming that  $Q$  is sufficiently small as in that case there are no forbidden matchings. Intuitively, this follows from the fact that forbidden matchings arise due to space constraints at the corners, and the region  $Q$  is concave.

More precisely, if the size of the rectangular hole is  $L_h \times L_v$  and the torus is  $N_h \times N_v$ , then we require

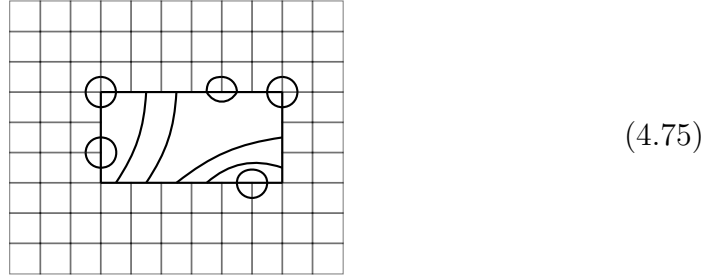
$$\min\{N_h, N_v\} > \frac{3}{2}(L_h + L_v) \quad (4.73)$$

The kernel of  $\Psi_R$  is non-empty if and only if for every connectivity pattern, there exists a loop pattern on  $R$  that is compatible with it. The following procedure produces such a loop pattern for an arbitrary inside connectivity pattern.

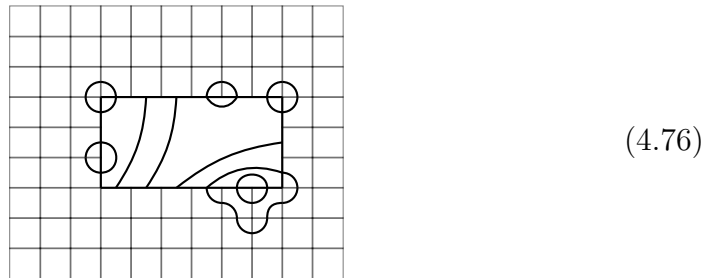


Since we work on the torus, we can draw the rectangle in the center of our lattice.

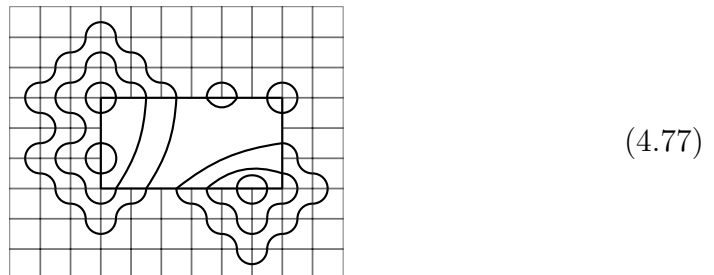
1. Close any nearest neighbours in a minimal way (as shown in the figures). Clearly, these cannot interfere with each other. This can be done within one tile from the hole.



2. Remove the connected pairs from the connectivity pattern. There must necessarily be at least one newly formed nearest neighbour pair. Connect these minimally, avoiding the bonds that are already closed. This can be done within two tiles from the hole.



3. Again remove the connected pairs from the connectivity pattern, creating new nearest neighbours. As long as there is enough space on the torus, these pairs can be closed minimally. For each nested bond, one more tile of space is needed



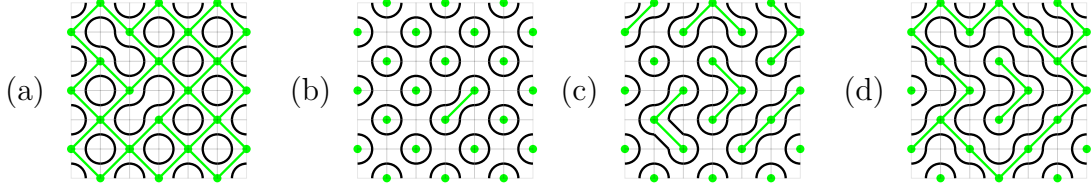


Figure 4.4: Typical configurations in the Fortuin-Kasteleyn expansion of the partition function of the Potts model. The green lines correspond to the clusters in the expansion. Each cluster configuration is associated with a unique loop pattern. (a) A typical configuration of the Potts model in the ordered phase, (b) a typical configuration in the disordered phase, (c) the Potts model at the phase transition point for  $Q > 4$ , (d) for values  $Q \leq 4$ . Only for the latter, loops of all length scales occur, whereas the bounded loop length in all other cases corresponds to a finite correlation length.

#### 4. Fill the rest of the loop pattern arbitrarily

For a hole of size  $L_h \times L_v$ , there can be at most  $\lceil \frac{L_h + L_v}{2} \rceil$  nested bonds. Therefore, if  $\min\{N_h, N_v\} > \frac{3}{2}(L_h + L_v)$ , then there is enough space in every direction for the above procedure to generate a compatible loop pattern.

### 4.1.4 Physical Interpretation of the State

In this section, we address the physical nature of our PEPS. This is most easily understood working in a sublattice rotated frame, i.e., after applying a Pauli- $X$  rotation on the B-sublattice. For  $\lambda = 0$ , we obtain a simple the classical state with a maximum number of bubbles (Fig. 4.4(a)). The other extreme,  $\lambda \rightarrow \infty$  corresponds to simply shifting that state by one lattice site (Fig. 4.4(b)) (shifting in the horizontal or vertical directions is equivalent). The nature of the state for finite  $\lambda$  can be inferred from mapping the norm of the state to the partition function of a classical  $Q$ -Potts model with  $Q = 16$ . In this mapping, which we will carry out in detail later in this section, the loops surround clusters of Potts spins that are aligned. Therefore,  $\lambda$  acquires the role of temperature in the Potts model with  $\lambda = 0$  corresponding to the perfectly ordered state. The most interesting case of  $\lambda = 1$  corresponds precisely to the phase transition in the Potts model. The transition is known to be of first-order in which regions of order (ABAB plaquettes) and disorder (BABA plaquettes) coexist. In particular, even at the transition, there is a characteristic length scale in the Potts model which translates to an exponential suppression of long loops in the PEPS.

Let us now establish such a mapping rigorously. Concretely, we will show that the staggered magnetization of the PEPS

$$\tilde{\sigma}_z(\vec{x}) := \begin{cases} \sigma_z(\vec{x}) & \text{if } \vec{x} \text{ is on the even sublattice} \\ -\sigma_z(\vec{x}) & \text{if } \vec{x} \text{ is on the odd sublattice} \end{cases} \quad (4.78)$$

is equal to an appropriately defined observable in the standard Potts model and decays exponentially even at  $\lambda = 1$ . In (4.78) and in the following we say that a plaquette  $\vec{x} = (x_1, x_2)$  is on the even (odd) sublattice if  $x_1 + x_2$  is even (odd). We refer to the  $\lambda = 1$ -PEPS simply by  $|\psi\rangle$ .

**Claim 4.7. (Exponential Decay of Staggered Magnetization)**

The correlator

$$C[\vec{x}, \vec{y}] := \frac{\langle \psi | \tilde{\sigma}_z(\vec{x}) \tilde{\sigma}_z(\vec{y}) | \psi \rangle}{\langle \psi | \psi \rangle} - \frac{\langle \psi | \tilde{\sigma}_z(\vec{x}) | \psi \rangle \langle \psi | \tilde{\sigma}_z(\vec{y}) | \psi \rangle}{\langle \psi | \psi \rangle^2} \quad (4.79)$$

decays exponentially.

*Proof.* Consider a classical  $Q$ -state Potts model with spins residing on the vertices of the *net lattice*. The net lattice is a square lattice rotated by  $45^\circ$  where the distance between the vertices is increased by a factor  $\sqrt{2}$  (the vertices are marked with green dots in figure 4.4). The classical spins take values  $\sigma \in \{1, \dots, Q\}$ . The Hamiltonian of the model is given by

$$H = - \sum_{\langle ij \rangle} \delta(\sigma_i, \sigma_j) \quad (4.80)$$

where  $\langle ij \rangle$  indicates nearest neighbours on the net lattice. For a plaquette of the original square lattice located at  $\vec{x}$ , define by  $\vec{x}_a$  and  $\vec{x}_b$  the two spins adjacent to that plaquette (the order will not matter for our purposes). Define the following “link” observable in the Potts model that acts on two spins

$$O_{\vec{x}}(\{\sigma\}) := \begin{cases} 1 & \text{if } \sigma_{\vec{x}_a} = \sigma_{\vec{x}_b} \\ \frac{1+Q}{1-Q} & \text{if } \sigma_{\vec{x}_a} \neq \sigma_{\vec{x}_b} \end{cases} \quad (4.81)$$

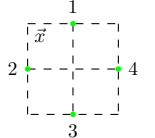
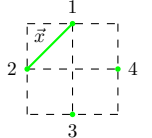
Note that  $\langle O \rangle = 1$  for perfect order and  $\langle O \rangle = -1$  for perfect disorder just as expected from the intuitive picture. Second, this link observable does *not* correspond to the usual observable in the Potts model. For example, the correlator  $\langle \sigma_{\vec{x}} \sigma_{\vec{y}} \rangle$  would be a four-point correlation function in terms of the Potts spin variables. On the other hand, usual Potts spin-spin correlators correspond to *non-local* correlators in the PEPS, namely asking whether two points lie on the same loop.

Consider the expectation value of  $O_{\vec{x}}$  in such a Potts model at inverse temperature  $\beta$ :

$$\begin{aligned} \langle O_{\vec{x}} \rangle &= \frac{1}{Z} \sum_{\{\sigma\}} O_{\vec{x}}(\{\sigma\}) \prod_{\langle ij \rangle} e^{-\beta \delta(\sigma_i, \sigma_j)} \\ &= \frac{1}{Z} \sum_{\{\sigma\}} O_{\vec{x}}(\{\sigma\}) \prod_{\langle ij \rangle} [1 + v \delta(\sigma_i, \sigma_j)], \end{aligned} \quad (4.82)$$

where  $v = e^\beta - 1$ . We now expand the product in the spirit of the Fortuin-Kasteleyn expansion [129, 130], yielding  $2^E$  terms, where  $E$  is the number of edges of the net lattice.

$$\dots = \frac{1}{Z} \left( \underbrace{\sum_{\{\sigma\}} O_{\vec{x}}(\{\sigma\})}_{\text{Diagram 1}} + v \underbrace{\sum_{\{\sigma\}} O_{\vec{x}}(\{\sigma\}) \delta(\sigma_1, \sigma_2) + \dots}_{\text{Diagram 2}} \right) \quad (4.83)$$

Here we have associated subgraphs  $G'$  of the net lattice  $G$  to each of the terms in the expansion, where  $G'$  has an edge between  $i$  and  $j$  if the expansion term contains



$\delta(\sigma_i, \sigma_j)$ . Let us investigate each sum individually. The first sum runs over  $Q^4$  configurations. In  $Q^3$  of those,  $\sigma_{\vec{x}_a} = \sigma_{\vec{x}_b}$ , implying  $O_{\vec{x}}(\{\sigma\}) = 1$ . In the other  $Q^3(Q-1)$  terms,  $\sigma_{\vec{x}_a} \neq \sigma_{\vec{x}_b}$  and  $O_{\vec{x}}(\{\sigma\}) = (1+Q)/(1-Q)$ . Therefore, the sum evaluates to

$$\sum_{\{\sigma\}} O_{\vec{x}}(\{\sigma\}) = Q^3 + Q^3(Q-1) \frac{1+Q}{1-Q} = -Q^4 \quad (4.84)$$

The second sum contains  $Q^3$  configurations and because there is a  $\delta$ -function between spins 1 and 2,  $\sigma_{\vec{x}_a} = \sigma_{\vec{x}_b}$  in all of them,

$$\sum_{\{\sigma\}} O_{\vec{x}}(\{\sigma\}) \delta(\sigma_1, \sigma_2) = Q^3 \quad (4.85)$$

Adding all these of contributions yields

$$\langle O_{\vec{x}} \rangle = \frac{1}{Z} \sum_{G' \subseteq G} Q^{n(G')} v^{b(G')} \tilde{O}_{\vec{x}}(G') \quad (4.86)$$

where  $n(G')$  is the number of connected components in  $G'$ ,  $b(G')$  is the number of bonds and

$$\tilde{O}_{\vec{x}}(G') = \begin{cases} 1 & \text{if } G' \text{ has a link at } \vec{x} \\ -1 & \text{otherwise} \end{cases} \quad (4.87)$$

Each subgraph  $G'$  of the net lattice can be associated to a unique loop pattern  $L(G')$  on the square lattice (figure 4.4), such that for the number of closed loops we have

$$n_{L(G')} = n(G') + c(G') \quad \text{and} \quad (4.88)$$

$$\tilde{O}_{\vec{x}}(G') = \langle L(G') | \tilde{\sigma}_z(\vec{x}) | L(G') \rangle, \quad (4.89)$$

where  $c(G')$  is the number of circuits in  $G'$ . Plugging Euler's relation

$$n(G') = c(G') - b(G') - V, \quad (4.90)$$

with  $V$  the number of vertices in  $G$  and (4.88) into (4.86) yields

$$\begin{aligned} \langle O_{\vec{x}} \rangle &= \frac{1}{Z} \sum_{G' \subseteq G} \sqrt{Q}^{n(G')} \sqrt{Q}^{n(G')} v^{b(G')} \tilde{O}_{\vec{x}}(G') \\ &= \frac{\sqrt{Q}^{-V}}{Z} \sum_{G' \subseteq G} \sqrt{Q}^{n(G')+c(G')} \left( \frac{v}{\sqrt{Q}} \right)^{b(G')} \tilde{O}_{\vec{x}}(G') \\ &= \frac{\sum_L \sqrt{Q}^{n_L} \left( \frac{v}{\sqrt{Q}} \right)^{b(G')} \langle L | \tilde{\sigma}_z(\vec{x}) | L \rangle}{\sum_L \sqrt{Q}^{n_L} \left( \frac{v}{\sqrt{Q}} \right)^{b(G')}} \\ &\xrightarrow{\beta \rightarrow \log(1+\sqrt{Q})} \frac{\sum_L \sqrt{Q}^{n_L} \langle L | \tilde{\sigma}_z(\vec{x}) | L \rangle}{\sum_L \sqrt{Q}^{n_L}} \\ &\xrightarrow{Q \rightarrow 16} \frac{\langle \psi | \tilde{\sigma}_z(\vec{x}) | \psi \rangle}{\langle \psi | \psi \rangle} \end{aligned} \quad (4.91)$$

This argument can be repeated for the correlator

$$\langle O_{\vec{x}} O_{\vec{y}} \rangle = \frac{\langle \psi | \tilde{\sigma}_z(\vec{x}) \tilde{\sigma}_z(\vec{y}) | \psi \rangle}{\langle \psi | \psi \rangle}, \quad (4.92)$$

thereby showing that

$$C[\vec{x}, \vec{y}] = \langle O_{\vec{x}} O_{\vec{y}} \rangle - \langle O_{\vec{x}} \rangle \langle O_{\vec{y}} \rangle, \quad (4.93)$$

i.e. the staggered  $\sigma_z$  correlation function in the  $\lambda = 1$ -PEPS equal to the link-link correlation of a classical  $Q = 16$  Potts model at  $\beta = \log(1 + \sqrt{Q})$ . The model is known to undergo a phase transitions at that point for all values of  $Q$ . While this transition is critical for  $Q \leq 4$  [131–139], it is of first order for  $Q > 4$  [140, 141], implying that the local correlator (4.93) decays exponentially.  $\square$

A more general, alternative proof invokes the mapping between the norm of the PEPS to a Potts partition function. To this end, define the tensor network using tensors (4.6) with independent variables on every site, i.e.:

$$|\psi(\lambda_{(1,1)}, \lambda_{(1,2)}, \dots, \lambda_{(N_h, N_v)})\rangle =: |\psi(\vec{\lambda})\rangle, \quad (4.94)$$

Taking derivatives with respect to different  $\lambda$  will yield the expectation value of some local diagonal operator acting on e.g., one site,  $D_{\text{PEPS}}(\vec{x})$

$$\frac{\partial}{\partial \lambda_{\vec{x}}} \log \langle \psi(\vec{\lambda}) | \psi(\vec{\lambda}) \rangle = \frac{\langle \psi(\vec{\lambda}) | D_{\text{PEPS}}(\vec{x}) | \psi(\vec{\lambda}) \rangle}{\langle \psi | \psi \rangle} \quad (4.95)$$

Introducing the effective coupling strengths  $\vec{\beta}$  via

$$\lambda_{\vec{x}} = \begin{cases} \sqrt{\frac{e^{\beta_{\vec{x}}}-1}{\sqrt{Q}}} & \text{if } \vec{x} \text{ is on the even sublattice} \\ \sqrt{\frac{\sqrt{Q}}{e^{\beta_{\vec{x}}}-1}} & \text{if } \vec{x} \text{ is on the odd sublattice} \end{cases}, \quad (4.96)$$

one can directly calculate that

$$\langle \psi(\vec{\lambda}) | \psi(\vec{\lambda}) \rangle = C(\vec{\beta}) \underbrace{\sum_L \sqrt{Q}^{n_L} \prod_{\vec{x}} \left( \frac{e^{\beta_{\vec{x}}}-1}{\sqrt{Q}} \right)^{b_{\vec{x}}(L)}}_{Z_{\text{inhom Potts}}}, \quad (4.97)$$

where  $b_{\vec{x}}(L)$  is 1 if  $G'(L)$  has a bond at  $\vec{x}$  and 0 otherwise. Here,  $Z_{\text{inhom Potts}}$  is the partition function of a Potts model with different effective couplings between every pair of spins, given by (4.96). The constant is given by

$$C(\vec{\beta}) = \prod_{\vec{x} \text{ odd}} \left( \frac{e^{\beta_{\vec{x}}}-1}{\sqrt{Q}} \right) \quad (4.98)$$

Therefore,

$$\frac{\langle \psi(\vec{\lambda}) | D_{\text{PEPS}}(\vec{x}) | \psi(\vec{\lambda}) \rangle}{\langle \psi | \psi \rangle} = \frac{\partial \beta_{\vec{x}}}{\partial \lambda_{\vec{x}}} \frac{\partial}{\partial \beta_{\vec{x}}} \log \left( C(\vec{\beta}) Z_{\text{inhom Potts}} \right) \quad (4.99)$$

$$(4.100)$$

As usual, taking logarithmic derivatives of the partition function will yield some classical observable  $D_{\text{Potts}}(\vec{x})$ :

$$\dots = \langle D_{\text{Potts}}(\vec{x}) \rangle \quad (4.101)$$

In particular, the point  $\vec{\lambda} = \vec{1}$  corresponds to the original Potts model at its phase transition with all coupling strengths equal.

$$\langle D_{\text{PEPS}}(\vec{x}) \rangle_{\lambda=1} = \langle D_{\text{Potts}}(\vec{x}) \rangle_{\beta=1+\sqrt{Q}}, \quad (4.102)$$

Taking higher derivatives yields three-point and higher order correlators. In our case,  $Q = 16$  and all such operators decay exponentially even at the phase transition. This argument can be expanded by linearity to conclude that all diagonal correlators of the PEPS must decay exponentially.

Finally, for non-orthogonal loop states  $\langle 0|1 \rangle \neq 0$ , the mapping has to be carried out with respect to two *coupled* Potts models, whose phase diagram is also known [142–144]. As the nature of the phase transition remains unchanged, we expect the correlation function to behave in the same manner as derived above.

Of course, the preceding discussion makes no statements about non-classical correlation functions (i.e., those that are not diagonal in the  $\sigma^z$ -basis). It has been observed in other loop models that all diagonal correlators can decay exponentially and there is still a *critical* off-diagonal operator in the system [132]. To rule out such a possibility, we investigate the  $\lambda = 1$ -PEPS with a Corner Transfer Matrix algorithm. First, we use a single-site MPS ansatz for the fixed point of the transfer matrix. The corresponding zero-dimensional channel operator has two leading real eigenvalues with opposite sign that are degenerate to machine precision at boundary bond dimension  $\chi = 256$ . This is precisely what we would expect at the boundary of a plaquette phase: the one-site ansatz forces the fixed point to form a non-injective 2-periodic cat state MPS, where the fixed points correspond to the “+”- and “-”-superposition of the ordered and disordered (shifted) state. The transfer matrix therefore likely realizes imaginary time evolution under two coupled Majumdar-Ghosh-type chains. This evidence is corroborated by the fact that the boundary channel acquires a unique fixed point when allowing a two-site unit cell. Overall, our findings are compatible with a plaquette state that spontaneously breaks translation symmetry at  $\lambda = 1$ .

## 4.2 Parent Hamiltonians

In the following, we will study how our  $SU(2)$ -invariant wave function can appear as a ground state. To this end, we will construct its parent Hamiltonian and subsequently characterize its ground space, both for open boundary conditions (OBC) and on the torus. In particular, we will show that the parent Hamiltonian possesses the intersection property and that we can obtain a unique ground state with OBC by gapping out the boundary. For the remainder of this section, we will focus on  $\lambda = 1$ .

### 4.2.1 Construction of the Hamiltonian and intersection property

To construct a parent Hamiltonian, we use (1.24) and (1.25). In this case, the Hamiltonian acts on a  $2 \times 2$  plaquette. We introduce the notation

$$H = \sum_{x,y} h_{(x,y)} \quad (4.103)$$

where  $(x, y)$  is the top left spin of  $h_{(x,y)}$ , and the sum runs over all  $x$  and  $y$  on the patch, according to the chosen boundary conditions. By construction,  $H \geq 0$  and  $h_{(x,y)} |\psi_{N_x \times N_y}(A, X)\rangle = 0$  for all  $X$ , and thus, any  $|\psi_{N_x \times N_y}(A, X)\rangle$  is a ground state of  $H$ .

The remaining question is thus to understand whether these states fully span the ground space of  $H$ . As mentioned in section 1.1, for OBC, this is known as the intersection property, i.e., the intersection of the ground spaces of the  $h_{(x,y)}$  is given by the PEPS with arbitrary boundary on the larger patch.

In order to understand the structure of an arbitrary ground state of  $H$ , let us consider the action of  $h$  in terms of the loop picture. It is convenient to introduce the following notation for loop states on  $2 \times 2$  plaquettes:

$$\begin{aligned}
 \left| \begin{array}{|c|c|} \hline \oplus & \oplus \\ \hline \end{array} \right\rangle &= |B\rangle \\
 \left| \begin{array}{|c|c|} \hline \oplus & \ominus \\ \hline \end{array} \right\rangle &= |E_1\rangle & \left| \begin{array}{|c|c|} \hline \ominus & \oplus \\ \hline \end{array} \right\rangle &= |E_2\rangle \\
 \left| \begin{array}{|c|c|} \hline \oplus & \oplus \\ \hline \end{array} \right\rangle &= |E_3\rangle & \left| \begin{array}{|c|c|} \hline \oplus & \oplus \\ \hline \end{array} \right\rangle &= |E_4\rangle \\
 \left| \begin{array}{|c|c|} \hline \oplus & \oplus \\ \hline \end{array} \right\rangle &= |O_1\rangle & \left| \begin{array}{|c|c|} \hline \oplus & \oplus \\ \hline \end{array} \right\rangle &= |O_2\rangle & \left| \begin{array}{|c|c|} \hline \oplus & \oplus \\ \hline \end{array} \right\rangle &= |O_3\rangle \\
 \left| \begin{array}{|c|c|} \hline \oplus & \oplus \\ \hline \end{array} \right\rangle &= |O_4\rangle & \left| \begin{array}{|c|c|} \hline \oplus & \oplus \\ \hline \end{array} \right\rangle &= |O_5\rangle & \left| \begin{array}{|c|c|} \hline \oplus & \oplus \\ \hline \end{array} \right\rangle &= |O_6\rangle \\
 \left| \begin{array}{|c|c|} \hline \oplus & \oplus \\ \hline \end{array} \right\rangle &= |O_7\rangle & \left| \begin{array}{|c|c|} \hline \oplus & \oplus \\ \hline \end{array} \right\rangle &= |O_8\rangle & \left| \begin{array}{|c|c|} \hline \oplus & \oplus \\ \hline \end{array} \right\rangle &= |O_9\rangle \\
 \left| \begin{array}{|c|c|} \hline \oplus & \oplus \\ \hline \end{array} \right\rangle &= |O_{10}\rangle & \left| \begin{array}{|c|c|} \hline \oplus & \oplus \\ \hline \end{array} \right\rangle &= |O_{11}\rangle
 \end{aligned} \quad (4.104)$$

We will refer to  $|B\rangle$  as *bubbles*,  $|E_i\rangle$  as *tadpoles*, and  $|O_i\rangle$  as *bubble-free states*. Furthermore, define

$$|\phi\rangle = \frac{1}{2\sqrt{2}} \left[ 2|B\rangle + \sum_{i=1}^4 |E_i\rangle \right] \quad (4.105)$$

Then, each local term has 12 possible ground states:

$$|O_i\rangle, \quad i = 1, \dots, 11 \quad \text{and} \quad |\phi\rangle. \quad (4.106)$$

Taking a general state  $|g\rangle = \sum_i o_i |O_i\rangle + \sum_i e_i |E_i\rangle + b|B\rangle$ , a direct calculation reveals that  $h|g\rangle = 0$  if and only if  $e_i = e_j \forall i, j$  and  $e_i = b/2 \forall i$ . This is, in order to be a ground state of  $h$ , the states  $|B\rangle$  and  $|E_i\rangle$  must appear with the relative amplitudes  $2 : 1 : 1 : 1 : 1$ , as in  $|\phi\rangle$  – and this is the *only* condition in order to be a ground state.

We can thus interpret the Hamiltonian as defining a random walk on the space of loop configurations,

$$2 \begin{array}{|c|} \hline \text{⊙} \\ \hline \end{array} \Leftrightarrow \begin{array}{|c|} \hline \text{⊕} \\ \hline \end{array} \Leftrightarrow \begin{array}{|c|} \hline \text{⊗} \\ \hline \end{array} \Leftrightarrow \begin{array}{|c|} \hline \text{⊖} \\ \hline \end{array} \Leftrightarrow \begin{array}{|c|} \hline \text{⊙} \\ \hline \end{array} \quad (4.107)$$

i.e., any two states coupled by the transition (4.107) must appear in any ground state in superposition with the given relative amplitude. Differently speaking, for any orbit of the random walk (4.107) acting on all sites, there is at most one ground state per orbit. In the following, we will call such a move between loop configurations a *surgery move* and use the notation  $L' = \sigma(L)$  to describe the fact that loop patterns  $L'$  and  $L$  are related by such a move. We will denote *sequences* of surgery moves by capital letters, e.g.  $\Sigma = \sigma_1 \dots \sigma_M$ .

We will now use this interpretation to prove that for  $H$  on an OBC rectangle, there is exactly one ground state per connectivity pattern, this is, the ground space is given by

$$\mathcal{S}_{N_h \times N_v} := \text{span}\{|\psi_{N_h \times N_v}(A, X)\rangle | X \in \mathbb{C}^{(2N_h + 2N_v)}\}$$

– this is precisely the intersection property. In particular, it entails that the degeneracy of the parent Hamiltonian is given by  $\mathcal{N}(N_h, N_v)$ .

To start with, note that each surgery move leaves the connectivity pattern invariant, i.e.,  $\langle K|h|L\rangle = 0$  if  $K \in C_p \neq C_q \ni L$ . The Hamiltonian is therefore block diagonal in the loop basis

$$H = \bigoplus_p H_p, \quad (4.108)$$

where the  $H_p$  are supported on  $V(C_p)$ . Now pick the basis spanned by applying the PEPS to the dual boundary vectors  $|\psi_p\rangle := \{|\psi_{N_h \times N_v}(A, m^*(p))\rangle\}_p$  of  $\mathcal{S}_{N_h \times N_v}$ , cf. Eq. (4.16). Each of these states is by construction a ground state of  $H$ , and lives in the corresponding block  $V(C_p)$  of the Hamiltonian. It thus remains to show that the random walk defined by  $H$  couples any two configurations  $L, L' \in C_p$ : As argued above, this uniquely fixes the ratios of the coefficients  $\sum_{L \in C_p} c_L |L\rangle$  for any given  $p$ , which thus must be equal to those of  $|\psi_p\rangle$ . (Note that the fact that  $|\psi_p\rangle$  is a ground state implies that the ratio must be independent of the chosen path  $\Sigma(L) = L'$  of surgery moves.). Differently speaking, the random walk (4.107) should be ergodic in the space of loop states with a fixed connectivity pattern.

We proceed to demonstrate such ergodicity in two steps: First, as we have shown in 4.1.2, for any given connectivity pattern  $p$ , we can define a canonical pattern  $L_0$ . Second, we will now show that any  $L \in C_p$  can be connected to  $L_0$  through a sequence  $\Sigma_0$  of surgery moves,  $L_0 = \Sigma_0(L)$ , and thus, any two  $L, L' \in C_p$  are connected through a sequence  $\Sigma$  which goes through  $L_0$ ,

$$L = \Sigma_0^{-1}(\Sigma'_0(L')) , \quad (4.109)$$

where  $L_0 = \Sigma'_0(L')$ .

The algorithm to arrive at the canonical loop pattern from an arbitrary starting pattern from surgery moves contains three steps:

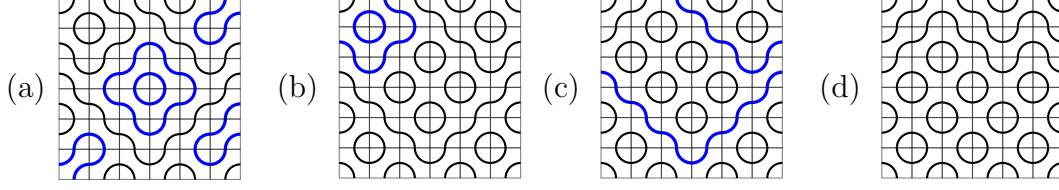


Figure 4.5: Bringing a given loop pattern (a) into the canonical pattern with the same boundary matching (d). In step 1, tadpoles and larger bubbles are cut off into small bubbles (b). Every path is shortened as much as possible in step 2 (c). The remaining ambiguity is the trajectory of longer paths. For the sake of uniqueness, they are moved as close as possible to the north-west boundary (d).

1. Tadpoles and larger bubbles are cut off.
2. All paths are consecutively made as short as possible. Any path with non-minimal length must necessarily contain both vertical and horizontal *bay-type* plaquettes (Fig. 4.5b). This pair must necessarily contain a loop in their inside. The loop can be moved through the bay by three consecutive surgery moves. If the bays had previously been adjacent, the path is now shorter, otherwise the bays are now closer together. Therefore, any path can be made as short as possible. Note that any surgery move only acts on one path plus a surrounding loop so previously shortened paths will always stay shortest during the application of further elementary moves in this step.
3. Every path now exclusively consists of *up-* and *down-*moves, the order of which may still differ from the canonical loop pattern, i.e. the path might not run as close as possible to the north-west boundary of the patch (Fig. 4.5c). For the pattern to be compatible with the same boundary matching, the area between the current and the desired trajectory for any given path must be filled with small bubbles. We are finished after moving all the bubbles through the appropriate bays.

This implies that (up to normalisation), on a OBC patch of size  $N_h \times N_v$ ,

$$|\psi_p\rangle = \sum_{L \in C_p} 2^{n_L} |L\rangle \quad (4.110)$$

is the unique ground state of  $H$  in sector  $p$ , i.e.,  $H$  has one ground state per connectivity pattern  $C_p$ , and the space of all ground states is given by  $\mathcal{S}_{N_h \times N_v}$ .

### 4.2.2 Open boundary conditions and unique ground state

We have just seen that the parent Hamiltonian possesses the intersection property – the ground space manifold on any rectangular patch is precisely given by those configurations which can be obtained by choosing arbitrary boundary conditions. In the following, we will show that, for  $N_h, N_v$  even, it is possible to gap out the boundary, this is, to add boundary terms to the parent Hamiltonian which yield a unique ground state.

To this end, we target

$$|\psi\rangle = \begin{array}{c} \begin{array}{ccc} \begin{array}{|c|c|} \hline A & A \\ \hline \end{array} & \cdots & \begin{array}{|c|c|} \hline A & A \\ \hline \end{array} \\ \begin{array}{|c|} \hline A \\ \hline \end{array} & & \begin{array}{|c|} \hline A \\ \hline \end{array} \\ \hline \vdots & & \vdots \\ \begin{array}{|c|c|} \hline A & A \\ \hline \end{array} & \cdots & \begin{array}{|c|c|} \hline A & A \\ \hline \end{array} \\ \begin{array}{|c|} \hline A \\ \hline \end{array} & & \begin{array}{|c|} \hline A \\ \hline \end{array} \\ \hline \end{array} \end{array} \quad (4.111)$$

as the unique ground state, and proceed by constructing its parent Hamiltonian. In the bulk, the parent Hamiltonian will be the same as before. On the boundary, however, extra terms appear. Specifically, we consider a  $2 \times 1$  tile

$$\begin{array}{|c|c|} \hline A & A \\ \hline \end{array} \quad (4.112)$$

at either boundary, and define

$$\mathcal{R}_{(2n-1,1),(2n,1)} := \text{span} \left\{ \begin{array}{|c|} \hline \begin{array}{|c|c|} \hline A & A \\ \hline \end{array} \\ \hline X \end{array} \mid X \in (\mathbb{C}^2)^{\otimes 4} \right\} \quad (4.113)$$

(and rotated versions thereof) and the corresponding parent Hamiltonian

$$h'_{(x_1,y_1),(x_2,y_2)} = \mathbb{1} - \Pi_{\mathcal{R}_{(x_1,y_1),(x_2,y_2)}} \quad (4.114)$$

It is easy to check that  $h'$ , together with the original parent Hamiltonian on the corresponding  $2 \times 2$  patch, has exactly the same ground space as the “true” parent Hamiltonian derived from that patch of  $|\psi\rangle$  *including* the boundary condition (and containment, which suffices for  $|\psi\rangle$  to be a ground state, holds trivially). On the other hand, the parent Hamiltonians on the shifted patches remain unchanged. Thus,

$$\begin{aligned} H' &:= H + \sum_{n=1}^{N_h/2} [h'_{(2n-1,1),(2n,1)} + h'_{(2n-1,N_v),(2n,N_v)}] \\ &\quad + \sum_{n=1}^{N_v/2} [h'_{(1,2n-1),(1,2n)} + h'_{(N_h,2n-1),(N_h,2n)}] \end{aligned} \quad (4.115)$$

is a parent Hamiltonian of  $|\psi\rangle$ , and has  $|\psi\rangle$  as a ground state.

Let us now show that this ground state is unique. To this end, note that ground states of  $h'$  on a  $2 \times 1$  patch are spanned by the states

$$\begin{aligned} |\theta_1\rangle &= \begin{array}{|c|c|} \hline \diagup & \diagdown \\ \hline \end{array} + \begin{array}{|c|c|} \hline \diagdown & \diagup \\ \hline \end{array} + 2 \begin{array}{|c|c|} \hline \diagup & \diagup \\ \hline \end{array} , \\ |\theta_2\rangle &= \begin{array}{|c|c|} \hline \diagdown & \diagdown \\ \hline \end{array} . \end{aligned} \quad (4.116)$$

Thus,  $h'$  imposes the additional constraint that in any ground state the states in  $|\theta_1\rangle$  must appear as superpositions with the corresponding weights. Arguing as before,

this fixes the relative amplitudes of any two loop patterns coupled by the additional surgery move

$$\begin{array}{|c|} \hline \text{Diagram 1} \\ \hline \end{array} \Leftrightarrow \begin{array}{|c|} \hline \text{Diagram 2} \\ \hline \end{array} \Leftrightarrow 2 \begin{array}{|c|} \hline \text{Diagram 3} \\ \hline \end{array} \quad (4.117)$$

on the corresponding  $2 \times 1$  patches, and rotated versions thereof. Crucially, unlike the bulk moves, this new surgery move allows us to change the connectivity class. Equipped with both the original (bulk) surgery moves as well as the additional surgery move (4.117) obtained from  $h'$  allows us to transform any any loop pattern to a loop pattern in the “minimal” connectivity class

$$p_{\min} = \begin{array}{|c|} \hline \text{Diagram 4} \\ \hline \end{array} \quad (4.118)$$

**Claim 4.8.** For every loop pattern  $L$ , there exists a sequence  $\Sigma$  of bulk moves (4.107) and boundary moves (4.117), such that

$$p(\Sigma(L)) = p_{\min}, \quad (4.119)$$

where  $p_{\min}$  is given by (4.118).

*Proof.* We are going to construct  $\Sigma$  explicitly, starting from an arbitrary loop pattern  $L$ . We begin in the top left corner. Combining boundary moves on the first horizontal and vertical dominos and potentially a bulk move on the plaquette in the top left corner, we can transform the top left corner of  $L$  into

$$\begin{array}{|c|} \hline \text{Diagram 5} \\ \hline \end{array} \quad (4.120)$$

We proceed similarly for all other corners:

$$\begin{array}{|c|} \hline \text{Diagram 6} \\ \hline \end{array} \quad (4.121)$$

Now we continue sequentially, column by column. If the top domino looks like  $\begin{array}{|c|} \hline \text{Diagram 7a} \\ \hline \end{array}$  or  $\begin{array}{|c|} \hline \text{Diagram 7b} \\ \hline \end{array}$ , transform it into  $\begin{array}{|c|} \hline \text{Diagram 7c} \\ \hline \end{array}$  using (4.117). If it is in the  $\begin{array}{|c|} \hline \text{Diagram 7d} \\ \hline \end{array}$ -state, we will see now that the corresponding plaquette can be brought into the  $|B\rangle$  state, after which the bubble is cut off and the boundary move is applicable again.

There are two scenarios: In the first, the top  $\begin{array}{|c|} \hline \text{Diagram 7d} \\ \hline \end{array}$ -domino has a bubble or tadpole underneath it:

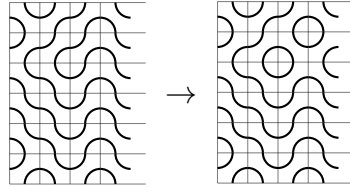
$$\begin{array}{|c|} \hline \text{Diagram 8} \\ \hline \end{array} \quad (4.122)$$



In this case, the bubble can be moved up to the topmost plaquette using bulk moves. It can then be cut off to transform the top domino into  $\begin{smallmatrix} \diagup & \diagdown \\ \diagdown & \diagup \end{smallmatrix}$ . In the second scenario there is no bubble or tadpole in the column:


(4.123)

Then, there must necessarily be  $N_v$  paths passing through the column left to right. Only  $N_v - 4$  of them can originate from the west boundary, since  $4 + 4k$  out of the  $N_v + 4k$  boundary points to the left of the  $k$ -th column are already connected with their nearest neighbours. Therefore, at least two pairs of paths must actually be a single path, which has a tadpole to the left of the column. This tadpole can be moved into the column upon which we recover situation 1, e.g.:


(4.124)

The bottom tile is transformed into  $\begin{smallmatrix} \diagup & \diagdown \\ \diagdown & \diagup \end{smallmatrix}$  in the same manner to arrive at


(4.125)

After fixing the top and bottom dominos column by column, we apply the same procedure to the left and right boundary. Evidently, once a boundary domino is in the correct state (e.g.,  $\begin{smallmatrix} \diagup & \diagdown \\ \diagdown & \diagup \end{smallmatrix}$  for top dominos), it will never be touched again during this procedure, allowing us to sequentially bring the connectivity pattern into minimal form.  $\square$

We have thus established that the minimal connectivity pattern can be reached from arbitrary starting loop patterns. On the other hand, we have seen in Sec. 4.2.1 that any two loop patterns in a given connectivity class – specifically, the minimal one above – are connected through bulk surgery moves. Thus, it follows that any two loop patterns can be connected by combining bulk and boundary surgery moves, and thus, the relative amplitudes of all loop patterns are fixed and therefore equal to those found in  $|\psi\rangle$ , Eq. (4.111). We thus infer that  $|\psi\rangle$  is the unique ground state of  $H'$ .

### 4.2.3 Periodic Boundary Conditions

Let us now study the ground space structure of the parent Hamiltonian (4.103) on a system with periodic boundary conditions (PBC); recall from Sec. 4.1 that this requires  $N_h$  and  $N_v$  to be even. To this end, we will resort to the description of the PEPS in terms of the tensor  $\tilde{A}$ , Eq. (4.1), rather than  $A$  (see Sec. 4.1). Note that due to the gauge relation (4.5) between them, both  $A$  and  $\tilde{A}$  have the same parent Hamiltonian.

Let us first consider an approach which allowed to fully characterize the ground space for  $G$ -injective PEPS with finite symmetry group  $G$  [20]. (In the following, all matrices are applied from left to right and top to bottom by convention.) First, note that the fundamental symmetry is stable under concatenation, e.g.

$$\begin{aligned}
 & \text{Diagram 1} = \text{Diagram 2} = \text{Diagram 3} \\
 & \text{Diagram 1: Two } \tilde{A} \text{ tensors connected horizontally. Each has } U_g \text{ on top and } U_g^\dagger \text{ on bottom vertical legs.} \\
 & \text{Diagram 2: Same as Diagram 1, but } U_g \text{ and } U_g^\dagger \text{ are on the horizontal legs.} \\
 & \text{Diagram 3: A single } \tilde{A} \text{ tensor with two horizontal legs, each having } U_g \text{ and } U_g^\dagger \text{ on its vertical legs.}
 \end{aligned} \tag{4.126}$$

i.e., any closed loop of symmetry operators leaves a simply connected patch invariant. This is particularly interesting when we consider closed boundary conditions:

$$\begin{aligned}
 & \text{Diagram 1} = \text{Diagram 2} = \text{Diagram 3} \\
 & \text{Diagram 1: Two } \tilde{A} \text{ tensors connected vertically. Left horizontal legs have } U_g^\dagger. \text{ A dashed vertical line passes through.} \\
 & \text{Diagram 2: A complex diagram with multiple } U_g \text{ and } U_g^\dagger \text{ tensors and a dashed vertical line.} \\
 & \text{Diagram 3: Same as Diagram 1, but the dashed vertical line is moved to the right.}
 \end{aligned} \tag{4.127}$$

Virtual string operators of the form  $U_g^{\otimes N_v}$  which wrap vertically around the torus can therefore be freely moved around the torus, and correspondingly horizontal loops  $V_h^{\otimes N_h}$ , i.e., the state

$$|\psi_{N_h \times N_v}\{U_g, V_h\}\rangle = \dots \tag{4.128}$$

on the torus is independent of the position of the strings, as long as  $[U_g, V_h] = 0$  (otherwise, the strings might not be movable where they intersect).

It is now clear that any such state  $|\psi_{N_h \times N_v}\{U_g, V_h\}\rangle$  is a ground state of the parent Hamiltonian  $H = \sum h_{(x,y)}$ , since for any local term  $h_{(x,y)}$ , the strings can be moved such that they are outside the region where  $h_{(x,y)}$  acts. In the case of  $G$ -injective PEPS with finite symmetry group, it could be shown that these states precisely parameterize the full ground space of  $H$  [20]. For abelian groups, all  $(g, h)$  yield linearly independent ground states  $|\psi_{N_h \times N_v}\{U_g, V_h\}\rangle$ , while for non-abelian groups, linear dependencies arise as certain  $(g, h)$  yield identical states.

Let us now consider the case of  $G = SU(2)$ . Clearly,

$$\mathcal{S}' = \text{span} \{ |\psi_{N_h \times N_v}\{U, V\}\rangle \mid U, V \in SU(2), [U, V] = 0 \} \quad (4.129)$$

is inside the ground space of  $H$ . What is the dimension of  $\mathcal{S}'$ ? Without loss of generality, we can restrict to  $U = \text{diag}(e^{i\phi}, e^{-i\phi})$  – otherwise, we conjugate each  $\tilde{A}$  with the unitary which diagonalises  $U$ , leaving the state invariant. Then (up to basis permutations),

$$\begin{aligned} U^{\otimes N_v} &= e^{iN_v\phi} \mathbb{1}_{\binom{N_v}{0}} \oplus e^{i(N_v-2)\phi} \mathbb{1}_{\binom{N_v}{1}} \oplus \\ &\quad \dots \oplus e^{-iN_v\phi} \mathbb{1}_{\binom{N_v}{N_v}}, \end{aligned} \quad (4.130)$$

for arbitrary values of  $\phi$ , and thus, the closure  $U_g^{\otimes N_v}$  on its own parametrizes a  $(N_v + 1)$ -dimensional subspace (e.g. by choosing Fourier angles  $\phi_k = 2\pi k / (2N_v + 1)$ ,  $k = -N_v/2, \dots, N_v/2$ ). In order to satisfy  $[U, V] = 0$ , we must have  $V = \text{diag}(e^{i\theta}, e^{-i\theta})$ , and thus,  $\mathcal{S}'$  is at most  $(N_h + 1)(N_v + 1)$ -dimensional. However, it is easy to see that there is at least one more redundancy: By conjugating each  $\tilde{A}$  with the Pauli  $X$ -operator, we map  $\phi \rightarrow -\phi$ ,  $\theta \rightarrow -\theta$ . This reduces the number of possibilities by a factor of 2, except at  $\phi = \theta = 0$ .

If the remaining states are linearly independent, we have

$$\dim \mathcal{S}' = \frac{(N_h + 1)(N_v + 1) + 1}{2}. \quad (4.131)$$

We now show rigorously that these *string-inserted states* are indeed linearly independent. We begin by making some useful definitions:

**Definition 4.8.** For a tuple of  $(j, k) \in \mathbb{Z}^2$ , define a *generalized greatest common divisor*

$$g(j, k) = \begin{cases} \gcd(j, |k|) & \text{if } j, k \neq 0 \\ j & \text{if } k = 0, j > 0 \\ |k| & \text{if } j = 0, |k| > 0 \\ 1 & \text{if } j=k=0 \end{cases} \quad (4.132)$$

and make the following observations:

- The winding number of a non-trivial loop in, say, the horizontal direction is equivalent to the difference of how many times that loop crosses the  $U$ -subset of the right boundary vs. how many times it crosses the  $\bar{U}$ -subset of the right boundary cf. (4.128). An equivalent statement holds for non-trivial winding in the vertical direction.

- If in a given loop pattern  $L$  there is a loop winding non-trivially around the torus  $j$  times in the horizontal direction and  $k$  times in the vertical direction, then *all* non-trivial loops have winding number  $(j, k)$  or  $(-j, -k)$  (in fact, half of the loops will have winding number  $(j, k)$  and the other half  $(-j, -k)$ ). Therefore, we may denote the winding sector of such a loop pattern by  $W(L) = (j, k)$ . To remove ambiguity, we enforce  $j \geq 0$ .
- A loop cannot wind around the torus  $(j, k)$  times if  $g(j, k) \neq 1$ .
- For a loop pattern in a given winding sector  $(j, k)$ , the number of non-trivial loops is  $n_{NTL} \in \{2, 4, \dots, \min\{\lfloor N_h/j \rfloor, \lfloor N_v/k \rfloor\}\}$ . Therefore we redefine the winding sector of a loop pattern that has  $n_{NTL}/2$  loops wrapping around the torus  $(j, k)$  times and  $n_{NTL}/2$  loops wrapping around the torus  $(-j, -k)$  times as  $W(L) = (j \times n_{NTL}/2, k \times n_{NTL}/2)$ .

**Definition 4.9.** Given  $N_h, N_v$  even, we define the *index set*

$$I = \left\{ (x, y) \mid x = 0, \dots, N_v/2, \right. \\ \left. y = \begin{cases} 0, \dots, N_h/2 & \text{if } x = 0 \\ -N_h/2, \dots, N_h/2 & \text{if } x \neq 0 \end{cases} \right\} \quad (4.133)$$

Counting the number of elements in  $I$  reveals that

$$|I| = \frac{(N_h + 1)(N_v + 1) + 1}{2} \quad (4.134)$$

Besides these definitions, the following shorthand notation will be useful: we denote

$$\widetilde{N}_h := N_h + 1 \quad (4.135)$$

$$\widetilde{N}_v := N_v + 1. \quad (4.136)$$

Let us also introduce the states

$$|j, k\rangle := \sum_{\substack{L \text{ s.t.} \\ W(L)=(j,k)}} 2^{n_L} |L\rangle \quad (4.137)$$

where  $W(L)$  is the winding number from definition 4.8. By orthogonality of the physical basis states, different  $|j, k\rangle$  are clearly orthogonal:

$$\langle j, k | j', k' \rangle := \delta_{jj', kk'} ||j, k||^2 \quad (4.138)$$

and by the above observations  $||j, k||^2 \neq 0$  for all  $(j, k) \in I$ . Next, we define the operators

$$D_\phi = \begin{pmatrix} e^{i\phi} & 0 \\ 0 & e^{-i\phi} \end{pmatrix} \quad (4.139)$$

$$W_{N_v}(\phi) := \bigotimes_{i=1}^{N_v/2} D_\phi \otimes \bar{D}_\phi \quad (4.140)$$

$$\tilde{W}_{N_v}^l := W_{N_v} \left( \frac{\pi l}{N_v} \right) \quad (4.141)$$

which, in turn allow us to define the states

$$|\psi_{\phi,\theta}\rangle := |\psi\{D_\phi, D_\theta\}\rangle \quad (4.142)$$

$$|\tilde{\psi}_{l,m}\rangle := |\psi_{\phi=\frac{\pi l}{N_v}, \theta=\frac{\pi m}{N_h}}\rangle \quad (4.143)$$

Here, we have used the notation introduced in (4.128), but suppressed the dependence of  $|\psi\rangle$  on  $N_h$  and  $N_v$  (and we will continue to do so for the remainder of this section). Finally, we can Fourier transform (4.143)

$$|\phi_{k_x, k_y}\rangle := \frac{1}{\widetilde{N_v N_h}} \sum_{l=0}^{N_v} \sum_{m=0}^{N_h} e^{2\pi i \left( \frac{k_x l}{N_v} + \frac{k_y m}{N_h} \right)} |\tilde{\psi}_{l,m}\rangle \quad (4.144)$$

and define the  $M$ -matrix

$$M_{(jk),(lm)} := \left[ 2 \cos \left( \frac{\pi j l}{g(j,k) \widetilde{N_v}} + \frac{\pi k m}{g(j,k) \widetilde{N_h}} \right) \right]^{2g(j,k)} \quad (4.145)$$

for any set of integers  $j, k, l$  and  $m$ . To show that  $\dim \mathcal{S}' = |I|$ , we use a “sandwich”-bound from below and above.

**Claim 4.9. (Bound from above)**

$$\dim \mathcal{S}' \leq |I| \quad (4.146)$$

*Proof.* Starting from the definition of  $\mathcal{S}'$ , we can first restrict the unitaries  $U$  and  $V$  to be diagonal, i.e.

$$\mathcal{S}' = \text{span}\{|\psi_{\phi,\theta}\rangle \mid \phi, \theta \in [0, 2\pi]\} \quad (4.147)$$

This is because any state that is generated by non-diagonal  $U$  and  $V$  is related to a state with  $U$  and  $V$  diagonal by conjugating the whole network with  $S$ , where  $S$  is the unitary that simultaneously diagonalises  $U$  and  $V$ . Because of the fundamental symmetry of the PEPS tensor, this conjugation leaves the state invariant.

As a first step, we are going to show that

$$\mathcal{S}' = \text{span}\{|\tilde{\psi}_{l,m}\rangle\}_{l=0,\dots,N_v}^{m=0,\dots,N_h} \quad (4.148)$$

Because  $|\psi_{\phi,\theta}\rangle$  depends linearly on  $W_{N_v}(\phi) \otimes W_{N_h}(\theta)$ , it is sufficient to show that

$$\text{span}\{W_{N_v}(\phi) \otimes W_{N_h}(\theta)\} = \text{span}\left\{\tilde{W}_{N_v}^l \otimes \tilde{W}_{N_h}^m\right\}_{l=0,\dots,N_v}^{m=0,\dots,N_h} \quad (4.149)$$

Clearly,

$$\text{span}\{W_{N_v}(\phi) \otimes W_{N_h}(\theta)\} \supseteq \text{span}\left\{\tilde{W}_{N_v}^l \otimes \tilde{W}_{N_h}^m\right\}_{l=0,\dots,N_v}^{m=0,\dots,N_h} \quad (4.150)$$

and we will prove the reverse inclusion by showing that

$$\begin{aligned}
 \widetilde{N}_v \widetilde{N}_h &\geq \dim \text{span}\{W_{N_v}(\phi) \otimes W_{N_h}(\theta)\} \\
 &\geq \dim \text{span} \left\{ \widetilde{W}_{N_v}^l \otimes \widetilde{W}_{N_h}^m \right\}_{\substack{l=0,\dots,N_v \\ m=0,\dots,N_h}} \\
 &\geq \widetilde{N}_v \widetilde{N}_h
 \end{aligned} \tag{4.151}$$

The first inequality of (4.151) follows by expanding the operator

$$\begin{aligned}
 W_{N_v}(\phi) &= e^{iN_v\phi} \mathbb{1}_{\binom{N_v}{0}} \oplus e^{i(N_v-2)\phi} \mathbb{1}_{\binom{N_v}{1}} \oplus \\
 &\quad \dots \oplus e^{-iN_v\phi} \mathbb{1}_{\binom{N_v}{N_v}},
 \end{aligned} \tag{4.152}$$

which, for general values of  $\phi$  spans an  $\widetilde{N}_v$ -dimensional space. The second inequality in (4.151) is a trivial conclusion of (4.150).

To see the validity of the third inequality, consider the matrix whose columns are made up of the distinct diagonal entries of  $\widetilde{W}_{N_v}^l$  for  $l = \frac{N_v}{2}, \frac{N_v}{2} - 1, \dots, 0, N_v, N_v - 1, \dots, \frac{N_v}{2} + 1$ :

$$\begin{aligned}
 F_{N_v} &= \begin{pmatrix} \text{diag}(\widetilde{W}_{N_v}^{N_v/2}) & \text{diag}(\widetilde{W}_{N_v}^{N_v/2-1}) & \dots \end{pmatrix} \\
 &= \begin{pmatrix} 1 & 1 & 1 & 1 \\ 1 & \omega & \omega^2 & \omega^3 \\ 1 & \omega^2 & \omega^4 & \omega^6 & \dots \\ 1 & \omega^3 & \omega^6 & \omega^9 \\ & \vdots & & \ddots \end{pmatrix}
 \end{aligned} \tag{4.153}$$

which is simply  $\widetilde{N}_v$  times the  $\widetilde{N}_v \times \widetilde{N}_v$  discrete Fourier matrix (we have set  $\omega = \exp(2\pi i/\widetilde{N}_v)$ ), and therefore has full rank equal to  $\widetilde{N}_v$ . Applying these arguments to both tensor factors individually yields (4.151).

Finally, we will prove that

$$\text{span}\{|\tilde{\psi}_{l,m}\rangle\}_{\substack{l=0,\dots,N_v \\ m=0,\dots,N_h}} = \text{span}\{|\tilde{\psi}_{l,m}\rangle\}_{(l,m) \in I} \tag{4.154}$$

by showing that for each  $(l, m) \notin I$ , there exists an  $(l', m') \in I$  such that  $|\tilde{\psi}_{l,m}\rangle = |\tilde{\psi}_{l',m'}\rangle$ . The key observation is that

$$|\psi\{U, V\}\rangle = |\psi\{XUX^\dagger, XVX^\dagger\}\rangle \tag{4.155a}$$

$$|\psi\{U, V\}\rangle = |\psi\{-U, V\}\rangle \tag{4.155b}$$

$$|\psi\{U, V\}\rangle = |\psi\{U, -V\}\rangle \tag{4.155c}$$

which follows from the fact that conjugating the whole tensor network with  $iX \in SU(2)$  leaves the state invariant and the numbers of  $U$ s and  $V$ s are both even. Inserting

$$\begin{aligned}
 U &= \text{diag}(\exp(\pi i l/\widetilde{N}_v), \exp(-\pi i l/\widetilde{N}_v)) \quad \text{and} \\
 V &= \text{diag}(\exp(\pi i m/\widetilde{N}_h), \exp(-\pi i m/\widetilde{N}_h)),
 \end{aligned} \tag{4.156}$$

we obtain

$$|\tilde{\psi}_{l,m}\rangle = |\tilde{\psi}_{-l,-m}\rangle \quad (4.157a)$$

$$|\tilde{\psi}_{l,m}\rangle = |\tilde{\psi}_{l \pm \widetilde{N}_v, m}\rangle \quad (4.157b)$$

$$|\tilde{\psi}_{l,m}\rangle = |\tilde{\psi}_{l, m \pm \widetilde{N}_h}\rangle \quad (4.157c)$$

Using (4.157a) - (4.157c), for each  $(l, m) \in [0, \dots, N_v] \times [0, \dots, N_h]$  we can now find an  $(l', m') \in I$  such that  $|\tilde{\psi}_{l,m}\rangle = |\tilde{\psi}_{l', m'}\rangle$  which imply (4.154) and, together with (4.148) show that

$$\dim \mathcal{S}' \leq |I| \quad (4.158)$$

□

**Claim 4.10. (Bound from below)**

$$\dim \mathcal{S}' \geq |I| \quad (4.159)$$

*Proof.* Because of (4.148) and the  $|\phi_{k_x, k_y}\rangle$  being linear combinations of the  $|\tilde{\psi}_{l,m}\rangle$  via (4.144), it is clear that

$$\mathcal{S}' \supseteq \text{span}\{|\phi_{k_x, k_y}\rangle\}_{(k_x, k_y) \in I} \quad (4.160)$$

Also, from the observations made in the beginning of this section and (4.137) and (4.145), we see that

$$|\tilde{\psi}_{l,m}\rangle = \sum_{(jk) \in I} M_{(jk), (lm)} |j, k\rangle \quad (4.161)$$

The matrix elements of  $M$  can be simplified using the binomial theorem. For better readability, we are going to suppress the argument of  $g = g(j, k)$ .

$$\begin{aligned} M_{(jk), (lm)} &= \left[ 2 \cos \left( \frac{jl\pi}{\widetilde{N}_v g} + \frac{km\pi}{\widetilde{N}_h g} \right) \right]^{2g} \\ &= \left[ e^{\frac{\pi i}{g} \left( \frac{jl}{\widetilde{N}_v} + \frac{km}{\widetilde{N}_h} \right)} + e^{-\frac{\pi i}{g} \left( \frac{jl}{\widetilde{N}_v} + \frac{km}{\widetilde{N}_h} \right)} \right]^{2g} \\ &= \sum_{a=0}^{2g} e^{\frac{2\pi i}{g} \left( \frac{jl}{\widetilde{N}_v} + \frac{km}{\widetilde{N}_h} \right) (a-g)} \binom{2g}{a} \end{aligned} \quad (4.162)$$

Plugging (4.161) and (4.162) into (4.144) yields

$$\begin{aligned} |\phi_{(k_x, k_y)}\rangle &= \sum_{(jk) \in I} \sum_{a=0}^{2g} \binom{2g}{a} |j, k\rangle \\ &\quad \times \underbrace{\frac{1}{\widetilde{N}_v} \sum_{l=0}^{N_v} \left[ e^{\frac{2\pi i}{\widetilde{N}_v} \left( \frac{j}{g} (a-g) - k_x \right)} \right]^l}_{\delta_{\frac{j}{g} (a-g) - k_x \in \widetilde{N}_v \mathbb{Z}}} \\ &\quad \times \underbrace{\frac{1}{\widetilde{N}_h} \sum_{m=0}^{N_h} \left[ e^{\frac{2\pi i}{\widetilde{N}_h} \left( \frac{k}{g} (a-g) - k_y \right)} \right]^m}_{\delta_{\frac{k}{g} (a-g) - k_y \in \widetilde{N}_h \mathbb{Z}}} \end{aligned} \quad (4.163)$$

In principle, the constraints only enforce e.g.,

$$\frac{k}{g}(a - g) - k_y = n\widetilde{N}_h \quad (4.164)$$

for  $n \in \mathbb{Z}$ . However, we will now show that if  $|n| \geq 1$ , then it follows that  $|a - g| > g$  which entails that either  $a < 0$  or  $a > 2g$ , in both cases the summation on  $a$  will be empty. Rearranging (4.164) and taking the absolute value yields

$$\begin{aligned} |a - g| &= \frac{|n\widetilde{N}_h + k_y|}{|k|}g \\ &\geq \frac{|n|\widetilde{N}_h - |k_y|}{|k|}g \\ &> \widetilde{N}_h \frac{|n| - 1/2}{|k|}g \\ &> \frac{\widetilde{N}_h}{2} \frac{2}{\widetilde{N}_h}g \\ &= g, \end{aligned} \quad (4.165)$$

$$(4.166)$$

where we have used that  $|a + b| > |a| - |b|$ ,  $|n| \geq 1$ ,  $|k_y| < N_h/2$  and  $|k| < N_h/2$ . This argument can be carried out for the constraints originating from both the summation over  $l$  and  $m$ , leaving us with:

$$\frac{j}{g}(a - g) = k_x \quad (4.167)$$

$$\frac{k}{g}(a - g) = k_y \quad (4.168)$$

These equations mean that

$$\langle j, k | \phi_{(k_x, k_y)} \rangle = \begin{cases} \binom{2g}{k_x g / j + g} & \text{if } k_x/k_y = j/k \\ 0 & \text{otherwise} \end{cases} \quad (4.169)$$

In particular, by orthogonality of the  $|j, k\rangle$ , sectors with different  $k_x/k_y$  are mutually orthogonal. As a final step, we will investigate the sector that is spanned by the vectors

$$\{|\phi_{(k_x, k_y)}\rangle\}_{\substack{(k_x, k_y) \in I \\ k_x/k_y = p/q}} \quad (4.170)$$

for a fixed, completely reduced fraction  $p/q$ . The vectors in this set have the form  $|\phi_{(p, q)}\rangle, |\phi_{(2p, 2q)}\rangle, \dots$ . Since

$$\langle p, q | \phi_{(bp, bq)} \rangle = \binom{2}{b+1}, \quad (4.171)$$

only  $|\phi_{(1p, 1q)}\rangle$  has non-zero overlap with  $|p, q\rangle$ . Therefore,  $|\phi_{(1p, 1q)}\rangle$  must necessarily be linearly independent from all other vectors in that sector. We can therefore



remove  $|\phi_{(1p,1q)}\rangle$  from  $\{|\phi_{(k_x,k_y)}\rangle\}_{(k_x,k_y)\in I, k_x/k_y=p/q}$  and check the remaining basis vectors for linear independence. Indeed we can iterate this procedure to show that in the remaining set, there exists exactly one vector that has non-zero overlap with  $|bp,bq\rangle$ , which is  $|\phi_{(bp,bq)}\rangle$ . Therefore,

$$\dim \text{span}\{|\phi_{(k_x,k_y)}\rangle\}_{(k_x,k_y)\in I} = |I| \quad (4.172)$$

and by equation (4.160), it follows that

$$\dim \mathcal{S}' \geq |I| \quad (4.173)$$

□

We have shown that there is a polynomial number of ground states spanned by string-inserted states. One might think that this parameterizes the full ground space of  $H$ , just as for  $G$ -injective PEPS with finite  $G$ . However, this is not the case. To see this, consider an arbitrary bit-string  $b \in \{0,1\}^{N_h}$ . Then, we define the product state  $|v(b)\rangle$  by stacking  $N_v$  copies of  $b$  on top of each other and then identifying  $0 \rightarrow |0\rangle$  and  $1 \rightarrow |1\rangle$ , for example

$$|v(0101)\rangle = \begin{array}{|c|c|c|c|c|} \hline \text{---} & \text{---} & \text{---} & \text{---} & \text{---} \\ \hline \text{---} & \text{---} & \text{---} & \text{---} & \text{---} \\ \hline \text{---} & \text{---} & \text{---} & \text{---} & \text{---} \\ \hline \text{---} & \text{---} & \text{---} & \text{---} & \text{---} \\ \hline \end{array} \quad (4.174)$$

Horizontally stacked states  $|h(b)\rangle$  are defined accordingly. Clearly, there are  $2^{N_h} + 2^{N_v} - 2$  of these states (since only the all-0 and all-1 states are doubly counted). Finally, all of them are ground states, since, by definition, no plaquette locally looks like any of  $|B\rangle = \begin{smallmatrix} 0 & 1 \\ 1 & 0 \end{smallmatrix}$ ,  $|E_1\rangle = \begin{smallmatrix} 0 & 0 \\ 1 & 0 \end{smallmatrix}$ ,  $|E_2\rangle = \begin{smallmatrix} 0 & 1 \\ 0 & 0 \end{smallmatrix}$ ,  $|E_3\rangle = \begin{smallmatrix} 1 & 1 \\ 1 & 0 \end{smallmatrix}$  or  $|E_4\rangle = \begin{smallmatrix} 0 & 1 \\ 0 & 1 \end{smallmatrix}$ , even across the boundary. Note that in all of these configurations, the winding of the loops around the torus is maximal in at least one direction (horizontally or vertically). We call these states *isolated states*, as they are not coupled to any other loop configuration by the Hamiltonian.

We therefore find that the ground space degeneracy of  $H$  is at least *exponential* in  $N_v$  and  $N_h$ , and thus cannot be parametrized by strings of symmetry operations alone. In fact, e.g. the states

$$|v(0101)\rangle = \begin{array}{|c|c|c|c|c|} \hline \text{---} & \text{---} & \text{---} & \text{---} & \text{---} \\ \hline \text{---} & \text{---} & \text{---} & \text{---} & \text{---} \\ \hline \text{---} & \text{---} & \text{---} & \text{---} & \text{---} \\ \hline \text{---} & \text{---} & \text{---} & \text{---} & \text{---} \\ \hline \end{array} \quad |v(1010)\rangle = \begin{array}{|c|c|c|c|c|} \hline \text{---} & \text{---} & \text{---} & \text{---} & \text{---} \\ \hline \text{---} & \text{---} & \text{---} & \text{---} & \text{---} \\ \hline \text{---} & \text{---} & \text{---} & \text{---} & \text{---} \\ \hline \text{---} & \text{---} & \text{---} & \text{---} & \text{---} \\ \hline \end{array} \quad (4.175)$$

are indistinguishable by any such string operation. It is worth pointing out, however, that all of these ground states are isolated and in the sector with maximal winding number, so it might still be possible that in the remaining sectors, the ground space can be parametrized succinctly in terms of the symmetry.

### 4.3 Conclusion

In this chapter, we have extended our study of symmetric PEPS to a non-abelian continuous symmetry. We investigated a class of  $SU(2)$ -invariant PEPS with the fundamental representation of  $SU(2)$ , and studied their entanglement properties and

their relation to local Hamiltonians. First, we have introduced the most general form of tensors invariant under the fundamental representation of  $SU(2)$ . From the local tensor, we have constructed local parent Hamiltonians acting on  $2 \times 2$  sites, and characterized their ground space structure. For open boundaries, we have found that the ground space on rectangular patches on any size is always exactly parameterized by the PEPS, i.e., the intersection property is fulfilled. We were further able to show that by choosing appropriate Hamiltonian terms at the boundary, the system acquires a unique ground state. On a system with periodic boundary conditions, we have found a ground space degeneracy which grows with the system size. We were able to attribute this to at least two distinct mechanisms: First, closing the boundaries with symmetry twists of  $SU(2)$ , in analogy to finite symmetry groups, yields a linearly growing number of ground states; and second, extremal isolated spin configurations yield an exponentially growing number of states. Regarding the entanglement properties of the state, we found that the zero Renyi entropy has a logarithmic correction to the area law scaling and that there are further geometric restrictions on long and thin bipartitions. Finally, we have mapped certain correlation functions of the PEPS to a classical Potts model. Using this mapping, it becomes clear that the physics of the isotropic ( $\lambda = 1$ ) point is that of a translation symmetry breaking plaquette state.

We are now equipped with a rigorous proof for the intersection property in a PEPS with a continuous symmetry. It would be interesting to find a more general (and potentially simpler) symmetry-based proof. Also, isolated states seem to be common in the study of PEPS with continuous symmetries. Can a general proof for their existence be constructed? Another interesting question concerns the existence critical points in the non-abelian case.

An interesting observation is that, for periodic boundaries and  $\lambda = 1$ , we obtain exactly the wave function of a quantum loop model  $|\psi_{N_h \times N_v}(A, \text{PBC})\rangle = \sum_L d^{n_L} |L\rangle$  which was studied in [137, 138]. The main focus of those works is the case where the so called *topological weight* is  $d = 2 \cos\left(\frac{\pi}{k+2}\right) < 2$  for  $k$  a positive integer. In that case, a Hamiltonian with a finite number of ground states on the torus in the thermodynamic limit can be found, in contrast to the exponential degeneracy we find in our model. The topological weight in our PEPS wave function is given by the bond dimension  $d = 2$ . While our construction can be extended to any integer  $d > 2$ , it is unclear whether a PEPS description with constant bond dimension exists for the quantum loop models investigated in the above references.

Finally, when computing diagonal observables, the PEPS contraction coincides with the result of a Monte Carlo simulation [145]. This might indicate that PEPS with continuous symmetries beyond this model are susceptible to Monte Carlo schemes, and replacing the computationally heavy PEPS contraction in such a manner may prove useful e.g., in variational calculations.

## Chapter 5

# Subsystem Symmetry Protected Topological Order

In this chapter we will consider elementary tensors whose symmetry is not described by a simple group action of the form (2.3) but follows a more anisotropic form. The resulting states differ from the wave functions considered so far: The PEPS actually have a *physical* symmetry and this symmetry is neither local, nor global, but an intermediate *subsystem* symmetry. They are the unique ground states of gapped 2D Hamiltonians on periodic boundary conditions. Still, these states can not be deformed into a product state as long as the subsystem symmetries are respected. We therefore speak about *subsystem symmetry-protected topological* (SSPT) order. We have encountered topological order protected by global symmetries in chapter 1, where we investigated the AKLT chain. Natural generalizations to two-dimensional SPT order protected by *global* symmetries have also been obtained [146, 147]. While states with subsystem symmetries generally also exhibit global symmetries (obtained by applying many symmetries at once), the stronger symmetry condition entails its own set of interesting consequences: First, such symmetries can be shown to be necessary in the context of measurement-based quantum computation, that is, the ground state in certain SSPT phases can be exploited as a resource to perform universal quantum computation [148–151]. Second, subsystem symmetries can be subjected to a generalized gauging procedure, yielding novel *fracton* phases of matter in three dimensions [152–155].

One example of such an SSPT ordered phase is the *Cluster Phase*. In this chapter the center stage is taken by the Cluster phase’s ground state entanglement entropy. In section 5.1, we investigate the Renormalization Group fixed point deep in the phase and show that it exhibits a subtractive correction to the area law. This correction is identical to the correction in topologically ordered phases and thus weakens measurements of the entanglement entropy as a phase classification mechanism. On the other hand, recent studies conjectured this correction to be *spurious*, only appearing at special points in the phase. In section 5.2, we show that the opposite is the case: We give both analytical and numerical evidence that the correction persists everywhere in the phase, except at certain fine-tuned points. We discuss our conclusions and open questions in 5.3.

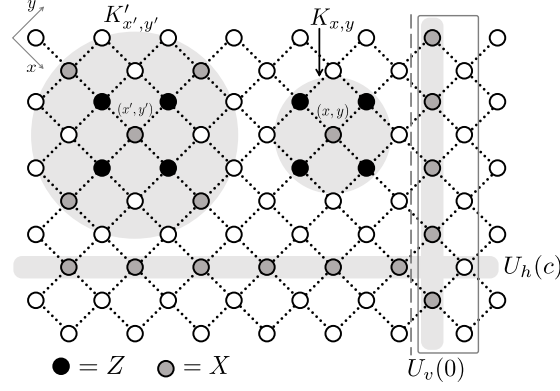


Figure 5.1: The rotated square lattice on a cylinder with circumference  $N = 5$ . The horizontal and vertical line symmetries  $U_h$  and  $U_v$  are shown as well as an entanglement cut next to a vertical subsystem symmetry. Also shown are the terms of the stabilizer parent Hamiltonian both at the Cluster ( $K$ ) as well as the  $|\theta = \pi\rangle$  point ( $K'$ ). Figure courtesy of D. T. Stephen and reprinted with permission ©The American Physical Society (2019).

## 5.1 The Cluster State

The purpose of this section is to set the stage by introducing the *Cluster state*, which is both a paradigmatic example of SSPT order and our point of departure to explore the surrounding quantum phase in the next section.

Throughout the first part of this chapter, we will work with a PEPS on the two-dimensional square lattice that is rotated by  $45^\circ$  (Fig. 5.1). To facilitate notation, throughout this chapter we will use  $X, Y, Z$  to mean the Pauli matrices.

### 5.1.1 Symmetries

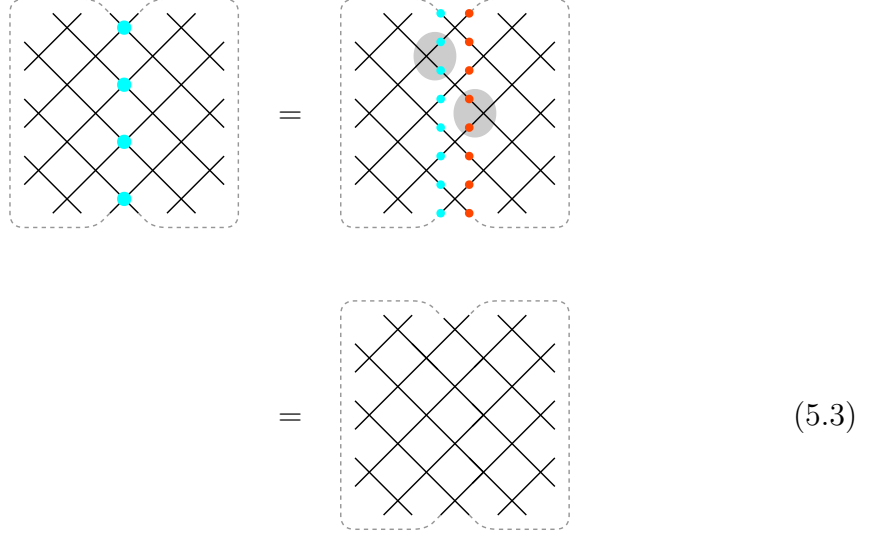
We will now define symmetries of an elementary PEPS-tensor in such a way that the resulting state is symmetric under the application of a unitary that is acting strictly along a line of the (rotated) lattice (the lines  $U_h(c)$  and  $U_v(0)$  shaded in gray in Fig. 5.1). To this end, consider a bond dimension  $D = 2$ -tensor  $C_1$  with physical dimension  $d = 2$  and the following constraints

$$\begin{aligned}
 & \begin{array}{c} \diagup \\ | \\ \textcircled{C_1} \\ | \\ \diagdown \end{array} = \begin{array}{c} X \\ \diagup \\ \textcircled{C_1} \\ \diagdown \\ X \end{array} = \begin{array}{c} Z \\ \diagup \\ \textcircled{C_1} \\ \diagdown \\ Z \end{array} \\
 & = \begin{array}{c} Z \\ \diagup \\ \textcircled{C_1} \\ \diagdown \\ X \end{array} = \begin{array}{c} \diagup \\ \textcircled{C_1} \\ \diagdown \\ Z \end{array} \quad (5.1)
 \end{aligned}$$

The solution to the above constraints is given by the following one-parameter family of fiducial states

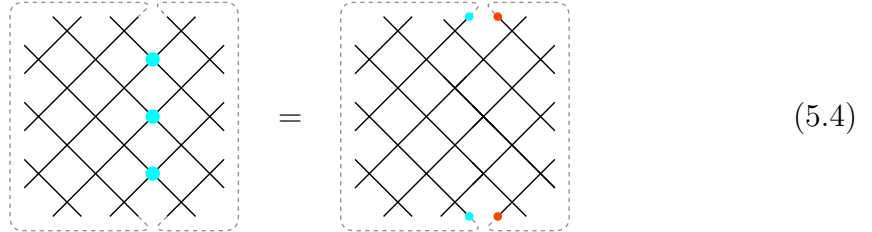
$$|C_1\rangle = |\alpha_+\rangle \begin{vmatrix} 0 & + \\ 0 & + \end{vmatrix} + |\alpha_-\rangle \begin{vmatrix} 1 & - \\ 1 & - \end{vmatrix} \quad (5.2)$$

with  $|\alpha_\pm\rangle = \cos(\alpha) |+\rangle \pm \sin(\alpha) |-\rangle$ . Denoting  $\bullet = X$ ,  $\bullet = Z$ , we can apply a string of  $X$  across the lattice:



$$(5.3)$$

and



$$(5.4)$$

for the adjacent line. We have applied the symmetries (5.2) in the shaded areas. We make the following two observations: First, when periodic boundary conditions are imposed, the line-symmetries become actual physical symmetries of the state. Second, on open boundaries, the symmetry fractionalizes at the boundary in a non-trivial way: While neighbouring lines commute in the bulk, the corresponding virtual representations at the boundary anticommute. After blocking  $L \times L$  sites of a cylinder with circumference  $L$ , one therefore obtains an MPS with precisely the same symmetry properties as the AKLT state (1.27): The line-symmetry has turned into a single-site operator that pushes through to the virtual level as a non-trivial projective representation. Indeed, it can be proven rigorously, that the cluster state possesses “strong” SSPT order, i.e., it cannot be connected to a product state by a finite depth circuit, even if one allows the circuit to be merely *linearly symmetric*, i.e., to be comprised of gates that individually break the symmetry but can be grouped in such a way that the subcircuit along a lower-dimensional retains the relevant symmetry [156].

### 5.1.2 Parent Hamiltonian

We now set  $\alpha = \pi/4$  in (5.2) and denote the resulting state as  $|C\rangle$  (the *Cluster State*). A few features of the resulting state can be verified: First, for each computational basis state, one may assign the subgraph of the square lattice which has an edge between two qubits if and only if they are both in the  $|1\rangle$ -state. Then,  $|C\rangle$  is an equal-weight superposition over all computational basis states, where the sign of each term in the sum is  $(-1)^{n_e}$ , where  $n_e$  is the number of edges in the corresponding subgraph. This expression grants us access to the (non-symmetric) finite-depth unitary circuit that connects the Cluster state to a product state:

$$|C\rangle = \prod_e CZ_e |+\rangle^N, \quad (5.5)$$

where the product runs over all the edges of the lattice and

$$CZ = \begin{pmatrix} 1 & & & \\ & 1 & & \\ & & 1 & \\ & & & -1 \end{pmatrix}. \quad (5.6)$$

Using this expression, we readily see that

$$K_{(x,y)} |C\rangle = |C\rangle, \quad (5.7)$$

where  $K_{(x,y)} = X_{(x,y)} Z_{(x-1,y)} Z_{(x,y-1)} Z_{(x,y+1)} Z_{(x+1,y)}$ , as shown in Fig. 5.1. This is seen by plugging  $X_i CZ_{ij} = X_i Z_j$  and (5.5) into (5.7). Therefore,  $|C\rangle$  must be a ground state of the stabilizer Hamiltonian

$$H = - \sum_{(x,y)} K_{(x,y)} \quad (5.8)$$

and since there are as many independent constraints as there are qubits, it is the unique ground state on periodic boundary conditions.

### 5.1.3 Entropy

The fact that  $|C\rangle$  is a stabilizer state can be exploited to compute the von-Neumann entropy exactly. We choose to bipartition a long (the result will be independent of the length of the system due to the area law) cylinder of circumference  $L$  by a cut that runs along the compactified axis of the rotated cylinder (see Fig. 5.1). It has been shown in [157] that the entropy of a bipartition of a stabilizer state into regions  $A$  and  $B$  is given by

$$S(\rho_A) = |A| - \log |G_A|, \quad (5.9)$$

where  $G_A$  is the group generated by stabilizers acting exclusively within subregion  $A$ . The number of such generators is easy to count: Out of the  $|A|$  generators that act on  $A$ , there are  $L$  star operators  $K_{(x,y)}$  in the immediate vicinity of the boundary that act on both  $A$  and  $B$  (Fig. 5.1). However, the product of all  $K$  along the cut is precisely the line-symmetry (5.3) which is completely contained in  $A$ . Therefore  $\log |G_A| = 2^{|A|-L-1}$ , yielding

$$S(\rho_A) = L - \gamma, \quad (5.10)$$

where the offset  $\gamma = 1$  is independent of the size of the boundary. Owing to the way the subsystem symmetries lead to the  $\gamma$ -term, we call this offset the *Symmetry-Protected Entanglement Entropy (SPEE)*. A correction to the area law of the form (5.10) is familiar from the study of systems with intrinsic topological order. In such systems the ground state manifold is characterized by wave functions that cannot be continuously connected to any product state regardless of any symmetries imposed. They therefore form a phase of matter that is rather distinct from the present case. Detection of these topologically ordered phases is complicated by the fact that there is no local order parameter that can be measured. Instead, it has been put forward that one may use the entanglement entropy as a means to detect and classify such phases. Using a suitable partition of the system [33, 34] one may measure the entanglement entropy of a ground state and draw conclusions about the quantum dimension of the underlying topologically ordered phase. However, as we have just shown, under this scheme the 2D Cluster State is indistinguishable from e.g., the Toric Code (at least with the present partition).

It was argued in [158] that the detection mechanism is rescued by the fact that the correction of the Cluster State are *spurious*, i.e., there exist ground states in the “Cluster Phase” that display a *larger* correction to the area law. It is the purpose of the next section to show that these larger corrections are fine-tuned and - as long as the geometry remains as shown in Fig. 5.1 - the correction  $\gamma = 1$  is instead robust throughout the phase.

## 5.2 The Cluster Phase

We will now begin exploring the *Cluster Phase* that surrounds the zero correlation length Cluster State. In order to argue that the SPEE introduced in the previous section is universal within the phase, except at fine-tuned points, we first introduce an exactly solvable perturbation, then give a more general analytical argument and finally conduct a numerical experiment.

### 5.2.1 An Exactly Solvable Perturbation

To illustrate our arguments, let us choose one particular path within that phase that contains both the cluster state, as well as the state analyzed in [158], which was found to exhibit a larger correction to the entanglement entropy. To this end consider the states  $|\theta\rangle$  that are obtained by the following unitary circuit  $U(\theta)$  applied to the cluster state

$$|\theta\rangle = \prod_e [(H \otimes H)C\theta(H \otimes H)]_e |C\rangle \quad (5.11)$$

where, again, the product runs over all edges of the lattice and

$$H = \frac{1}{\sqrt{2}} \begin{pmatrix} 1 & 1 \\ 1 & -1 \end{pmatrix} \quad \text{and} \quad C\theta = \begin{pmatrix} 1 & & & \\ & 1 & & \\ & & 1 & \\ & & & e^{i\theta} \end{pmatrix} \quad (5.12)$$



This finite-depth circuit is readily seen to describe a path of states contained within the cluster phase, since each of the gates is diagonal in the local  $X$ -basis and therefore commutes with all the subsystem symmetries. Up to complex conjugation, the path is symmetric around  $\theta = \pi$ , so we consider  $\theta \in [0, \pi]$ . Let us now investigate the quantity  $\gamma(\theta)$  as defined by (5.10).

We have already shown that  $\gamma(0) = 1$ . For  $\theta = \pi$ , we can carry out a similar analysis, since the state is again a stabilizer state. This time, the operators stabilizing the state are enlarged versions of the star operator that has grown under the unitary evolution (cf. Fig. 5.1):

$$U(\pi)K_{(x,y)}U^\dagger(\pi) = X_{(x,y+2)}X_{(x,y-2)}Z_{(x-1,y)}Z_{(x,y-1)} \\ X_{(x,y)}Z_{(x,y+1)}Z_{(x+1,y)}X_{(x-2,y)}X_{(x+2,y)}. \quad (5.13)$$

Repeating the analysis of surrounding (5.9), we find that there are now two independent ways of multiplying stabilizers that act across the cut in such a way that their product yields an operator that is completely contained within subregion A, namely the star operators along a diagonal of distance one and two along the cut. The size of  $|G_A|$  is therefore  $2^{|A|-L-2}$  and therefore  $\gamma(\pi) = 2$ .

For intermediate values of  $\theta$ , there are several possibilities: First,  $\gamma$  could be a smooth function of  $\theta$  or there could be a jump for some value  $\theta > 0$ . In both cases we could immediately conclude that the correction  $\gamma = 1$  would not be universal within the phase. However, we will now show that  $\gamma = 1$  for all  $\theta$ , except at  $\theta = \pi$ , where a jump occurs. It follows that, at least along this particular path,  $\gamma = 1$  is universal.

Since, for intermediate values of  $\theta$ ,  $|\theta\rangle$  is not a stabilizer states we have to resort to a different method in order to compute the entanglement entropy, inspired by [159]: Fortunately, the calculation can be simplified using the knowledge of a short depth circuit that disentangles the state, namely

$$\prod_e CZ_e U(-\theta) |\theta\rangle = |+\rangle^N. \quad (5.14)$$

Moreover, the entanglement entropy is invariant under applying local unitaries to either subsystem. Applying those gates of  $\prod_e CZ_e U(-\theta)$  that act on edges that are contained exclusively in  $A$  or  $B$ , we obtain a new density matrix with the same entropy as  $\rho_A$ :

$$\rho'_A = \text{Tr}_B \prod_e [(H \otimes H)C\theta(H \otimes H)]_e CZ_e (|+\rangle \langle +|)^L \prod_e CZ_e [(H \otimes H)\overline{C\theta}(H \otimes H)]_e \quad (5.15)$$

The  $A(B)$ -subsystems now comprise the qubits immediately to the left (right) of the cut (Fig. 5.1). Crucially, we have reduced the computation to a *one-dimensional* one which is now amenable to tensor-network techniques. Since these techniques are straightforward for higher integer Renyi entropies, but hard for the von-Neumann entropy, we will focus on the Renyi 2-entropy  $S_2(A) = \text{Tr}(\rho'_A{}^2)$  from now on. We can set up an expression for  $\rho'_A{}^2$  in terms of a Matrix Product Density Operator (MPDO) (Fig. 5.2). For a cylinder of circumference  $L$ , there are two ways of contracting the network corresponding to  $\text{Tr}(\rho'_A{}^2)$ : First, one may set up  $\rho'_A{}^2$  first and then take



the trace, encountering an exponential overhead. It is much more advantageous to contract “from-top-to-bottom” (cf. Fig. 5.2). We can therefore rewrite:

$$\text{Tr}(\rho'_A(\theta)^2) = \text{Tr}(Q^L(\theta)), \quad (5.16)$$

for  $Q(\theta)$  the matrix defined in Fig. 5.2. The spectrum of  $Q(\theta)$  allows us to make statements even in the thermodynamic limit: If there is a unique largest eigenvalue with magnitude  $r$ , then for  $L \rightarrow \infty$ , we have that  $S_2(\theta) = Lr + \mathcal{O}(e^{-L})$ , i.e.,  $r$  is the prefactor of the area law and  $\gamma = 0$ . If there are multiple leading eigenvalues  $\lambda_k = re^{i\phi_k}$ , the entropy becomes

$$S_2(\theta) = L \log_2 r - \log_2 m + \mathcal{O}(e^{-L}) \quad (5.17)$$

with  $m = \sum_k e^{iL\phi_k}$ . Therefore,  $\gamma(\theta) = \log_2 m$  is non-zero if  $Q(\theta)$  has degenerate leading eigenvalues and it may oscillate with system size depending on the phase structure of these eigenvalues. From the definition of  $Q(\theta)$  (Fig. 5.2), we see that  $Q(\theta)$  is a matrix of size  $2^8 \times 2^8$  and can therefore be easily diagonalized, the result of which is shown in Fig. 5.3. For  $\theta \neq \pi$ , there are two largest eigenvalues, both of which are positive. We therefore have that  $\gamma = 1$ . For  $\gamma = \pi$  we find that the largest eigenvalues are  $1/4, -1/4, i/4$  and  $-i/4$  with degeneracies 8, 4, 2 and 2, respectively. Therefore

$$S_A^{(2)}(\pi) = \begin{cases} 2N - 4 & \text{if } 4 \mid N \\ 2N - 3 & \text{if } 2 \mid N \text{ and } 4 \nmid N \\ 2N - 2 & \text{if } 2 \nmid N \end{cases} \quad (5.18)$$

We conclude that  $\gamma = 1$  along the path (5.11), except at a single point  $\theta = \pi$ , where  $\gamma \in \{2, 3, 4\}$ , depending on the size of the system.

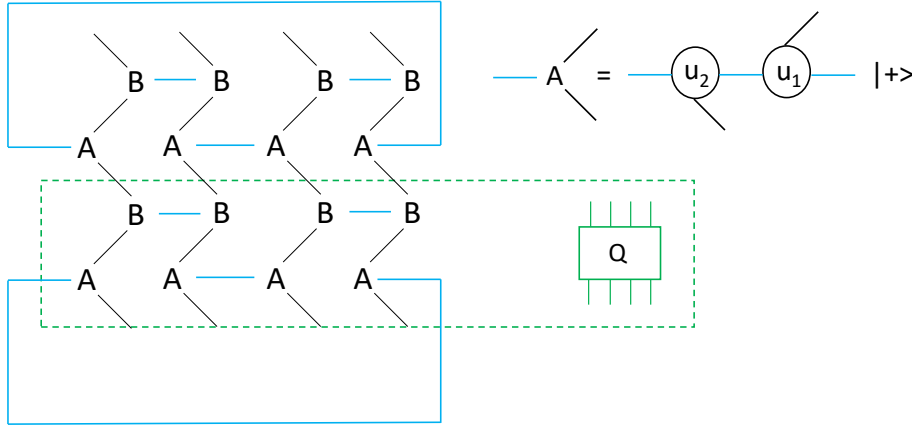


Figure 5.2: The network representing  $\text{Tr}(\rho'_A(\theta)^2)$  and the definition of the matrix  $Q(\theta)$ . Physical legs are shown in blue, virtual legs are black.  $u_1$  and  $u_2$  are obtained from the singular value decomposition of the two-body gates. The resulting  $A$ - and  $B$ -tensors each have bond dimension 4.

### 5.2.2 Generic Ground States

To bolster our case, we now consider generic ground states in the phase. Unfortunately, we cannot employ a direct dimensionality reduction as in section 5.2.1 since we do not have access to the precise form of the quantum circuits that create

those states from the Cluster state. Instead, we recall the bulk-boundary correspondence (1.47): The reduced density matrix of one half of a long cylinder of a PEPS can be written as  $\rho = U\sqrt{\sigma_L^T}\sigma_R\sqrt{\sigma_L^T}U^\dagger$ , where  $\sigma_L$  and  $\sigma_R$  are the left and right eigenvectors of the PEPS transfer matrix and  $U$  is an isometry. In particular, the entanglement entropy of such a region is identical to the entropy of the symmetrised fixed-point

$$\sigma := \sqrt{\sigma_L^T}\sigma_R\sqrt{\sigma_L^T}. \quad (5.19)$$

Equation (1.47) offers two distinct points of attack. First, we can exploit the symmetries of the tensor network (5.2) to *analytically* constrain  $\sigma$  at arbitrary points in the cluster phase. Second, we may consider small perturbations away from the Cluster Hamiltonian (5.8) and attempt to find  $\sigma$  *numerically*. We will explore both avenues in sections 5.2.2 and 5.2.3, respectively.

Before we carry out these analyses, we introduce a slightly different representation of the system that will be useful in the subsequent sections. The new representation is formed by blocking two sites (e.g.,  $(x, y)$  and  $(x+1, y)$ ) into a new unit cell. The new tensor has two physical indices that we call  $a$  and  $b$ . It can be checked that this tensor can be recompressed to bond dimension  $D = 2$ . The symmetries (5.2) induce the following symmetries for the blocked tensor:

$$\begin{aligned} \text{Diagram 1} &= \text{Diagram 2} = \text{Diagram 3} \\ &= \text{Diagram 4} \end{aligned} \quad (5.20)$$

The advantage is that we can now work on the more familiar *non-rotated* square lattice while keeping the line-symmetries parallel to the axes of the cylinder and the entanglement cut.

### An Analytic Argument

We now set up an analytic argument that shows that  $\gamma = 1$  throughout the phase under relatively weak assumptions. The structure of the argument proceeds as follows: First, we give an alternative proof for  $\gamma = 1$  in the Cluster state, based solely on the defining symmetry (5.2). Then, we use a theorem stating that those symmetries are robust everywhere within the phase.

The symmetries (5.20) concatenate to yield the following commutation relations

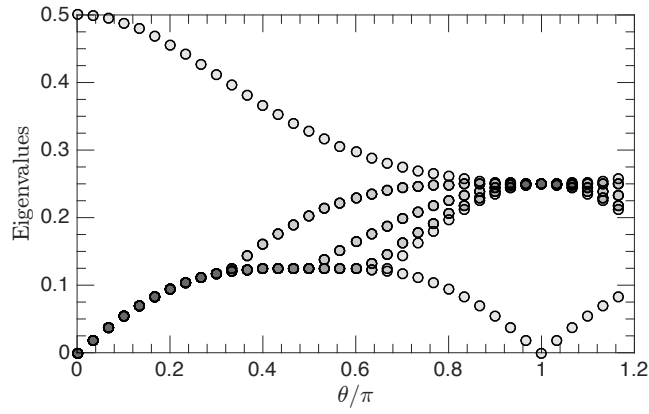


Figure 5.3: Absolute value of the 18 largest eigenvalues of the matrix  $Q(\theta)$  cf. Fig. (5.2). Each dot represents at least two degenerate eigenvalues and darker shading indicates larger degeneracies. The leading eigenvalue is two-fold degenerate everywhere except at  $\theta = \pi$ , where it is 16-fold degenerate. Figure reprinted with permission ©The American Physical Society (2019).

for the transfer matrix

$$\begin{aligned}
 & \text{Diagram 1} = \text{Diagram 2} = \text{Diagram 3} \\
 & \text{Diagram 4} = \text{Diagram 5} = \text{Diagram 6} \quad (5.21)
 \end{aligned}$$

The diagrams consist of horizontal lines intersected by diagonal lines. In the first three diagrams, the intersections are labeled with 'X' and 'Z'. The fourth diagram has 'X' labels on the left and right. The fifth and sixth diagrams have 'X' labels on the right. The diagrams are connected by equals signs, indicating they represent the same mathematical object.

Deep in the cluster phase, the fixed points  $\sigma_L$  and  $\sigma_R$  are unique and therefore satisfy

the above symmetries, i.e.,

$$[X_k, \sigma_{L/R}] = 0 \quad (5.22a)$$

$$[Z_k Z_{k+1}, \sigma_{L/R}] = 0 \quad (5.22b)$$

$$X^{\otimes N} \sigma_{L/R} = \sigma_{L/R} X^{\otimes N} = \sigma_{L/R} \quad (5.22c)$$

Hence, there are  $2N$  independent operators that stabilize the fixed point. The unique solution to these constraints is

$$\sigma_{L/R} = \frac{\mathbb{1} + X^{\otimes N}}{2}. \quad (5.23)$$

Since this is nothing but a projector on the even-parity subspace, the entanglement spectrum is

$$\lambda_1 = \dots = \lambda_{2^N/2} = 2/2^N \quad (5.24)$$

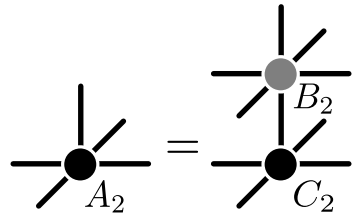
$$\lambda_{2^N/2+1} = \dots = \lambda_{2^N} = 0 \quad (5.25)$$

and

$$S = N - 1 \quad (5.26)$$

for all Rényi entropies.

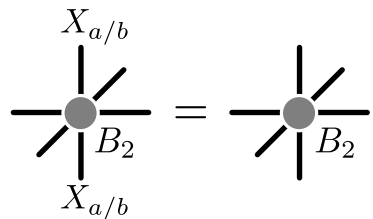
Next, we show that the above argument works everywhere in the Cluster phase, except at fine-tuned points. Small excursions into the surrounding phase are realized by adiabatic changes of the ground state wave function. Intuitively, such an evolution should be well captured by applying a PEPO to the initial tensor <sup>1</sup>



The diagram shows a tensor  $A_2$  (a black dot with four legs) equal to the sum of two tensors  $B_2$  and  $C_2$ . Tensor  $B_2$  is a grey dot with four legs, and tensor  $C_2$  is a black dot with four legs. The legs of  $A_2$  are horizontal, vertical, and diagonal. The legs of  $B_2$  and  $C_2$  are also horizontal, vertical, and diagonal, but their orientations are swapped relative to each other.

$$A_2 = B_2 + C_2 \quad (5.27)$$

In case of the cluster phase, this decomposition has the special property that



The diagram shows a tensor  $X_{a/b}$  (a grey dot with four legs) equal to the sum of two tensors  $B_2$ . The legs of  $X_{a/b}$  are horizontal, vertical, and diagonal. The legs of the  $B_2$  tensors are also horizontal, vertical, and diagonal, but their orientations are swapped relative to each other.

$$X_{a/b} = B_2 + B_2 \quad (5.28)$$

and this decomposition is valid *everywhere* within the phase [148]. The virtual space is seen to be decomposed into a *protected* ( $C_2$ ) and *junk* ( $B_2$ ) subspace. Crucially,

---

<sup>1</sup>Figures in equations (5.27) and (5.28) courtesy of D. T. Stephen and reprinted with permission ©The American Physical Society (2019).

the fact that  $X_{a/b}$  pushes through the PEPO-tensor is sufficient to prove (5.21) where all operators acting on the protected subspace. Furthermore, the fixed point of the modified transfer matrix continues to be unique by adiabaticity. Therefore, everywhere in the Cluster phase

$$\sigma_{L/R} = \left( \frac{\mathbb{1} + X^{\otimes N}}{2} \right)_{\text{protected}} \otimes \tilde{\sigma}_{L/R_{\text{junk}}} \quad (5.29)$$

and consequently, the entanglement spectrum is equivalent to the spectrum of

$$\sigma = \left( \frac{\mathbb{1} + X^{\otimes N}}{2} \right)_{\text{protected}} \otimes \tilde{\sigma}_{\text{junk}} \quad (5.30)$$

with  $\tilde{\sigma} = \sqrt{\tilde{\sigma}_L^T} \tilde{\sigma}_R \sqrt{\tilde{\sigma}_L^T}$ . Since the entropy is additive,

$$S = N - 1 + S(\tilde{\sigma}). \quad (5.31)$$

We conclude that  $\gamma = 1$  precisely, as long as  $\tilde{\sigma}$  is a generic full rank matrix.

### 5.2.3 Generic Perturbations - Numerics

We have numerically proven  $\gamma = 1$  along a specific path traversing the Cluster phase (section 5.2.1) and provided an argument why  $\gamma = 1$  generically. The purpose of this section is to numerically tackle generic points in the phase. We consider both symmetry-breaking as well as symmetry-preserving perturbations of the Cluster Hamiltonian (5.8)

$$\mathcal{H} = \mathcal{H}_C + \sum_{x,y} h'_{x,y} \quad (5.32)$$

According to our hypothesis, we should have  $\gamma = 1$  for small arbitrary perturbations that respect the line-symmetries and  $\gamma = 0$  for symmetry-breaking terms. Indeed, the numerical data we present in this subsection provides evidence for this hypothesis. Once we have confirmed our hypothesis and established the correctness of our numerical approach, we will then use the algorithm to probe a specific perturbation that breaks the line-symmetries but keeps what we will call *subsystem time reversal* symmetry. Surprisingly, we find that the SPEE (and hence the SSPT order) is robust to this perturbation, indicating a new phase of matter beyond the cluster phase.

To compute the ground state entropy we work in the blocked picture (5.20). An optimal PEPS tensor for the ground state is found variationally using an iPEPS algorithm [160, the optimization was done by M. Iqbal]. Technically, the algorithm works directly in the thermodynamic limit but since there is a finite correlation length, the same tensor should also describe with good accuracy the ground state on a large cylinder. We then cut the cylinder in half and use the bulk-boundary correspondence (1.47). Numerically, it is easiest to access the second Renyi entropy  $S_2(\rho) = -\log_2 \text{Tr} \rho^2$ . In terms of the fixed point this reads

$$S_2 = -\log_2 \text{Tr}(\sigma_R \sigma_L^T \sigma_R \sigma_L^T) \quad (5.33)$$

If the fixed points are well approximated by MPOs, the same technique we used in section 5.2.1 can be used theoretically, contracting it “from top to bottom”, cf. Fig. 5.2:

$$\text{Tr}(\sigma_R \sigma_L^T \sigma_R \sigma_L^T) = \text{Tr}(Q^L). \quad (5.34)$$

It remains to find an accurate MPO description of the fixed point tensors. From the fixed point tensors, the matrix  $Q$  is obtained and the leading eigenvalues are extracted. In the following,  $Q$  will always at most have two degenerate eigenvalues, so we will call the leading two eigenvalues  $\lambda_0$  and  $\lambda_1$ . In exact analogy with eq. (5.17), we have that  $\gamma = 1$  if the leading eigenvalue of  $Q$  is two-fold degenerate, while  $\gamma = 0$  if it is unique. Measuring the ratio  $\lambda_1/\lambda_0$  therefore gives us direct access to the SPEE.

### Benchmarking the Algorithm

We begin by studying four known models to determine if our algorithm is able to detect and locate the transition points faithfully. The first two will be symmetry-respecting while the latter two are symmetry-breaking. By definition of SSPT order, we expect the symmetry-respecting perturbation to only drive the system into a different phase if they are sufficiently strong, while the symmetry-breaking models may have topologically trivial phases in the immediate vicinity of the Cluster point. The data is shown in Fig. 5.4.

The first perturbation we consider is a local  $X$ -field

$$h'_{x,y} = -h_X X_{x,y}. \quad (5.35)$$

Our data indicate that  $\lambda_1/\lambda_0 = 1$  up to  $h_X = 1$ , where a sudden drop occurs. We explain this as follows: Clearly, for  $h_X \rightarrow \infty$  the system will go into a topologically trivial paramagnetic phase. At the same time, the perturbation respects the subsystem symmetries, so a phase transition must occur for some finite value of  $h_X$ . We can find this value using a simple Kramers-Wannier argument [161, 162]: The model is dual under  $h_X \rightarrow 1/h_X$ , by conjugating the Hamiltonian with  $\prod_e CZ_e$ , which maps  $K_{(x,y)} \leftrightarrow X_{(x,y)}$ . Therefore, if there is a single phase transition, it must occur at  $h_X = 1$ . Indeed this has been confirmed through a (non-local) mapping to the transverse-field Xu-Moore model [163–167]. The proposed algorithm therefore detects the phase transition successfully.

The second term we consider is the minimal perturbation containing  $Z$ -operators but still commuting with the line symmetries

$$h'_{x,y} = -J_{ZZZZ}^\circ Z_{x-1,y} Z_{x+1,y} Z_{x,y-1} Z_{x,y+1}. \quad (5.36)$$

The data for this perturbation again indicates that  $\lambda_1/\lambda_0 = 1$  up to a phase transition at  $J_{ZZZZ}^\circ$  at which a downward jump occurs. This time, conjugating by the unitary  $\prod_e CZ_e$  leaves the perturbation invariant, while the star operators are mapped into local  $X$ -fields. This is precisely the definition of the transverse-field Xu-Moore model and, by the argument from the last paragraph, there is a phase transition at  $J_{ZZZZ}^\circ = 1$ . Again, the existence and location of this transition is accurately predicted by our numerics.

Next, we benchmark our algorithm on perturbations that break the line symmetries. First consider the local field

$$h'_{x,y} = -h_Z Z_{x,y}. \quad (5.37)$$

Under  $\prod_e CZ_e$  this family of Hamiltonians maps to the trivial paramagnet (along an axis in the  $XZ$ -plane) and we expect  $\lambda_1/\lambda_0$  to deviate from 1 for any  $h_Z > 0$ . Indeed, this is consistent with our data.

Finally, we consider the term

$$h'_{x,y} = -J_{ZZ}^\times (Z_{x,y} Z_{x+1,y+1} + Z_{x,y} Z_{x-1,y+1}). \quad (5.38)$$

The reason to consider this term is two-fold: First, despite breaking the individual line symmetries, this perturbation commutes with the global  $\mathbb{Z}_2 \times \mathbb{Z}_2$ -symmetry of the cluster state (applying  $X$  to the whole  $A$  or  $B$ -sublattice). It was shown in [168, 169] that the cluster state possesses “weak” SPT order protected by this symmetry, that is, it can be connected to a product state by a circuit respecting the  $\mathbb{Z}_2 \times \mathbb{Z}_2$ -symmetry if translation invariance is not enforced. This perturbation therefore allows us to check if the SPEE is due to the line symmetries or if the overall weak SPT order is sufficient. Second, (5.38) is slightly richer than the previous perturbation, since  $\prod_e CZ_e$  maps the model to two uncoupled transverse field Ising models which undergo a symmetry-breaking transition at  $J_{ZZ}^\times \approx 0.3285$ . While not tailored to detect such transitions, we would like to find out whether signatures of the second-order phase transition are visible in the SPEE. The data shows that  $\lambda_1/\lambda_0 < 1$  for  $J_{ZZ}^\times > 0$ , confirming our first hypothesis that the global  $\mathbb{Z}_2 \times \mathbb{Z}_2$ -symmetry is not sufficient to protect the SPEE. Second, there is a clear signature of singular behaviour at the expected value of  $J_{ZZ}^\times$ , suggesting that the algorithm may even be useful to detect non-SSPT transitions.

### Applying the Algorithm - A New Phase of Matter

Having established the correctness of the algorithm in the previous subsection, we now turn to models that have not yet been studied. As a warm-up, we consider another symmetry-preserving term:

$$h'_{x,y} = -J_{XX} (X_{x,y} X_{x+1,y} + X_{x,y} X_{x,y+1}). \quad (5.39)$$

The reason to consider this additional perturbation is that we would like to strengthen the claim that  $\gamma = 1$  is generic for symmetric perturbations. By having access to a third such perturbation, we can construct small random combinations of the symmetry-respecting perturbations and validate that  $\gamma = 1$  is always fulfilled. For this particular choice we numerically find that  $\lambda_1/\lambda_0 = 1$  in a finite region, as expected. At  $-J_{XX} \approx 0.5$ , a sudden drop occurs, indicating the demise of the SSPT order. We also verified that  $\gamma = 1$  for a combination of (5.35), (5.36), (5.39) and (5.41) (to be defined in the next paragraph):

$$\begin{aligned} h'_{x,y} = & -0.1X_{x,y} - 0.05(X_{x,y}X_{x+1,y} + X_{x,y}X_{x,y+1}) \\ & - 0.05Z_{x-1,y}Z_{x+1,y}Z_{x,y-1}Z_{x,y+1} - 0.1Y_{x,y}. \end{aligned} \quad (5.40)$$

Finally, we come to the most interesting perturbation of this section:

$$h'_{x,y} = -h_Y Y_{x,y}. \quad (5.41)$$

Adding such a local  $Y$ -field breaks the line-symmetries and thus we would expect  $\lambda_1/\lambda_0 < 1$  for any  $h_Y > 0$ . However, our data clearly indicates  $\lambda_1/\lambda_0 = 1$  as long as  $h_Y < 1$  (cf. Fig. 5.5).

One tempting explanation for the robustness to  $Y$ -perturbations relies on the fact that the line symmetries considered so far are not necessary to protect the SSPT order. Indeed, it was shown in [170] that the Cluster state is symmetric under the application of a product of  $Y$ -operators in a fractal geometry. An immediate problem with this explanation is given in the discussion surrounding eq. (5.38). There, we found that the SPEE only exists in the presence of symmetries that are spatially close to the cut, which is not the case for the fractal symmetries. To deliver the final blow to the fractal hypothesis, we consider the perturbation

$$h'_{x,y} = -h_X X_{x,y} - h_Y Y_{x,y}, \quad (5.42)$$

which breaks both the line symmetries and the fractal symmetries explicitly. Still, our data shows that  $\gamma = 1$  for  $h_X^2 + h_Y^2 < 1$  (Fig. 5.5). Before we move on, let us make a comment about the effectiveness of  $\gamma$  as a detection mechanism for quantum phases. Note that one could measure the onset of paramagnetic order in the  $X$ - or  $Y$ -direction by using appropriate local order parameters. There is however, no clear choice of order parameter that remains reliable along the entire transition line. The SPEE, on the other hand, is agnostic to the phase that lies beyond the transition.

In this subsection, we have established that  $\gamma$  is a reliable indicator of non-trivial SSPT order. In fact, we have used it to show that the Cluster Phase is embedded in a larger SSPT phase, which will subsequently refer to as the *XY Phase*. What is the nature of this phase and which is the symmetry protecting it?

### Perturbation Theory

To resolve these questions, we turn to perturbation theory, which provides two benefits to the present discussion. First, with the cluster state as the reference state, perturbation theory may be carried out to *arbitrary* order analytically. Second, this analytical understanding yields a PEPS representation of the perturbed state (at any desired order). The latter will finally allow us to identify a symmetry that we hypothesise to protect the SSPT order. Crucially, this symmetry is again found to be geometrically close to the cut, unlike the fractal symmetries considered before.

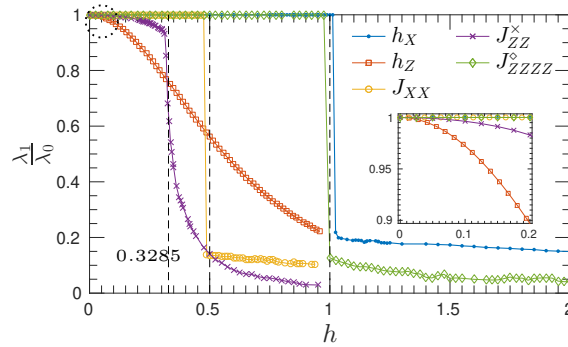


Figure 5.4: Ratio of the two largest eigenvalues of the matrix  $Q$  implicitly defined in (5.34). There is a correction  $\gamma = 1$  to the area law if  $\lambda_1/\lambda_0 = 1$  and  $\gamma = 0$  else. Inset: magnification of the region indicated by the dotted circle, showing that the symmetry breaking  $J_{ZZ}^X$  immediately destroys the SPEE. Figure courtesy of M. Iqbal and reprinted with permission ©The American Physical Society (2019).



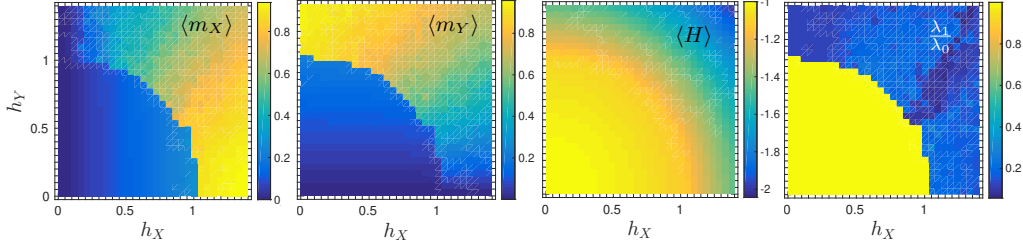


Figure 5.5: Phase diagram of the perturbation defined by (5.42). Shown are the  $X$ - and  $Y$ -magnetization as well as the ground state energy per site. The last diagram shows the ratio of the largest eigenvalues of the matrix  $Q$  and indicates that there is an extended SSPT phase in the absence of both the line- and fractal symmetries. Figure courtesy of M. Iqbal and reprinted with permission ©The American Physical Society (2019).

The starting point is the Hamiltonian  $\mathcal{H}(h_X, h_Y) = \mathcal{H}_C - \sum_{x,y} h_X X_j - h_Y Y_j$ . Here, and in the remainder of this subsection, we denote a site simply by  $j = (x, y)$  for shorter notation. Defining

$$V(h_X, h_Y) = (\mathcal{H}_C - E_C)^{-1} (\mathbb{1} - |C\rangle \langle C|) \sum_j h'_j, \quad (5.43)$$

the ground state, to first order in perturbation, is given by

$$\begin{aligned} |\psi(h_X, h_Y)\rangle &= [\mathbb{1} + V(h_X, h_Y)] |C\rangle \\ &= \left[ \mathbb{1} - \sum_j (\mathcal{H}_C - E_C)^{-1} (\mathbb{1} - |C\rangle \langle C|) (h_X X_j + h_Y Y_j) \right] |C\rangle \end{aligned} \quad (5.44)$$

$$= \left[ \mathbb{1} - \sum_j (\mathcal{H}_C - E_C)^{-1} (h_X X_j + h_Y Y_j) \right] |C\rangle \quad (5.45)$$

$$= \left[ \mathbb{1} - \sum_j \left( \frac{h_X}{8} X_j + \frac{h_Y}{10} Y_j \right) \right] |C\rangle \quad (5.46)$$

$$= \Lambda(h_X, h_Y)^{\otimes N} |C\rangle + \mathcal{O}(h_X^2, h_Y^2, h_X h_Y) \quad (5.47)$$

for

$$\Lambda(h_X, h_Y) = \mathbb{1} - \frac{h_X}{8} X - \frac{h_Y}{10} Y. \quad (5.48)$$

In going from (5.44) to (5.45), we have used that

$$\langle C | X_j | C \rangle = \langle + |^{\otimes N} \left( \prod_e CZ_e \right) X_j \left( \prod_{e'} CZ_{e'} \right) | + \rangle^{\otimes N} \quad (5.49)$$

$$= \langle + |^{\otimes N} \left( \prod_e CZ_e \right) \left( \prod_{e'} CZ_{e'} \right) X_j \prod_{j' \in N(j)} Z_{j'} | + \rangle^{\otimes N} \quad (5.50)$$

$$= \langle + | + \rangle^{N-4} \langle + | - \rangle^4 \quad (5.51)$$

$$= 0, \quad (5.52)$$

where  $N(j)$  is the set of vertices neighbouring  $j$ . Similarly  $\langle C | Y_j | C \rangle = 0 \quad \forall j$ , since

$$Y_j \left( \prod_e CZ_e \right) = \left( \prod_e CZ_e \right) Y_j \prod_{j' \in N(j)} Z_{j'} \quad (5.53)$$

To go from Eq. (5.45) to (5.46), we exploited the fact that

$$-H_C X_j |C\rangle = \sum_i K_i X_j |C\rangle \quad (5.54)$$

$$= \sum_{i \in N(j)} K_i X_j |C\rangle + \sum_{i \notin N(j)} K_i X_j |C\rangle \quad (5.55)$$

$$= - \sum_{i \in N(j)} X_j K_i |C\rangle + \sum_{i \notin N(j)} X_j K_i |C\rangle \quad (5.56)$$

$$= 4 \sum_{i \in N(j)} X_j |C\rangle + (4 - N) \sum_{i \notin N(j)} X_j |C\rangle \quad (5.57)$$

which implies that for all  $j$ ,  $X_j |C\rangle$  is an eigenstate of  $(\mathcal{H}_C - E_C)^{-1}$  with inverse energy  $1/8$  (note that  $j \notin N(j)$ ). The same statement holds for  $Y_j |C\rangle$  with inverse energy  $1/10$ . The first order perturbation is implemented by acting on the cluster state by acting with  $\Lambda$  on every site.

To reach higher orders in perturbation theory, we use

$$|\psi(h_X, h_Y)\rangle = e^{-V} |C\rangle. \quad (5.58)$$

This exponentiated version of perturbation theory is not only more natural in the language of Projected Entangled Pair Operators, but it is indeed the correct perturbative ansatz for a size-extensive many-body quantum wave function [171–173]. Therefore, we must evaluate terms like  $V^2 |C\rangle$ ,  $V^3 |C\rangle$ , and so on. We can use the machinery of [171] to write down PEPOs enacting the perturbations with increasing bond dimension for any given order. The extra bond dimension is needed to account for the fact that higher powers of  $V$  will introduce products of  $X$ s and  $Y$ s with different prefactors, depending on the geometry of the operator. For example, the second order contribution to the ground state contains both connected and disconnected contributions and is given by

$$\begin{aligned} & \left[ \frac{h_X^2}{16} \left( \frac{1}{8} \sum_{|i-j|=1} X_i X_j + \frac{1}{4} \sum_{|i-j|=\sqrt{2}} X_i X_j + \frac{1}{6} \sum_{|i-j|=2} X_i X_j + \frac{1}{8} \sum_{|i-j|>2} X_i X_j \right) \right. \\ & + \frac{h_Y^2}{20} \left( \frac{1}{6} \sum_{|i-j|=1} Y_i Y_j + \frac{1}{6} \sum_{|i-j|=\sqrt{2}} Y_i Y_j + \frac{1}{8} \sum_{|i-j|=2} Y_i Y_j + \frac{1}{10} \sum_{|i-j|>2} Y_i Y_j \right) \\ & + \frac{9h_X h_Y}{80} \left( \frac{1}{7} \sum_{|i-j|=1} X_i Y_j + \frac{1}{4} \sum_{|i-j|=\sqrt{2}} X_i Y_j + \frac{1}{7} \sum_{|i-j|=2} X_i Y_j + \frac{1}{9} \sum_{|i-j|>2} X_i Y_j \right) \\ & \left. - \frac{h_X h_Y}{80} \sum_i X_i Y_i \right] |C\rangle, \end{aligned} \quad (5.59)$$

where the first four terms sum over nearest neighbours, next-nearest neighbours, next-next-nearest neighbours, and all other pairings, respectively. For the sake of completeness, and in order to formulate our hypothesis about the protecting symmetry of the  $XY$ -phase, we write out one (not necessarily optimal) PEPO that

implements this correction (the order of the virtual legs is north, west, south, east):

$$\begin{aligned}
 B_{0,0,0,0} &= \mathbb{1} + aX + bY + cXY \\
 B_{0,0,0,1} &= B_{0,0,1,0} = B_{0,2,0,0} = B_{2,0,0,0} = dX \\
 B_{0,1,0,2} &= B_{1,0,2,0} = \mathbb{1} \\
 B_{1,1,0,0} &= B_{0,0,2,2} = B_{1,0,0,2} = B_{0,1,2,0} = e\mathbb{1} \\
 B_{0,0,0,3} &= B_{0,0,3,0} = B_{0,3,0,0} = B_{3,0,0,0} = fY \\
 B_{0,4,0,0} &= B_{0,0,0,5} = B_{4,0,0,0} = B_{0,0,5,0} = gY \\
 B_{0,5,0,4} &= B_{5,0,4,0} = \mathbb{1} \\
 B_{4,4,0,0} &= B_{4,0,0,5} = B_{0,0,5,5} = B_{0,4,5,0} = h\mathbb{1} \\
 B_{0,0,0,6} &= B_{0,0,6,0} = B_{0,7,0,0} = B_{7,0,0,0} = k_X X \\
 B_{0,0,0,7} &= B_{0,0,7,0} = B_{0,6,0,0} = B_{6,0,0,0} = k_Y Y \\
 B_{0,0,0,8} &= B_{0,8,0,0} = B_{11,0,0,0} = B_{0,11,0,0} = l_X X \\
 B_{0,9,0,0} &= B_{9,0,0,0} = B_{0,0,10,0} = B_{0,0,0,10} = l_Y Y \\
 B_{0,8,0,9} &= B_{8,0,9,0} = B_{0,10,0,11} = B_{10,0,11,0} = \mathbb{1} \\
 B_{10,8,0,0} &= B_{8,10,0,0} = B_{0,8,9,0} = B_{0,10,11,0} = B_{8,0,0,9} \\
 &= B_{9,0,0,11} = B_{0,0,11,9} = B_{0,0,10,11} = m\mathbb{1}
 \end{aligned} \tag{5.60}$$

$$\begin{aligned}
 a = d = \frac{h_X}{8}, \quad b = \frac{h_Y}{10}, \quad c = -\frac{h_X h_Y}{80}, \quad e = -\frac{191}{192}, \quad f = \frac{h_Y}{16} \sqrt{\frac{2}{3}}, \\
 g = \frac{h_Y}{20}, \quad h = \frac{8}{3}, \quad k_X = l_X = \frac{h_X}{280}, \quad k_Y = l_Y = h_Y, \quad m = \frac{35}{8}.
 \end{aligned}$$

The critical observation between (5.48) and (5.60) is that, for any virtual configuration of the PEPO tensor  $B$ , we have

$$XB_{ijkl}X = \overline{B_{ijkl}} \tag{5.61}$$

We will now argue why this holds to all orders in perturbation theory. First, as long as the action of  $V^n |C\rangle$  on the cluster state can be expressed as sums of Pauli strings of  $X$ s and  $Y$ s with real coefficients, one can always find a PEPO  $B$  which satisfied (5.61). In other words, we want to show that

$$V^n |C\rangle = \sum_{\mathbf{ab}} c_{\mathbf{ab}} P_{\mathbf{ab}} |C\rangle \tag{5.62}$$

for all  $n$ , where  $P_{\mathbf{ab}} = \bigotimes_k X^{a_k} Y^{b_k}$ ,  $\mathbf{a}$  and  $\mathbf{b}$  are bitstrings on the lattice and the  $c_{\mathbf{ab}}$  are real coefficients. We have seen explicitly that Eq. (5.62) holds for  $n = 1, 2$ . Now, assuming Eq. (5.62) holds for some  $n$ , we have,

$$\begin{aligned}
 V^{n+1} |C\rangle &= V \sum_{\mathbf{ab}} c_{\mathbf{ab}} P_{\mathbf{ab}} |C\rangle \\
 &= (\mathcal{H}_C - E_C)^{-1} (\mathbb{1} - |C\rangle \langle C|) \sum_{x,y} h'_{x,y} \sum_{\mathbf{ab}} c_{\mathbf{ab}} P_{\mathbf{ab}} |C\rangle \\
 &= \sum_{\mathbf{ab}} c'_{\mathbf{ab}} P_{\mathbf{ab}} |C\rangle,
 \end{aligned} \tag{5.63}$$

where  $c'_{\mathbf{ab}}$  are also real. Therein, we have used that the perturbation  $h'$  consists of Pauli- $X$ s and  $Y$ s with real coefficients and the fact that each product of Pauli matrices either maps the cluster state to an exact excitation or to itself, making  $(\mathcal{H}_C - E_C)^{-1}(\mathbb{1} - |C\rangle\langle C|)$  act simply as a multiplication of each of the  $c_{\mathbf{ab}}$  by a real number. So Eq. (5.62) holds for all  $n$  by induction.

Therefore, it is clear that, at any given order, the corresponding PEPO-tensor  $B$  describing the perturbation will again act as a real linear combination of  $\mathbb{1}$ ,  $X$ ,  $Y$  and  $XY$  for any given virtual state. We conclude that there must exist a region of convergence in  $(h_X, h_Y)$ -space around the cluster point in which the ground state is accurately described by a PEPO fulfilling Eq. (5.61) acting on the cluster state.

### Local Time Reversal

Having derived a general form for a state in the  $XY$ -phase, we will now identify the symmetry that is protecting its SSPT order. First, we draw inspiration from the one-dimensional Cluster state for which the perturbation (5.41) has also been considered. Despite the protecting symmetries ( $X$  on either sublattice) being broken by this perturbation, the ground state remains in the SPT phase as the Cluster state. The reason is that the Cluster state is additionally invariant under complex conjugation and the *product* of complex conjugation and the on-site symmetry is sufficient to protect the phase [174]. This combined symmetry action is called time reversal symmetry.

The important difference in the present case is that, unlike the  $\mathbb{Z}_2 \times \mathbb{Z}_2$ -symmetry of the 1D Cluster state, the protecting symmetries only act on subsystems. Indeed, the Hamiltonian (5.42) does *not* commute with the line symmetries followed by global complex conjugation. It *is* however invariant under conjugation by a line of  $X$  followed by  $\sigma \rightarrow \bar{\sigma}$  for all Pauli operators  $\sigma$  that act *on that same line*.

While such a *local* version of time-reversal symmetry is generally ill-defined, we can define its action on a wave function if a tensor network representation is given [175]. Then, let  $\mathcal{K}_{x,y}$  be an operator that locally conjugates the tensor at a given site. We are then led to define *local time reversal* operators

$$\begin{aligned} U_v^T(c) &= \prod_{x=1}^N X_{x,c-x} \mathcal{K}_{x,c-x}, \\ U_h^T(c) &= \prod_{x=-\infty}^{\infty} X_{x,c+x} \mathcal{K}_{x,c+x}. \end{aligned} \quad (5.64)$$

We hypothesise that the SSPT order of the Cluster phase is stable as long as a ground state description invariant under (5.64) exists.

We have given a first piece of evidence in section 5.2.3, the point of which was to show that ground states in the  $XY$ -phase are described by a PEPO fulfilling (5.64) to arbitrary orders in perturbation theory. On the other hand, it was confirmed numerically that taking random bond dimension 4 tensors satisfying (5.61) yields a SPEE of  $\gamma = 1$ , indicating that such local time reversal symmetry is sufficient for SSPT order.

### 5.3 Conclusion

In this chapter, we have studied anisotropic, mixed symmetries of an elementary PEPS tensor. These can give rise to physical subsystem symmetries and therefore make PEPS an excellent framework for studying SSPT ordered phases. Indeed, we extensively used the PEPS bulk-boundary correspondence to investigate corrections to the area law in the Cluster Phase. These corrections, as we have demonstrated, are *not* spurious, but they occur everywhere in the phase except at fine-tuned points. Their value coincides with the value for certain intrinsically topologically ordered phases. This somewhat awkward situation can be remedied by measuring the entanglement entropy across different cuts: we have confirmed numerically that the value  $\gamma = 1$  is unstable to deformations of the cut both in the cluster state as well as the family of bond dimension  $D = 2$ -PEPS in the cluster phase (5.2).

Using the novel numerical and analytical tools developed in this chapter, we discovered a new phase of matter that is compatible with *subsystem time-reversal symmetry*. The latter notion raises important questions: Since we defined subsystem time reversal in terms of an explicit PEPS representations, this suggests that the elementary tensor is not merely a *description* of the physical state but rather of fundamental importance. We leave an exhaustive study of the newly discovered phase as an open problem.

Our arguments can be generalized to other SSPT phases beyond the Cluster Phase. A difficulty is that the decomposition result (5.27) is particular to the Cluster Phase. On the other, our algorithm is universally applicable and can be used to show robustness in more general circumstances.

# Chapter 6

## Conclusion and Outlook

In this Thesis, we have furthered the understanding of symmetric PEPS. This was motivated by the fact that tensor networks are proven in one dimension and believed in higher dimensions to parameterize the ground states of realistic (i.e., local) Hamiltonians. Symmetry, on the other hand, is the essential ingredient to understand the universal features of the PEPS as demonstrated by MPS' and PEPS' ability to completely classify certain topological phases. The relation between symmetry and universality is exemplified by the fact that the both Six-Vertex model from chapter 2 and the Resonating Valence Bond in chapter 3 are described by the same field theory despite the microscopic details being completely different.

In chapter 2, we investigated the simplest continuous symmetry,  $U(1)$ . We showed that the max entanglement entropy in such states can be reduced to a counting problem. There are logarithmic corrections to the area law with a combinatorial universal prefactor. Besides the correction that depends on the size of the cut, there is another correction for “thin enough” subsystems. This geometric correction is not just reflected in the entanglement, but is also responsible for the non-invertibility of the PEPS, as well as an additional symmetry of the transfer matrix. Physically, large portions of the “Six-Vertex”- $U(1)$ -PEPS are dominated by either critical or symmetry-breaking behaviour. We explained this by proposing a virtual Lieb-Schultz-Matthis theorem. We also put forward an explicit construction of the low-lying excitations for the critical cases. Our criteria are fulfilled in cases that go beyond simple Rokhsar-Kivelson wavefunctions. They can be checked with one-dimensional transfer matrix calculations. This dimensional reduction is possible, because the PEPS is described by a classical 2+0D variant of conformal invariance which arises as the ground state of a 2+1D critical point with dynamical critical exponent  $z = 2$ .

Such connections with Conformal Field Theory are the backbone of chapter 3, where we have studied the Resonating Valence Bond state, focusing in particular on the kind with long-range singlets as it is a realistic description of certain frustrated magnets. Our goal was to resolve the following puzzle: the long-range RVB state was believed to possess an extended critical phase while at the same time long-range singlets destroy the  $U(1)$ -symmetry of the nearest-neighbour RVB which is crucial for the existence of the gapless virtual photons we have proposed in chapter 2. We reconcile these two observations by showing that the putative critical phase is actually *gapped*, albeit with a gap that is too small to detect for current numerical algorithms. To quantify this gap, we combined existing numerical tools with arguments from Conformal Field Theory, allowing us to write down a scaling hypothesis.

While this hypothesis works well for a range of models in between a proposed Quantum Dimer-Solidomer and the Resonating Valence Bond model, at the RVB point, we had to include subleading terms to set up a refined scaling hypothesis. This hypothesis was then shown to agree with the numerical data and can now be used to make predictions where numerical data is not available. Finally, we proposed a model in which an emergent  $U(1)$ -symmetry could actually be observed in a PEPS.

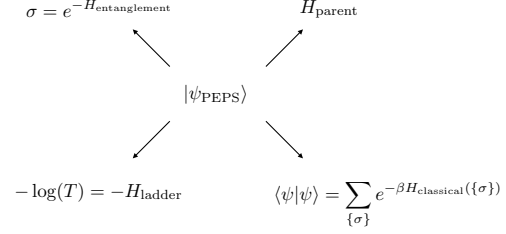
In chapter 4, we extended our analysis to the non-abelian group  $SU(2)$ . Due to the entangled nature of non-abelian singlets, the model could naturally be described as a loop model, corresponding to a Rokhsar-Kivelson line of classical systems with *non-local* interactions. The combinatorial universality class of the entropy counting problem was shown to be different from the  $U(1)$  case and compatible with a prefactor (number of generators/2) for the logarithmic correction. The physics of the PEPS is obtained from mapping its correlators to those of a classical Potts model and is essentially that of a cat state over one-site translations, corresponding to a symmetry breaking plaquette phase. In particular, there are no algebraic correlations and the model does not describe a continuous transition into a topologically ordered state, unlike the  $U(1)$  models. The PEPS also has a  $2 \times 2$ -local parent Hamiltonian, the ground space of which it succinctly characterizes on open boundary conditions (the *intersection property*). On a torus, there is both a polynomial number of ground states arising from inserting symmetry strings as well as an exponential number of frozen ground state configurations.

Taking a step back from continuous symmetries, we investigated a type of mixed virtual-physical anisotropic symmetry in chapter 5 that gives rise to subsystem symmetries. Along cuts running parallel to such rigid line-like symmetries, the entanglement entropy exhibits a constant correction to the area law, despite no intrinsic topological order in the system. We settled a recent debate about the universality of such corrections by showing that they persist everywhere in the Cluster phase except at fine-tuned points. In doing so, we provided an exactly solvable path through the phase, a generic analytical argument and a numerical algorithm to measure the Renyi 2-entropy. After testing the validity of the algorithm in a benchmark, we used it to discover a novel subsystem-symmetry protected topological phase in which the Cluster phase is embedded. A perturbative argument was provided to show that the protecting symmetry is most aptly described as a local version of time-reversal symmetry.

This research fills several gaps in the theory of symmetric PEPS, but it also opens up new avenues of inquiry. A central theme in this Thesis is *correspondence*. In all models that we have investigated we could not associate one Hamiltonian with the PEPS but *four*: the parent Hamiltonian, a classical Hamiltonian whose partition function equals the norm of the PEPS (and can thus be used to compute diagonal correlation functions), an entanglement Hamiltonian whose spectrum is the entanglement spectrum and that can be obtained from the fixed point of the transfer matrix and, finally, a ladder Hamiltonian which turned out to be quasi-local in the one example where it is accessible (3.15). A more general understanding of how these Hamiltonians are related is desirable. For example, we constructed ladder Hamiltonians with both critical and symmetry-breaking properties, but we know from chapter 1 that there is a third possibility: can there be a PEPS with symmetry protected topological order at the boundary? A natural candidate would be a 19-vertex model in the absence of an external field. In this case, the transfer matrix has



a commuting  $\mathbb{Z}_2 \times \mathbb{Z}_2$ -symmetry which can potentially push through the fixed point as a nontrivial projective representation. What is the interpretation of the entanglement degeneracy and the edge modes in terms of the corresponding classical model? A separate issue is that the classical Hamiltonian is only available when the PEPS has non-negative coefficients. The physical interpretation of quantum states which admit no non-negative representation is an interesting current problem [176, 177]. The ladder Hamiltonian, on the other hand, is hermitian only if the PEPS is reflection positive [178, chapter 9]. Non-hermitian Hamiltonians can have a number of exotic physical properties that have been the subject of recent studies [179, 180]. Which PEPS have such ladder Hamiltonians?



Another interesting relationship is that with PEPS with interacting chiral topological order. It is of great interest to find PEPS models that describe Fractional Quantum Hall states, but the quest has so far been unsuccessful. The problem is that the entanglement spectrum either turns out non-chiral or the bulk is critical. Ideally, one would like to gap out the bulk in one of these models, but in order to do that, a better understanding of the bulk criticality is required. For some of the models considered so far it can be explained in terms of a virtual  $U(1)$ -symmetry (cf. Proposition 2.2) [47], but others lack the symmetry. As we have shown in chapter 3, criticality can reemerge when immersing a  $U(1) \rightarrow \mathbb{Z}_2$ -breaking PEPS in an external electric field. In this context, it is also interesting to observe that the combinatorics obtained in chapter 4 for  $k$  applications of the transfer matrix is identical to the one obtained from the fusion rules of  $SU(2)_k$ , a Conformal Field Theory whose correlators coincide with the wavefunction amplitudes of certain Quantum Hall ground states.

Emergent symmetries can also be used to strengthen the expressivity of variational ansatzes. Currently, symmetries have to be encoded exactly in the local tensor is one would like them to be present in the optimized wave function. On the other hand, PEPS with continuous symmetries are now being used in variational optimization, often with great success, but the ansatz sometimes fails [68, 69]. Providing general proofs, for example for the value of the dynamical critical exponent  $z = 2$ , may answer the question as to when imposing those symmetries is appropriate.

On the topic of general proofs, a variant of the Hohenberg-Mermin-Wagner theorem for transfer matrices is desirable, particularly because there is no rigorous proof for zero-temperature quantum Hamiltonians to date. Implementing a symmetry breaking-potential on the level of the transfer matrix is straightforward, as well as probing the symmetry properties of the fixed point by using the Rayleigh quotient. An issue arises because one typically has to deal with critical fixed points that require infinite bond dimension in the thermodynamic limit. General proofs regarding the way a finite bond dimension MPS approaches the infinite- $\chi$ -limit (or a framework for dealing with  $\chi = \infty$  directly) would therefore be useful.

Another issue is that of alternative parent Hamiltonians. While quite successful, the construction of (1.24) and (1.25) suffers from discontinuities. This weakens the concept of smooth PEPS deformations, as they are not guaranteed to be the



ground states of continuously changing Hamiltonians. A further weakness is that the symmetries of the PEPS and the Hamiltonian are the same by construction. In particular, the parent Hamiltonian is not suited to describe symmetry-breaking scenarios. Fortunately, there is a lot of freedom in choosing parent Hamiltonians: one can, for example, freely change the excited space of the local Hamiltonian term and still keep the PEPS in its ground space. Another interesting question is which parent Hamiltonians appear in variationally optimized MPS. Finite  $\chi$  can be seen as a relevant perturbation to whichever Hamiltonian one is approximating and it would be interesting to study this perturbation on the Hamiltonian level. Such parent Hamiltonians become more and more nonlocal in the  $\chi \rightarrow \infty$ -limit, but the size of their support only grows as  $\log \chi$  even at criticality.

While criticality is commonplace in the phase diagram of  $U(1)$ -PEPS, there are no algebraically decaying correlations in the non-abelian case. In our model, this is because the weight per closed loop is so large that configurations with long loops are exponentially suppressed. Curiously, this loop fugacity is equal to the bond dimension squared and putting higher  $SU(N)$  on the links only reduces the correlation length further. Is it possible to construct a critical non-abelian model?

Another interesting direction concerns circumventing the computationally costly PEPS contraction. Expectation values of the  $SU(2)$ -PEPS (including the non-local “same-loop”-correlator) can be evaluated with a Monte Carlo algorithm. There is no reason why that should be restricted to the specific model and it would be exciting to combine the symmetry- and entanglement-based PEPS perspective with the strengths of Monte Carlo [181, 182], especially when going to three dimensions. In this regard, the perspective taken in chapter 5 could be fruitful to infer properties of 3D states without any numerical computation at all. Hopefully, the contributions of this Thesis will help to answer these and related questions.

# Bibliography

- [1] P. W. Andersen. “More is different”. In: *Science* 177.4047 (Aug. 1972), pp. 393–396. ISSN: 00368075. DOI: [10.1126/science.177.4047.393](https://doi.org/10.1126/science.177.4047.393). URL: <https://science.sciencemag.org/content/177/4047/393%20https://science.sciencemag.org/content/177/4047/393.abstract>.
- [2] D. M. Broun. “What lies beneath the dome?” In: *Nature Physics* 4.3 (2008), pp. 170–172. ISSN: 17452481. DOI: [10.1038/nphys909](https://doi.org/10.1038/nphys909). URL: <http://arxiv.org/abs/0711.2494>.
- [3] Thomas Häner and Damian S. Steiger. “0.5 Petabyte Simulation of a 45-Qubit Quantum Circuit”. In: *Proceedings of the International Conference for High Performance Computing, Networking, Storage and Analysis, SC 2017* (Apr. 2017). DOI: [10.1145/3126908.3126947](https://doi.org/10.1145/3126908.3126947). URL: <http://arxiv.org/abs/1704.01127%20http://dx.doi.org/10.1145/3126908.3126947>.
- [4] L. Landau. *The theory of phase transitions [3]*. 1936. DOI: [10.1038/138840a0](https://doi.org/10.1038/138840a0). URL: <https://www.nature.com/articles/138840a0>.
- [5] P. C. Hohenberg. “Existence of long-range order in one and two dimensions”. In: *Physical Review* 158.2 (June 1967), pp. 383–386. ISSN: 0031899X. DOI: [10.1103/PhysRev.158.383](https://doi.org/10.1103/PhysRev.158.383).
- [6] N. D. Mermin and H. Wagner. “Absence of ferromagnetism or antiferromagnetism in one- or two-dimensional isotropic Heisenberg models”. In: *Physical Review Letters* 17.22 (Nov. 1966), pp. 1133–1136. ISSN: 00319007. DOI: [10.1103/PhysRevLett.17.1133](https://doi.org/10.1103/PhysRevLett.17.1133).
- [7] V. Berezinskiĭ. “Destruction of Long-range Order in One-dimensional and Two-dimensional Systems Possessing a Continuous Symmetry Group. II. Quantum Systems”. In: *Soviet Journal of Experimental and Theoretical Physics* (1972). ISSN: 1063-7761.
- [8] J. M. kosterlitz and D. J. Thouless. “Ordering, metastability and phase transitions in two-dimensional systems”. In: *Journal of Physics C: Solid State Physics* (1973). ISSN: 00223719. DOI: [10.1088/0022-3719/6/7/010](https://doi.org/10.1088/0022-3719/6/7/010).
- [9] K. v. Klitzing, G. Dorda, and M. Pepper. “New Method for High-Accuracy Determination of the Fine-Structure Constant Based on Quantized Hall Resistance”. In: *Physical Review Letters* 45.6 (Aug. 1980), pp. 494–497. ISSN: 0031-9007. DOI: [10.1103/PhysRevLett.45.494](https://doi.org/10.1103/PhysRevLett.45.494). URL: <https://link.aps.org/doi/10.1103/PhysRevLett.45.494>.
- [10] M B Hastings. “An Area Law for One Dimensional Quantum Systems”. In: *Journal of Statistical Mechanics: Theory and Experiment* (May 2018). ISSN: 17425468. URL: <https://arxiv.org/abs/0705.2024v4>.

- [11] Steven R. White. “Density matrix formulation for quantum renormalization groups”. In: *Physical Review Letters* 69.19 (Nov. 1992), pp. 2863–2866. ISSN: 00319007. DOI: [10.1103/PhysRevLett.69.2863](https://doi.org/10.1103/PhysRevLett.69.2863). URL: <https://journals.aps.org/prl/abstract/10.1103/PhysRevLett.69.2863>.
- [12] R. B. Laughlin. “Anomalous quantum Hall effect: An incompressible quantum fluid with fractionally charged excitations”. In: *Physical Review Letters* 50.18 (May 1983), pp. 1395–1398. ISSN: 00319007. DOI: [10.1103/PhysRevLett.50.1395](https://doi.org/10.1103/PhysRevLett.50.1395). URL: <https://journals.aps.org/prl/abstract/10.1103/PhysRevLett.50.1395>.
- [13] Ian Affleck et al. “Rigorous results on valence-bond ground states in antiferromagnets”. In: *Physical Review Letters* 59.7 (Aug. 1987), pp. 799–802. ISSN: 00319007. DOI: [10.1103/PhysRevLett.59.799](https://doi.org/10.1103/PhysRevLett.59.799). URL: <https://journals.aps.org/prl/abstract/10.1103/PhysRevLett.59.799>.
- [14] F. D.M. Haldane. “Continuum dynamics of the 1-D Heisenberg antiferromagnet: Identification with the O(3) nonlinear sigma model”. In: *Physics Letters A* (1983). ISSN: 03759601. DOI: [10.1016/0375-9601\(83\)90631-X](https://doi.org/10.1016/0375-9601(83)90631-X).
- [15] F. D.M. Haldane. “Nonlinear field theory of large-spin Heisenberg antiferromagnets: Semiclassically quantized solitons of the one-dimensional easy-axis Néel state”. In: *Physical Review Letters* (1983). ISSN: 00319007. DOI: [10.1103/PhysRevLett.50.1153](https://doi.org/10.1103/PhysRevLett.50.1153).
- [16] H. Bethe. “Zur Theorie der Metalle”. In: *Zeitschrift für Physik* (1931). ISSN: 1434-6001. DOI: [10.1007/bf01341708](https://doi.org/10.1007/bf01341708).
- [17] N. Schuch, D Perez-Garcia, and J. I. Cirac. “Classification of gapped symmetric phases in one-dimensional spin systems”. In: *Physical Review B - Condensed Matter and Materials Physics* 84.16 (Oct. 2011), p. 165139. DOI: [10.1103/PhysRevB.84.165139](https://doi.org/10.1103/PhysRevB.84.165139).
- [18] Xie Chen, Zheng-Cheng Gu, and Xiao-Gang Wen. “Complete classification of 1D gapped quantum phases in interacting spin systems”. In: *Physical Review B - Condensed Matter and Materials Physics* 84.23 (Mar. 2011). DOI: [10.1103/PhysRevB.84.235128](https://doi.org/10.1103/PhysRevB.84.235128). URL: <http://arxiv.org/abs/1103.3323>  
<http://dx.doi.org/10.1103/PhysRevB.84.235128>.
- [19] Michael A. Levin and Xiao-Gang Wen. “String-net condensation: A physical mechanism for topological phases”. In: *Physical Review B - Condensed Matter and Materials Physics* 71.4 (Apr. 2004). DOI: [10.1103/PhysRevB.71.045110](https://doi.org/10.1103/PhysRevB.71.045110). URL: <http://arxiv.org/abs/cond-mat/0404617>  
<http://dx.doi.org/10.1103/PhysRevB.71.045110>.
- [20] Norbert Schuch, Ignacio Cirac, and David Perez-Garcia. “PEPS as ground states: degeneracy and topology”. In: *Annals of Physics* 325.10 (Jan. 2010), pp. 2153–2192. DOI: [10.1016/j.aop.2010.05.008](https://doi.org/10.1016/j.aop.2010.05.008). URL: <http://arxiv.org/abs/1001.3807>  
<http://dx.doi.org/10.1016/j.aop.2010.05.008>.
- [21] O. Buerschaper, M. Aguado, and G. Vidal. “Explicit tensor network representation for the ground states of string-net models”. In: *Physical Review B - Condensed Matter and Materials Physics* 79.8 (Sept. 2008). DOI: [10.1103/PhysRevB.79.085119](https://doi.org/10.1103/PhysRevB.79.085119). URL: <http://arxiv.org/abs/0809.2393>  
<http://dx.doi.org/10.1103/PhysRevB.79.085119>.

- [22] Mehmet Burak Şahinoğlu et al. “Characterizing Topological Order with Matrix Product Operators”. In: (Sept. 2014). URL: <http://arxiv.org/abs/1409.2150>.
- [23] T. B. Wahl et al. “Projected entangled-pair states can describe chiral topological states”. In: *Physical Review Letters* 111.23 (Aug. 2013). DOI: [10.1103/PhysRevLett.111.236805](https://doi.org/10.1103/PhysRevLett.111.236805). URL: <http://arxiv.org/abs/1308.0316%20http://dx.doi.org/10.1103/PhysRevLett.111.236805>.
- [24] Shuo Yang et al. “Chiral projected entangled-pair state with topological order”. In: *Physical Review Letters* 114.10 (Nov. 2014). DOI: [10.1103/PhysRevLett.114.106803](https://doi.org/10.1103/PhysRevLett.114.106803). URL: <http://arxiv.org/abs/1411.6618%20http://dx.doi.org/10.1103/PhysRevLett.114.106803>.
- [25] Didier Poilblanc. “Investigation of the chiral antiferromagnetic Heisenberg model using PEPS”. In: *Physical Review B* 96.12 (July 2017). DOI: [10.1103/PhysRevB.96.121118](https://doi.org/10.1103/PhysRevB.96.121118). URL: <http://arxiv.org/abs/1707.07844%20http://dx.doi.org/10.1103/PhysRevB.96.121118>.
- [26] Kasper Duivenvoorden et al. “Entanglement phases as holographic duals of anyon condensates”. In: *Physical Review B* 95.23 (Feb. 2017). DOI: [10.1103/PhysRevB.95.235119](https://doi.org/10.1103/PhysRevB.95.235119). URL: <http://arxiv.org/abs/1702.08469%20http://dx.doi.org/10.1103/PhysRevB.95.235119>.
- [27] Erez Zohar and Michele Burrello. “Building Projected Entangled Pair States with a Local Gauge Symmetry”. In: (Nov. 2015). DOI: [10.1088/1367-2630/18/4/043008](https://doi.org/10.1088/1367-2630/18/4/043008). URL: <http://arxiv.org/abs/1511.08426%20http://dx.doi.org/10.1088/1367-2630/18/4/043008>.
- [28] Erez Zohar et al. “Fermionic Projected Entangled Pair States and Local U(1) Gauge Theories”. In: *Annals of Physics* 363 (July 2015), pp. 385–439. DOI: [10.1016/j.aop.2015.10.009](https://doi.org/10.1016/j.aop.2015.10.009). URL: <http://arxiv.org/abs/1507.08837%20http://dx.doi.org/10.1016/j.aop.2015.10.009>.
- [29] Erez Zohar et al. “Projected Entangled Pair States with non-Abelian gauge symmetries: an SU(2) study”. In: *Annals of Physics* 374 (July 2016), pp. 84–137. DOI: [10.1016/j.aop.2016.08.008](https://doi.org/10.1016/j.aop.2016.08.008). URL: <http://arxiv.org/abs/1607.08115%20http://dx.doi.org/10.1016/j.aop.2016.08.008>.
- [30] Erez Zohar and J. Ignacio Cirac. “Combining Tensor Networks with Monte Carlo Methods for Lattice Gauge Theories”. In: *Physical Review D* 97.3 (Oct. 2017). DOI: [10.1103/PhysRevD.97.034510](https://doi.org/10.1103/PhysRevD.97.034510). URL: <http://arxiv.org/abs/1710.11013%20http://dx.doi.org/10.1103/PhysRevD.97.034510>.
- [31] Stefan Kühn et al. “Non-Abelian string breaking phenomena with matrix product states”. In: *Journal of High Energy Physics* 2015.7 (July 2015). ISSN: 10298479. DOI: [10.1007/JHEP07\(2015\)130](https://doi.org/10.1007/JHEP07(2015)130). URL: <https://arxiv.org/abs/1505.04441v3>.
- [32] Daniel Robaina, Mari Carmen Bañuls, and J. Ignacio Cirac. “Simulating 2+1d  $\mathbb{Z}_3$  lattice gauge theory with iPEPS”. In: (July 2020). URL: <http://arxiv.org/abs/2007.11630>.

- [33] Alexei Kitaev and John Preskill. “Topological entanglement entropy”. In: *Physical Review Letters* 96.11 (Oct. 2005). DOI: [10.1103/PhysRevLett.96.110404](https://doi.org/10.1103/PhysRevLett.96.110404). URL: <http://arxiv.org/abs/hep-th/0510092><http://dx.doi.org/10.1103/PhysRevLett.96.110404>.
- [34] Michael Levin and Xiao-Gang Wen. “Detecting topological order in a ground state wave function”. In: *Physical Review Letters* 96.11 (Oct. 2005). DOI: [10.1103/PhysRevLett.96.110405](https://doi.org/10.1103/PhysRevLett.96.110405). URL: <http://arxiv.org/abs/cond-mat/0510613><http://dx.doi.org/10.1103/PhysRevLett.96.110405>.
- [35] D. Perez-Garcia et al. “Matrix product state representations”. In: *Quantum Information and Computation* 7.5-6 (July 2007), pp. 401–430. ISSN: 15337146. URL: <https://arxiv.org/abs/quant-ph/0608197v2>.
- [36] Andras Molnar et al. “Normal projected entangled pair states generating the same state”. In: (Apr. 2018). DOI: [10.1088/1367-2630/aae9fa](https://doi.org/10.1088/1367-2630/aae9fa). URL: <http://arxiv.org/abs/1804.04964><http://dx.doi.org/10.1088/1367-2630/aae9fa>.
- [37] Jacob C. Bridgeman and Christopher T. Chubb. “Hand-waving and Interpretive Dance: An Introductory Course on Tensor Networks”. In: (Mar. 2016). DOI: [10.1088/1751-8121/aa6dc3](https://doi.org/10.1088/1751-8121/aa6dc3). URL: <http://arxiv.org/abs/1603.03039><http://dx.doi.org/10.1088/1751-8121/aa6dc3>.
- [38] T. Nishino and K. Okunishi. “Corner Transfer Matrix Renormalization Group Method”. In: *Journal of the Physical Society of Japan* 65.4 (July 1995), pp. 891–894. DOI: [10.1143/JPSJ.65.891](https://doi.org/10.1143/JPSJ.65.891). URL: <http://arxiv.org/abs/cond-mat/9507087><http://dx.doi.org/10.1143/JPSJ.65.891>.
- [39] Roman Orus and Guifre Vidal. “Simulation of two dimensional quantum systems on an infinite lattice revisited: corner transfer matrix for tensor contraction”. In: *Physical Review B - Condensed Matter and Materials Physics* 80.9 (May 2009). DOI: [10.1103/PhysRevB.80.094403](https://doi.org/10.1103/PhysRevB.80.094403). URL: <http://arxiv.org/abs/0905.3225><http://dx.doi.org/10.1103/PhysRevB.80.094403>.
- [40] Philippe Corboz, T. M. Rice, and Matthias Troyer. “Competing states in the t-J model: uniform d-wave state versus stripe state”. In: *Physical Review Letters* 113.4 (Feb. 2014). DOI: [10.1103/PhysRevLett.113.046402](https://doi.org/10.1103/PhysRevLett.113.046402). URL: <http://arxiv.org/abs/1402.2859><http://dx.doi.org/10.1103/PhysRevLett.113.046402>.
- [41] M. T. Fishman et al. “Faster Methods for Contracting Infinite 2D Tensor Networks”. In: *Physical Review B* 98.23 (Nov. 2017). DOI: [10.1103/PhysRevB.98.235148](https://doi.org/10.1103/PhysRevB.98.235148). URL: <http://arxiv.org/abs/1711.05881><http://dx.doi.org/10.1103/PhysRevB.98.235148>.
- [42] Michael M Wolf. *Quantum Channels & Operations Guided Tour*. Tech. rep. 2012.
- [43] J Ignacio Cirac et al. “Entanglement spectrum and boundary theories with projected entangled-pair states”. In: *PHYSICAL REVIEW B* 83 (2011), p. 245134. DOI: [10.1103/PhysRevB.83.245134](https://doi.org/10.1103/PhysRevB.83.245134).



- [44] J. Eisert, M. Cramer, and M. B. Plenio. “Area laws for the entanglement entropy - a review”. In: *Reviews of Modern Physics* 82.1 (Aug. 2008), pp. 277–306. DOI: [10.1103/RevModPhys.82.277](https://doi.org/10.1103/RevModPhys.82.277). URL: <http://arxiv.org/abs/0808.3773><http://dx.doi.org/10.1103/RevModPhys.82.277>.
- [45] Norbert Schuch et al. “Resonating valence bond states in the PEPS formalism”. In: *Physical Review B - Condensed Matter and Materials Physics* 86.11 (Mar. 2012). DOI: [10.1103/PhysRevB.86.115108](https://doi.org/10.1103/PhysRevB.86.115108). URL: <http://arxiv.org/abs/1203.4816><http://dx.doi.org/10.1103/PhysRevB.86.115108>.
- [46] Didier Poilblanc et al. “Topological and Entanglement Properties of Resonating Valence Bond wavefunctions”. In: *Physical Review B - Condensed Matter and Materials Physics* 86.1 (Feb. 2012). DOI: [10.1103/PhysRevB.86.014404](https://doi.org/10.1103/PhysRevB.86.014404). URL: <http://arxiv.org/abs/1202.0947><http://dx.doi.org/10.1103/PhysRevB.86.014404>.
- [47] Didier Poilblanc, Norbert Schuch, and Ian Affleck. “SU(2) chiral edge modes of a critical spin liquid”. In: *Physical Review B* 93.17 (Feb. 2016). DOI: [10.1103/PhysRevB.93.174414](https://doi.org/10.1103/PhysRevB.93.174414). URL: <http://arxiv.org/abs/1602.05969><http://dx.doi.org/10.1103/PhysRevB.93.174414>.
- [48] Thorsten B. Wahl et al. “Symmetries and boundary theories for chiral Projected Entangled Pair States”. In: *Physical Review B - Condensed Matter and Materials Physics* 90.11 (May 2014). DOI: [10.1103/PhysRevB.90.115133](https://doi.org/10.1103/PhysRevB.90.115133). URL: <http://arxiv.org/abs/1405.0447><http://dx.doi.org/10.1103/PhysRevB.90.115133>.
- [49] Anna Hackenbroich, Antoine Sterdyniak, and Norbert Schuch. “Interplay of SU(2), point group and translation symmetry for PEPS: application to a chiral spin liquid”. In: *Physical Review B* 98.8 (May 2018). DOI: [10.1103/PhysRevB.98.085151](https://doi.org/10.1103/PhysRevB.98.085151). URL: <http://arxiv.org/abs/1805.04531><http://dx.doi.org/10.1103/PhysRevB.98.085151>.
- [50] Erez Zohar et al. “Fermionic Projected Entangled Pair States and Local U(1) Gauge Theories”. In: *Annals of Physics* 363 (July 2015), pp. 385–439. DOI: [10.1016/j.aop.2015.10.009](https://doi.org/10.1016/j.aop.2015.10.009). URL: <http://arxiv.org/abs/1507.08837><http://dx.doi.org/10.1016/j.aop.2015.10.009>.
- [51] N. Schuch, Ignacio Cirac, and David Pérez-García. “PEPS as ground states: Degeneracy and topology”. In: *Annals of Physics* (2010). ISSN: 00034916. DOI: [10.1016/j.aop.2010.05.008](https://doi.org/10.1016/j.aop.2010.05.008).
- [52] Philippe Flajolet and Robert Sedgewick. *Analytic combinatorics*. 2009. ISBN: 9780511801655. DOI: [10.1017/CB09780511801655](https://doi.org/10.1017/CB09780511801655).
- [53] Eddy Ardonne, Paul Fendley, and Eduardo Fradkin. “Topological Order and Conformal Quantum Critical Points”. In: *Annals of Physics* 310.2 (Nov. 2003), pp. 493–551. DOI: [10.1016/j.aop.2004.01.004](https://doi.org/10.1016/j.aop.2004.01.004). URL: <http://arxiv.org/abs/cond-mat/0311466><http://dx.doi.org/10.1016/j.aop.2004.01.004>.
- [54] Eduardo Fradkin and Joel E. Moore. “Entanglement entropy of 2D conformal quantum critical points: hearing the shape of a quantum drum”. In: *Physical Review Letters* 97.5 (May 2006). DOI: [10.1103/PhysRevLett.97.050404](https://doi.org/10.1103/PhysRevLett.97.050404). URL: <http://arxiv.org/abs/cond-mat/0605683><http://dx.doi.org/10.1103/PhysRevLett.97.050404>.

- [55] Daniel S. Rokhsar and Steven A. Kivelson. “Superconductivity and the quantum hard-core dimer gas”. In: *Physical Review Letters* 61.20 (Nov. 1988), pp. 2376–2379. ISSN: 00319007. DOI: [10.1103/PhysRevLett.61.2376](https://doi.org/10.1103/PhysRevLett.61.2376).
- [56] Michael P. Zaletel, Jens H. Bardarson, and Joel E. Moore. “Logarithmic terms in entanglement entropies of 2D quantum critical points and shannon entropies of spin chains”. In: *Physical Review Letters* 107.2 (July 2011), p. 020402. ISSN: 00319007. DOI: [10.1103/PhysRevLett.107.020402](https://doi.org/10.1103/PhysRevLett.107.020402).
- [57] H. Francis Song et al. “Entanglement Entropy of the Two-Dimensional Heisenberg Antiferromagnet”. In: *Physical Review B - Condensed Matter and Materials Physics* 83.22 (Mar. 2011). DOI: [10.1103/PhysRevB.83.224410](https://doi.org/10.1103/PhysRevB.83.224410). URL: <http://arxiv.org/abs/1103.1636><http://dx.doi.org/10.1103/PhysRevB.83.224410>.
- [58] Jean Marie Stéphan et al. “Entanglement in gapless resonating-valence-bond states”. In: *New Journal of Physics* (2013). ISSN: 13672630. DOI: [10.1088/1367-2630/15/1/015004](https://doi.org/10.1088/1367-2630/15/1/015004).
- [59] Hyejin Ju et al. “Entanglement scaling in two-dimensional gapless systems”. In: *Physical Review B - Condensed Matter and Materials Physics* 85.16 (Apr. 2012), p. 165121. ISSN: 10980121. DOI: [10.1103/PhysRevB.85.165121](https://doi.org/10.1103/PhysRevB.85.165121).
- [60] Bohdan Kulchytskyy, Lauren E. Hayward Sierens, and Roger G. Melko. “Universal divergence of the Rényi entropy of a thinly sliced torus at the Ising fixed point”. In: *Physical Review B* 100.4 (July 2019), p. 045139. ISSN: 24699969. DOI: [10.1103/PhysRevB.100.045139](https://doi.org/10.1103/PhysRevB.100.045139).
- [61] Elliott H. Lieb. “Exact solution of the problem of the entropy of two-dimensional ice”. In: *Physical Review Letters* (1967). ISSN: 00319007. DOI: [10.1103/PhysRevLett.18.692](https://doi.org/10.1103/PhysRevLett.18.692).
- [62] Elliott H. Lieb. “Residual Entropy of Square Ice”. In: *Physical Review* (1967). ISSN: 0031899X. DOI: [10.1103/PhysRev.162.162](https://doi.org/10.1103/PhysRev.162.162).
- [63] Bill Sutherland. “Exact solution of a two-dimensional model for hydrogen-bonded crystals”. In: *Physical Review Letters* (1967). ISSN: 00319007. DOI: [10.1103/PhysRevLett.19.103](https://doi.org/10.1103/PhysRevLett.19.103).
- [64] R. J. Baxter. “Exactly Solved Models in Statistical Mechanics”. In: 1985. DOI: [10.1142/9789814415255\\_{\\\_}0002](https://doi.org/10.1142/9789814415255_{\_}0002).
- [65] Eddy Ardonne, Paul Fendley, and Eduardo Fradkin. “Topological order and conformal quantum critical points”. In: *Annals of Physics* (2004). ISSN: 00034916. DOI: [10.1016/j.aop.2004.01.004](https://doi.org/10.1016/j.aop.2004.01.004).
- [66] Jonah Herzog-Arbeitman, Sebastian Mantilla, and Inti Sodemann. “Solving the quantum dimer and six-vertex models one electric field line at a time”. In: *Physical Review B* (2019). ISSN: 24699969. DOI: [10.1103/PhysRevB.99.245108](https://doi.org/10.1103/PhysRevB.99.245108).
- [67] Olav F. Syljuasen and Sudip Chakravarty. “Resonating plaquette phase of a quantum six-vertex model”. In: *Physical Review Letters* 96.14 (Sept. 2005). DOI: [10.1103/PhysRevLett.96.147004](https://doi.org/10.1103/PhysRevLett.96.147004). URL: <http://arxiv.org/abs/cond-mat/0509624><http://dx.doi.org/10.1103/PhysRevLett.96.147004>.

- [68] Philippe Corboz et al. “Finite Correlation Length Scaling with Infinite Projected Entangled-Pair States”. In: *Physical Review X* 8.3 (July 2018), p. 031031. ISSN: 21603308. DOI: [10.1103/PhysRevX.8.031031](https://doi.org/10.1103/PhysRevX.8.031031).
- [69] Michael Rader and Andreas M. Läuchli. “Finite Correlation Length Scaling in Lorentz-Invariant Gapless iPEPS Wave Functions”. In: *Physical Review X* 8.3 (Mar. 2018). DOI: [10.1103/PhysRevX.8.031030](https://doi.org/10.1103/PhysRevX.8.031030). URL: <http://arxiv.org/abs/1803.08566><http://dx.doi.org/10.1103/PhysRevX.8.031030>.
- [70] S. V. Isakov et al. “Dynamics at and near conformal quantum critical points”. In: *Physical Review B - Condensed Matter and Materials Physics* 83.12 (Dec. 2010). DOI: [10.1103/PhysRevB.83.125114](https://doi.org/10.1103/PhysRevB.83.125114). URL: <http://arxiv.org/abs/1012.3806><http://dx.doi.org/10.1103/PhysRevB.83.125114>.
- [71] Elliott Lieb, Theodore Schultz, and Daniel Mattis. “Two Soluble Models of an Antiferromagnetic Chain”. In: *Condensed Matter Physics and Exactly Soluble Models*. Springer Berlin Heidelberg, 2004, pp. 543–601. DOI: [10.1007/978-3-662-06390-3\\_{\\\_}35](https://doi.org/10.1007/978-3-662-06390-3_{\_}35).
- [72] Ian Affleck and Elliott H. Lieb. “A proof of part of Haldane’s conjecture on spin chains”. In: *Letters in Mathematical Physics* 12.1 (July 1986), pp. 57–69. ISSN: 03779017. DOI: [10.1007/BF00400304](https://doi.org/10.1007/BF00400304).
- [73] Masanori Yamanaka, Masaki Oshikawa, and Ian Affleck. *Non-perturbative approach to Luttinger’s theorem in one dimension*. Tech. rep. 1997.
- [74] Masaki Oshikawa, Masanori Yamanaka, and Ian Affleck. “Magnetization plateaus in spin chains: “Haldane gap” for half-integer spins”. In: *Physical Review Letters* 78.10 (Oct. 1996), pp. 1984–1987. DOI: [10.1103/PhysRevLett.78.1984](https://doi.org/10.1103/PhysRevLett.78.1984). URL: <http://arxiv.org/abs/cond-mat/9610168><http://dx.doi.org/10.1103/PhysRevLett.78.1984>.
- [75] Yoshiko Ogata and Hal Tasaki. “Lieb–Schultz–Mattis Type Theorems for Quantum Spin Chains Without Continuous Symmetry”. In: *Communications in Mathematical Physics* 372.3 (Dec. 2019), pp. 951–962. ISSN: 14320916. DOI: [10.1007/s00220-019-03343-5](https://doi.org/10.1007/s00220-019-03343-5).
- [76] J. I. Cirac et al. “Matrix product density operators: Renormalization fixed points and boundary theories”. In: *Annals of Physics* 378 (Mar. 2017), pp. 100–149. ISSN: 1096035X. DOI: [10.1016/j.aop.2016.12.030](https://doi.org/10.1016/j.aop.2016.12.030).
- [77] M. B. Hastings. “Lieb–Schultz–Mattis in Higher Dimensions”. In: *Physical Review B - Condensed Matter and Materials Physics* 69.10 (May 2003). DOI: [10.1103/PhysRevB.69.104431](https://doi.org/10.1103/PhysRevB.69.104431). URL: <http://arxiv.org/abs/cond-mat/0305505><http://dx.doi.org/10.1103/PhysRevB.69.104431>.
- [78] Richard P. (Richard Phillips) Feynman. *Statistical mechanics : a set of lectures*. Reading (Mass.): W.A. Benjamin, 1972, p. 354. ISBN: 9780805325089.
- [79] R. Moessner and L. Sondhi. “Three-dimensional resonating-valence-bond liquids and their excitations”. In: *Physical Review B - Condensed Matter and Materials Physics* 68.18 (Nov. 2003), p. 184512. ISSN: 1550235X. DOI: [10.1103/PhysRevB.68.184512](https://doi.org/10.1103/PhysRevB.68.184512).



- [80] Michael Hermele, Matthew P.A. Fisher, and Leon Balents. “Pyrochlore photons: The U(1) spin liquid in a  $S=1/2$  three-dimensional frustrated magnet”. In: *Physical Review B - Condensed Matter and Materials Physics* 69.6 (Feb. 2004), p. 064404. ISSN: 1550235X. DOI: [10.1103/PhysRevB.69.064404](https://doi.org/10.1103/PhysRevB.69.064404).
- [81] V. Zauner et al. “Transfer Matrices and Excitations with Matrix Product States”. In: (Aug. 2014). DOI: [10.1088/1367-2630/17/5/053002](https://doi.org/10.1088/1367-2630/17/5/053002). URL: <http://arxiv.org/abs/1408.5140>[20http://dx.doi.org/10.1088/1367-2630/17/5/053002](http://dx.doi.org/10.1088/1367-2630/17/5/053002).
- [82] Jutho Haegeman, Tobias J. Osborne, and Frank Verstraete. “Post-matrix product state methods: To tangent space and beyond”. In: *Physical Review B - Condensed Matter and Materials Physics* 88.7 (Aug. 2013), p. 075133. ISSN: 10980121. DOI: [10.1103/PhysRevB.88.075133](https://doi.org/10.1103/PhysRevB.88.075133).
- [83] P. C. Hohenberg. “Existence of long-range order in one and two dimensions”. In: *Physical Review* 158.2 (June 1967), pp. 383–386. ISSN: 0031899X. DOI: [10.1103/PhysRev.158.383](https://doi.org/10.1103/PhysRev.158.383).
- [84] Mohammad F. Maghrebi, Zhe Xuan Gong, and Alexey V. Gorshkov. “Continuous Symmetry Breaking in 1D Long-Range Interacting Quantum Systems”. In: *Physical Review Letters* 119.2 (July 2017), p. 023001. ISSN: 10797114. DOI: [10.1103/PhysRevLett.119.023001](https://doi.org/10.1103/PhysRevLett.119.023001).
- [85] C. L. Henley. “Relaxation time for a dimer covering with height representation”. In: *Journal of Statistical Physics* 89.3-4 (July 1996), pp. 483–507. DOI: [10.1007/BF02765532](https://doi.org/10.1007/BF02765532). URL: <http://arxiv.org/abs/cond-mat/9607222>[20http://dx.doi.org/10.1007/BF02765532](http://dx.doi.org/10.1007/BF02765532).
- [86] Roderich Moessner and Kumar S. Raman. “Quantum Dimer Models”. In: Springer, Berlin, Heidelberg, 2011, pp. 437–479. DOI: [10.1007/978-3-642-10589-0\\_17](https://doi.org/10.1007/978-3-642-10589-0_17).
- [87] P. W. Anderson. “Resonating valence bonds: A new kind of insulator?” In: *Materials Research Bulletin* (1973). ISSN: 00255408. DOI: [10.1016/0025-5408\(73\)90167-0](https://doi.org/10.1016/0025-5408(73)90167-0).
- [88] P. W. Anderson. “The resonating valence bond state in  $\text{La}_2\text{CuO}_4$  and superconductivity”. In: *Science* (1987). ISSN: 00368075. DOI: [10.1126/science.235.4793.1196](https://doi.org/10.1126/science.235.4793.1196).
- [89] Steven A. Kivelson, Daniel S. Rokhsar, and James P. Sethna. “Topology of the resonating valence-bond state: Solitons and high- $T_c$  superconductivity”. In: *Physical Review B* (1987). ISSN: 01631829. DOI: [10.1103/PhysRevB.35.8865](https://doi.org/10.1103/PhysRevB.35.8865).
- [90] P. W. Kasteleyn. “The statistics of dimers on a lattice. I. The number of dimer arrangements on a quadratic lattice”. In: *Physica* 27.12 (Dec. 1961), pp. 1209–1225. ISSN: 00318914. DOI: [10.1016/0031-8914\(61\)90063-5](https://doi.org/10.1016/0031-8914(61)90063-5).
- [91] K. S.D. Beach. “Master equation approach to computing RVB bond amplitudes”. In: *Physical Review B - Condensed Matter and Materials Physics* (2009). ISSN: 10980121. DOI: [10.1103/PhysRevB.79.224431](https://doi.org/10.1103/PhysRevB.79.224431).
- [92] Ling Wang et al. “Constructing a gapless spin-liquid state for the spin-1/2 J 1-J2 heisenberg model on a square lattice”. In: *Physical Review Letters* (2013). ISSN: 00319007. DOI: [10.1103/PhysRevLett.111.037202](https://doi.org/10.1103/PhysRevLett.111.037202).

- [93] A. Fabricio Albuquerque and Fabien Alet. “Critical correlations for short-range valence-bond wave functions on the square lattice”. In: *Physical Review B - Condensed Matter and Materials Physics* (2010). ISSN: 10980121. DOI: [10.1103/PhysRevB.82.180408](https://doi.org/10.1103/PhysRevB.82.180408).
- [94] Ying Tang, Anders W. Sandvik, and Christopher L. Henley. “Properties of resonating-valence-bond spin liquids and critical dimer models”. In: *Physical Review B - Condensed Matter and Materials Physics* (2011). ISSN: 10980121. DOI: [10.1103/PhysRevB.84.174427](https://doi.org/10.1103/PhysRevB.84.174427).
- [95] Ji Yao Chen and Didier Poilblanc. “Topological Z2 resonating-valence-bond spin liquid on the square lattice”. In: *Physical Review B* (2018). ISSN: 24699969. DOI: [10.1103/PhysRevB.97.161107](https://doi.org/10.1103/PhysRevB.97.161107).
- [96] A. Yu Kitaev. “Fault-tolerant quantum computation by anyons”. In: *Annals of Physics* (2003). ISSN: 00034916. DOI: [10.1016/S0003-4916\(02\)00018-0](https://doi.org/10.1016/S0003-4916(02)00018-0).
- [97] Chetan Nayak et al. “Non-Abelian anyons and topological quantum computation”. In: *Reviews of Modern Physics* (2008). ISSN: 00346861. DOI: [10.1103/RevModPhys.80.1083](https://doi.org/10.1103/RevModPhys.80.1083).
- [98] Jean-Marie Stéphan et al. “Entanglement in gapless resonating valence bond states”. In: *New Journal of Physics* 15 (July 2012). DOI: [10.1088/1367-2630/15/1/015004](https://doi.org/10.1088/1367-2630/15/1/015004). URL: <http://arxiv.org/abs/1207.3820><http://dx.doi.org/10.1088/1367-2630/15/1/015004>.
- [99] H. N.V. Temperley and Michael E. Fisher. *Dimer problem in statistical mechanics-an exact result*. 1961. DOI: [10.1080/14786436108243366](https://doi.org/10.1080/14786436108243366). URL: <https://www.tandfonline.com/doi/abs/10.1080/14786436108243366>.
- [100] Michael E. Fisher and John Stephenson. “Statistical mechanics of dimers on a plane lattice. II. Dimer correlations and monomers”. In: *Physical Review* 132.4 (Nov. 1963), pp. 1411–1431. ISSN: 0031899X. DOI: [10.1103/PhysRev.132.1411](https://doi.org/10.1103/PhysRev.132.1411). URL: <https://journals.aps.org/pr/abstract/10.1103/PhysRev.132.1411>.
- [101] Richard Kenyon. “Conformal invariance of Domino tiling”. In: *Annals of Probability* 28.2 (Oct. 2000), pp. 759–795. ISSN: 00911798. DOI: [10.1214/aop/1019160260](https://doi.org/10.1214/aop/1019160260). URL: <https://arxiv.org/abs/math-ph/9910002v1>.
- [102] Richard Kenyon. “Dominos and the Gaussian free field”. In: *Annals of Probability* 29.3 (July 2001), pp. 1128–1137. ISSN: 00911798. DOI: [10.1214/aop/1015345599](https://doi.org/10.1214/aop/1015345599). URL: <https://arxiv.org/abs/math-ph/0002027v1>.
- [103] Fabien Alet et al. “Interacting classical dimers on the square lattice”. In: *Physical Review Letters* (2005). ISSN: 00319007. DOI: [10.1103/PhysRevLett.94.235702](https://doi.org/10.1103/PhysRevLett.94.235702).
- [104] Nicolas Allegra. “Exact solution of the 2d dimer model: Corner free energy, correlation functions and combinatorics”. In: *Nuclear Physics B* 894 (May 2015), pp. 685–732. ISSN: 05503213. DOI: [10.1016/j.nuclphysb.2015.03.022](https://doi.org/10.1016/j.nuclphysb.2015.03.022). URL: <https://arxiv.org/abs/1410.4131v4>.
- [105] Jané Kondev and Christopher L. Henley. “Kac-Moody symmetries of critical ground states”. In: *Nuclear Physics B* 464.3 (Apr. 1996), pp. 540–575. ISSN: 05503213. DOI: [10.1016/0550-3213\(96\)00064-8](https://doi.org/10.1016/0550-3213(96)00064-8). URL: <https://arxiv.org/abs/cond-mat/9511102v1>.

- [106] Philippe Di Francesco, Pierre Mathieu, and David Sénéchal. *Conformal Field Theory*. Graduate Texts in Contemporary Physics. New York, NY: Springer New York, 1997. ISBN: 978-1-4612-7475-9. DOI: [10.1007/978-1-4612-2256-9](https://doi.org/10.1007/978-1-4612-2256-9). URL: <http://link.springer.com/10.1007/978-1-4612-2256-9>.
- [107] Eduardo Fradkin et al. “On bipartite Rokhsar-Kivelson points and Cantor deconfinement”. In: *Physical Review B - Condensed Matter and Materials Physics* 69.22 (Nov. 2003). DOI: [10.1103/PhysRevB.69.224415](https://doi.org/10.1103/PhysRevB.69.224415). URL: <http://arxiv.org/abs/cond-mat/0311353%20http://dx.doi.org/10.1103/PhysRevB.69.224415>.
- [108] Eduardo Fradkin et al. “Bipartite Rokhsar-Kivelson points and Cantor deconfinement”. In: *Physical Review B - Condensed Matter and Materials Physics* (2004). ISSN: 01631829. DOI: [10.1103/PhysRevB.69.224415](https://doi.org/10.1103/PhysRevB.69.224415).
- [109] Claudio Castelnovo et al. “High-Temperature Criticality in Strongly Constrained Quantum Systems”. In: (Dec. 2005). DOI: [10.1103/PhysRevB.73.144411](https://doi.org/10.1103/PhysRevB.73.144411). URL: <http://arxiv.org/abs/cond-mat/0512258%20http://dx.doi.org/10.1103/PhysRevB.73.144411>.
- [110] Kedar Damle, Deepak Dhar, and Kabir Ramola. “Resonating valence bond wave functions and classical interacting dimer models”. In: *Physical Review Letters* (2012). ISSN: 00319007. DOI: [10.1103/PhysRevLett.108.247216](https://doi.org/10.1103/PhysRevLett.108.247216).
- [111] S. L. Sondhi et al. “Continuous quantum phase transitions”. In: *Reviews of Modern Physics* (1997). ISSN: 00346861. DOI: [10.1103/revmodphys.69.315](https://doi.org/10.1103/revmodphys.69.315).
- [112] M. Suzuki. “The dimer problem and the generalized X-model”. In: *Physics Letters A* (1971). ISSN: 03759601. DOI: [10.1016/0375-9601\(71\)90901-7](https://doi.org/10.1016/0375-9601(71)90901-7).
- [113] Ruben Verresen, Nick G. Jones, and Frank Pollmann. “Topology and Edge Modes in Quantum Critical Chains”. In: *Physical Review Letters* (2018). ISSN: 10797114. DOI: [10.1103/PhysRevLett.120.057001](https://doi.org/10.1103/PhysRevLett.120.057001).
- [114] Philippe Di Francesco, Pierre Mathieu, and David Sénéchal. *Conformal field theory*. Graduate texts in contemporary physics. New York, NY: Springer, 1997. DOI: [10.1007/978-1-4612-2256-9](https://doi.org/10.1007/978-1-4612-2256-9). URL: <https://cds.cern.ch/record/639405>.
- [115] N. E. Bonesteel. “Valence bonds and the Lieb-Schultz-Mattis theorem”. In: *Physical Review B* (1989). ISSN: 01631829. DOI: [10.1103/PhysRevB.40.8954](https://doi.org/10.1103/PhysRevB.40.8954).
- [116] Mahito Kohmoto and Yonathan Shapir. “Antiferromagnetic correlations of the resonating-valence-bond state”. In: *Physical Review B* 37.16 (June 1988), pp. 9439–9442. ISSN: 01631829. DOI: [10.1103/PhysRevB.37.9439](https://doi.org/10.1103/PhysRevB.37.9439).
- [117] S. Liang, B. Doucot, and P. W. Anderson. “Some New variational resonating-valence-bond-type wave functions for the spin-1/2 antiferromagnetic heisenberg model on a square lattice”. In: *Physical Review Letters* (1988). ISSN: 00319007. DOI: [10.1103/PhysRevLett.61.365](https://doi.org/10.1103/PhysRevLett.61.365).
- [118] Didier Poilblanc et al. “Resonating-valence-bond superconductors with fermionic projected entangled pair states”. In: *Physical Review B - Condensed Matter and Materials Physics* (2014). ISSN: 1550235X. DOI: [10.1103/PhysRevB.89.241106](https://doi.org/10.1103/PhysRevB.89.241106).

- [119] Marek M. Rams, Piotr Czarnik, and Lukasz Cincio. “Precise Extrapolation of the Correlation Function Asymptotics in Uniform Tensor Network States with Application to the Bose-Hubbard and XXZ Models”. In: *Physical Review X* (2018). ISSN: 21603308. DOI: [10.1103/PhysRevX.8.041033](https://doi.org/10.1103/PhysRevX.8.041033).
- [120] S. Lukyanov and A. Zamolodchikov. “Exact expectation values of local fields in quantum sine-Gordon model”. In: *Nuclear Physics B* 493.3 (Nov. 1996), pp. 571–587. DOI: [10.1016/S0550-3213\(97\)00123-5](https://doi.org/10.1016/S0550-3213(97)00123-5). URL: <http://arxiv.org/abs/hep-th/9611238> and [http://dx.doi.org/10.1016/S0550-3213\(97\)00123-5](http://dx.doi.org/10.1016/S0550-3213(97)00123-5).
- [121] M. R. Norman. “Colloquium: Herbertsmithite and the search for the quantum spin liquid”. In: *Reviews of Modern Physics* (2016). ISSN: 15390756. DOI: [10.1103/RevModPhys.88.041002](https://doi.org/10.1103/RevModPhys.88.041002).
- [122] A. V. Gorshkov et al. “Two-orbital SU(N) magnetism with ultracold alkaline-earth atoms”. In: *Nature Physics* 6.4 (May 2009), pp. 289–295. DOI: [10.1038/NPHYS1535](https://doi.org/10.1038/NPHYS1535). URL: <http://arxiv.org/abs/0905.2610> and <http://dx.doi.org/10.1038/NPHYS1535>.
- [123] Michael Hermele, Victor Gurarie, and Ana Maria Rey. “Mott insulators of ultracold fermionic alkaline earth atoms: Underconstrained magnetism and chiral spin liquid”. In: *Physical Review Letters* 103.13 (Sept. 2009), p. 135301. ISSN: 00319007. DOI: [10.1103/PhysRevLett.103.135301](https://doi.org/10.1103/PhysRevLett.103.135301).
- [124] Ji-Yao Chen et al. “SU(3)<sub>1</sub> Chiral Spin Liquid on the Square Lattice: a View from Symmetric PEPS”. In: (Dec. 2019). URL: <http://arxiv.org/abs/1912.13393>.
- [125] H. Weyl, G. Rumer, and E. Teller. “Eine für die Valenztheorie geeignete Basis der binären Vektorinvarianten”. In: *Nachrichten von der Gesellschaft der Wissenschaften zu Göttingen, Mathematisch-Physikalische Klasse* 1932 (1932), pp. 499–504.
- [126] Riichiro Saito. “A Proof of the Completeness of the Non Crossed Diagrams in Spin 1/2 Heisenberg Model”. In: *journal of the physical society of japan* 59.2 (Nov. 1990), pp. 482–491. ISSN: 13474073. DOI: [10.1143/JPSJ.59.482](https://doi.org/10.1143/JPSJ.59.482). URL: <https://journals.jps.jp/doi/abs/10.1143/JPSJ.59.482>.
- [127] Ruben Pauncz. *Spin Eigenfunctions*. Springer US, 1979. DOI: [10.1007/978-1-4684-8526-4](https://doi.org/10.1007/978-1-4684-8526-4).
- [128] Markus Fulmek. “Asymptotics of the average height of 2-watermelons with a wall”. In: (July 2006). URL: <http://arxiv.org/abs/math/0607163>.
- [129] F. Y. Wu. “The Potts model”. In: *Reviews of Modern Physics* 54.1 (Jan. 1982), pp. 235–268. ISSN: 00346861. DOI: [10.1103/RevModPhys.54.235](https://doi.org/10.1103/RevModPhys.54.235). URL: <https://journals.aps.org/rmp/abstract/10.1103/RevModPhys.54.235>.
- [130] C. M. Fortuin and P. W. Kasteleyn. “On the random-cluster model. I. Introduction and relation to other models”. In: *Physica* 57.4 (Feb. 1972), pp. 536–564. ISSN: 00318914. DOI: [10.1016/0031-8914\(72\)90045-6](https://doi.org/10.1016/0031-8914(72)90045-6).

- [131] Paul Fendley, Sergei V. Isakov, and Matthias Troyer. “Fibonacci topological order from quantum nets”. In: *Physical Review Letters* 110.26 (Oct. 2012). DOI: [10.1103/PhysRevLett.110.260408](https://doi.org/10.1103/PhysRevLett.110.260408). URL: <http://arxiv.org/abs/1210.5527><http://dx.doi.org/10.1103/PhysRevLett.110.260408>.
- [132] Matthias Troyer et al. “Local interactions and non-Abelian quantum loop gases”. In: *Physical Review Letters* 101.23 (May 2008). DOI: [10.1103/PhysRevLett.101.230401](https://doi.org/10.1103/PhysRevLett.101.230401). URL: <http://arxiv.org/abs/0805.2177><http://dx.doi.org/10.1103/PhysRevLett.101.230401>.
- [133] Michael H. Freedman. “A magnetic model with a possible Chern-Simons phase”. In: *Communications in Mathematical Physics* 234.1 (Oct. 2001), pp. 129–183. URL: <http://arxiv.org/abs/quant-ph/0110060>.
- [134] Michael Freedman, Chetan Nayak, and Kirill Shtengel. “An extended Hubbard model with ring exchange: a route to a non-Abelian topological phase”. In: *Physical Review Letters* 94.6 (Dec. 2003). DOI: [10.1103/PhysRevLett.94.066401](https://doi.org/10.1103/PhysRevLett.94.066401). URL: <http://arxiv.org/abs/cond-mat/0312273><http://dx.doi.org/10.1103/PhysRevLett.94.066401>.
- [135] Michael Freedman, Chetan Nayak, and Kirill Shtengel. “A Line of Critical Points in 2+1 Dimensions: Quantum Critical Loop Gases and Non-Abelian Gauge Theory”. In: *Physical Review Letters* 94.14 (Aug. 2004). DOI: [10.1103/PhysRevLett.94.147205](https://doi.org/10.1103/PhysRevLett.94.147205). URL: <http://arxiv.org/abs/cond-mat/0408257><http://dx.doi.org/10.1103/PhysRevLett.94.147205>.
- [136] Paul Fendley and Eduardo Fradkin. “Realizing non-Abelian statistics”. In: *Physical Review B - Condensed Matter and Materials Physics* 72.2 (Feb. 2005). DOI: [10.1103/PhysRevB.72.024412](https://doi.org/10.1103/PhysRevB.72.024412). URL: <http://arxiv.org/abs/cond-mat/0502071><http://dx.doi.org/10.1103/PhysRevB.72.024412>.
- [137] Paul Fendley. “Topological order from quantum loops and nets”. In: *Annals of Physics* 323.12 (Apr. 2008), pp. 3113–3136. DOI: [10.1016/j.aop.2008.04.011](https://doi.org/10.1016/j.aop.2008.04.011). URL: <http://arxiv.org/abs/0804.0625><http://dx.doi.org/10.1016/j.aop.2008.04.011>.
- [138] Paul Fendley. “Quantum loop models and the non-abelian toric code”. In: 1 (Nov. 2007), p. 4. URL: <http://arxiv.org/abs/0711.0014>.
- [139] C. Domb and J.L. Lebowitz. *PHASE TRANSITIONS AND CRITICAL PHENOMENA. VOL. 11*. Nov. 1987.
- [140] Vincent Beffara and Hugo Duminil-Copin. “The self-dual point of the two-dimensional random-cluster model is critical for  $q \geq 4$ ”. In: (June 2010). URL: <http://arxiv.org/abs/1006.5073>.
- [141] Hugo Duminil-Copin et al. “Discontinuity of the phase transition for the planar random-cluster and Potts models with  $q \geq 4$ ”. In: (Nov. 2016). URL: <http://arxiv.org/abs/1611.09877>.
- [142] Paul Fendley and Jesper L Jacobsen. *Critical points in coupled Potts models and critical phases in coupled loop models*. Tech. rep. Mar. 2008. URL: <https://arxiv.org/abs/0803.2618v1>.



- 
- [143] Vladimir Dotsenko et al. “Coupled Potts models: Self-duality and fixed point structure”. In: *Nuclear Physics B* 546.3 (Dec. 1998), pp. 505–557. DOI: [10.1016/S0550-3213\(99\)00097-8](https://doi.org/10.1016/S0550-3213(99)00097-8). URL: <http://arxiv.org/abs/cond-mat/9812227>[http://dx.doi.org/10.1016/S0550-3213\(99\)00097-8](http://dx.doi.org/10.1016/S0550-3213(99)00097-8).
- [144] Vl. S. Dotsenko et al. “Universality of coupled Potts models”. In: *Nuclear Physics B* 631.3 (Dec. 2001), pp. 426–446. DOI: [10.1016/S0550-3213\(02\)00213-4](https://doi.org/10.1016/S0550-3213(02)00213-4). URL: <http://arxiv.org/abs/cond-mat/0112120>[http://dx.doi.org/10.1016/S0550-3213\(02\)00213-4](http://dx.doi.org/10.1016/S0550-3213(02)00213-4).
- [145] Adam Nahum et al. “Phase transitions in three-dimensional loop models and the CP<sub>n</sub>-1 sigma model”. In: *Physical Review B - Condensed Matter and Materials Physics* 88.13 (Oct. 2013), p. 134411. ISSN: 10980121. DOI: [10.1103/PhysRevB.88.134411](https://doi.org/10.1103/PhysRevB.88.134411). URL: <https://journals.aps.org/prb/abstract/10.1103/PhysRevB.88.134411>.
- [146] Michael Levin and Zheng Cheng Gu. “Braiding statistics approach to symmetry-protected topological phases”. In: *Physical Review B - Condensed Matter and Materials Physics* 86.11 (Sept. 2012), p. 115109. ISSN: 10980121. DOI: [10.1103/PhysRevB.86.115109](https://doi.org/10.1103/PhysRevB.86.115109).
- [147] Xie Chen et al. “Symmetry-protected topological orders in interacting bosonic systems”. In: *Science* 338.6114 (Dec. 2012), pp. 1604–1606. ISSN: 10959203. DOI: [10.1126/science.1227224](https://doi.org/10.1126/science.1227224).
- [148] Robert Raussendorf et al. “Computationally Universal Phase of Quantum Matter”. In: *Physical Review Letters* (2019). ISSN: 10797114. DOI: [10.1103/PhysRevLett.122.090501](https://doi.org/10.1103/PhysRevLett.122.090501).
- [149] R. Raussendorf and H. J. Briegel. “A one-way quantum computer”. In: *Physical Review Letters* 86.22 (May 2001), pp. 5188–5191. ISSN: 00319007. DOI: [10.1103/PhysRevLett.86.5188](https://doi.org/10.1103/PhysRevLett.86.5188).
- [150] Robert Raussendorf et al. “Symmetry-protected topological phases with uniform computational power in one dimension”. In: *Physical Review A* 96.1 (July 2017). ISSN: 24699934. DOI: [10.1103/PhysRevA.96.012302](https://doi.org/10.1103/PhysRevA.96.012302).
- [151] David T. Stephen et al. “Computational Power of Symmetry-Protected Topological Phases”. In: *Physical Review Letters* 119.1 (July 2017), p. 010504. ISSN: 10797114. DOI: [10.1103/PhysRevLett.119.010504](https://doi.org/10.1103/PhysRevLett.119.010504).
- [152] Wilbur Shirley, Kevin Slagle, and Xie Chen. “Foliated fracton order from gauging subsystem symmetries”. In: *SciPost Physics* 6.4 (June 2018). DOI: [10.21468/SciPostPhys.6.4.041](https://doi.org/10.21468/SciPostPhys.6.4.041). URL: <http://arxiv.org/abs/1806.08679><http://dx.doi.org/10.21468/SciPostPhys.6.4.041>.
- [153] Sagar Vijay, Jeongwan Haah, and Liang Fu. “Fracton topological order, generalized lattice gauge theory, and duality”. In: *Physical Review B* 94.23 (Dec. 2016), p. 235157. ISSN: 24699969. DOI: [10.1103/PhysRevB.94.235157](https://doi.org/10.1103/PhysRevB.94.235157).
- [154] Dominic J. Williamson. “Fractal symmetries: Ungauging the cubic code”. In: *Physical Review B* 94.15 (Oct. 2016), p. 155128. ISSN: 24699969. DOI: [10.1103/PhysRevB.94.155128](https://doi.org/10.1103/PhysRevB.94.155128).
- [155] Aleksander Kubica and Beni Yoshida. “Ungauging quantum error-correcting codes”. In: (May 2018). URL: <http://arxiv.org/abs/1805.01836>.

- [156] Trithep Devakul, Dominic J. Williamson, and Yizhi You. “Classification of subsystem symmetry-protected topological phases”. In: *Physical Review B* (2018). ISSN: 24699969. DOI: [10.1103/PhysRevB.98.235121](https://doi.org/10.1103/PhysRevB.98.235121).
- [157] Alioscia Hamma, Radu Ionicioiu, and Paolo Zanardi. “Bipartite entanglement and entropic boundary law in lattice spin systems”. In: (). DOI: [10.1103/PhysRevA.71.022315](https://doi.org/10.1103/PhysRevA.71.022315).
- [158] Dominic J Williamson, Arpit Dua, and Meng Cheng. *Spurious topological entanglement entropy from subsystem symmetries*. Tech. rep.
- [159] Liujun Zou and Jeongwan Haah. “Spurious long-range entanglement and replica correlation length”. In: *Physical Review B* 94.7 (Aug. 2016), p. 075151. ISSN: 24699969. DOI: [10.1103/PhysRevB.94.075151](https://doi.org/10.1103/PhysRevB.94.075151).
- [160] Laurens Vanderstraeten et al. “Gradient methods for variational optimization of projected entangled-pair states”. In: *Physical Review B* 94.15 (Oct. 2016), p. 155123. ISSN: 24699969. DOI: [10.1103/PhysRevB.94.155123](https://doi.org/10.1103/PhysRevB.94.155123).
- [161] H. A. Kramers and G. H. Wannier. “Statistics of the two-dimensional ferromagnet. Part II”. In: *Physical Review* 60.3 (Aug. 1941), pp. 263–276. ISSN: 0031899X. DOI: [10.1103/PhysRev.60.263](https://doi.org/10.1103/PhysRev.60.263).
- [162] G. H. Wannier. “The statistical problem in cooperative phenomena”. In: *Reviews of Modern Physics* 17.1 (Jan. 1945), pp. 50–60. ISSN: 00346861. DOI: [10.1103/RevModPhys.17.50](https://doi.org/10.1103/RevModPhys.17.50).
- [163] Cenke Xu and J. E. Moore. “Strong-weak coupling self-duality in the two-dimensional quantum phase transition of  $p + ip$  superconducting arrays”. In: *Physical Review Letters* 93.4 (July 2004), pp. 047003–1. ISSN: 00319007. DOI: [10.1103/PhysRevLett.93.047003](https://doi.org/10.1103/PhysRevLett.93.047003).
- [164] Andrew C. Doherty and Stephen D. Bartlett. “Identifying phases of quantum many-body systems that are universal for quantum computation”. In: *Physical Review Letters* 103.2 (Aug. 2009), p. 020506. ISSN: 00319007. DOI: [10.1103/PhysRevLett.103.020506](https://doi.org/10.1103/PhysRevLett.103.020506).
- [165] Yizhi You et al. “Subsystem symmetry protected topological order”. In: *Physical Review B* (2018). ISSN: 24699969. DOI: [10.1103/PhysRevB.98.035112](https://doi.org/10.1103/PhysRevB.98.035112).
- [166] Román Orús et al. “Bounds on universal quantum computation with perturbed two-dimensional cluster states”. In: *Physical Review A - Atomic, Molecular, and Optical Physics* 87.6 (June 2013), p. 062312. ISSN: 10502947. DOI: [10.1103/PhysRevA.87.062312](https://doi.org/10.1103/PhysRevA.87.062312).
- [167] Henning Kalis et al. “Fate of the cluster state on the square lattice in a magnetic field”. In: *Physical Review A - Atomic, Molecular, and Optical Physics* 86.2 (Aug. 2012), p. 022317. ISSN: 10502947. DOI: [10.1103/PhysRevA.86.022317](https://doi.org/10.1103/PhysRevA.86.022317).
- [168] Xie Chen et al. “Symmetry protected topological orders and the group cohomology of their symmetry group”. In: *Physical Review B - Condensed Matter and Materials Physics* 87.15 (Apr. 2013), p. 155114. ISSN: 10980121. DOI: [10.1103/PhysRevB.87.155114](https://doi.org/10.1103/PhysRevB.87.155114).
- [169] Jacob Miller and Akimas A. Miyake. “Hierarchy of universal entanglement in 2D measurement-based quantum computation”. In: *npj Quantum Information* 2.1 (Nov. 2016), pp. 1–6. ISSN: 20566387. DOI: [10.1038/npjqi.2016.36](https://doi.org/10.1038/npjqi.2016.36).

- [170] David T. Stephen et al. “Subsystem symmetries, quantum cellular automata, and computational phases of quantum matter”. In: *Quantum* 3 (June 2018), p. 142. DOI: [10.22331/q-2019-05-20-142](https://doi.org/10.22331/q-2019-05-20-142). URL: <http://arxiv.org/abs/1806.08780><http://dx.doi.org/10.22331/q-2019-05-20-142>.
- [171] Laurens Vanderstraeten et al. “Bridging Perturbative Expansions with Tensor Networks”. In: *Physical Review Letters* 119.7 (Aug. 2017), p. 070401. ISSN: 10797114. DOI: [10.1103/PhysRevLett.119.070401](https://doi.org/10.1103/PhysRevLett.119.070401).
- [172] M. B. Hastings and Xiao Gang Wen. “Quasiadiabatic continuation of quantum states: The stability of topological ground-state degeneracy and emergent gauge invariance”. In: *Physical Review B - Condensed Matter and Materials Physics* 72.4 (July 2005), p. 045141. ISSN: 10980121. DOI: [10.1103/PhysRevB.72.045141](https://doi.org/10.1103/PhysRevB.72.045141).
- [173] Karel Van Acoleyen et al. “Entanglement of Distillation for Lattice Gauge Theories”. In: *Physical Review Letters* 117.13 (Sept. 2016), p. 131602. ISSN: 10797114. DOI: [10.1103/PhysRevLett.117.131602](https://doi.org/10.1103/PhysRevLett.117.131602).
- [174] Ruben Verresen, Roderich Moessner, and Frank Pollmann. “One-dimensional symmetry protected topological phases and their transitions”. In: *Physical Review B* 96.16 (Oct. 2017), p. 165124. ISSN: 24699969. DOI: [10.1103/PhysRevB.96.165124](https://doi.org/10.1103/PhysRevB.96.165124).
- [175] Xie Chen and Ashvin Vishwanath. “Towards Gauging Time-Reversal Symmetry: A Tensor Network Approach”. In: *Physical Review X* 5.4 (Nov. 2015), p. 041034. ISSN: 2160-3308. DOI: [10.1103/physrevx.5.041034](https://doi.org/10.1103/physrevx.5.041034).
- [176] M B Hastings. *How Quantum Are Non-Negative Wavefunctions?* Tech. rep. 2020.
- [177] Oliver Buerschaper. “Twisted injectivity in projected entangled pair states and the classification of quantum phases”. In: *Annals of Physics* (2014). ISSN: 1096035X. DOI: [10.1016/j.aop.2014.09.007](https://doi.org/10.1016/j.aop.2014.09.007).
- [178] Eduardo Fradkin. *Field theories of condensed matter physics, second edition*. Vol. 9780521764445. Cambridge University Press, Jan. 2010, pp. 1–838. ISBN: 9781139015509. DOI: [10.1017/CB09781139015509](https://doi.org/10.1017/CB09781139015509).
- [179] Flore K. Kunst and Vatsal Dwivedi. “Non-Hermitian systems and topology: A transfer-matrix perspective”. In: *Physical Review B* 99.24 (Dec. 2018). DOI: [10.1103/PhysRevB.99.245116](https://doi.org/10.1103/PhysRevB.99.245116). URL: <http://arxiv.org/abs/1812.02186><http://dx.doi.org/10.1103/PhysRevB.99.245116>.
- [180] Flore K. Kunst et al. “Biorthogonal Bulk-Boundary Correspondence in Non-Hermitian Systems”. In: *Physical Review Letters* 121.2 (May 2018). DOI: [10.1103/PhysRevLett.121.026808](https://doi.org/10.1103/PhysRevLett.121.026808). URL: <http://arxiv.org/abs/1805.06492><http://dx.doi.org/10.1103/PhysRevLett.121.026808>.
- [181] Sergey Bravyi, David Gosset, and Ramis Movassagh. “Classical algorithms for quantum mean values”. In: (Sept. 2019). URL: <http://arxiv.org/abs/1909.11485>.
- [182] Mingpu Qin. “Combination of Tensor Network States and Green’s function Monte Carlo”. In: (June 2020). URL: <http://arxiv.org/abs/2006.15608>.



# Acknowledgements

First, I would like to express my sincere gratitude to my advisors Prof. Norbert Schuch and Prof. Ignacio Cirac for their guidance and patience that made this project possible. They not only provided knowledge and encouragement, but also a great deal of freedom for my research. I would also like to thank Prof. Jan von Delft for being so helpful in establishing ties with the LMU, as well as Prof. Barbara Ercolano, Prof. Roland Kersting and Prof. Emiliano Cortez for being on my committee.

I am indebted to Dr. Mohsin Iqbal, David Stephen, Dr. Ji-Yao Chen, Prof. Paul Fendley, Dr. Laurens Vanderstraeten, Dr. Michele Burrello and Prof. Frank Pollmann for particularly illuminating discussions. Special thanks go to Dr. Ruben Verresen from whom I learned enormously. It is hard to say in words just how helpful our conversations were. Extra kudos for being able to explain all of modern physics in terms of the Quantum Ising Chain.

I would like to thank current and former colleagues and staff at the Max-Planck-Institute of Quantum Optics, including Nicola Pancotti, Cosimo Rusconi, Annie Park, Caroline de Groot, David Malz, Johannes Knörzer, Anna Hackenbroich, Oriana Diessel, Tommaso Guaita, Marti Perarnau-Llobet, Andrea Kluth, Regina Jasny, Ivana Kurecic, Lorenzo Piroli, Giacomo Giudice, Patrick Emonts, Julian Roos, Andrew Goldsborough, Manuel Rispler and Tao Shi for their help, good attitude and thrilling ping-pong matches, as well as David Stephen, Daniel Robaina and Vitaly Wirthl for the jam sessions and Irene Papaefstathiou for the food.

A massive thank you goes to Nicola, Ruben, Andras, Cosimo and all former flatmates at the Leo flat: without you, I'm sure I would have gone crazy. Okay, maybe not more crazy, but a worse kind of crazy.

Thanks also to Nina for the support, as well as the help in preparing the document. Due to an injury, I was unable to use my hands while preparing this Thesis and her help was tremendously useful. Also extremely useful was the free eye-tracking software offered by the guys at Talon which, together with Dragon NaturallySpeaking, Serenade, Tobii 4C and a foot switch allowed me to keep a reasonable level of productivity even without using my hands.

Thanks to Elisa for walking part of the way with me and providing me with so much encouragement. A great deal of gratitude goes to Haikal. I'm not sure if there is a single person from whom I learned more about life. Thanks for changing me for the better, man. I would also like to thank Ilyas Khan for support and encouragement over the past 6 years.

Last, but maybe most importantly, I am deeply indebted to my family, Rita and Karl-Heinz Dreyer, Helena Lang and Luna. I have no idea where I would be without their support over the past three decades. Many thanks go to my mom for giving me "psychological air" to breath whenever I need it. And finally, gratitude goes to my deceased *Opa* Horst. You were always so proud. I only realize now, how you

kept everything together and how much I would like to be like you. It's sad that I didn't get to tell you this, but I hope that you are in a good place now.

Funding from the Max-Planck Society and from the European Union through the grants WASCOSYS (No. 636201) and QENOCOB A (No. 742102) is gratefully acknowledged.